

# **MODEL FOR THE BOUNCING PROCESS OF AN AIR BUBBLE INTERACTING WITH AN INCLINED WALL**

by

**RONAL ABEL DE LA CRUZ ARAUJO**

A thesis submitted in partial fulfillment of the requirements for the degree of

MASTER OF SCIENCE

in

MECHANICAL ENGINEERING

UNIVERSITY OF PUERTO RICO

MAYAGÜEZ CAMPUS

2011

Approved by:

---

Silvina Cancelos, Ph.D  
President, Graduate Committee

---

Date

---

Gustavo Gutierrez, Ph.D  
Member, Graduate Committee

---

Date

---

Jaime Benitez, Ph.D  
Member, Graduate Committee

---

Date

---

Miguel Canals, Ph.D  
Representative of Graduate Studies

---

Date

---

Gustavo Gutierrez, Ph.D  
Chairperson of the Department

---

Date

Abstract of Dissertation Presented to the Graduate School  
of the University of Puerto Rico in Partial Fulfillment of the  
Requirements for the Degree of Master of Science

## **MODEL FOR THE BOUNCING PROCESS OF AN AIR BUBBLE INTERACTING WITH AN INCLINED WALL**

by

RONAL ABEL DE LA CRUZ ARAUJO

2011

Chair: SILVINA CANCELOS  
Major Department: MECHANICAL ENGINEERING

### **ABSTRACT**

A model to predict the bouncing of an air bubble rising through an unbounded quiescent liquid and impinging on an inclined wall has been derived. This model is an extension to three dimensions of previous models in one and two dimensions based on the following methodology: Resolution of the bubble motion equation in an unbounded fluid in which an additional Bubble-Wall Interaction Force (BWIF) or often called the *wall force* is included to account for the excess pressure exerted in the fluid film between the wall and the top surface of the bubble when it approaches the wall. This force is obtained as the integral of the excess pressure calculated from the solution of the lubrication equation. In order to solve the resulting system of equations a numerical method was developed. This numerical method was a finite difference method in which the derivatives were approximated using a Taylor series expansion of second order accuracy.

We have considered bubbles of diameter 0.3-2 mm which correspond to Reynolds numbers ( $Re$ ) from 8 to 600 and Weber numbers ( $We$ ) from 0.003 to 1.7.  $Re$  and  $We$  were

calculated using the terminal velocity of the bubble. The numerical simulations predicted the bubble position during the bouncing process which was successfully validated with experimental data for the case of a horizontal wall. Also, the bubble velocity, deformation of the top surface of the bubble, excess pressure on the fluid film and the forces on the bubble were predicted.

From the simulations results it was concluded that the bouncing process of a bubble is governed by the Reynolds Number, the Weber number and the wall inclination. For the case of a horizontal wall the model predicted the axisymmetry of the bubble deformation and excess pressure profile of the physical phenomenon. For the case of a wall with one inclination the results predicted asymmetrical behavior, which is consistent with previous experimental visualizations and model predictions. In the case of a wall inclined in two directions the bubble deformation and excess pressure profile were predicted asymmetrical in the two tangential directions. It was also observed that as the wall inclination increases the asymmetry increases and the rebound amplitude and the wall force decreases. The numerical simulations showed that the rebound of a deformable bubble against a wall is essentially governed by the balance between the wall force and added mass force in the normal direction to the wall, and the drag and the buoyancy forces in the tangential directions.

Unlike previous three-dimensional numerical studies which were no able to predict bubble bounce on the wall; our model was able to compute several bubble bounces on an inclined wall with two angles. Moreover for the case of a horizontal wall the numerical results are in good agreement with experimental data.

Resumen de Disertación Presentado a Escuela Graduada  
de la Universidad de Puerto Rico como requisito parcial de los  
Requerimientos para el grado de Maestría en Ciencias

## **MODELO PARA EL PROCESO DE REBOTE DE UNA BURBUJA DE AIRE INTERACTUANDO CON UN PARED INCLINADA**

Por

RONAL ABEL DE LA CRUZ ARAUJO

2011

Consejera: SILVINA CANCELOS  
Departamento: INGENIERÍA MECÁNICA

### **RESUMEN**

Un modelo para predecir el proceso de rebote de una burbuja de aire ascendiendo en un líquido ilimitado y en reposo e incidiendo sobre una pared inclinada ha sido desarrollado. Este modelo es una extensión a tres dimensiones de previos modelos en una y dos dimensiones basados en la siguiente metodología: Resolución de la ecuación de movimiento de la burbuja en un fluido ilimitado en el cual una fuerza adicional de interacción de la burbuja con la pared (BWIF) o a menudo llamada la *fuerza de la pared* es incluida con el fin de tener en cuenta el exceso de presión ejercido entre la pared y la parte superior de la burbuja cuando esta se aproxima a la pared. Esta fuerza es obtenida como la integral del exceso de presión calculado a partir de la solución de la ecuación de lubricación. Con el fin de resolver el sistema resultante de ecuaciones un método numérico ha sido desarrollado. Este método numérico usa el método de diferencias finitas, en el cual la derivadas fueron aproximadas usando expansión en series de Taylor de Segundo orden.

Se consideraron burbujas de diámetros entre 0.3 y 2mm los cuales corresponden a números de Reynolds( $Re$ ) entre 8 y 600 y a números de Weber ( $We$ ) entre 0.003 y 1.7. Los  $Re$  y

Se fueron calculados usando la velocidad terminal de la burbuja. Las simulaciones numéricas predijeron la posición de la burbuja durante el proceso de rebote, la cual fue satisfactoriamente validada con datos experimentales para el caso de una pared horizontal. También han sido predichos la velocidad de la burbuja, la deformación de la parte superior de la burbuja, el exceso de presión sobre la capa fluida y las fuerzas sobre la burbuja.

De los resultados de las simulaciones se concluyó que el proceso de rebote de una burbuja es gobernado por el número de Reynolds, el número de Weber y la inclinación de la pared. Para el caso de una pared horizontal el modelo predice la axisimetría de la deformación y del perfil de exceso de presión del fenómeno físico. Para el caso de una pared con una inclinación los resultados predijeron comportamiento asimétrico, lo cual es consistente con previas visualizaciones experimentales o predicciones de previos modelos. En el caso de una pared inclinada en dos direcciones el perfil de exceso de presión y la deformación de la burbuja resultaron ser predichos asimétricos en las dos direcciones tangenciales. También se observó que a medida que la inclinación de la pared crece la asimetría también crece y la amplitud del rebote y la fuerza de la pared decrecen. Las simulaciones numéricas mostraron que el rebote de una burbuja deformable contra una pared es esencialmente gobernada por el balance entre la fuerza de la pared y la fuerza de masa agregada en la dirección normal a la pared y entre la fuerza de arrastre y la fuerza boyante en las direcciones tangenciales.

Estudios numéricos previamente reportados en tres dimensiones, no fueron capaces de predecir el rebote de la burbuja sobre la pared. Sin embargo, nuestro modelo fue capaz de calcular varios rebotes de la burbuja sobre una pared inclinada con dos ángulos. Además, para el caso de una pared horizontal los resultados numéricos concuerdan bien con datos experimentales.

Copyright © 2011

by

RONAL ABEL DE LA CRUZ ARAUJO

*To my family...*

## ACKNOWLEDGMENTS

This research was supported by the Puerto Rico Space Grant Consortium through a NASA-IDEAS ER grant and by the Nuclear Regularity Commission through the grant No. NRC-38-10-922.

I want to express my gratitude to the following people, without their help this work would have not been possible:

To my advisor, Professor *Silvina Cancelos*, for presenting me the problem of the bubble-wall interaction, for her patience and for guiding me in the elaboration of the solution of this problem. Thanks for her instruction and assistance in this work. .... you have helped me more than you think.

To my Graduate Committee members: Professors *J. Benitez* and *G. Gutierrez*.

To Professors of the Department of Mechanical Engineering for giving me the opportunity to pursue my graduate studies; Specially to Professors *N. Venkataraman*, *F. Just*, *O. Ruiz*, *S. Leonardi*, *V. Pandya* and *S. Coutin*.

To *A. Blagg*, for her invaluable help with my thesis corrections.

To my parents *A. De La Cruz* and *C. Araujo*, my brother and my sisters for their support and encouragement. Spetial thanks to my wife *Dioni* and my kids *Ronal Isaac* and *Ronal Junior* - the source of my inspiration.... I love you!

Also, I extend my gratitude to *F. Guzmán*, *G. Quevedo*, *J. Olivencia*, and *G. Zucchi* my professors in Perú. Thanks you so much!

# TABLE OF CONTENTS

ABSTRACT.....	ii
RESUMEN .....	iv
ACKNOWLEDGMENTS .....	viii
TABLE OF CONTENTS.....	ix
LIST OF TABLES .....	xi
LIST OF FIGURES .....	xii
LIST OF ABBREVIATIONS.....	xviii
1. INTRODUCTION.....	1
2. BACKGROUND.....	8
2.1 Overview .....	8
2.2 Jump condition at the interface: Laplace Formula.....	9
2.3 Single particle motion in a large fluid domain.....	13
2.3.1 Low Reynolds number flow .....	14
2.3.2 High Reynolds number flow .....	17
2.4 Drag and added mass correlations.....	18
2.5 Characteristics of bubbles .....	22
2.5.1 Shape of bubbles in motion: shape-maps .....	22
2.5.2 Terminal velocity.....	25
2.6 Hydrodynamic lubrication theory .....	30
3. BUBBLE-WALL INTERACTION MODEL .....	36
3.1 IMPLEMENTATION OF THE GENERAL MODEL .....	36
3.1.1 Excess pressure model in the liquid film drainage .....	43
3.1.2 System of equations.....	45
3.1.3 Initial and boundary conditions .....	49
3.1.4 Normal vector and matrix transformation .....	52
3.2 ONE-DIMENSIONAL BUBBLE-WALL INTERACTION MODEL.....	53
3.3 TWO-DIMENSIONAL BUBBLE-WALL INTERACTION MODEL.....	57
3.4 THREE-DIMENSIONAL BUBBLE-WALL INTERACTION MODEL.....	61
4. NUMERICAL SOLUTION OF THE BWI MODEL.....	65
4.1 OVERVIEW.....	65

4.2 INTERACTION OF A BUBBLE WITH A HORIZONTAL WALL.....	66
4.2.1 Problem statement .....	66
4.2.2 Discretization of the film drainage equation .....	67
4.2.3 Discretization of the bubble motion equation.....	76
4.2.4 Computational algorithms .....	79
4.3 INTERACTION OF A BUBBLE WITH AN INCLINED WALL.....	85
4.3.1 Problem statement .....	85
4.3.2 Discretization of the film drainage equation .....	88
4.3.3 Discretization of the bubble motion equation.....	94
4.3.4 Computational algorithm.....	98
5. BWI RESULTS AND ANALYSIS.....	102
5.1 INTERACTION WITH A HORIZONTAL WALL .....	104
5.1.1 Computer codes analysis .....	104
5.1.2 Bouncing Prediction of a bubble using the 1D-BWI model.....	110
5.1.3 Comparison with previous results .....	121
5.1.4 Critical radius for the rebound of an air bubble in water.....	127
5.2 INTERACTION WITH AN INCLINED WALL .....	131
5.2.1 Computer code analysis.....	131
5.2.2 Comparison with the 1D-Model .....	134
5.2.3 Prediction of bubble motion when interacting with a wall with one inclination.	139
5.2.4 Prediction of bubble motion when interacting with a wall with two inclinations.	143
.....	143
6. CONCLUSIONS AND FUTURE WORKS.....	154
6.1 Conclusions .....	154
6.2 Future works.....	157
REFERENCES .....	159
APPENDIX A.....	163
APPENDIX B .....	167
APPENDIX C .....	169
APPENDIX D.....	175

## LIST OF TABLES

Table 1: Drag and added mass correlations for spherical bubbles and spherical rigid particles. ....	20
Table 2: Drag and added mass correlation for deformable bubbles. ....	21
Table 3: Data used for runs .....	127
Table B.1: Forward difference representations of $O(\Delta x)$ .....	167
Table B.2: Backward difference representations of $O(\Delta x)$ .....	167
Table B.3: Central difference representations of $O(\Delta x)^2$ .....	167
Table B.4: Forward difference representations of $O(\Delta x)^2$ .....	168
Table B.5: Backward difference representations of $O(\Delta x)^2$ .....	168
Table B.6: Central-mixed derivatives of $O((\Delta x)^2, (\Delta z)^2)$ .....	168

## LIST OF FIGURES

Figure 2.1: Curved interface between two fluids .....	10
Figure 2.2: Geometrical parameters of a deformed bubble close to wall .....	22
Figure 2.3: Shape-map of bubbles rising in an unbounded liquid (Clift et al. 1978) .....	24
Figure 2.4: Terminal Velocities for a spherical bubble as function of its equivalent diameter: The several correlations specified in Table 1 are represented; Experimental data is obtained from Clift et.al. (1978).....	27
Figure 2.5: (a) Terminal velocities for air bubbles rising in water at 20°C (Clift et al. 1978); (b) Drag coefficient as function of Re for air bubbles rising in water.....	28
Figure 2.6: Schematic of fluid film between two solid surfaces .....	30
Figure 3.1: Bubble-wall interaction geometry: $X'Y'Z'$ is a fixed reference frame with $Y'$ vertical and horizontal plane $X'Z'$ , $XYZ$ is a reference frame fixed to the solid wall, and $xyz$ is a moving reference frame.....	39
Figure 3.2: Boundary and initial conditions of bubble-wall interaction.....	50
Figure 3.3: (a) Outward pointing normal vector to the bubble surface; (b) $X'Y'Z'$ and $XYZ$ rectangular Cartesian coordinate systems.....	52
Figure 3.4: 1D-BWI geometry: a) Nomenclature; b) Cartesian and cylindrical coordinates .....	54
Figure 3.5: 2D-BWI geometry: a) $XY$ plane and nomenclature; b) Perspective in 3D.....	58
Figure 4.1: Discretization of spatial domain .....	68
Figure 4.2: Numerical domain for 1D-BWI.....	69
Figure 4.3: Central and boundary nodes for 1D-BWI.....	70
Figure 4.4: Explicit scheme for 1D-BWI .....	70
Figure 4.5: (a) Five point stencil represented by the filled nodes; (b) Implicit scheme for 1D-BWI..	74
Figure 4.6: Structure of the main program <i>Exp_1D_BWI</i> .....	82
Figure 4.7: Structure of the main program <i>Impl_1D_BWI</i> .....	84

Figure 4.8: Numerical domain for BWI in Cartesian coordinates.....	90
Figure 4.9: Discrete spatial domain for BWI in Cartesian coordinates: Open symbols as the square, circle and triangle are called <i>boundary nodes</i> and the closed circles within the discontinuous closed line are called <i>central nodes</i> .....	91
Figure 4.10: Implicit scheme for film drainage equation in Cartesian coordinates.....	92
Figure 4.11: Structure of the main program <i>main3D_BWI</i> .....	101
Figure 5.1: Comparison results from implicit and explicit codes: (a) Non-dimensional normal velocity vs Non-dimensional time for a bubble of $R=1$ mm, $Re=407$ and $We=0.566$ ; (b) Amplified view, time range 1.3-1.8; (c) Amplified view, time range 0-0.5 .....	105
Figure 5.2: Comparison results from implicit and explicit codes: (a) Non-dimensional position vs Non-dimensional time for a bubble of $R=1$ mm , $Re=407$ and $We=0.566$ ; (b) Amplified view of the first rebound.....	106
Figure 5.3: Non-dimensional velocity vs non-dimensional time for a bubble for different values of spatial grid resolution: (a) Non- dimensional time range:0-8; (b) Amplified view about the second maximum value of velocity .....	108
Figure 5.4: Non-dimensional velocity vs non-dimensional time for a bubble for different values of spatial grid resolution: (a) Non- dimensional time range:0-8; (b) Amplified view non-dimensional time range:5.2-6.7 .....	109
Figure 5.5: Non-dimensional velocity (a) and position (b) vs non-dimensional time for a bubble of radius $R= 0.4$ mm, $Re= 92$ $We=0.143$ and $Eo= 0.08476$ immersed in purified water and interacting with a horizontal wall. ....	110
Figure 5.6: Evolution of the fluid film thickness profile during the first rebound for a bubble of radius $R= 0.4$ mm, $Re= 92$ , $We=0.143$ and $Eo= 0.08476$ immersed in purified water and interacting with a horizontal wall: (a) Before the first rebound; (a.1) amplified view of (a) around $r = 0$ ; (b) After the first rebound; (b.1) amplified view of (b) around $r = 0$ . The first rebound occur at 13.61ms.....	113
Figure 5.7: Evolution of the fluid film thickness profile during the second rebound for a bubble of radius $R= 0.4$ mm, $Re= 92$ , $We=0.143$ and $Eo= 0.08476$ immersed in purified water and interacting with a horizontal wall: (a) Before the second rebound; (a.1) amplified view of (a) around $r = 0$ ; (b) After the second rebound; (b.1) amplified view of (b) around $r = 0$ . The second rebound occur at 23.31ms .....	114

Figure 5.8: Evolution of the excess pressure profile during the first rebound for a bubble of radius  $R= 0.4$  mm,  $Re= 92$ ,  $We=0.143$  and  $Eo= 0.08476$  immersed in purified water and interacting with a horizontal wall: (a) Before the first rebound; (b) After the first rebound;. The first rebound occur at 13.61ms ..... 115

Figure 5.9: Evolution of the excess pressure profile during the second rebound for a bubble of radius  $R= 0.4$  mm,  $Re= 92$ ,  $We=0.143$  and  $Eo= 0.08476$  immersed in purified water and interacting with a horizontal wall: (a) Before the second rebound; (b) After the second rebound. The second rebound occur at 23.31ms ..... 116

Figure 5.10: Time evolution of the forces exerted on a bubble of radius  $R= 0.4$  mm,  $Re= 92$ ,  $We=0.143$  and  $Eo= 0.08476$  immersed in purified water and interacting with a horizontal wall. .... 118

Figure 5.11: Non-dimensional velocity and position vs non-dimensional time for a bubble of radius  $R= 0.4$  mm. (a) and (b) bubble immersed in contaminated water ; (c) and (d) velocity and position comparison for a bubble immersed in a contaminated and a purified system. .... 119

Figure 5.12: Time evolution of the forces exerted on a bubble of radius  $R=0.4$ mm immersed in purified and contaminated system and interacting with a horizontal wall..... 120

Figure 5.13: Centroid velocity (a) and centroid position (b) of a bubble of radius  $R=0.79$ mm,  $Re=410$ ,  $We=1.463$  and  $Eo=0.3283$ . Discontinuous line: Present 1D-BWI model with Moore’s Correlation. Continuous line: Present 1D-BWI model with Bozzano & Dente’s Correlation. Circles: Experimental data from Tsao & Koch (1997)..... 122

Figure 5.14: Difference between the present 1D model B (drag correlation from Bozzano & Dente, (2009)) specified in Fig. 5.13 and the experimental data from Tsao & Koch, (1997).. 122

Figure 5.15: Excess pressure and film thickness profiles of a bubble of radius  $R=0.79$ mm,  $Re=410$ ,  $We=1.463$ ,  $Eo=0.3283$  during the first rebound. (a) and (c) are the fluid film thickness and excess pressure profile before the 1<sup>st</sup> rebound at 12.4 ms (1), 13.12ms (2), 13.90ms (3), 14.58ms (4), 15.31ms (5), and 16.04ms (6). (b) and (d) are the fluid film thickness and excess pressure profile after 1<sup>st</sup> rebound at 16.35 ms (7), 17.08ms (8), 17.81ms (9), 18.53 ms (10), 19.26ms (11), and 20.00ms (12). (a.1) and (b.1) are amplified view of (a) and (b) respectively. The 1<sup>st</sup> rebound occur at  $t = 16.346$ ms. .... 124

Figure 5.16: Time evolution of the forces exerted on a bubble of radius  $R=0.79$  mm,  $Re=410$  and  $We=1.463$  immersed in purified system and interacting with a horizontal wall..... 125

Figure 5.17: Centroid position of a bubble of  $R=0.79\text{mm}$ ,  $Re=410$  and  $We=1.463$ . Continuous line: present 1Dmodel A with drag correlation from Moore (1965); Continuous bold line: present 1D model B with drag correlation from Bozzano & Dente, (2009); Discontinuous bold line: Previous model 1D from Moraga et al. (2005); Circles: experimental data from Tsao & Koch, (1997). ..... 126

Figure 5.18: Non-dimensional velocity, position and wall force vs non-dimensional time for bubble radius  $R=400\mu\text{m}$ ,  $R=350\mu\text{m}$  and  $R=300\mu\text{m}$ . ..... 128

Figure 5.19: Non-dimensional velocity, position and wall force vs non-dimensional time for bubble radius  $R=250\mu\text{m}$ ,  $R=240\mu\text{m}$  and  $R=230\mu\text{m}$ . ..... 129

Figure 5.20: Non-dimensional velocity, position and wall force vs non-dimensional time for bubble radius  $R=210\mu\text{m}$ ,  $R=200\mu\text{m}$  and  $R=150\mu\text{m}$ . ..... 130

Figure 5.21: Normal position of a Bubble respect to a horizontal wall for different values of spatial grid resolution using 3D-BWI and 1D-BWI codes. Bubble in clean system with characteristics given by  $R=0.79\text{mm}$ ,  $Re=410$ ,  $We=1.463$  and  $EO= 0.3283$ . In 3D-BWI code, the angles  $\theta = 0^\circ$  and  $\alpha = 0^\circ$  were used. .... 133

Figure 5.22: Position vs Grid Resolution at time  $t = 0.035\text{s}$  (35ms) from Fig. 5.21 ..... 133

Figure 5.23: Centroid position of a bubble of  $R=0.79\text{mm}$ ,  $Re=410$  and  $We=1.463$  immersed in a clean system and interacting with a horizontal wall; Continuous bold line: present Cartesian coordinates 3D-BWI model; Discontinuous bold line: Present cylindrical coordinates 1D-BWI model; Circles: experimental data from Tsao & Koch, (1997). ..... 134

Figure 5.24: Time evolution of the non-dimensional fluid film thickness during the first rebound of a bubble of  $R=0.79\text{mm}$ ,  $Re=410$  and  $We=1.463$  immersed in a clean system and interacting with a horizontal wall. The first rebound occur at  $t = 16.346 \text{ ms}$  ..... 136

Figure 5.25: Non-dimensional excess pressure profile of a bubble before the first rebound ( $t=12.15\text{ms}$ ) and after the first rebound ( $t=20.66\text{ms}$ ). Bubble immersed in clean system with characteristics given by  $R=0.79\text{mm}$ ,  $Re=410$  and  $We=1.463$ . The first rebound occur at  $t = 16.346 \text{ ms}$ . ..... 137

Figure 5.26: Non-dimensional excess pressure profile on a bubble during the first rebound. Bubble characteristics are given by  $R=0.79\text{mm}$ ,  $Re=410$  and  $We=1.463$ . The first rebound occur at  $t = 16.346 \text{ ms}$ . ..... 138

Figure 5.27: Normal Velocity (a), Tangential velocity (b), Normal position (c) and Tangential position (d) of a bubble immersed in a contaminated system and rising towards a wall inclined at $\theta = 20^\circ$ . The bubble characteristics are given by $R=0.51\text{mm}$ , $Re=103$ , $We=0.24$ and $Eo=0.1938$ .....	140
Figure 5.28: Excess pressure profile time $t=3.6$ (non-dimensional) of a bubble immersed in a contaminated system and rising towards a wall inclined at $\theta = 20^\circ$ . The bubble characteristics are given by $R=0.51\text{mm}$ , $Re=103$ , $We=0.24$ and $Eo=0.1938$ . The first rebound occur at non-dimensional time $t = 3.844$ . The non-dimensional excess pressure $p^*=0.625$ is zero in dimensional form. ....	141
Figure 5.29: Normal velocities (a) and normal positions (b) of a bubble immersed in a contaminated system and rising towards a wall with several inclinations. The bubble characteristics are given by $R=0.4\text{mm}$ , $V_T=0.086\text{m/s}$ , $Re=68.8$ , $We=0.08$ and $Eo=0.08476$	142
Figure 5.30: Normal wall forces on a bubble immersed in a contaminated system and rising towards a wall with several angles of inclination. The bubble characteristics are given by $R=0.4\text{mm}$ , $V_T=0.086\text{m/s}$ , $Re=68.8$ , $We=0.08$ and $Eo=0.08476$ .....	143
Figure 5.31: Velocities (a), (b) and (c) and positions (d), (e), and (f) of a bubble immersed in a clean system and rising towards a wall inclined at $\theta = 10^\circ$ and $\alpha = 10^\circ$ . The bubble characteristics are given by $R=0.79\text{mm}$ , $Re=410$ and $We=1.463$ . ....	145
Figure 5.32: Tangential forces in x-direction (a), Normal forces in y-direction (b) and tangential forces in z-direction(c) of a bubble immersed in a clean system and rising towards a wall inclined at $\theta = 10^\circ$ and $\alpha = 10^\circ$ . The bubble characteristics are given by $R=0.79\text{mm}$ , $Re=410$ and $We=1.463$ . One unit of non-dimensional force corresponds to about $264.6 \mu\text{N}$ . .	146
Figure 5.33: Fluid film thickness during the first rebound of a bubble immersed in a clean system and rising towards a wall inclined at $\theta = 10^\circ$ and $\alpha = 10^\circ$ . The bubble characteristics are given by $R=0.79\text{mm}$ , $Re=410$ and $We=1.463$ . The first rebound occur at $t=17.48\text{ms}$ .....	147
Figure 5.34: Non-dimensional film thickness during the first rebound of a bubble immersed in a clean system and rising towards a wall inclined at $\theta = 10^\circ$ and $\alpha = 10^\circ$ . (a) $h^*(x^*,0)$ before and after the first rebound; (a.1) Amplified view of (a) around $x^* = 0$ . The bubble characteristics are given by $R=0.79\text{mm}$ , $Re=410$ and $We=1.463$ . The first rebound occur at $17.48\text{ms}$ .....	148

Figure 5.35: Excess pressure profile (surface) during the first rebound of a bubble immersed in a clean system and rising towards a wall inclined at $\theta = 10^\circ$ and $\alpha = 10^\circ$ . The bubble characteristics are given by $R=0.79\text{mm}$ , $Re=410$ and $We=1.463$ . The first rebound occur at 17.48ms.....	149
Figure 5.36: Excess pressure profile (contour fill) during the first rebound of a bubble immersed in a clean system and rising towards a wall inclined at $\theta = 10^\circ$ and $\alpha = 10^\circ$ . The bubble characteristics are given by $R=0.79\text{mm}$ , $Re=410$ and $We=1.463$ . The first rebound occur at 17.48ms.....	150
Figure 5.37: Excess pressure profile (contour lines) during the first rebound of a bubble immersed in a clean system and rising towards a wall inclined at $\theta = 10^\circ$ and $\alpha = 10^\circ$ . The bubble characteristics are given by $R=0.79\text{mm}$ , $Re=410$ and $We=1.463$ . The first rebound occur at 17.48ms.....	151
Figure A 1: Coordinate system to describe the flow around a rigid sphere .....	164
Figure D1: Structure of the subroutine ODE (n) specified in main program Exp_1D_BWI .....	175
Figure D2: Structure of the subroutine PDE(n) specified in main program Exp_1D_BWI.....	176
Figure D3: Structure of the subroutine PDE(n) specified in main program Exp_1D_BWI (continuation).....	177
Figure D4: Structure of the subroutine pressure term specified in subroutine ODE (n) as shown in Fig. D1 .....	178
Figure D5: Structure of the subroutine ODE (n) specified in main program Impl_1D_BWI.....	188
Figure D6: Structure of the subroutine <i>PDE (n)</i> which is called by the main program <i>Impl_1D_BWI</i> .....	189
Figure D7: Structure of the subroutine ODEs_solver called by the program main3D_BWI.....	202
Figure D8: Structure of the subroutine ODEs_solver called by the program main3D_BWI (continuation).....	203
Figure D9: Structure of the subroutine PDE_solver called by the program main3D_BWI .....	204
Figure D10: Structure of the subroutine <i>PDE_solver</i> called by the program <i>main3D_BWI</i> (continuation).....	205

## LIST OF ABBREVIATIONS

1D	One-Dimensional
1D-BWI	One - Dimensional Bubble -Wall Interaction
2D	Two-Dimensional
2D-BWI	Two - Dimensional Bubble -Wall Interaction
3D	Three-Dimensional
3D-BWI	Three - Dimensional Bubble -Wall Interaction
BCs	Boundary Conditions
BWI	Bubble-Wall Interaction
BWIF	Bubble-Wall Interaction Force
CMFD	Computational Multiphase Fluid Dynamics
FDE	Finite Difference Equation
ICs	Initial Conditions
ODE	Ordinary Differential Equation
PDE	Partial Differential Equation

# 1. INTRODUCTION

Bubble-wall and bubble-bubble interaction play a major role in many industrial multiphase processes. Some applications of bubble-wall interaction are found in nuclear reactors cooling, pharmaceutical processes, medical applications (for example interaction bubble-bubble or bubble-wall in echography), drag reduction using injected microbubbles with which has been intensively studied for its application on sea transport (Kodama et al. 2004).

In order to obtain a complete description of bubbly flows, it is not only necessary to consider the equations governing the motion of the bulk fluid and the dispersed phase, but also the boundary conditions for these equations. Very often, it is difficult to choose the adequate boundary conditions for the bubbles interacting with solid wall boundaries since many behaviors have been observed, such as: bubbles sliding along the wall, bouncing or “sticking” on the wall, coalescence and disaggregation (Tsao & Koch, 1997).

Clift et al. (1978) and Michaelides (2006) have reported studies of the motion of drops, bubbles and particles far from a wall considering spherical or spheroid form. They provided motion equations for bubbles, drops or solid particles immersed in an unbounded fluid domain based on the force balance at the bubble centroid. They considered the buoyancy, added mass, drag and history forces, caused by the action of the gravity and the interaction of the bubble (or a particle, or a drop) with the surrounding fluid. The drag and added mass forces depend on the instantaneous Reynolds number. In order to represent this

dependence, empirical correlations for the drag and added mass coefficients were used. They provided useful drag and added mass correlations for drops and particles for a wide range of Reynolds numbers. They described the bubble motion in an unbounded fluid domain as well as the mass transfer between bubbles and the fluid. However, they offered limited information on the behavior of bubbles when they are close to a rigid wall that could lead to bubble bouncing.

Despite the progressive increase in computational power, numerical studies of bubbly flows predict the behavior of a bubble away from the wall, or use the concept of restitution coefficient to model the force due to bubble-wall interaction when the bubble is near the wall, or simply do not consider the effect of the walls. But as mentioned before, the bubble-wall interaction is very important in practical applications and the motion of a deformable bubble in the vicinity of a rigid wall is an essential prerequisite for the development of many Eulerian / Lagrangian numerical codes devoted to the simulation of bubbly flows (Canot et al. 2003), therefore, we need a rigorous model for the bubble-wall interaction so that we can obtain results suitable for use in Computational Multiphase Fluid Dynamics (CMFD).

Restitution coefficients have been used in two-phase flows numerical codes in order to consider the impact between a solid particle/bubble or between a solid particle/bubble and solid wall. This restitution coefficient has been defined as the ratio of the particle/bubble velocity after the rebound to the solid particle/bubble velocity before the impact. This coefficient has been experimentally determined and most of the publications in this field have been devoted to solid particle-wall interactions (Sondergaard et al. 1990; Gondret et al. 2002).

One of the first attempts to determine the bouncing of a bubble on a wall, was done by Shopov et al. (1990). They used a finite element method to solve the Navier-Stokes equations to study the unsteady viscous flow induced by a deformable gas bubble in the wall proximity for Reynolds numbers smaller than 60. Their results showed the bubble deformation in the wall proximity. However, the bubble bouncing process was not fully obtained. The failure to describe the bouncing effect relies on the difficulty to simultaneously solve the thin liquid film entrapped between the bubble and the wall and the larger scale of the outer flow.

An experimental analysis of a bubble bouncing on a wall has been conducted by Tsao & Koch (1997). They performed experimental observations on the motion of a bubble near a horizontal and an inclined wall immersed in purified water (water free of contaminants at the surface) for high Reynolds number and bubbles with radius between 0.5mm and 0.8mm. They observed that the bubble bounced several times from the wall and obtained a series of experimental data that served as a validation tool for analytical or numerical results of future investigations (Moraga et al. 2005; Podvin et al. 2008).

Klaseboer et al. (2001) implemented a one dimensional model to determine the trajectory of a drop impinging on a rigid horizontal wall considering the drag, added mass and history forces as well as the buoyancy force, and finally, in order to account for the bouncing effect, instead of using the restitution coefficient, they studied the film drainage between the drop and the wall. The force due to this effect, hereafter called wall force, was computed by integrating the excess pressure produced in the fluid film. They proposed the following algorithm: (i) calculate the force on the thin layer using the lubrication equation, (ii) with the BWIF and the other forces mentioned above, they solved the motion equation

that provides the drop velocity as a function of time. Their model was successfully tested with various experimental data. Also, their model was applied to a particular case of bubble-wall interaction (bubble radius of 0.79mm and surface tension of 73mN/m). Moraga et al. (2005) implemented the model proposed by Klaseboer et al. (2001) to study the motion of a bubble interacting with a horizontal wall. Their results were validated using the experimental data measured by Tsao & Koch, (1997). Moraga et al. (2005) found a correlation for the wall force that depends on the Weber ( $We$ ), Reynolds ( $Re$ ) and Eotvos ( $EO$ ) numbers calculated using the bubble terminal velocity, which is a steady velocity that the bubble reaches away from the wall when the buoyancy force is balanced by the drag force. The proposed function enables the computation of the bubble position in time without the need of solving the lubrication equation.

A two dimensional numerical study for a bubble bouncing on a horizontal wall was conducted by Canot et al. (2003) in which they coupled an analytical model based on lubrication theory with a boundary element method to simulate the bubble bouncing. Their results have been compared satisfactorily with experimental data from Tsao & Koch (1997). An extension of this model to three-dimensions has been developed by the same authors but in this case their simulation results did not predict the bouncing process of the bubble despite it impacted with a horizontal wall.

Most recently, Podvin et al. (2008) extended the model derived by Klaseboer et al. (2001) and Moraga et al. (2005) to two-dimensions. In a similar manner to that used by Moraga et al. (2005), an expression for the wall force was determined. The bubble diameters studied were from 1mm to 2mm for Reynolds numbers in the order of 100, moderate deformation effects (i.e. Weber numbers on the order of 1) and several angles of inclination.

Their model did not predict satisfactorily the bouncing process when the bubble impacted on a wall with inclinations greater than  $60^\circ$ .

Tsao & Koch, (1997) provided reliable experimental data of the interaction of a bubble with a wall, which was used to validate the innovative concept of the film drainage between the bubble and the wall modeled by the lubrication theory, derived by Klaseboer et al. (2001), continued by Moraga et al. (2005) for one- dimension and Podvin et al. (2008) for two dimensions. However, in order to consider more complex surfaces (e.g. ship hulls) it is still necessary to extend this model to three-dimensions and so it can be suitable for use in CMFD. Also, due to the fact that in the last years a vast number of new correlations for drag and added mass coefficients have been obtained (Michaelides, 2003; Bozzano & Dente, 2009), it is necessary to implement this correlations into previous models with the aim of improving the bubble motion prediction.

The purpose of this research is to extend the model derived by Klaseboer et al. (2001) to three-dimensions in order to study the motion of a bubble with constant volume rising in an unbounded isothermal quiescent liquid and impinging on an immersed rigid wall. The immersed wall can be horizontal, or with one or two inclinations. We solved two equations in three-dimension: the film drainage equation, that describes the bubble-wall interaction based on the lubrication theory, and the motion equation that fully describes the transient motion of the bubble centroid near the wall. The motion equation includes the wall force, the drag force, the added mass force, and the buoyancy force. A particular objective is to evaluate other correlations for drag and added mass coefficients for a clean bubble (free of contaminants on the bubble surface) and for a contaminated bubble (with the presence of contaminants on the bubble surface) in order to improve the accuracy of the model when

compared to the available experimental data. Another particular aim is obtain an expression for the film force as a function of dimensionless numbers, such as the Reynolds ( $Re$ ), the Weber ( $We$ ), and the Eotvos ( $EO$ ), similarly to what was previously developed by Moraga et al. (2005) and Podvin et al. (2008); so that it is suitable for use in numerical simulations on multiphase flow.

In order to model the bouncing process of a bubble impinging with a horizontal, one inclination or two inclinations wall; a three-dimensional model was derived in Cartesian coordinates without considering any symmetry conditions. We assumed that the fluid (water in this case) is at rest with respect to an inertial reference system and that the liquid is isothermal and unbounded (i.e. the side walls of its container do not affect the upward motion of the bubble). Therefore, thermal effects, the effect of the side walls, and the effect of fluid velocity are not considered. We investigated correlations to determine the most appropriate forms of the drag and added mass coefficients such that they take into consideration the deformation of the bubble. By doing this, we can control the drag force and the added mass force. Simulations for Reynolds numbers on the order of 100, Weber numbers on the order of 1, and bubble size ranging from 0.3-2mm were used. We also assumed that the bubble near the wall does not break up into smaller bubbles, but it only undergoes small deformations (due to moderate Weber numbers). Moraga et al. (2005) and Podvin et al. (2008) showed that in the region where the bouncing of the bubble is calculated (several bubble diameter away from the wall), variations of hydrostatic pressure cause negligible changes in bubble volume and consequently, the buoyancy force remains constant throughout the rebound phenomenon.

For the wall force, the film drainage equation was solved to determine the excess pressure. Once this pressure was determined the total force was obtained by integrating the excess pressure over the surface area of the bubble facing the wall.

In order to determine the bubble trajectory in 3D, the following algorithm was used: (i) appropriate boundary conditions and initial conditions for the bubble motion and the film drainage equations were established. (ii) Non-dimensional equations and boundary conditions were obtained using the Reynolds, Weber and Eotvos numbers. (iii) Since the film drainage equation is a non-linear equation, it cannot be solved analytically; in addition, the motion equation depends on the excess pressure obtained from the film drainage equation, consequently, the coupled system of equations was solved numerically with an iterative procedure. (iv) The finite difference method was used to solve the problem, by discretizing the domain and using second order accuracy for the derivatives and the implicit/explicit method to iterate over time.

In Chapter 2, the necessary theoretical background is presented. In Chapter 3 the equations of the proposed bubble-wall interaction model are presented. Chapter 4 presents the numerical techniques used to solve the model proposed in Chapter 3. In Chapter 5 simulation results of the bubble-wall interaction model are presented and discussed. Conclusions and future work on this area are provided in Chapter 6.

## 2. BACKGROUND

### 2.1 Overview

The background necessary to understand the model used to study the interaction of a bubble with an inclined wall is studied in the present chapter. The dynamic behavior, mass transfer and heat transfer on bubbles, drops and solid particles immersed in a fluid may be treated similarly (Clift et al. 1978; Michaelides, 2006). For instance, in order to model the dynamic behavior and make experimental measurements for its validation; the bubbles, drops and solid particles are studied as bodies immersed in a fluid (Michaelides, 2006). Hence, fluid mechanics theory is applied to obtain the velocity, shear stress, and pressure fields of the fluid around the immersed body; then the body velocity and its trajectory are determined by applying Newton's second law to the forces exerted on the body. Significant experimental, analytical and numerical publications are devoted to study the dynamic behavior of bubbles, drops and solid particles with regular and complex shapes (such as spheres, prolate ellipsoids, oblate ellipsoids, cylinders, spherical caps, wobbling and others) when immersed in a fluid (Brennen, 2005; Happel & Brenner, 1991; Clift et al. 1978; Michaelides, 2003). The fluid motion inside of a bubble or a drop is also a matter of continuous research interest. This fluid motion is decisive when the values of fluid viscosity inside and outside of the bubble or drop are of the same order of magnitude (Michaelides, 2003). The fluid motion inside of the bubble is also crucial when heat and mass transfer are present (Ruiz, 2002). In the present thesis we study air bubbles in water with constant

temperature. Since the air viscosity is very small compared with water viscosity and the temperature is constant, the internal motion does not need to be considered.

The fluid inside and outside of a bubble or a drop are separated by a surface called *interface*. From a molecular approach, an interface is interpreted as a film with a certain thickness and from a mechanical approach the interface is considered without thickness, i.e. non-material surface (Michaelides, 2006). The interface presents a tension resistance called the *surface* or *interfacial tension* which produces a pressure difference between two immiscible fluids in contact when the interface is curved (Adamson et al. 1997). The pressure difference at the interface, bubble motion and the shape of the bubble when in motion are presented in this chapter.

Another subject detailed here is a study of the lubrication theory, which must be coupled to the bubble motion equation to model the bubble-wall interaction when the bubble approaches the wall. This model is derived in Chapter 3 and solved in Chapter 4.

## **2.2 Jump condition at the interface: Laplace Formula**

When two immiscible liquids or a liquid and a gas or a solid phase are in contact, *surface or interface phenomenon* occurs. This phenomenon is characteristic of the liquids. An interesting example is the aquatic insect which can walk on the free surface of water without sinking since its weight is compensated by the resistance to deformation offered by the water surface. This ability of the liquids to support tension is quantified by the *surface tension coefficient* ( $\sigma$ ) (Adamson et al. 1997). The surface tension coefficient is defined as the force per unit length exerted perpendicularly to any line on the surface, and is expressed in N/m. The value of the surface tension coefficient of a liquid depends on the nature of the

substances in contact at the interface. It also depends on the degree of contamination at the interface with impurities. It has been showned that the surface tension coefficient of liquids decreases as temperature increases; this is named the *Marangoni effect* (Brennen, 2005).

If we consider a steady interface between two fluids at rest (Fig. 2.1), the curvature of the interface causes the pressure on the concave side (below surface  $m$  in Fig. 2.1(a)) to be greater than on the convex side (above surface  $m$  in Fig. 2.1(a)). The difference of these two pressures is called *capillary pressure*, and it is often referred to as *jump condition*. It is calculated by the *Laplace formula* (Adamson et al. 1997) which is derived below.

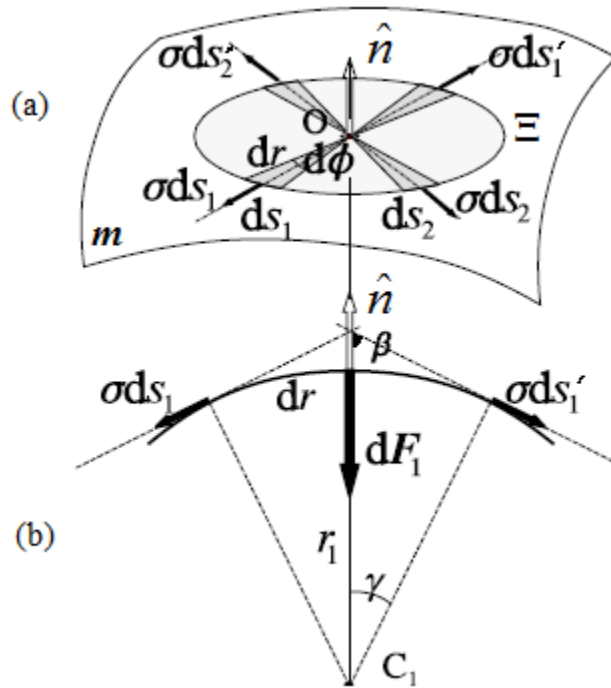


**Figure 2.1:** Curved interface between two fluids

In order to derive Laplace formula we consider the curved interface as shown in Fig. 2.1. The surface limited by the line  $\Xi$  over the curved surface  $m$ , can be approximated as a circle with center  $O$  and area  $dS = \pi(dr)^2$ . Two neighboring diameters determine two arcs  $ds_1$  and  $ds_1'$  with  $ds_1 = ds_1' = d\phi dr$ ; the surface tension causes a force on these two arcs of

magnitudes  $\sigma ds_1$  and  $\sigma ds'_1$  of equal magnitude and with the direction shown Fig. 2.1(b). The resultant of these two forces is  $d\vec{F}_1$  in the direction normal to the surface  $m$  pointing towards the center of curvature  $C_1$  and with magnitude  $dF_1$ ,

$$dF_1 = 2\sigma ds_1 \cos \beta = 2\sigma ds_1 \sin \gamma = 2\sigma d\phi dr \frac{dr}{r_1} = 2\sigma d\phi dr^2 \frac{1}{r_1}$$

A pair of neighboring diameters perpendicular to the previous one, determine another pair of arcs  $ds_2 = ds'_2$  on  $\Xi$ . Once again the surface tension over these arcs creates the forces  $\sigma ds_2$  and  $\sigma ds'_2$  with a resultant  $d\vec{F}_2$  directed toward a center of curvature  $C_2$ , which differs from  $C_1$  (Fig. 2.1(b)). The magnitude of this force is  $dF_2 = 2\sigma d\phi dr^2 \frac{1}{r_2}$ .

Consequently the total force acting on the curve  $\Xi$  in the direction normal to the surface  $m$  is:

$$dF = dF_1 + dF_2 = 2\sigma d\phi dr^2 \left( \frac{1}{r_1} + \frac{1}{r_2} \right).$$

The Gauss theorem (Adamson et al. 1997) shows that for any pair of mutually perpendicular sections normal to the surface  $m$ , with center at the point  $O$ , we can write,

$$\frac{1}{r_1} + \frac{1}{r_2} = \frac{1}{R_1} + \frac{1}{R_2} = \text{mean curvature of } m \text{ in } O$$

where  $R_1$  and  $R_2$  are the principal radii of curvature of surface  $m$  in  $O$ . Therefore we can write

$$dF = 2\sigma d\phi dr^2 \left( \frac{1}{R_1} + \frac{1}{R_2} \right)$$

Integrating the previous equation from 0 to  $\frac{\pi}{2}$  with respect to  $d\phi$  we have,

$$dF = 2\sigma \frac{\pi}{2} dr^2 \left( \frac{1}{R_1} + \frac{1}{R_2} \right) = \sigma dS \left( \frac{1}{R_1} + \frac{1}{R_2} \right),$$

Given that  $\frac{dF}{dS} = \Delta p$ , where  $\Delta p$  is the capillarity pressure, the expression finally yields

$$\Delta p = \sigma \left( \frac{1}{R_1} + \frac{1}{R_2} \right) \quad (2.1)$$

Eq. (2.1) is denominated the *Laplace formula*, which relates the pressure difference between both sides of a generic interface with the surface tension of the liquid and the mean curvature of the mentioned interface. Eq. (2.1) is derived for a generic interface. Therefore, it can be applied for liquid-gas (bubbles) and liquid-liquid (drops) interfaces.

A significant result that can be obtained from Eq. (2.1) is that if the interface is flat (i.e.  $R_1, R_2 \rightarrow \infty$ ), the pressure is equal on both sides of the surface. Also, if a spherical interface is considered, like in the case of a bubble (i.e.  $R_1 = R_2 = R$ ),  $\Delta p = \sigma \frac{2}{R} = p_b - p$ , where  $p_b$  and  $p$  are the pressure inside and outside of the bubble respectively.

If the surface  $m$  (Fig. 2.1(a)) is given as a differentiable function,  $z = m(x, y)$ , then the mean curvature can be computed as the divergence of the normal vector,  $\hat{n}$  directed as shown in Fig. 2.1 (Do Carmo, 1976).

The normal vector is defined as;

$$\hat{n} = \frac{\vec{\nabla} m}{|\vec{\nabla} m|} = \frac{\left( \frac{\partial m}{\partial x}, \frac{\partial m}{\partial y}, -1 \right)}{\sqrt{1 + \left( \frac{\partial m}{\partial x} \right)^2 + \left( \frac{\partial m}{\partial y} \right)^2}} \quad (2.2)$$

Hence, the mean curvature is expressed as,

$$\frac{1}{R_1} + \frac{1}{R_2} = \vec{\nabla} \cdot \hat{n} = \frac{\left(1 + \left(\frac{\partial m}{\partial y}\right)^2\right) \frac{\partial^2 m}{\partial x^2} - 2 \frac{\partial m}{\partial x} \frac{\partial m}{\partial y} \frac{\partial^2 m}{\partial x \partial y} + \left(1 + \left(\frac{\partial m}{\partial x}\right)^2\right) \frac{\partial^2 m}{\partial y^2}}{\left(1 + \left(\frac{\partial m}{\partial x}\right)^2 + \left(\frac{\partial m}{\partial y}\right)^2\right)^{\frac{3}{2}}} \quad (2.3)$$

Equation (2.3) constitutes a useful expression to relate the jump pressure with an arbitrary surface that describes the interface.

### 2.3 Single particle motion in a large fluid domain.

In this section we consider an isothermal Newtonian fluid and an immersed particle without considering mass transfer to or from the fluid. Therefore, the fundamental physical laws governing the motion of immersed particles in fluids are the mass and linear momentum conservation equations traditionally known as the *continuity* and *Navier-Stokes* equations. For incompressible fluids with constant viscosity and neglecting body forces, these equations become:

*Continuity equation:*

$$\vec{\nabla} \cdot \vec{u} = \text{div}(\vec{u}) = 0 \quad (2.4)$$

*Navier-Stokes equation:*

$$\rho_f \frac{D\vec{u}}{Dt} = -\nabla P + \mu_f \nabla^2 \vec{u} \quad (2.5)$$

where  $P$  and  $\vec{u}$  are the pressure and velocity fields of the fluid around the particle,  $\rho_f$  and  $\mu_f$  are the density and viscosity of the fluid respectively, and  $t$  is the time. If we have the solution for Eqs. (2.4) and (2.5) for a fluid around an immersed particle we can determine the pressure (normal stress) and shear stress at the surface of the particle. Hence, the total force

applied by the fluid on a particle is determined by integrating the normal and tangential forces which are produced by the normal and shear stress at the surface respectively (Bird et al. 2006). This total force is commonly named the *hydrodynamic force*.

The solution of Eqs. (2.4) and (2.5) for bubbles and drops is different from that of solid particles, since no slip and no normal flow is applied at the particle boundary, but there is no reason to attribute no slip to the surface of a drop or bubble. A degree of tangential slip at the surface of a drop or bubble immersed in liquid with certain degree of purity has been reported (Michaelides, 2006; Klaseboer et al. 2001; Clift et al. 1978; Michaelides, 2003; Moore, 1965). Hence, for bubbles and drops in a pure system, the continuity of tangential stress at the bubble interface can be applied. The effects of the degree of slip at the surface on the bubble motion are presented in section 2.4 and 2.5.2.

We studied first the hydrodynamic force on solid particles because these results can be easily extended for drops and bubbles using correction factors that are described in sections 2.3.2 and 2.4.

### **2.3.1 Low Reynolds number flow**

Due to the non-linearity of the Navier-Stokes equation it has not been easy to determine an analytical expression for the hydrodynamic force from Eqs. (2.4) and (2.5). In most cases, these equations have to be solved numerically. In the present section, we present the historic perspective on the progress made by scientists in determining the hydrodynamic force for specific restricted conditions.

In 1831 Poisson studied the hydrodynamic force on a rigid sphere within an inviscid fluid by solving the potential flow equations (i.e. no viscous terms) (Michaelides 2003). He

determined that the force exerted by a non-viscous fluid on the sphere was  $\frac{1}{2}m_f \frac{d(\vec{V} - \vec{U}_\infty)}{dt}$  when the sphere was accelerated in the fluid (Brennen 1982), where  $m_f$  is the mass of a fluid occupying the same volume as the sphere,  $\vec{V} = \vec{V}(t)$  is the sphere velocity,  $\vec{U}_\infty = \vec{U}_\infty(t)$  is the uniform velocity of fluid and  $t$  is time. What Poisson obtained was the expression for what is now called, the added mass force, in which the added mass coefficient has a value of  $\frac{1}{2}$  (a derivation of the added mass force is presented in appendix A). When the sphere has a constant relative velocity with respect to the fluid, the potential inviscid flow predicts that the hydrodynamic force is zero (D'Alembert paradox) due to the symmetry of the pressure field around the particle, however, experimental data shows that in a finite time the solid would stop. A detailed solution of the D' Alembert paradox can be found in Bird et al. (2006) and Clift et al. (1978).

George G. Stokes was the first to analyze the motion of a sphere inside a viscous fluid (Michaelides 2003). Considering a flow with low velocities (creeping flow), he neglected the convective terms from Eq. (2.5) and obtained the following equation:

$$\rho_f \frac{\partial \vec{u}}{\partial t} = -\nabla P + \mu_f \nabla^2 \vec{u} \quad (2.6)$$

Eq. (2.6) is called the *Stokes equation*. Solving it for steady state conditions when the fluid moves around a sphere or vice versa, Stokes determined that the force felt by the sphere due to the presence of the fluid was  $6\pi R\mu_f \vec{V}$  (Bird et al. 2006), where  $\mu_f$  is the fluid viscosity,  $R$  and  $\vec{V}$  are the radius and velocity of the sphere respectively. This force is now called *Stokes's law* or *Stokes drag force* (Michaelides 2003). A derivation of this drag force is presented in appendix A. A full unsteady solution of Stokes equation was developed independently in

1885 by Boussinesq and in 1888 by Basset to determine the hydrodynamic force on a rigid sphere exerted by the motion of an unsteady viscous fluid around it (Michaelides, 1997; Clift et al. 1978; Basset, 1888). A derivation of this subject is beyond the scope of this thesis; the reader can find this derivation in Clift et al. (1978) pages 285 to 287. For a sphere moving in a fluid of uniform velocity  $\vec{U} = \vec{U}_\infty(t)$  far from the sphere, the results of both Boussinesq and Basset for the transient hydrodynamic force may be written as (Michaelides 2003),

$$\vec{F}_{hydrod} = -6\pi R\mu_f (\vec{V} - \vec{U}_\infty) - \frac{1}{2}m_f \frac{d(\vec{V} - \vec{U}_\infty)}{dt} - 6R^2 \sqrt{\pi\mu_f \rho_f} \int_0^t \frac{1}{\sqrt{t-\tau}} \frac{d(\vec{V} - \vec{U}_\infty)}{d\tau} d\tau \quad (2.7)$$

The first term in the right hand of Eq. (2.7) is the steady term exerted by the viscous fluid and is identical to the Stokes's law, the second term considers part of the transient motion of the surrounding fluid and is the same as that derived by Poisson (1831). This term is often called the *added mass* or the *virtual mass force* and it arises because the acceleration of the particle requires acceleration of the surrounding fluid. The last term called the *Basset force* is due to the diffusion of the vorticity around the sphere, and is often called the *history force*. Past accelerations are included in this term;  $t - \tau$  represents the time elapsed since the past acceleration, and  $(t - \tau)^{-1/2}$  is called the *kernel*  $K(t - \tau)$ . Eq. (2.7) is strictly valid for unsteady creeping flow which is satisfied only when the Reynolds number of the sphere,

$$Re_s = \frac{2R\rho_f |\vec{V} - \vec{U}_\infty|}{\mu_f} \text{ approaches zero (Michaelides, 2006).}$$

After Basset, several scientists worked to extend the results of creeping flow to other shapes of solid particles, bubbles or drops. These subjects are thoroughly explained by Clift et al. (1978). Relevant results are, for example, that the added mass force depends on the shape of the particle, that the drag force depends on the shape and degree of slip at surface,

and that the history force is affected by the vorticity of the surrounding fluid and it is different depending upon the type of particle (solid particles, drops or bubbles). Including the body force (in this case the gravity force) the unsteady creeping flow motion equation for particles without volume change moving in a large stagnant fluid domain ( $\vec{U}_\infty = 0$ ) can be written as follows,

$$\rho_p Vol \frac{d\vec{V}(t)}{dt} = (\rho_f - \rho_p) Vol \vec{g} - C_d \frac{\pi}{4} Re_V R \mu_f \vec{V} - C_{am} \rho_f Vol \frac{d\vec{V}(t)}{dt} - C_h 6R^2 \sqrt{\pi \mu_f \rho_f} \int_0^t \frac{1}{\sqrt{t-\tau}} \frac{d\vec{V}(\tau)}{d\tau} d\tau \quad (2.8)$$

where the subscript  $p$  refers to the particle properties, the gravity acceleration is denoted by  $\vec{g}$ ,  $Vol$  represents the particle volume,  $Re_V$  is the instantaneous Reynolds number defined as  $Re_V = 2\rho_f RV / \mu_f$ ,  $C_d$  and  $C_{am}$  are the drag and added mass coefficients which have distinct values for different particles (bubbles, drops or solid particles) and shapes (for a spherical rigid particle,  $C_d = 24 / Re_V$  and  $C_{am} = 1/2$ ), and  $C_h$  is the history force coefficient that takes into account the particle shape (Clift et al. 1978). In section 2.4 we have organized a table with relevant correlations for the drag and added mass coefficients.

### 2.3.2 High Reynolds number flow

Since Basset, many attempts have been made to solve the full Navier-Stokes equation for a particle immersed in a stagnant fluid and to derive an expression for the transient hydrodynamic force. For large Reynolds numbers, the inertia terms neglected in creeping flow ( $Re_V \ll 1$ ), have to be considered (Clift et al. 1978). The most classic study on this subject was published by Ossen in 1910 (Michaelides, 2003) who considered the inertia terms on the Navier-Stokes equation and using an asymptotic method he obtained an expression for the hydrodynamic force valid for finite Reynolds numbers ( $Re_V < 1$ ). The drag

coefficient obtained is often called the “*Ossen’s drag coefficient*”,  $C_d = 24/Re_v(1 + 3/8Re_v)$ .

Michaelides, (2006) and Clift et al. (1978) have detailed the contributions made by several scientists to determine the velocity and pressure fields around solid particles, bubbles and drops for high Reynolds number flow.

In 1964 Odar and Hamilton treated the three terms in the hydrodynamic force, Eq. (2.7), separately and multiplied each one of them with a correction function to account for the higher Reynolds numbers (Michaelides, 2003). Hence the equation of motion, Eq. (2.8), remains essentially the same for higher  $Re_v$ ; however, the correlation for drag and added mass coefficients are changed and the history term has been expressed using the kernel  $K(t - \tau)$  (Klaseboer et al. 2001). Finally the equation of motion becomes,

$$\rho_p Vol \frac{d\vec{V}(t)}{dt} = (\rho_f - \rho_p) Vol \vec{g} - C_d \frac{\pi}{4} Re_v R \mu_f \vec{V} - C_{am} \rho_f Vol \frac{d\vec{V}(t)}{dt} - C_h 6R^2 \sqrt{\pi \mu_f \rho_f} \int_0^t K(t - \tau) \frac{d\vec{V}(t)}{d\tau} d\tau \quad (2.9)$$

In the last 30 years the technique of separating the transient hydrodynamic force in three independent components and using empirical correlations for the drag and added mass coefficients has become popular since the results of Eq. (2.9) obtained numerically agree with experimental data (Michaelides, 2003).

## 2.4 Drag and added mass correlations.

The viscosity ratio,  $k = \mu_p / \mu_f$  (the particle viscosity is replaced by its respective viscosities in the case of a bubble or a drop), the contamination at the surface, and the boundary layer around the surface are three characteristics that determine the difference of drag and added mass coefficients between a bubble, a drop and a rigid particle. A finite value of  $k$  produces an internal circulation in the bubble, and hence a vorticity lower than for a rigid

sphere. When  $k \rightarrow \infty$  or  $k \rightarrow 0$ , the internal circulation is negligible, therefore in most cases, the internal circulation of bubbles is neglected. A system free of contaminants permits a full slip at the bubble surface so that it behaves like an inviscid sphere for creeping flow. However, a small concentration of contaminants produces a shear stress at the surface that affects the bubble shape, and therefore the drag and added mass forces. The separation phenomenon of fluid from the surface is different for bubbles than for rigid particles, since for bubbles the boundary layer is much thinner and remains attached to the surface longer than for a comparable rigid particle (Clift et al. 1978). Few efforts have been made to solve the hydrodynamic force using the internal circulation in bubbles and including the concept of an inner and outer boundary layer on the bubble surface; the most recent study was reported by Feng & Michaelides (2001).

Table 1 shows some correlations for the drag and added mass coefficients for a spherical rigid particle and a spherical bubble for a wide range of  $Re_V$  and for slip and no slip condition at the surface. Note that the added mass does not depend on surface contamination or the degree of slip at the surface of the particle, but only on the shape.

**Table 1:** Drag and added mass correlations for spherical bubbles and spherical rigid particles.

CORRELATION	REFERENCES	RANGE	PARTICLE TYPE
$C_d = \frac{24}{Re_v}$ Stokes' law	Clift et al. (1978)	$Re_v < 0.5$	- Rigid particle $k \rightarrow \infty$
$C_d = \frac{24}{Re_v} (1 + 0.15 Re_v^{0.4})$ Schiller and Nauman's law	Clift et al. (1978)	$Re_v < 800$	- No slip condition on the surface. - Rigid particle, also applies for quasi-rigid bubble.
$C_d = \frac{16}{Re_v}$	Michaelides, (2006)	$Re_v < 0.5$	- Slip at surface of a rigid particle - Inviscid bubble $k \rightarrow 0$
$C_d = \frac{48}{Re_v}$	Levich, (1962) Michaelides, (2006) Clift et al. (1978)	$5 < Re_v < 1000$	- Inviscid bubble $k \rightarrow 0$ - Calculated using irrotational flow theory - Clean system
$C_d = \frac{48}{Re_v} \left( 1 - \frac{2.21}{Re_v^{1/2}} + O(Re_v^{-5/8}) \right)$	Moore, (1963)	$40 < Re_v < 1000$	- Bubble in clean system - Calculate the thin boundary layer dissipation see (Moore, 1963)
$C_d = \frac{48}{Re_v} \left( 1 + \frac{3}{2} k \right)$	Harper & Moore, (1968)	$5 < Re_v < 1000$	- Slip at surface of a rigid particle - For a finite value of $k$ in bubbles - Bubbles in clean system
$C_d(Re_v, k) = \left\{ \begin{array}{l} \frac{2-k}{2} C_d(Re_v, 0) + \\ \frac{4k}{6+k} C_d(Re_v, 2) \end{array} \right\}$ where $C_d(Re_v, 0) = \frac{48}{Re_v} \left( 1 + \frac{2.21}{Re_v^{1/2}} - \frac{2.14}{Re_v} \right)$ , $C_d(Re_v, 2) = 17.0 Re_v^{-2/3}$	Feng & Michaelides, (2001)	$5 < Re_v < 1000$ $0 \leq k \leq 2$	- For viscous particles (bubbles and drops). - Solve the boundary layer on the viscous particle. - Clean system
$C_{AM} = 0.5$ Poisson's result	Michaelides, (2003)	any range	Bubbles and rigid particles. Only for spherical shaped bodies

Deformable bubbles and drops can be approximated as spheres when the difference in length of their two principal axes is less than or equal to 5% (Michaelides, 2006). When the bubble shape cannot be approximated as a sphere the drag and added mass coefficient are changed to account for the deformation. The bubble deformation can be caused by two different conditions: the first is due to fact that the buoyancy force is greater than the surface force due to the surface tension, this condition generally occurs at large Reynolds numbers,

$Re_V$ ; the second condition of deformation is produced when the bubble impacts on a wall in which the kinetic energy of the bubble motion is converted to deformation energy and viscous dissipation energy (Tsao & Koch, 1997), and if the deformation energy is sufficiently large it is converted again to kinetic energy and the bubble rebounds several times on the wall until the deformation energy is balanced with the other energies involved in the phenomenon of bubble-wall interaction. Table 2 shows typical correlations for the drag and added mass coefficients for a deformable bubble when it moves in an unbounded fluid and when it moves in a fluid and impacts with an immersed wall.

**Table 2:** Drag and added mass correlation for deformable bubbles.

CORRELATION	REFERENCES	RANGE	PARTICLE TYPE
$C_d = \frac{48}{Re_V} C(y)$	Van der Geld, (2002)	$Re_V > 100$	-Small spherical deformable bubbles -Clean system. -Considers the effect of the wall proximity.
$C_d = \frac{24}{Re_V} C(y) (1 + 0.15 Re_V^{0.4})$	Moraga et al. (2005) Podvin et al. (2008)	$Re_V < 100$ $R < 500 \mu m$	- Small deformable bubbles -Contaminated system. -Considers the effect of the wall proximity.
$C_d = \frac{48}{Re_V} G(\chi) \left( 1 + \frac{H(\chi)}{Re_V^{1/2}} \right)$	Moore, (1965) Moraga et al. (2005) Podvin et al. (2008)	$10^2 < Re_V < 10^3$ $\chi < 4$	-Deformable bubble in unbounded fluid - Clean system - Solves the boundary layer at surface
$C_{am} = \frac{3}{2} (C(y))^{1/2} - 1$	Moraga et al. (2005) Van der Geld, (2002)	Depends from wall proximity	-Small deformable bubbles -Takes account the effect of the wall proximity -Used for clean or no clean system.
$C_{am} = \frac{\alpha}{2 - \alpha}$	Klaseboer et al. (2001) Tsao & Koch, (1997)	Depends of bubble deformation	- Small deformable bubbles -Takes account the effect of the wall proximity -Used for clean or no clean system.
$C_{am} = 0.62 \chi - 0.12$ Approximation result of Lamb correlation for $C_{am}$	Klaseboer et al. (2001) Moraga et al. (2005)	Depends of bubble deformation	- Clean or no clean surface of the bubble. $0 < \chi < 2.5$

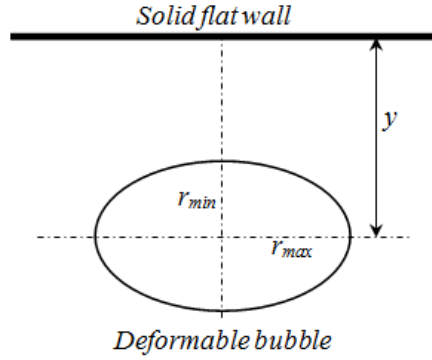


**Figure 2.2:** Geometrical parameters of a deformed bubble close to wall

In Table 2,  $\chi$  refers to the bubble aspect ratio,  $y$  is the distance of the bubble centroid from a wall (Fig. 2.2) and  $R$  is the *equivalent radius* defined as the radius of a spherical bubble with the same volume as the deformed bubble (Clift et al. 1978). The functions  $G(\chi)$ ,  $H(\chi)$ ,  $\alpha(\chi)$  and  $C(y)$  are defined as follows:

$$G(\chi) = \frac{1}{3} \chi^{4/3} (\chi^2 - 1)^{3/2} \frac{\left( \sqrt{\chi^2 - 1} - (2 - \chi^2) \cos^{-1}\left(\frac{1}{\chi}\right) \right)}{\left( \chi^2 \cos^{-1}\left(\frac{1}{\chi}\right) - \sqrt{\chi^2 - 1} \right)^2}, \quad \alpha = \frac{2\chi^2}{\chi^2 - 1} \left( 1 - \frac{1}{\sqrt{\chi^2 - 1}} \cos^{-1}\left(\frac{1}{\chi}\right) \right)$$

$$H(\chi) = 0.0195\chi^4 - 0.2134\chi^3 + 1.7026\chi^2 - 2.1461\chi - 1.5732, \quad C(y) = \left( 1 - \left( \frac{R}{2y} \right)^3 \right)^{-2}, \quad \chi = \frac{r_{\max}}{r_{\min}}$$

## 2.5 Characteristics of bubbles

### 2.5.1 Shape of bubbles in motion: shape-maps

Bubbles and drops are characterized by the properties of the fluid inside and outside, their size, and the local gravity acceleration when they are in motion in an unbounded continuous fluid. The shape of bubbles and drops is determined by the interaction of the surface tension and the shear stress exerted by the surrounding fluid. A dimensional analysis was developed by Haberman & Morton, (1953) to determine the dimensionless groups

necessary to describe the shape of deformed bubbles when freely rising in a column of water under the action of gravity.

The main variables that influence the shape of bubbles are:

- The bubble terminal velocity,  $V_T$ , which is the steady velocity the bubble reaches when the drag and buoyancy force are balanced.
- The characteristic length, which is often taken as the diameter of the volume-equivalent sphere,  $d_e$
- The density of the surrounding fluid,  $\rho_f$
- The density of fluid inside the bubble,  $\rho_b$  (bubble density)
- The viscosity of fluid inside the bubble,  $\mu_b$  (bubble viscosity)
- The viscosity of the surrounding fluid,  $\mu_f$
- The surface tension coefficient of the interface,  $\sigma$
- The gravitational acceleration,  $g$

Having into account the above mentioned variables and using the Buckingham theorem (Shames, 2003) it can be proven that we need five independent dimensionless groups to describe the bubble shape (Haberman & Morton, 1953; Michaelides, 2006). These numbers are listed below:

- Reynolds Number,  $Re = \frac{\rho_f V_T 2R}{\mu_f}$ , calculated with the bubble terminal velocity.
- Eotvos Number,  $Eo = \frac{g(\rho_f - \rho_b)d_e^2}{\sigma}$
- Morton Number,  $Mo = \frac{g\mu_f^4}{\rho_f \sigma^3}$

- Density ratio,  $\lambda = \frac{\rho_b}{\rho_f}$
- Viscosity ratio,  $k = \frac{\mu_b}{\mu_f}$

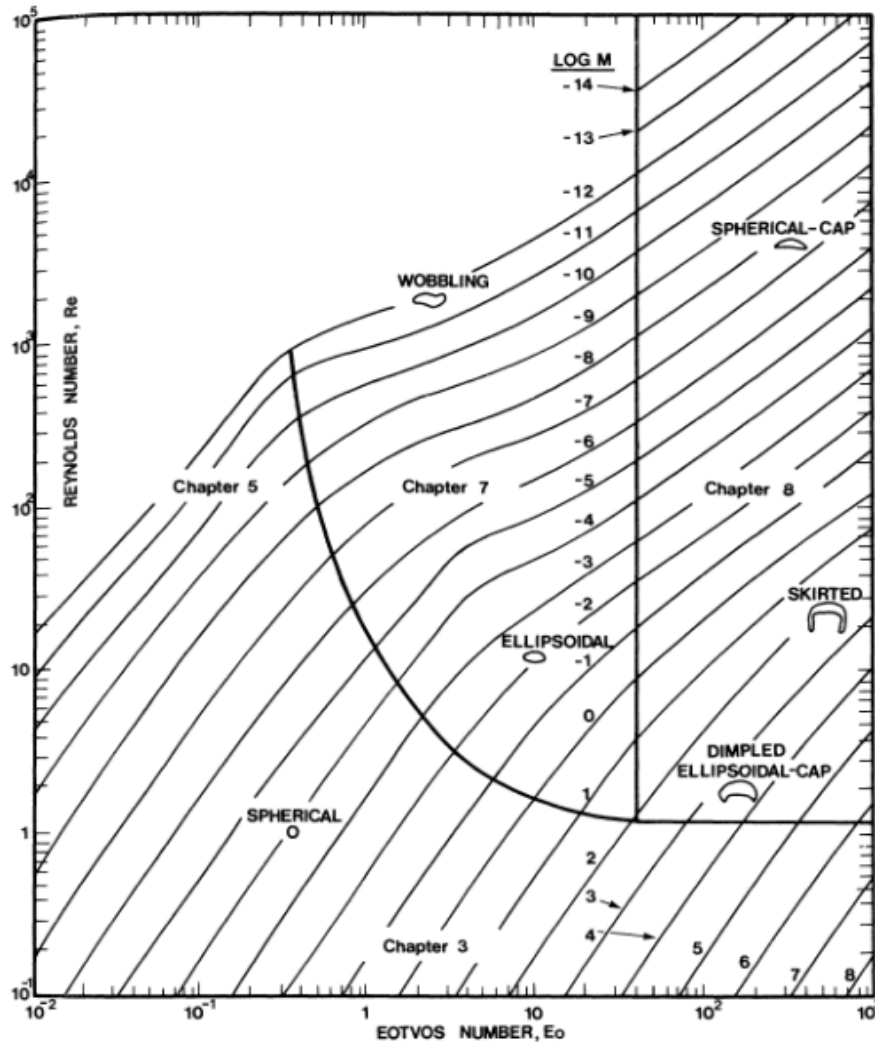


**Figure 2.3:** Shape-map of bubbles rising in an unbounded liquid (Clift et al. 1978)

The density and viscosity of bubbles is very small (1/1000) compared with the density and viscosity of the surrounding fluid (Michaelides, 2006), consequently, they can be neglected. Also, the gravitational acceleration at the earth's surface is almost constant, therefore, the list

of important physical variables is reduced to five ( $V_T, d_e, \rho_f, \mu_f, \sigma$ ) and the independent dimensionless groups are reduced to two, for example  $(Re, Eo)$ ,  $(Re, Mo)$  or  $(Re, We)$ . The  $We$  is another dimensionless number which is sometimes used and it is defined as  $We = \rho_f V_T^2 d_e / \sigma$ . By choosing one of these pairs, we may construct two-dimensional diagrams that help determine the bubble shape. These diagrams are called “shape-maps”. In Fig. 2.3 a shape-map for a bubble rising freely in a fluid is shown, in which  $Re$  vs  $Eo$  are plotted for several Morton numbers,  $Mo$  (denoted by  $M$  in the figure). In this figure, we can see that for  $10^{-2} < Eo < 10^3$  and  $Re < 2$  the bubble is spherical; for  $2 < Re < 10^3$  and  $Eo < 1$ , the bubble still retains its spherical shape; for  $2 < Re < 10^3$  and  $1 < Eo < 12$  the bubble results in an ellipsoidal shape; and for  $Re > 2$  and  $Eo$  of order  $10^2$  the bubble assumes large deformations ranging from ellipsoidal-cap to spherical-cap. The spherical-cap, dimpled ellipsoidal-cap skirted and Wobbling bubble shapes (see Fig. 2.3) are not of interest in the present thesis.

## 2.5.2 Terminal velocity

As it was mentioned above, the velocity that a bubble reaches rising in an unbounded fluid is called the *terminal velocity* ( $V_T$ ). The terminal velocity is obtained by balancing the drag and buoyancy forces on the bubble. An expression for the terminal velocity can be derived from Eq. (2.9). When the bubble moves at the terminal velocity, the acceleration is

zero and Eq. (2.9) is reduced to  $\frac{4}{3}\pi R^3(\rho_f - \rho_b)g = C_d Re \frac{\pi}{4} R \mu_f V_T$ , from which an expression

for  $V_T$  can be obtained:

$$V_T = \sqrt{\frac{8}{3} R \left( 1 - \frac{\rho_b}{\rho_f} \right) g \frac{1}{C_d}} \quad (2.10)$$

Since the drag coefficient is a function of  $Re$  and it varies with  $V_T$ , in most cases Eq. (2.10) is solved numerically. The terminal velocity ( $V_T$ ) of an air bubble as a function of its equivalent diameter ( $d_e$ ) for several of the drag correlations listed in Table 1 is shown in Fig. 2.4 along with experimental data. In this figure the contamination at the surface of the bubble plays a determinant role. For small bubbles ( $d_e < 0.6$  mm) the experimental terminal velocities for contaminated and uncontaminated water are the same; in this case a small concentration of contaminants at the surface are sufficient to prevent the slip at the surface, then the bubble behaves as a rigid particle and the Schiller & Nauman's correlation (see Table 1) is in good agreement with experimental data. For moderate bubble sizes ( $0.6 \text{ mm} < d_e < 1.2$  mm) the terminal velocity depends on water purity; the results obtained using several of the correlations listed in Table 1 for a clean system, present the same behavior as the experimental data for a bubble in pure water. However, the values of terminal velocities calculated using the correlations are higher than the experimental data because these correlations were obtained with the assumption of a clean system, which in practice is not straightforward to carry out.

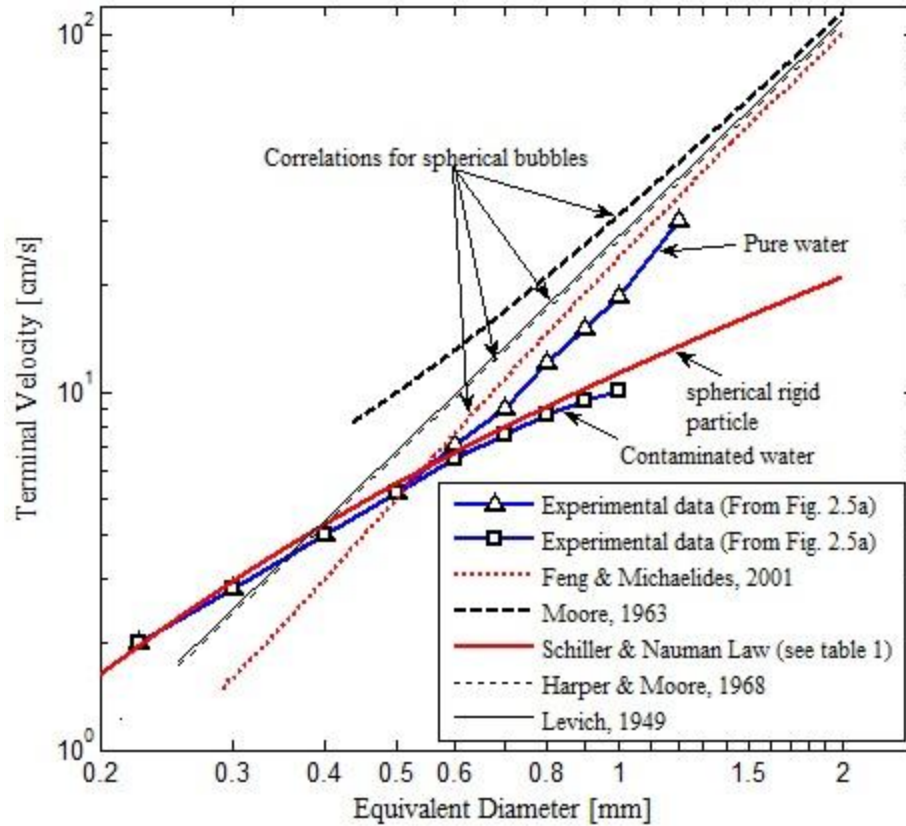
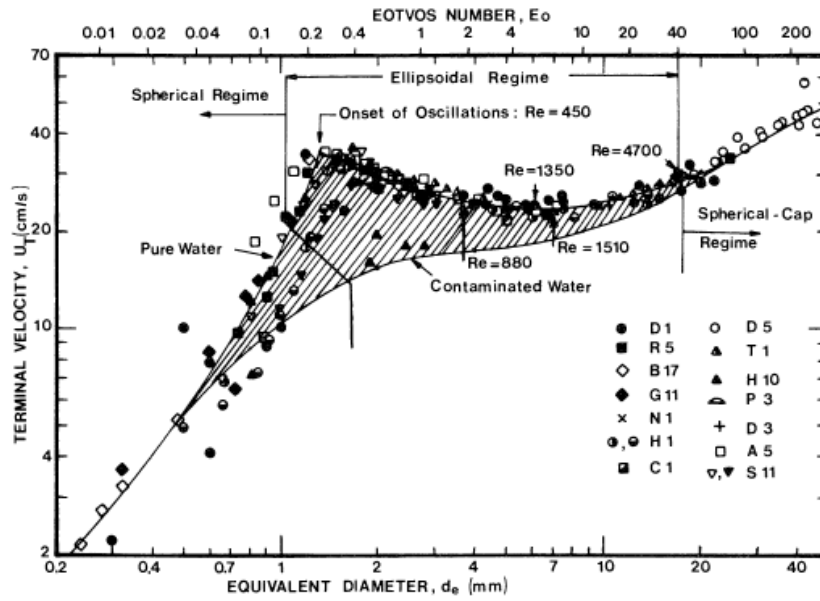


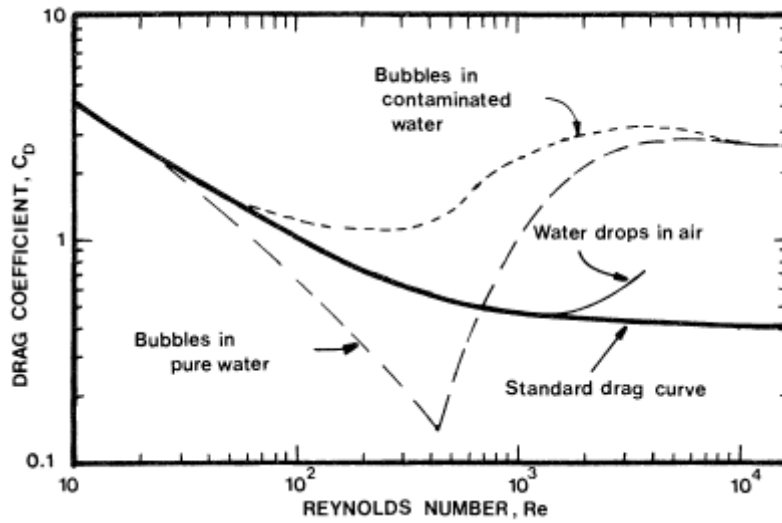
**Figure 2.4:** Terminal Velocities for a spherical bubble as function of its equivalent diameter: The several correlations specified in Table 1 are represented; Experimental data is obtained from Clift et.al. (1978).

A larger number of experimental data for deformable air bubbles rising freely in pure and contaminated water for a wide range of equivalent diameters has been reported in the literature (Clift et al. 1978). The experimental data are shown in Fig. 2.5 in which the uppermost curve in Fig. 2.5(a) indicates the terminal velocities for a bubble of equivalent diameter  $d_e$  rising in distilled water (Clift et al. 1978). On the other hand, the lowermost curve in Fig. 2.5(a) represents the terminal velocity of bubbles rising in contaminated water (Clift et al. 1978). The symbols Fig. 2.5(a) represent experiments with different degrees of contamination. The corresponding drag coefficients of the two curves shown in Fig. 2.5(a)

are shown in Fig. 2.5(b) in comparison with the standard drag curve for a solid spherical particle.



(a)



(b)

**Figure 2.5:** (a) Terminal velocities for air bubbles rising in water at 20°C (Clift et al. 1978); (b) Drag coefficient as function of  $Re$  for air bubbles rising in water

Recently, Bozzano & Dente, (2009) have proposed two correlations for the drag coefficient for a deformable bubble, which have good agreement with the uppermost and lowermost continuous lines in Fig. 2.5(a). These correlations are:

$$C_d = Def \cdot f \quad (2.11)$$

where,  $Def = \left(\frac{2r_{max}}{2R}\right)^2 = \frac{10(1+1.3Mo^{1/6})+3.1Eo}{10(1+1.3Mo^{1/6})+Eo}$ , and the value of the function  $f$  depends on

the impurities present in the liquid. For bubbles in clean system  $f$  is given by,

$$f = \frac{48}{Re} \left( \frac{\sqrt{1+0.25Re}}{\sqrt{1+0.25Re}+1} \right) \left( \frac{3/2 + \mu_f / \mu_b}{1 + \mu_f / \mu_b} \right) \left( \frac{1+12Mo^{1/3}}{1+36Mo^{1/3}} \right) + f_\infty \quad (2.12)$$

with  $f_\infty = 0.9 \frac{Eo^{3/2}}{1.4(1+30Eo^{3/2})+Eo^{3/2}}$

For bubbles in contaminated system,  $f$  is given by,

$$f = \begin{cases} \frac{48}{Re} \left( \frac{\sqrt{1+0.25Re}}{\sqrt{1+0.25Re}+1} \right) \left( \frac{3/2 + \mu_f / \mu_b}{1 + \mu_f / \mu_b} \right) \left( \frac{1+12Mo^{1/3}}{1+36Mo^{1/3}} \right) + 0.45 & \text{if } f_\infty < 0.45 \\ \frac{48}{Re} \left( \frac{\sqrt{1+0.25Re}}{\sqrt{1+0.25Re}+1} \right) \left( \frac{3/2 + \mu_f / \mu_b}{1 + \mu_f / \mu_b} \right) \left( \frac{1+12Mo^{1/3}}{1+36Mo^{1/3}} \right) + f_\infty & \text{if } f_\infty \geq 0.45 \end{cases} \quad (2.13)$$

In Eq. (2.11), the deformation is considered by the term called  $Def$  (this value is 1 for spherical bubbles) in which  $r_{max}$  represent the maximum radius as shown in Fig. 2.2 and  $R$  is the equivalent bubble radius. The term  $f$  in Eq. (2.11) is called the friction factor.

In summary, the terminal velocity of a bubble is very sensitive to the impurities present in the fluid around it. A bubble retains its spherical shape only when its equivalent diameter is less than 1mm (see Fig. 2.5(a)). For  $d_e > 1$ mm (see Fig. 2.5(a)) large deformations such as ellipsoids and spherical caps are observed.

## 2.6 Hydrodynamic lubrication theory

The excess pressure generated in a thin film of fluid between two surfaces that undergo relative motion is recognized as *hydrodynamic lubrication*. This excess pressure enables a load to be transmitted between the surfaces with very low friction since the surfaces are completely separated by the fluid film. The hydrodynamic lubrication theory was first formulated in 1886 by Osborne Reynolds and validated using the experimental observations made in 1883 by B. Tower (Reynolds 1886). The current theories of elastohydrodynamic lubrication, thermo-hydrodynamic lubrication, and turbulent hydrodynamic lubrication were developed as an extension of Reynolds' lubrication theory (Hori, 2006). In this section, Reynolds lubrication theory is derived .

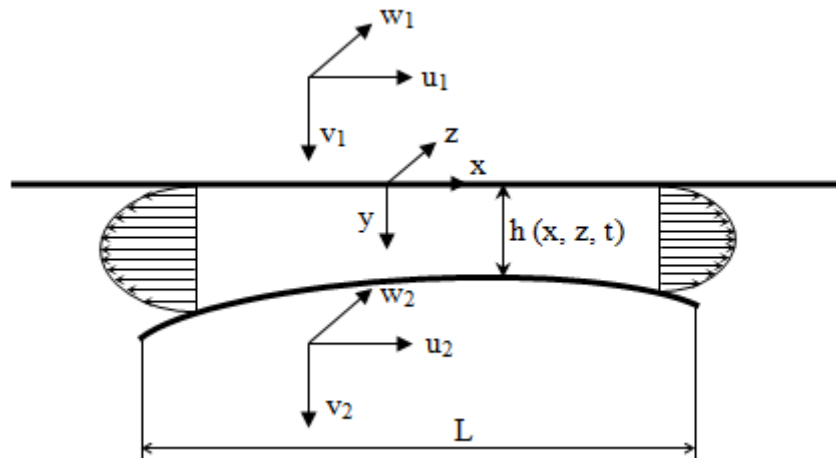


**Figure 2.6:** Schematic of fluid film between two solid surfaces

Osborne Reynolds, in his paper on hydrodynamic lubrication (Reynolds 1886), wrote as an introduction:

*LUBRICATION, or the action of oils and others viscous fluids to diminish friction and wear between solid surfaces, does not appear to have hitherto formed a subject for theoretical treatment. Such treatment may have been prevented by the obscurity*

*of the physical actions involved, which belong to a class as yet but little known, namely, the boundary or surface actions of fluids; but the absence of such treatment has also been owing to the want of any general laws discovered by experiment.*

.....

*On reading Mr. Tower's report it occurred to the author as possible that, in the case of the oil bath, the film of oil might be sufficiently thick for the unknown boundary actions to disappear, in which case the results would be deductible from the equations of hydrodynamics.*

Reynolds' lubrication equation is a second-order differential equation describing the pressure in the fluid film between two solid surfaces that undergo relative motion. This equation is derived from the Navier-stokes equation and the continuity equation using the Reynolds assumptions which are described here. The fluid film between two solid surfaces shown in Fig. 2.6 is considered. In order to obtain an equation of hydrodynamic lubrication for our case, the upper surface is assumed to be a plane. The axes of a rectangular coordinate system,  $x$ ,  $y$ , and  $z$  are taken as shown in the figure. The  $x$  and  $z$  axes are on the upper surface and  $y$  axis is perpendicular to it. The fluid velocities in the directions  $x$ ,  $y$ , and  $z$  are denoted by  $u$ ,  $v$ , and  $w$  respectively and the velocity of the upper and lower surface are  $u_1, v_1, w_1$  and  $u_2, v_2, w_2$  respectively. The gap between the two surfaces, or the film thickness of fluid, is denoted by  $h(x, z, t)$  with  $t$  being time. The essence of lubrication theory is that a film thickness of fluid  $h$  is very small compared with the dimension of the surfaces and that the radii curvature of the surfaces is very large compared with  $h$  such that the surfaces are nearly parallel. Assumptions based on this are as follows (Hori, 2006):

1. The flow is laminar.
2. The gravity and inertia forces acting on the fluid can be ignored compared with the viscous forces.
3. Compressibility of the fluid is negligible.
4. The fluid is Newtonian and the coefficient of viscosity is constant.
5. Fluid pressure does not change across the film thickness.
6. The rate of change of the velocity  $u$  and  $w$  in the  $x$  and  $z$  directions is negligible compared with the rate of change in the  $y$  direction. Hence,  $\frac{\partial u}{\partial x}, \frac{\partial u}{\partial z} \ll \frac{\partial u}{\partial y}$  and

$$\frac{\partial w}{\partial x}, \frac{\partial w}{\partial z} \ll \frac{\partial w}{\partial y}.$$

7. There is no slip between the fluid and the solid surface.

From assumptions 1 to 4, the continuity and Navier-Stokes equations are written as follows:

$$\vec{\nabla} \cdot \vec{u} = 0 \tag{2.14}$$

$$\nabla P = \mu_f \nabla^2 \vec{u} \tag{2.15}$$

Using assumptions 5 and 6 Eqs. (2.14) and (2.15) can be expressed in Cartesian coordinates as:

$$\frac{\partial P}{\partial x} = \mu_f \frac{\partial^2 u}{\partial y^2} \tag{2.16}$$

$$\frac{\partial P}{\partial y} = 0 \tag{2.17}$$

$$\frac{\partial P}{\partial z} = \mu_f \frac{\partial^2 w}{\partial y^2} \tag{2.18}$$

$$\frac{\partial u}{\partial x} + \frac{\partial v}{\partial y} + \frac{\partial w}{\partial z} = 0 \tag{2.19}$$

Equations (2.16) and (2.18) can be obtained from the Navier-Stokes Equation for incompressible fluids with constant viscosity and neglecting the convective term and body forces (Eq. (2.5)). The unsteady and convective terms in Eq. (2.5) for the  $x$  and  $z$  directions have typical magnitudes of  $\rho_f U_0^2 / R \sim \rho_f W_0^2 / R$ , while the viscous term scales as  $\mu_f U_0 / h^2 \sim \mu_f W_0 / h^2$ . Since assumption 2 assumes inertia terms are negligible compare with the viscous term, then  $\rho_f U_0^2 / R \ll \mu_f U_0 / h^2$  and consequently  $Re(h/R)^2 \ll 1$  with  $Re = \rho_f U_0 L / \mu_f$ . Here  $L$  is the characteristic length (see Fig. 2.6) and  $U_0, W_0$ , and  $V_0$  are the characteristic velocities associated with the motion, which in this case is the terminal velocity of the bubble.

The flow velocities  $u$  and  $w$  can be obtained by integrating Eqs. (2.16) and (2.18) twice. From the assumption 7 the boundary conditions for the velocities are:

$$\left. \begin{array}{l} \text{at } y=0 \quad u = u_1, \quad w = w_1 \\ \text{at } y=h \quad u = u_2, \quad w = w_2 \end{array} \right\} \quad (2.20)$$

Hence, the fluid velocities can be written as:

$$u(y) = \frac{1}{2\mu_f} \frac{\partial P}{\partial x} (y^2 - yh) + \left(1 - \frac{y}{h}\right) u_1 + \frac{y}{h} u_2 \quad (2.21)$$

$$w(y) = \frac{1}{2\mu_f} \frac{\partial P}{\partial z} (y^2 - yh) + \left(1 - \frac{y}{h}\right) w_1 + \frac{y}{h} w_2 \quad (2.22)$$

Integrating the continuity equation Eq. (2.19) in the film thickness direction from  $y=0$  to  $y=h$  gives:

$$v \Big|_0^h = - \int_0^h \frac{\partial u}{\partial x} dy - \int_0^h \frac{\partial w}{\partial z} dy \quad (2.23)$$

Here  $v(h) = v_2$  and  $v(0) = v_1$ . Integrating the two terms on the right hand side of Eq. (2.23) we obtain:

$$\frac{\partial}{\partial x} \left( \frac{h^3}{12\mu_f} \frac{\partial p}{\partial x} \right) + \frac{\partial}{\partial z} \left( \frac{h^3}{12\mu_f} \frac{\partial p}{\partial z} \right) = \left\{ \begin{array}{l} (v_2 - v_1) + \left( \frac{u_1 - u_2}{2} \right) \frac{\partial h}{\partial x} + \frac{h}{2} \frac{\partial}{\partial x} (u_1 + u_2) + \\ \left( \frac{w_1 - w_2}{2} \right) \frac{\partial h}{\partial z} + \frac{h}{2} \frac{\partial}{\partial z} (w_1 + w_2) \end{array} \right\} \quad (2.24)$$

Eq. (2.24) is named the *generalized Reynolds' lubrication equation* because it is derived without the rigid body assumption (Hori, 2006). If both surfaces are rigid, the third and fifth term on the right hand side of Eq. (2.24) are zero, and  $v_1$  and  $v_2$  are only functions of time.

Velocities  $v_1$  and  $v_2$  can be related to film height as follow (Hamrock et al. 2004).

Observing that  $h$  is a function of  $x$ ,  $z$ , and  $t$ , the total derivative of  $h$  can be written as:

$$\frac{Dh}{Dt} = \frac{\partial h}{\partial t} + \frac{\partial h}{\partial x} \frac{dx}{dt} + \frac{\partial h}{\partial z} \frac{dz}{dt} \quad (2.25)$$

Since  $y=h(x,z,t)$  and  $\frac{dy}{dt} = v$ ,  $\frac{dx}{dt} = u$ , and  $\frac{dz}{dt} = w$ , then  $\frac{Dh}{Dt} = v = \frac{\partial h}{\partial t} + \frac{\partial h}{\partial x} u + \frac{\partial h}{\partial z} w$ . Using

the boundary conditions at the lower interface in Fig. 2.6 and assuming the upper interface is fixed ( $u_1 = v_1 = w_1 = 0$ ) we obtain:

$$v_2 = \frac{\partial h}{\partial t} + \frac{\partial h}{\partial x} u_2 + \frac{\partial h}{\partial z} w_2 \quad (2.26)$$

with  $u_1 = v_1 = w_1 = 0$  and replacing Eq. (2.26) in Eq. (2.24) we obtain:

$$\frac{\partial}{\partial x} \left( \frac{h^3}{12\mu_f} \frac{\partial p}{\partial x} \right) + \frac{\partial}{\partial z} \left( \frac{h^3}{12\mu_f} \frac{\partial p}{\partial z} \right) = \frac{\partial h}{\partial t} + \frac{\partial}{\partial x} \left( \frac{hu_2}{2} \right) + \frac{\partial}{\partial z} \left( \frac{hw_2}{2} \right) \quad (2.27)$$

Leal, (2007) provided an alternative derivation of the lubrication equation Eq. (2.24) using an asymptotic approximation in which the variable under analysis is defined as  $\varepsilon = h/L$

where  $L$  represents a characteristic length of the surfaces. Indeed, the lubrication approximation makes sense when  $\varepsilon \ll 1$ .

### 3. BUBBLE-WALL INTERACTION MODEL

#### 3.1 IMPLEMENTATION OF THE GENERAL MODEL

In this chapter, a mathematical model to describe the dynamic behavior of a bubble rising vertically in a large quiescent fluid domain and bouncing against an immersed flat solid wall is developed. The body force, hydrodynamic force and the wall force applied on the center of gravity of the bubble need to be considered in order to derive the bubble motion equation. Using the gravity force as a unique body force, the hydrodynamic force as described in Chapter 2 and the wall force (denoted by  $\vec{F}_w$ ), the bubble equation of motion in an inertial reference frame can be written as follows:

$$m_b \frac{d\vec{V}}{dt} = \vec{F}_b + \vec{F}_d + \vec{F}_{am} + \vec{F}_w \quad (3.1)$$

Equation (3.1) applies Newton's second law to the bubble's center of gravity. In this equation  $m_b$  and  $\vec{V}$  represent the mass and centroid velocity of the bubble, and the forces acting on the bubble are denoted by  $\vec{F}$  in which the subscripts  $b$ ,  $d$ ,  $am$ , and  $w$  indicate the buoyancy, drag, added mass, and the bubble-wall interaction forces. It has been reported that the kernel of the history force for bubbles decays faster than for solid particles (Lovalenti & Brady, 1993), which causes the history force to be rapidly negligible (Klaseboer et al. 2001). Domgin et al. (1998) have also conducted an experimental and numerical study on the influence of the history term, and concluded that the history term may be neglected for bubbly flows. Therefore, we have chosen not to consider the history force in Eq. (3.1). Expressing the velocity and the forces in Eq. (3.1) in a Cartesian coordinate system we have,

$$\vec{F}_b = F_{bx}\hat{i} + F_{by}\hat{j} + F_{bz}\hat{k} \quad (3.2)$$

$$\vec{F}_d = F_{dx}\hat{i} + F_{dy}\hat{j} + F_{dz}\hat{k} \quad (3.3)$$

$$\vec{F}_{am} = F_{amx}\hat{i} + F_{amy}\hat{j} + F_{amz}\hat{k} \quad (3.4)$$

$$\vec{F}_w = F_{wx}\hat{i} + F_{wy}\hat{j} + F_{wz}\hat{k} \quad (3.5)$$

$$\vec{V} = U\hat{i} + V\hat{j} + W\hat{k} \quad (3.6)$$

where  $U$ ,  $V$ , and  $W$  represent the components of bubble centroid velocity in X, Y, and Z directions respectively, the unit vectors in the X, Y and Z directions are denoted by  $\hat{i}$ ,  $\hat{j}$ , and  $\hat{k}$ .

In this research, we considered a deformable gas bubble rising vertically in a fluid by the action of gravity and impinging against a rigid wall. The fluid outside the bubble was assumed *isotropic* and *isothermal* at rest. It was also considered that the liquid was *saturated* with air at ambient conditions. The fluid inside the bubble was assumed to be a gas with uniform and constant properties. The assumption of saturated air in the liquid implies that there is no mass transfer between the inside and outside of the bubble because the surrounding fluid does not permit a highest air concentration (Bird et al. 2006) and therefore the bubble mass remains constant throughout the bouncing process. Moreover if mass diffusion occurs the characteristic time of mass diffusion without thermal effects is  $\tau_{massdiff} = 4R^2 / D_{AB}$  (Michaelides, 2003) where  $D_{AB}$  is the diffusivity of air in water. This time is greater than or comparable with the total time of the bouncing process observed by Tsao & Koch, (1997). For a bubble of radius  $R=0.79\text{mm}$  and using  $D_{AB}=0.26\text{cm}^2/\text{s}$  at  $25^\circ\text{C}$  (Benitez, 2002), we obtain  $\tau_{massdiff} = 96\text{ms}$  which is comparable with the rebound time of this

bubble which occurs in about 100ms. Therefore, the assumption of constant mass is justified. The BWIF acts only on the region of the bubble that impacts the wall, and in the remaining region acts only the hydrostatic pressure of the surrounding fluid. Hence, we can assume that the gas bubble has a constant density during the bouncing process. This assumption is not applied in cases where thermal effects and non-saturated fluids are considered Clift et al. (1978). Without mass transfer and with gas density constant, the bubble maintains a constant volume during the bouncing process. Clearly, the bubble shape is variable; therefore we have used the equivalent radius to define the force in Eq. (3.1). Considering the equivalent radius  $R$  and density  $\rho_b$  of a bubble when it moves in a liquid, the terms in Eq. (3.1) can be expressed as,

$$m_b = \rho_b \frac{4}{3} \pi R^3 \quad (3.7)$$

$$\vec{F}_b = (\rho_l - \rho_b) \frac{4}{3} \pi R^3 \vec{g} \quad (3.8)$$

$$\vec{F}_d = -C_d Re_v \frac{\pi}{4} \mu_l R \vec{V} \quad (3.9)$$

$$\vec{F}_{am} = -C_{am} \rho_l \frac{4}{3} \pi R^3 \frac{d\vec{V}}{dt} \quad (3.10)$$

In this case, the Reynolds number, related to the instantaneous velocity, is denoted by  $Re_v$  and is defined as,

$$Re_v = \frac{\rho_l 2R |\vec{V}|}{\mu_l} = \frac{\rho_l 2R \sqrt{U^2 + V^2 + W^2}}{\mu_l} \quad (3.11)$$

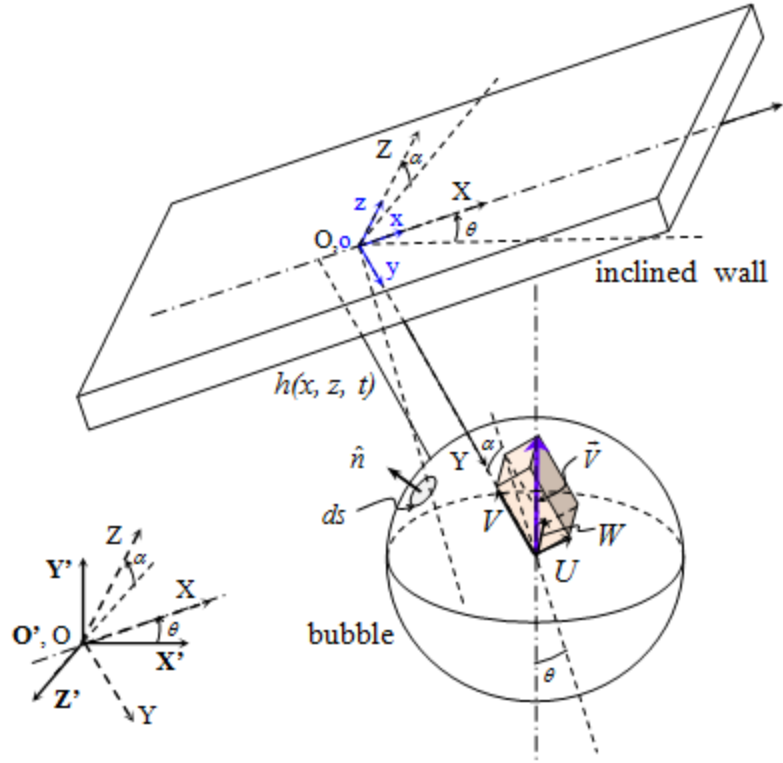


**Figure 3.1:** Bubble-wall interaction geometry:  $\mathbf{X}'\mathbf{Y}'\mathbf{Z}'$  is a fixed reference frame with  $\mathbf{Y}'$  vertical and horizontal plane  $\mathbf{X}'\mathbf{Z}'$ ,  $\mathbf{XYZ}$  is a reference frame fixed to the solid wall, and  $\mathbf{xyz}$  is a moving reference frame.

Figure 3.1 shows a sketch of the geometry used to derive our bubble wall interaction (BWI) model. The fixed reference frame  $\mathbf{X}'\mathbf{Y}'\mathbf{Z}'$  (rectangular Cartesian coordinate system with  $\mathbf{Y}'$  vertical) indicated in the figure is used as a straightforward representation of the directions of the buoyancy force and terminal velocity. The rectangular Cartesian coordinate system  $\mathbf{XYZ}$  (with  $\mathbf{Y}$  being normal to the wall) and origin  $\mathbf{O}$ , is fixed to the wall. The origin  $\mathbf{O}$  of this reference frame coincides with the normal projection of the bubble centroid onto the wall at initial time  $t=0$ . The solid wall is fixed and has two inclinations represented by the angles  $\theta$  and  $\alpha$ . The  $\mathbf{XYZ}$  reference frame is used to determine the bubble trajectory (Eq. (3.1)) and the buoyancy force and the terminal velocity initially expressed in the reference frame  $\mathbf{X}'\mathbf{Y}'\mathbf{Z}'$  were written in the reference frame  $\mathbf{XYZ}$  by means of a transformation matrix  $[\mathbf{L}]$  defined in section 3.1.4. A moving  $\mathbf{xyz}$  reference frame has been used to compute the

excess pressure because if we use the XYZ fixed reference, the solution of the lubrication equation becomes very difficult (Hori, 2006). The origin of this moving reference frame moves with the resultant bubble tangential velocity relative to the wall.

The effect of the wall is considered through the BWIF (or wall force). The objective of this thesis is to model this force as the result of the force exerted by the excess pressure generated in the fluid film due to the hydrodynamic lubrication phenomenon. This is a systematization and extension of the idea proposed by Klaseboer et al. (2001), Moraga et al. (2005), and Podvin et al. (2008).

The dynamic of a bubble rising vertically (see Fig. 3.1) in a fluid and bouncing against an immersed wall can be explained as follows: far from the wall, the bubble moves steadily with the terminal velocity. The added mass force ( $\vec{F}_{am}$ ) and the excess pressure are zero, therefore, there is no wall force, and the drag and buoyancy forces are equal. When the bubble approaches the wall, the excess pressure in the film increases, and as a result the wall force increases and the bubble decelerates. The added mass force simultaneously appears due to this deceleration. As the thickness of the fluid film decreases, the wall force increases; if the wall force produced by the excess pressure is greater than the sum of the buoyancy, added mass and drag forces in the y direction (see Fig. 3.1); the bouncing process is initiated.

To use the lubrication theory that describes the thin film drainage between the wall and the top of the bubble we must assume that: 1) The excess pressure is uniform across the film thickness i.e. only depends of  $x$  and  $z$  directions, and 2) the variations of fluid velocities  $u$  and  $w$  in the  $x$  and  $z$  directions are small compared with their variations in the  $y$  direction,

hence the following approximations are assumed:  $\frac{\partial u}{\partial x}, \frac{\partial u}{\partial z} \ll \frac{\partial u}{\partial y}$  and  $\frac{\partial w}{\partial x}, \frac{\partial w}{\partial z} \ll \frac{\partial w}{\partial y}$ . A

validation parameter of the lubrication equation is  $\varepsilon = \frac{h}{R} \ll 1$  (Leal, 2007) which indicates

that the film thickness must be small compared with the bubble radius; this ensures that the assumption 1 holds. The bubble deformation should also be small so that the second assumption is reasonably satisfied; therefore, the other validation parameters are

$$\frac{\partial h}{\partial x} \text{ and } \frac{\partial h}{\partial z} \ll 1 \text{ (Klaseboer et al. 2001).}$$

For a bubble with velocities  $U$  and  $W$  tangential to wall in the  $x$ -direction and  $z$ -direction respectively and approaching a wall as shown in Fig 3.1; in the  $xyz$  coordinate system, the lubrication equation, Eq. (2.27), can be written as,

$$\frac{\partial h}{\partial t} + \frac{U}{2} \frac{\partial h}{\partial x} + \frac{W}{2} \frac{\partial h}{\partial z} = \frac{1}{12\mu} \frac{\partial}{\partial x} \left( h^3 \frac{\partial p}{\partial x} \right) + \frac{1}{12\mu} \frac{\partial}{\partial z} \left( h^3 \frac{\partial p}{\partial z} \right) \quad (3.12)$$

Equation (3.12) considers the deformation of the bubble in the  $y$  direction since  $\frac{\partial h}{\partial t}$  is not

assumed constant along  $x$  and  $z$  directions. The deformations in the  $x$  and  $z$  directions are not

considered because the terms  $\frac{\partial U}{\partial x}$  and  $\frac{\partial W}{\partial z}$  are neglected in this equation; this terms are

neglected since we assume small deformations ( $\frac{\partial h}{\partial x}$  and  $\frac{\partial h}{\partial z} \ll 1$ ) which indicates that in the

area of deformation the surfaces (bubble surface and wall) are nearly parallel and the tangential deformations are very small compared with the normal deformation.

The hydrodynamic lubrication equation has been derived using no-slip conditions at the boundaries (solid surfaces). Several publications show that in a fluid free of contaminants, the bubble motion is more accurately described using the slip condition at the interface, or in other words, when there is no shear stress at the interface (Michaelides, 2006; Podvin et al. 2008). Apart from a contaminated or uncontaminated fluid the other important

factor that determines the degree of slip is the viscosity ratio between the bubble viscosity and the viscosity of the liquid around it. Due to the fact that is difficult to control water purity in experimental work, we use limiting cases, mobile (slip) and immobile (no-slip) bubble interface, to evaluate the relevance of each condition. If we assume mobile interface the shear stress at bubble surface has to be zero and a modified lubrication equation is obtained (Klaseboer et al. 2001; Podvin et al. 2008). This modified lubrication equation which is equivalent to Eq. (3.12) is given by,

$$\frac{\partial h}{\partial t} + \frac{U}{2} \frac{\partial h}{\partial x} + \frac{W}{2} \frac{\partial h}{\partial z} = \frac{1}{3\mu} \frac{\partial}{\partial x} \left( h^3 \frac{\partial p}{\partial x} \right) + \frac{1}{3\mu} \frac{\partial}{\partial z} \left( h^3 \frac{\partial p}{\partial z} \right) \quad (3.13)$$

Expressing Eqs. (3.12) and (3.13) in invariant form, we obtain,

$$\frac{\partial h}{\partial t} + \frac{1}{2} \vec{V}_s \cdot \vec{\nabla}_s h = \frac{1}{M\mu_l} \vec{\nabla}_s \cdot (h^3 \vec{\nabla}_s p) \quad (3.14)$$

where  $M = 3$  for a mobile interface and  $M = 12$  for an immobile interface.  $\vec{\nabla}_s$  is the portion of the gradient operator that involves the coordinates in the plane of the flat wall (these are  $x$ ,  $z$ ); similarly,  $\vec{V}_s$  represents the resultant bubble velocity on the plane of the wall. Both  $\vec{\nabla}_s$  and  $\vec{V}_s$  are expressed as functions of the unit vectors  $\hat{i}$  and  $\hat{j}$  in the form

$$\vec{\nabla}_s := \frac{\partial}{\partial x} \hat{i} + \frac{\partial}{\partial z} \hat{k} \quad (3.15)$$

$$\vec{V}_s := U\hat{i} + W\hat{k} \quad (3.16)$$

It can be observed that, the  $x$  and  $z$  are perpendicular directions on the plane perpendicular to the film thickness  $h(x, z, t)$  (see Fig. 3.1).

In general problems of hydrodynamic lubrication between solid surfaces the geometry is known a priori and one can almost always choose a reference frame such that the film

thickness is independent of time, or if a variation of  $h$  with time,  $\frac{\partial h}{\partial t}$ , exists, it is constant in space since the surfaces are rigid solids. Therefore, the lubrication problems are principally based on computing the excess pressure produced in the film drainage. In our case, a model for the excess pressure produced on the thin film of lubrication in accordance with the bubble deformation has been published. Hence, contrary to the classical problems of hydrodynamic lubrication, our aim is to calculate the film thickness  $h(x, z, t)$ , and with this result compute the excess pressure field and then the wall force. Finally, we will include the wall force in Eq. (3.1) to solve for the centroid velocity of the bubble.

### 3.1.1 Excess pressure model in the liquid film drainage

In order to establish an excess pressure model for the film drainage, the ability of the liquid-air interface to support small tensions quantified by the surface tension coefficient is considered. We used the model established by Klaseboer et al. (2001), Moraga et al. (2005) and Podvin et al. (2008) which is described as follows. Locally the pressure difference (pressure jump) inside and just outside of the bubble depends on the local surface tension and the local principal curvature radii (see section 2.2). The surface tension here is constant since we assume an isotropic and isothermal system. In consequence, the pressure jump depends only on the local curvatures, as follows

$$P_l - P_b = -\sigma \left( \frac{1}{R_x} + \frac{1}{R_z} \right) \quad (3.17)$$

where  $P_l$  and  $P_b$  represent the pressure outside and inside the bubble respectively,  $R_x$  and  $R_z$  are curvature radii in the orthogonal directions  $x$  and  $z$ . Eq. (3.17) is a general expression

for an arbitrary deformation of the bubble. If the bubble is spherical, the curvature radii are equal. Therefore, Eq. (3.17) yields,

$$P_l - P_b = -2\frac{\sigma}{R} \quad (3.18)$$

Assuming that the pressure inside the bubble is uniform and constant during the bouncing process, the excess pressure in the film,  $p$ , can be computed as the difference of the jump pressures between the initial spherical interface and the deformed interface of the bubble in the wall proximity.

$$p = 2\frac{\sigma}{R} - \sigma\left(\frac{1}{R_x} + \frac{1}{R_z}\right) \quad (3.19)$$

In the bouncing process, the deformation is considered to take place on the top surface of the bubble which faces the wall (see Fig. 3.2) within a small circle of radius  $r < r_{max}$  with  $r_{max} \ll R$ . When computing the excess pressure, it is difficult to establish a  $r_{max}$  but we can assume a negligible excess pressure at  $r > r_{max}$ , so we do not commit an error if we take  $r_{max} \approx R$ . This assumption should be verified a posteriori.

The curvatures in Eq. (3.19) can be expressed as a function of the film thickness  $h(x,z,t)$  and

if the deformation is small, we have  $\frac{\partial h}{\partial x}$  and  $\frac{\partial h}{\partial z} \ll 1$ . Therefore, the mean curvature in Eq.

(3.19) can be approximated using Eq. (2.3) as follows (Podvin et al. 2008),

$$\frac{1}{R_x} + \frac{1}{R_z} \cong \frac{\partial^2 h}{\partial x^2} + \frac{\partial^2 h}{\partial z^2} := \nabla_s^2 h \quad (3.20)$$

Considering small deformation, Eq. (3.19) in invariant form yields

$$p = \sigma\left(\frac{2}{R} - \nabla_s^2 h\right) \quad (3.21)$$

Finally, we can define the bubble-wall interaction force as follows

$$\vec{F}_w := -\iint_s p \hat{n} ds = -\iint_s \sigma \left( \frac{2}{R} - \nabla^2_s h \right) \hat{n} ds \quad (3.22)$$

The unit vector normal to the bubble surface as shown in Fig. 3.2 is denoted by  $\hat{n}$  and the region where the excess pressure is non-zero is denoted by  $S$ .

### 3.1.2 System of equations

For many engineering applications, the dimensions of the bubbles are very small compared with the dimensions of the surfaces where the bouncing phenomenon occurs. For instance, with the aim of reducing the drag on ships (Kodama et al. 2004), bubbles ranging from 0.5 mm to 1.0 mm in diameter have been impinged on the surface of ship hulls which have an approximate length of 100 m. It has also been reported that the distance travelled by the bubble during the bouncing motion is of the same order of magnitude as the bubble size (Tsao & Koch, 1997). Hence, the curvature radius of the surface is very large compared with the curvature radius of the bubble, and therefore the local bubble-wall interaction can be viewed as the interaction of a bubble with an inclined flat wall. For this reason, the governing equations of the BWI model are formulated for the most general case as the interaction of a bubble with a flat wall inclined in two directions (see Fig. 3.1). Using Eqs. (3.1), (3.7-3.10), (3.14), (3.21), and (3.22) we proposed the following governing equations for the bubble-wall interaction where the wall is flat with two inclinations, as shown in Fig. 3.1.

*Bubble equation of motion*

$$\frac{4}{3} \pi R^3 \rho_b \frac{d\vec{V}}{dt} = (\rho_l - \rho_b) \frac{4}{3} \pi R^3 g \hat{e}_b - C_d Re_v \frac{\pi}{4} \mu_l R \vec{V} - C_{am} \rho_l \frac{4}{3} \pi R^3 \frac{d\vec{V}}{dt} - \iint_s p \hat{n} ds \quad (3.23)$$

*Film drainage equation*

$$\frac{\partial h}{\partial t} + \frac{1}{2} \vec{V}_s \cdot \vec{\nabla}_s h = \frac{1}{M\mu_l} \vec{\nabla}_s \cdot (h^3 \vec{\nabla}_s p) \quad (3.24)$$

*Excess pressure equation*

$$p = \sigma \left( \frac{2}{R} - \nabla_s^2 h \right) \quad (3.25)$$

where  $\hat{e}_b$  is the unit vector of the buoyancy force expressed in the coordinate system XYZ.

The remaining variables have been previously mentioned. Eqs. (3.23-3.25) represent a system of 5 equations (3 from vector equation Eq. (3.23), and 2 from Eqs. (3.24) and (3.25)) and 5 unknown variables (components of bubble centroid velocity  $U(t)$ ,  $V(t)$ , and  $W(t)$ , excess pressure in the fluid film  $p(x,z,t)$ , and the film thickness  $h(x,z,t)$ ). If we are able establish adequate boundary and initial conditions, the proposed system of equations can be solved. Therefore, the bubble position as function of time becomes straightforward to compute. Indeed, the bubble position vector  $\vec{\chi}_b(t)$  related to the bubble velocity  $\vec{V}(t)$  is given by,

$$\vec{\chi}_b(t) = \vec{\chi}_b(t=0) + \int_0^t \vec{V}(t) dt \quad (3.26)$$

Here  $\vec{\chi}_b = X_b \hat{i} + Y_b \hat{j} + Z_b \hat{k}$ , where  $X_b$ ,  $Y_b$ , and  $Z_b$  are the position vector components in the  $X$ ,  $Y$ , and  $Z$  directions respectively (see Fig.3.1). The bubble velocity components are given in Eq. (3.6). For a full solution of Eq. (3.26) the initial position vector must be known at  $t=0$ .

To compare our results with the available experimental data we express the proposed system of equations, Eqs. (3.23-3.25), in a non-dimensional form using the following non-dimensional parameters and non-dimensional numbers.

$$x^* := \frac{x}{R} \quad , \quad z^* := \frac{z}{R} \quad (3.27)$$

$$X_b^* := \frac{X_b}{R} \quad , \quad Y_b^* := \frac{Y_b}{R} \quad , \quad Z_b^* := \frac{Z_b}{R} \quad (3.28)$$

$$U^* := \frac{U}{|\vec{V}_T|} \quad , \quad V^* := \frac{V}{|\vec{V}_T|} \quad , \quad W^* := \frac{W}{|\vec{V}_T|} \quad (3.29)$$

$$t^* := t \frac{|\vec{V}_T|}{R} \quad , \quad h^* := \frac{h}{hnd} \quad (3.30)$$

$$Re = \frac{\rho_l |\vec{V}_T| 2R}{\mu_l} \quad , \quad We = \frac{\rho_l |\vec{V}_T|^2 2R}{\sigma} \quad , \quad Eo = \frac{4g(\rho_l - \rho_b)R^2}{\sigma} \quad (3.31)$$

$$Re_V = \frac{\rho_l 2R \sqrt{U^2 + V^2 + W^2}}{\mu_l} = \frac{\rho_l 2R |\vec{V}_T| \sqrt{U^{*2} + V^{*2} + W^{*2}}}{\mu_l} = Re \sqrt{U^{*2} + V^{*2} + W^{*2}} \quad (3.32)$$

where the equivalent radius  $R$  of the bubble is the characteristic dimension for spatial coordinates, the magnitude of the bubble terminal velocity  $|\vec{V}_T|$  is the characteristic velocity, and  $hnd$  is the characteristic fluid film thickness. Note that  $|\vec{V}_T| = |\vec{V}'_T|$ , where  $\vec{V}_T$  and  $\vec{V}'_T$  are vectors expressed in XYZ and X'Y'Z' Cartesian coordinate systems respectively. Special care has been taken in defining the characteristic time since the time in the bouncing phenomena is on the order of  $10^{-3}$  seconds (Tsao & Koch, 1997). We use a characteristic time

$t_c$  defined as *the time that it takes the bubble to travel a distance equal to its radius*,  $t_c = \frac{R}{|\vec{V}_T|}$ ,

as used by Moraga et al. (2005) and Podvin et al. (2008).  $Re$  and  $We$  are the Reynolds and Weber numbers based on the terminal velocity and the bubble diameter and  $EO$  is the Eotvos number. Finally, the instantaneous Reynolds number is denoted by  $Re_v$  (see Eq. 3.32). Using these definitions, Eqs. (3.23-3.25) may be written in a non-dimensional form, as follows:

*Non-dimensional bubble equation of motion*

$$\frac{2}{3} \left( \frac{\rho_b}{\rho_l} + C_{am} \right) \frac{d\vec{V}^*}{dt^*} = \frac{1}{3} \frac{EO}{We} \hat{e}_b - \frac{C_d Re_v \vec{V}^*}{4Re} - \frac{2}{\pi We} \iint_{s^*} \hat{n} ds^* - \frac{1}{\pi We} \frac{hnd}{R} \iint_{s^*} p^* \hat{n} ds^* \quad (3.33)$$

*Non-dimensional film drainage equation*

$$C_1 \left[ \frac{\partial h^*}{\partial t^*} + \frac{1}{2} \vec{V}_s^* \cdot \vec{\nabla}_s^* h^* \right] = \vec{\nabla}_s^* \cdot (h^{*3} \vec{\nabla}_s^* p^*) \quad (3.34)$$

*Non-dimensional excess pressure equation*

$$p^* = -\nabla_s^{*2} h^* \quad (3.35)$$

where,

$$C_1 := M \frac{We}{Re} \left( \frac{R}{hnd} \right)^3 \quad (3.36)$$

$$\vec{\nabla}_s^* := \frac{\partial}{\partial x^*} \hat{i} + \frac{\partial}{\partial z^*} \hat{k} \quad (3.37)$$

$$\vec{V}_s^* := U^* \hat{i} + W^* \hat{k} \quad (3.38)$$

$$\vec{V}^* := U^* \hat{i} + V^* \hat{j} + W^* \hat{k} \quad (3.39)$$

As a result of the non-dimensionalization of the proposed system of equations the characteristic force is  $2\pi\rho_l |\vec{V}_T^-|^2 R^2$ . Therefore, the non-dimensional force can be expressed as,

$$\vec{F}_i^* := \frac{\vec{F}_i}{2\pi\rho_l |\vec{V}_T|^2 R^2} \quad (3.40)$$

where  $i$  represents a generic force on the bubble. Finally, the non-dimensional forces can be written as,

$$\vec{F}_b^* := \frac{1}{3} \frac{Eo}{We} \hat{e}_b \quad (3.41)$$

$$\vec{F}_d^* := -\frac{C_d Re_v \vec{V}^*}{4Re} \quad (3.42)$$

$$\vec{F}_{am}^* := -\frac{2}{3} C_{am} \frac{d\vec{V}^*}{dt^*} \quad (3.43)$$

$$\vec{F}_w^* := -\frac{2}{\pi We} \iint_{s^*} \hat{n} ds^* - \frac{1}{\pi We} \left( \frac{hnd}{R} \right) \iint_{s^*} p^* \hat{n} ds^* \quad (3.44)$$

### 3.1.3 Initial and boundary conditions

Adequate initial and boundary conditions (ICs and BCs) must be established to solve the system of equations derived in the previous section. As initial condition we assumed that the bubble rises vertically at the terminal velocity, which implies that, the added mass and wall forces are zero since the velocity variation and the excess pressure are zero. This condition occurs at a large initial liquid film height. As boundary conditions we assumed that outside of the region  $S$  (see Fig. 3.2) on the bubble surface, the excess pressure is zero and the bubble is no longer deformed by the wall. Therefore, the bubble surface moves with the centroid velocity.

Figure 3.2 provides a sketch of the initial geometry of the bubble where  $S$  is the initial region on the bubble with non-zero excess pressure (the boundary of  $S$  is initially assumed to be a circumference of radius  $r = r_{\max}$ ),  $h_\infty$  is the initial film height at  $(x, z) = (0, 0)$ , and  $\vec{V}_T'$

and  $\hat{e}'_b$  are the bubble terminal velocity and the unit vector of the buoyancy force both expressed in  $\mathbf{X}'\mathbf{Y}'\mathbf{Z}'$  fixed reference frame.

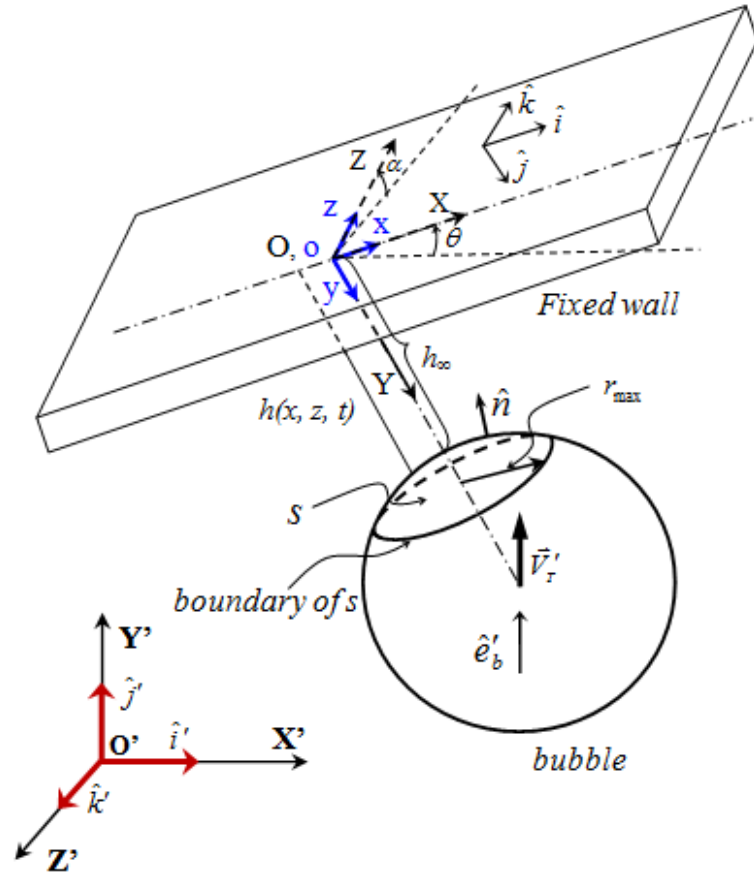


Figure 3.2: Boundary and initial conditions of bubble-wall interaction

The components of a vector in the XYZ Cartesian coordinate system are related to the components in the  $\mathbf{X}'\mathbf{Y}'\mathbf{Z}'$  Cartesian coordinate system according to the transformation law  $[\vec{v}_T] = [L][\vec{v}'_T]$ , where  $[L]$  is the transformation matrix (Reddy & Corporation, 2007) and it is defined in the next section. The transformation law is very useful to formulate the initial conditions of our problem and is detailed below. Thus, expressed in mathematical form, the ICs and BCs are,

$$\begin{aligned}
\text{at } t = 0 \quad & \begin{cases} \vec{V}(0) = \vec{V}_T \\ h(x, z, 0) = h_\infty + \frac{r^2}{2R} \\ p(x, z, 0) = 0 \end{cases} & \text{at } t > 0 \quad & \begin{cases} \left. \frac{\partial h}{\partial t} \right|_{\text{boundary of } S} = V = \frac{dY_b}{dt} \\ p|_{\text{boundary of } S} = 0 \end{cases} \\
& \text{initial conditions} & & \text{boundary conditions}
\end{aligned} \tag{3.45}$$

The initial spherical or ellipsoidal shape of a bubble is well represented by the parabolic film height profile  $h(x, z, 0) = h_\infty + \frac{r^2}{2R}$  provided that  $r$  is small, where  $r = (x^2 + z^2)^{1/2}$ . This parabolic profile is a Taylor series approximation of a hemispherical surface of radius  $R$ . This choice verifies the initial condition  $p = 0$  at  $t = 0$  in Eq. (3.25). In the non-dimensional form the ICs and BCs become,

$$\begin{aligned}
\text{at } t = 0 \quad & \begin{cases} \vec{V}^*(0) = 1\hat{e}_b \\ p^*(x^*, z^*, 0) = -2R/hnd \\ h^*(x^*, z^*, 0) = \frac{h_\infty}{hnd} + \frac{R}{2hnd}(x^{*2} + z^{*2}) \end{cases} & \text{at } t > 0 \quad & \begin{cases} \left. \frac{\partial h^*}{\partial t^*} \right|_{\text{boundary } S^*} = \frac{R}{hnd} V^* = \frac{R}{hnd} \frac{dY_b^*}{dt^*} \\ p^*|_{\text{boundary } S^*} = -2\frac{R}{hnd} \end{cases} \\
& \text{initial conditions} & & \text{boundary conditions}
\end{aligned} \tag{3.46}$$

In order to compute the bubble centroid position  $\vec{X}_b$ , the following initial relationship is considered,

$$\text{at } t = 0 \quad \begin{cases} X_b(0) = 0 \\ Y_b(0) = h_\infty + R \\ Z_b(0) = 0 \end{cases} \tag{3.47}$$

In non-dimensional form, it becomes,

$$\text{at } t^* = 0 \quad \begin{cases} X_b^*(0) = 0 \\ Y_b^*(0) = \frac{h_\infty + R}{R} \\ Z_b^*(0) = 0 \end{cases} \quad (3.48)$$

### 3.1.4 Normal vector and matrix transformation

The unit vector normal to the bubble surface pointing outward as shown in Fig. 3.3(a) is a function of fluid film height as follows,

$$\hat{n} = \frac{\vec{\nabla}f}{|\vec{\nabla}f|} \quad (3.49)$$

$$\text{where, } f : h(x, z, t) - y = 0 \quad (3.50)$$

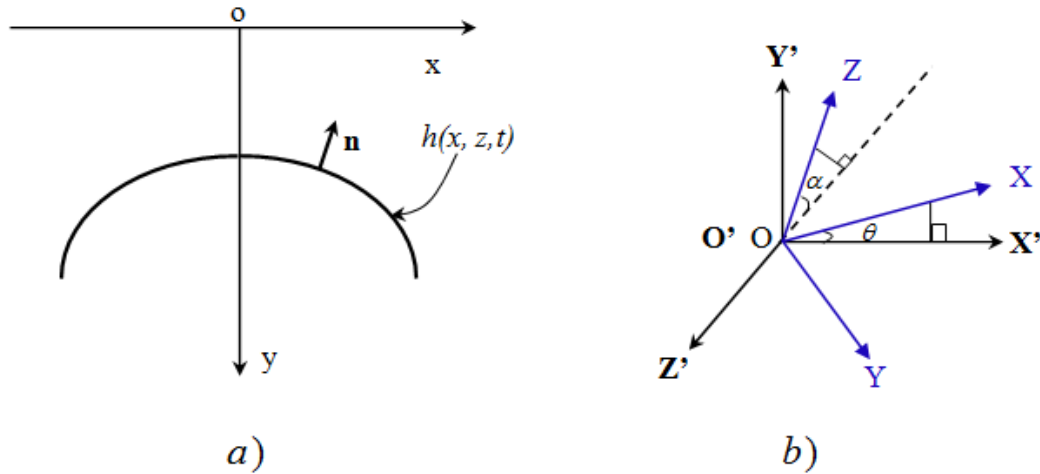


**Figure 3.3:** (a) Outward pointing normal vector to the bubble surface; (b)  $X'Y'Z'$  and  $XYZ$  rectangular Cartesian coordinate systems

Replacing Eq. (3.50) in Eq. (3.49), we obtain

$$\hat{n} = \frac{\frac{\partial h}{\partial x} \hat{i} - \hat{j} + \frac{\partial h}{\partial z} \hat{k}}{\sqrt{1 + \left(\frac{\partial h}{\partial x}\right)^2 + \left(\frac{\partial h}{\partial z}\right)^2}} \quad (3.51)$$

Considering that the XYZ coordinate system is a composition of a rotation around the  $\mathbf{Z}'$  axes by an angle  $\theta$  and rotation around  $\mathbf{X}'$  by an angle  $180^\circ + \alpha$  (see Fig. 3.1 and Fig 3.3(b)), the transformation law, according to the XYZ and  $\mathbf{X}'\mathbf{Y}'\mathbf{Z}'$  rectangular coordinates system as shown in Fig. 3.3(b) is obtained as:

$$\begin{bmatrix} i \\ j \\ k \end{bmatrix} = \begin{bmatrix} \cos \theta & \sin \theta & 0 \\ \sin \theta \cos \alpha & -\cos \theta \cos \alpha & -\sin \alpha \\ -\sin \theta \sin \alpha & \cos \theta \sin \alpha & -\cos \alpha \end{bmatrix} \begin{bmatrix} i' \\ j' \\ k' \end{bmatrix} \quad (3.52)$$

Therefore, the transformation matrix is

$$[L] = \begin{bmatrix} \cos \theta & \sin \theta & 0 \\ \sin \theta \cos \alpha & -\cos \theta \cos \alpha & -\sin \alpha \\ -\sin \theta \sin \alpha & \cos \theta \sin \alpha & -\cos \alpha \end{bmatrix} \quad (3.53)$$

The next sections are devoted to establishing the specific equation systems with their respective ICs and BCs for one-, two-, and three-dimensional BWI.

## 3.2 ONE-DIMENSIONAL BUBBLE-WALL INTERACTION MODEL

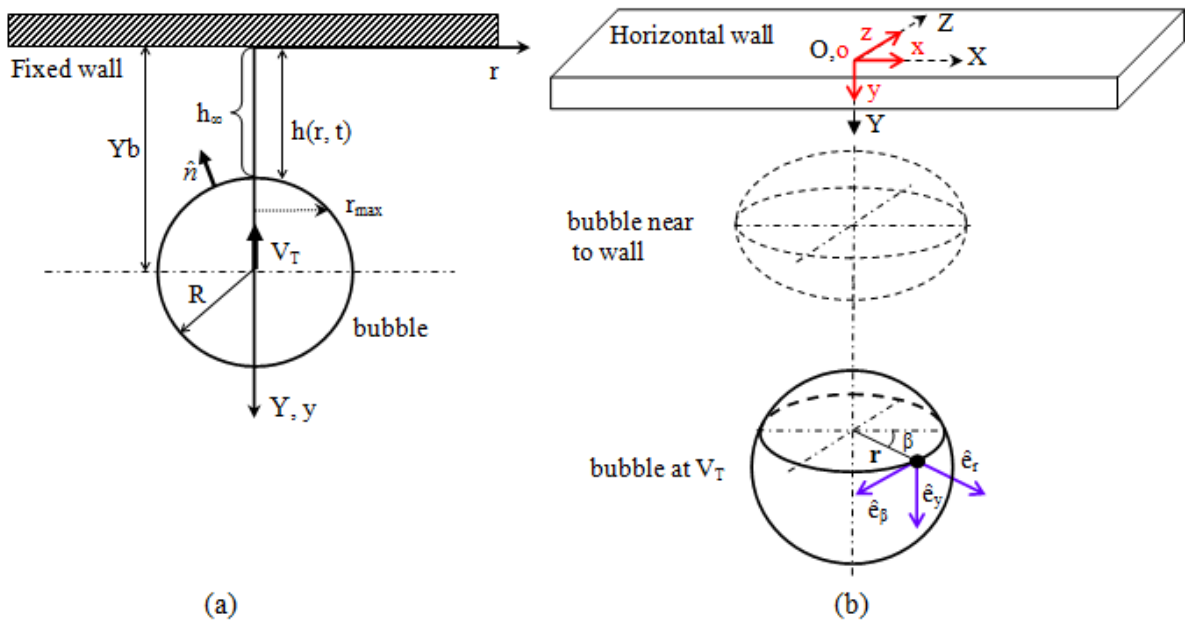
Using the assumptions and equations from section 3.1, a one-dimensional bubble-wall interaction (1D-BWI) model is developed in the present section. If we consider a bubble rising in a fluid and interacting with a rigid flat horizontal wall in which the angles  $\theta$  and  $\alpha$  are zero, the resulting velocities  $U$  and  $W$  in Fig. 3.1 are zero (i.e.,  $\vec{V}_s = 0$ ). Therefore, the bubble motion results in only one dimension (i.e., in the vertical direction). From the assumption that the fluid is isothermal and isotropic and the wall sufficiently large, an *axisymmetric deformation* on the top surface of the bubble is implied. Hence, in this case it is convenient to use cylindrical coordinates.

Figure 3.4 shows a schematic of a one-dimensional bubble-wall interaction (1D-BWI) where instead of  $(x, y, z)$  Cartesian coordinates system we use the  $(r, \beta, y)$  cylindrical coordinates. The unit vectors in  $r, \beta,$  and  $y$  directions are  $\hat{e}_r, \hat{e}_\beta,$  and  $\hat{e}_y$  respectively. In this coordinate system, the fluid film height and excess pressure are functions of  $r$  and  $t$  only (i.e.,  $h = h(r, t)$  and  $p = p(r, t)$ ) provided that the axisymmetric condition is satisfied. Furthermore, the bubble motion in cylindrical coordinates results in the  $Y$  direction only (see Fig. 3.4(a)).

In  $(r, \beta, y)$  coordinates the operators  $\bar{\nabla}_s$  and  $\nabla_s^2$  are written as:

$$\bar{\nabla}_s = \frac{\hat{e}_r}{r} \frac{\partial}{\partial r} ( \quad ) + \frac{\hat{e}_\beta}{r} \frac{\partial}{\partial \beta} ( \quad ) \quad (3.54)$$

$$\nabla_s^2 = \frac{1}{r} \frac{\partial}{\partial r} \left( r \frac{\partial}{\partial r} ( \quad ) \right) + \frac{1}{r^2} \frac{\partial^2}{\partial \beta^2} ( \quad ) \quad (3.55)$$



**Figure 3.4:** 1D-BWI geometry: a) Nomenclature; b) Cartesian and cylindrical coordinates

The centroid velocity of the bubble,  $\vec{V}$ , in  $(r, \beta, y)$  cylindrical coordinate system, has only one component which is in the  $y$ -direction, so

$$\vec{V} = V \hat{e}_y \quad (3.56)$$

The unit vector of the buoyancy force also yields

$$\hat{e}_b = -\hat{e}_y \quad (3.57)$$

Further, from the axisymmetric deformation condition, the film pressure causes zero wall force in the  $r$  direction. The net BWI force on the bubble is then in  $y$  direction only. Thus, using the projected area of  $S$  onto the wall, the wall force can be written as,

$$-\iint_S p \hat{n} ds = \hat{e}_y \int_0^{r_{\max}} 2\pi p r dr \quad (3.58)$$

Here the surface  $S$  is limited by a circumference  $r=r_{\max}$  at any time. But  $r_{\max}$  is not constant with time, such that the projected area onto XZ plane (see Fig 3.4(b)) varies with time. Substituting Eqs. (3.54-3.58) into Eqs. (3.23-3.25), the system of equations for 1D-BWI model is given by,

$$\frac{4}{3} \pi R^3 (\rho_b + C_{am} \rho_l) \frac{dV}{dt} = -(\rho_l - \rho_b) \frac{4}{3} \pi R^3 g - C_d \text{Re}_v \frac{\pi}{4} R \mu_l V + \int_{r=0}^{r=r_{\max}} 2\pi p r dr \quad (3.59)$$

$$\frac{\partial h}{\partial t} = \frac{1}{M\mu_l} \frac{1}{r} \frac{\partial}{\partial r} \left( r h^3 \frac{\partial p}{\partial r} \right) \quad (3.60)$$

$$p = \sigma \left\{ \frac{2}{R} - \frac{1}{r} \frac{\partial}{\partial r} \left( r \frac{\partial h}{\partial r} \right) \right\} \quad (3.61)$$

The BCs and ICs are

$$\begin{array}{l}
\text{at } t = 0 \left\{ \begin{array}{l} V(0) = -|\vec{V}_T| \\ h(r,0) = h_\infty + \frac{r^2}{2R} \\ p(r,0) = 0 \\ Y_b(0) = h_\infty + R \end{array} \right. \\
\text{initial conditions}
\end{array}
\quad
\begin{array}{l}
\text{at } t > 0 \left\{ \begin{array}{l} \left. \frac{\partial h}{\partial r} \right|_{r=0} = 0 \quad \text{symmetry condition} \\ \left. \frac{\partial p}{\partial r} \right|_{r=0} = 0 \quad \text{symmetry condition} \\ \left. \frac{\partial h}{\partial t} \right|_{r=r_{\max}} = V = \frac{dY_b}{dt} \\ p|_{r=r_{\max}} = 0 \end{array} \right. \\
\text{boundary conditions}
\end{array}
\quad (3.62)$$

Before we present the equations for 1D-BWI model in the non-dimensional form, we need to consider the following two expressions:

$$-\iint_s \hat{n} ds^* = \int_0^{r_{\max}^*} \hat{e}_y 2\pi r^* dr^* = \hat{e}_y \pi (r_{\max}^*)^2 \quad (3.63)$$

$$-\iint_s p^* \hat{n} ds^* = \hat{e}_y 2\pi \int_0^{r_{\max}^*} p^* r^* dr^* \quad (3.64)$$

Eq. (3.63) and Eq. (3.64) are valid as long as the hypothesis of small deformation of the

bubble ( $\frac{\partial h}{\partial x} \ll 1$ ) holds and the deformation in  $x$  is symmetrical (see section 3.3 for more

details).

Finally Eqs. (3.59-3.61) in non-dimensional form become,

$$\frac{2}{3} \left( \frac{\rho_b}{\rho_l} + C_{am} \right) \frac{dV^*}{dt^*} = -\frac{1}{3} \frac{Eo}{We} - \frac{C_d \text{Re}_V V^*}{4 \text{Re}} + \frac{2}{We} (r_{\max}^*)^2 + \frac{2}{We} \frac{hnd}{R} \int_0^{r_{\max}^*} p^* r^* dr^* \quad (3.65)$$

$$C_1 \frac{\partial h^*}{\partial t^*} = \frac{1}{r^*} \frac{\partial}{\partial r^*} \left( r^* h^{*3} \frac{\partial p^*}{\partial r^*} \right) \quad (3.66)$$

$$p^* = -\frac{1}{r^*} \frac{\partial}{\partial r^*} \left( r^* \frac{\partial h^*}{\partial r^*} \right) \quad (3.67)$$

where,

$$r^* := \frac{r}{R}, \quad r_{\max}^* := \frac{r_{\max}}{R} \quad (3.68)$$

$$V^* := \frac{V}{|\vec{V}_T|}, \quad \text{Re}_V := \text{Re}|V| \quad (3.69)$$

The non-dimensional BCs and ICs become,

$$\begin{aligned} \text{at } t^* = 0 \quad & \left\{ \begin{array}{l} V^*(0) = -1 \\ p^*(r^*, 0) = -2 \frac{R}{hnd} \\ h^*(r^*, 0) = \frac{h_\infty}{hnd} + \frac{1}{2} \frac{R r^{*2}}{hnd} \\ Y_b^*(0) = \frac{h_\infty + R}{R} \end{array} \right. & \text{initial conditions} \\ \text{at } t^* > 0 \quad & \left\{ \begin{array}{l} \left. \frac{\partial h^*}{\partial r^*} \right|_{r^*=0} = 0 \text{ (symmetry condition)} \\ \left. \frac{\partial p^*}{\partial r^*} \right|_{r^*=0} = 0 \text{ (symmetry condition)} \\ \left. \frac{\partial h^*}{\partial t^*} \right|_{r^*=r_{\max}^*} = \frac{R}{hnd} V^* = \frac{R}{hnd} \frac{dY_b^*}{dt^*} \\ \left. p^* \right|_{r^*=r_{\max}^*} = -2 \frac{R}{hnd} \end{array} \right. & \text{boundary conditions} \end{aligned} \quad (3.70)$$

### 3.3 TWO-DIMENSIONAL BUBBLE-WALL INTERACTION MODEL

Using the assumptions and equations from section 3.1, a two-dimensional bubble-wall interaction (2D-BWI) model is developed in the present section. Fig. 3.5 is a sketch of the geometry of the 2D-BWI model, where a bubble rises vertically at terminal velocity on a quiescent fluid by the action of gravity and impacts on a solid wall with an angle of inclination  $\theta$  relative to the horizontal. Unlike the 1D-BWI model, in this case the bubble motion is no longer in one direction but instead is in two directions on the XY plane (see Fig 3.5(a)). In the Z direction the bubble deformation is symmetric, a result obtained from the assumption of a very large wall and a quiescent fluid far from the bubble. This implies that the net force is zero in the Z direction and also that the Z component of bubble velocity,  $W$ , retains its zero initial value. On the other hand, the bubble top surface deformation in the X

direction is no longer symmetric since the bubble has a velocity  $U$  tangential to the wall, i.e., in the  $X$  direction. This produces a nonsymmetrical excess pressure field, and as a consequence a nonsymmetrical deformation of the bubble top surface.

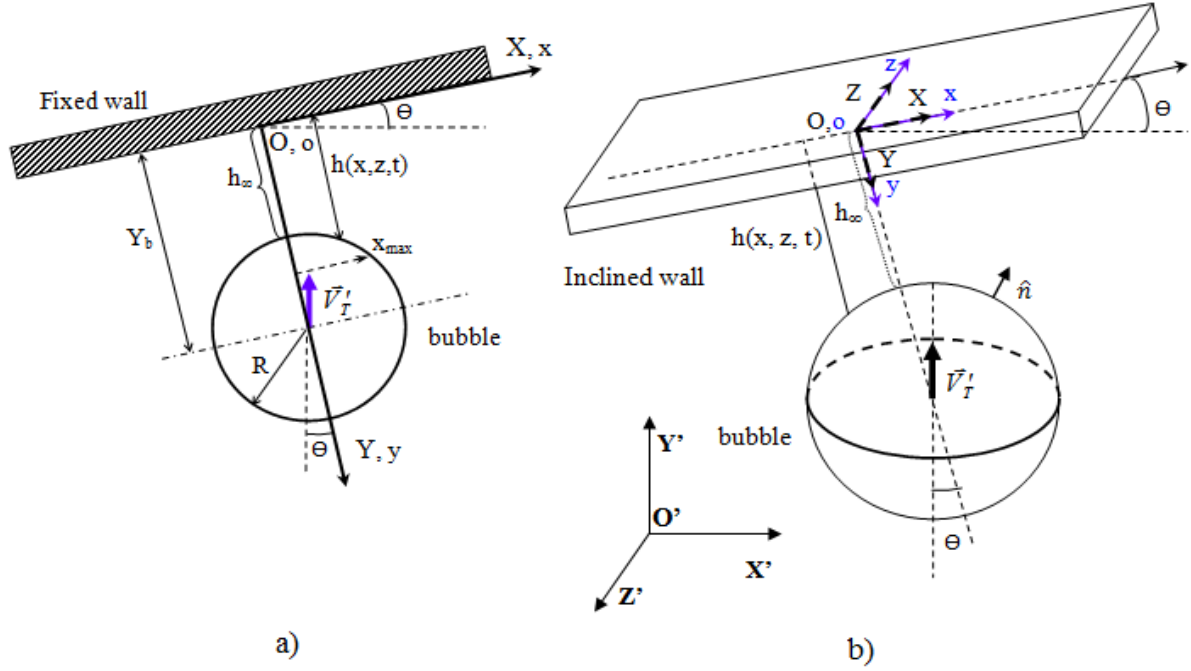


**Figure 3.5:** 2D-BWI geometry: a) XY plane and nomenclature; b) Perspective in 3D

Using the transformation law from Eq. (3.52) with  $\alpha = 0$ , we can express the coordinate transformation of the terminal velocity and the unit vector of buoyancy force in the XYZ coordinate system by,

$$\begin{bmatrix} e_{bx} \\ e_{by} \\ e_{bz} \end{bmatrix} = \begin{bmatrix} \cos \theta & \sin \theta & 0 \\ \sin \theta & -\cos \theta & 0 \\ 0 & 0 & 1 \end{bmatrix} \begin{bmatrix} 0 \\ 1 \\ 0 \end{bmatrix} \quad (3.71)$$

$$\begin{bmatrix} V_{Tx} \\ V_{Ty} \\ V_{Tz} \end{bmatrix} = \begin{bmatrix} \cos \theta & \sin \theta & 0 \\ \sin \theta & -\cos \theta & 0 \\ 0 & 0 & 1 \end{bmatrix} \begin{bmatrix} 0 \\ |\vec{V}_T'| \\ 0 \end{bmatrix} \quad (3.72)$$

From Eqs. (3.71) and (3.72), we obtain

$$\hat{e}_b = e_{bx}\hat{i} + e_{by}\hat{j} = \sin(\theta)\hat{i} - \cos(\theta)\hat{j} \quad (3.73)$$

$$\vec{V}_T = V_{Tx}\hat{i} + V_{Ty}\hat{j} = |\vec{V}'_T|\sin(\theta)\hat{i} - |\vec{V}'_T|\cos(\theta)\hat{j} \quad (3.74)$$

with the hypothesis of small deformation of the bubble,  $\frac{\partial h}{\partial x} \ll 1$  and  $\frac{\partial h}{\partial z} \ll 1$ , the normal

vector from Eq. (3.51) can be approximated as,

$$\hat{n} = \frac{\partial h}{\partial x}\hat{i} - 1\hat{j} + \frac{\partial h}{\partial z}\hat{k} \quad (3.75)$$

Hence, the wall force becomes,

$$-\iint_s p\hat{n}ds = -\iint_s p(\hat{i}n_x + \hat{j}n_y + \hat{k}n_z)dxdz = -\iint_s p\left(\hat{i}\frac{\partial h}{\partial x} - 1\hat{j} + \hat{k}\frac{\partial h}{\partial z}\right)dxdz \quad (3.76)$$

But by the symmetric condition in z direction, it results that  $-\iint_s p\frac{\partial h}{\partial z}dxdz = 0$  so the last

equation can be rewritten as,

$$-\iint_s p\hat{n}ds = -\iint_s p\left(\hat{i}\frac{\partial h}{\partial x} - 1\hat{j}\right)dxdz \quad (3.77)$$

Replacing Eqs. (3.73), (3.74) and (3.77) into Eqs. (3.23-3.25) the system of equations for the 2D-BWI model can be written as follows,

$$\frac{4}{3}\pi R^3(\rho_b + C_{am}\rho_l)\frac{dU}{dt} = (\rho_l - \rho_b)\frac{4}{3}\pi R^3 g \sin(\theta) - C_d \text{Re}_v \frac{\pi}{4} R\mu_l U - \iint_s p\frac{\partial h}{\partial x}dxdz \quad (3.78)$$

$$\frac{4}{3}\pi R^3(\rho_b + C_{am}\rho_l)\frac{dV}{dt} = -(\rho_l - \rho_b)\frac{4}{3}\pi R^3 g \cos(\theta) - C_d \text{Re}_v \frac{\pi}{4} R\mu_l V + \iint_s p dxdz \quad (3.79)$$

$$\frac{\partial h}{\partial t} + \frac{U}{2}\frac{\partial h}{\partial x} = \frac{1}{M\mu_l}\left\{\frac{\partial}{\partial x}\left(h^3\frac{\partial p}{\partial x}\right) + \frac{\partial}{\partial z}\left(h^3\frac{\partial p}{\partial z}\right)\right\} \quad (3.80)$$

$$p = \sigma\left\{\frac{2}{R} - \left(\frac{\partial^2 h}{\partial x^2} + \frac{\partial^2 h}{\partial z^2}\right)\right\} \quad (3.81)$$

The ICs and BCs are

$$\begin{array}{l}
 \left. \begin{array}{l}
 U(0) = |\vec{V}_T'| \sin(\theta) \\
 V(0) = -|\vec{V}_T'| \cos(\theta) \\
 h(x, z, 0) = h_\infty + \frac{x^2 + z^2}{2R} \\
 p(x, z, 0) = 0 \\
 Y_b(0) = h_\infty + R \\
 X_b(0) = 0
 \end{array} \right\} \text{at } t = 0 \quad \begin{array}{l}
 \text{initial conditions}
 \end{array} \\
 \left. \begin{array}{l}
 \left. \begin{array}{l}
 \frac{\partial h}{\partial t} \Big|_{\text{boundary of } S} = V = \frac{dY_b}{dt} \\
 p \Big|_{\text{boundary of } S} = 0
 \end{array} \right\} \text{at } t > 0 \\
 \text{boundary conditions}
 \end{array} \right\} \quad (3.82)
 \end{array}$$

The boundary of the surface  $S$  has the same significance as in section 3.1 (see Fig. 3.2). As we can see, Eqs. (3.78-3.81) constitute a coupled system of 4 equations in which the bubble centroid velocities  $U(t)$  and  $V(t)$ , the excess pressure field in the fluid film between the bubble and the wall  $p(x, z, t)$ , and the top interface of the bubble  $h(x, z, t)$  are determined.

In the non-dimensional form the approximated normal vector  $\hat{n}$  is given by

$$\hat{n} = \frac{\partial h}{\partial x} \hat{i} - 1 \hat{j} + \frac{\partial h}{\partial z} \hat{k} = \frac{hnd}{R} \frac{\partial h^*}{\partial x^*} \hat{i} - 1 \hat{j} + \frac{hnd}{R} \frac{\partial h^*}{\partial z^*} \hat{k} \quad (3.83)$$

Finally, in the non-dimensional form, the 2D-BWI model is expressed as:

$$\frac{2}{3} \left( \frac{\rho_b}{\rho_l} + C_{am} \right) \frac{dU^*}{dt^*} = \frac{1}{3} \frac{Eo}{We} \sin(\theta) - \frac{C_d Re_v U^*}{4 Re} - \frac{2}{\pi We} \frac{hnd}{R} \left\{ \iint_{s^*} \frac{\partial h^*}{\partial x^*} dx^* dz^* + \frac{1}{2} \left( \frac{hnd}{R} \right) \iint_{s^*} p^* \frac{\partial h^*}{\partial x^*} dx^* dz^* \right\} \quad (3.84)$$

$$\frac{2}{3} \left( \frac{\rho_b}{\rho_l} + C_{am} \right) \frac{dV^*}{dt^*} = -\frac{1}{3} \frac{Eo}{We} \cos(\theta) - \frac{C_d Re_v V^*}{4 Re} + \frac{2}{\pi We} \left\{ \iint_{s^*} dx^* dz^* + \frac{1}{2} \left( \frac{hnd}{R} \right) \iint_{s^*} p^* dx^* dz^* \right\} \quad (3.85)$$

$$C_1 \left\{ \frac{\partial h^*}{\partial t^*} + \frac{U^*}{2} \frac{\partial h^*}{\partial x^*} \right\} = \left\{ \frac{\partial}{\partial x^*} \left( h^{*3} \frac{\partial p^*}{\partial x^*} \right) + \frac{\partial}{\partial z^*} \left( h^{*3} \frac{\partial p^*}{\partial z^*} \right) \right\} \quad (3.86)$$

$$p^* = - \left( \frac{\partial^2 h^*}{\partial x^{*2}} + \frac{\partial^2 h^*}{\partial z^{*2}} \right) \quad (3.87)$$

where,  $Re_V = Re \sqrt{U^{*2} + V^{*2}}$  is the instantaneous Reynolds number.

The BCs and ICs become,

$$\begin{aligned}
 \text{at } t = 0 \left\{ \begin{array}{l} Y_b^*(0) = \frac{h_\infty + R}{R}, X_b^*(0) = 0 \\ U^*(0) = 1 \sin(\theta) \\ V^*(0) = -1 \cos(\theta) \\ p^*(x^*, z^*, 0) = -2 \frac{R}{hnd} \\ h^*(x^*, z^*, 0) = \frac{h_\infty}{hnd} + \frac{1}{2} \frac{R}{hnd} (x^{*2} + z^{*2}) \end{array} \right. & \quad \text{initial conditions} \\
 \text{at } t > 0 \left\{ \begin{array}{l} \left. \frac{\partial h^*}{\partial t^*} \right|_{\text{boundary of } S^*} = \frac{R}{hnd} V^* = \frac{R}{hnd} \frac{dY_b^*}{dt^*} \\ p^* \Big|_{\text{boundary of } S^*} = -2 \frac{R}{hnd} \end{array} \right. & \quad \text{boundary conditions}
 \end{aligned} \quad (3.88)$$

### 3.4 THREE-DIMENSIONAL BUBBLE-WALL INTERACTION MODEL

Using the assumptions and equations from section 3.1, a three-dimensional bubble-wall interaction (3D-BWI) model is developed in the present section. Fig. 3.1 and Fig. 3.2 show the geometry considered in the present case. A relevant difference here is that the deformation in  $z$  direction is no longer symmetric. The normal vector, terminal velocity, and the unit vector of the buoyancy force expressed in XYZ Cartesian coordinate system are,

$$\hat{n} = \frac{\partial h}{\partial x} \hat{i} - 1 \hat{j} + \frac{\partial h}{\partial z} \hat{k} = \frac{hnd}{R} \frac{\partial h^*}{\partial x^*} \hat{i} - 1 \hat{j} + \frac{hnd}{R} \frac{\partial h^*}{\partial z^*} \hat{k} \quad (3.89)$$

$$\vec{V}_T = V_{Tx} \hat{i} + V_{Ty} \hat{j} + V_{Tz} \hat{k} = |\vec{V}'_T| \sin(\theta) \hat{i} - |\vec{V}'_T| \cos(\theta) \cos(\alpha) \hat{j} + |\vec{V}'_T| \cos(\theta) \sin(\alpha) \hat{k} \quad (3.90)$$

$$\hat{e}_b = \hat{i} \sin(\theta) - \hat{j} \cos(\theta) \cos(\alpha) + \hat{k} \cos(\theta) \sin(\alpha) \quad (3.91)$$

Therefore, the system of equations for the 3D-BWI model is,

$$\frac{4}{3} \pi R^3 (\rho_b + C_{am} \rho_l) \frac{dU}{dt} = (\rho_l - \rho_b) \frac{4}{3} \pi R^3 g \sin(\theta) - C_d \text{Re}_v \frac{\pi}{4} R \mu_l U - \iint_s p \frac{\partial h}{\partial x} dx dz \quad (3.92)$$

$$\frac{4}{3} \pi R^3 (\rho_b + C_{am} \rho_l) \frac{dV}{dt} = -(\rho_l - \rho_b) \frac{4}{3} \pi R^3 g \cos(\theta) \cos(\alpha) - C_d \text{Re}_v \frac{\pi}{4} R \mu_l V + \iint_s p dx dz \quad (3.93)$$

$$\frac{4}{3} \pi R^3 (\rho_b + C_{am} \rho_l) \frac{dW}{dt} = (\rho_l - \rho_b) \frac{4}{3} \pi R^3 g \cos(\theta) \sin(\alpha) - C_d \text{Re}_v \frac{\pi}{4} R \mu_l W - \iint_s p \frac{\partial h}{\partial z} dx dz \quad (3.94)$$

$$\frac{\partial h}{\partial t} + \frac{U}{2} \frac{\partial h}{\partial x} + \frac{W}{2} \frac{\partial h}{\partial z} = \frac{1}{M \mu_l} \left\{ \frac{\partial}{\partial x} \left( h^3 \frac{\partial p}{\partial x} \right) + \frac{\partial}{\partial z} \left( h^3 \frac{\partial p}{\partial z} \right) \right\} \quad (3.95)$$

$$p = \sigma \left\{ \frac{2}{R} - \left( \frac{\partial^2 h}{\partial x^2} + \frac{\partial^2 h}{\partial z^2} \right) \right\} \quad (3.96)$$

with their BCs and ICs given by

$$\begin{aligned} \text{at } t = 0 \quad & \left\{ \begin{array}{l} U(0) = |\vec{V}'_T| \sin(\theta) \\ V(0) = -|\vec{V}'_T| \cos(\theta) \cos(\alpha) \\ W(0) = |\vec{V}'_T| \cos(\theta) \sin(\alpha) \\ p(x, z, 0) = 0 \\ Y_b(0) = h_\infty + R \\ X_b(0) = 0, Z_b(0) = 0 \\ h(x, z, 0) = h_\infty + \frac{x^2 + z^2}{2R} \end{array} \right. \\ & \text{initial conditions} \end{aligned} \quad \begin{aligned} \text{at } t > 0 \quad & \left\{ \begin{array}{l} \left. \frac{\partial h}{\partial t} \right|_{\text{boundary of } S} = V = \frac{dY_b}{dt} \\ p|_{\text{boundary of } S} = 0 \end{array} \right. \\ & \text{boundary conditions} \end{aligned} \quad (3.97)$$

The dimensionless system of equations becomes,

$$\frac{2}{3} \left( \frac{\rho_b}{\rho_l} + C_{am} \right) \frac{dU^*}{dt^*} = \left\{ \begin{array}{l} \frac{1}{3} \frac{Eo}{We} \sin(\theta) - \frac{C_d Re_v U^*}{4Re} - \\ \frac{2}{\pi We} \frac{hnd}{R} \left\{ \iint_{s^*} \frac{\partial h^*}{\partial x^*} dx^* dz^* + \frac{1}{2} \left( \frac{hnd}{R} \right) \iint_{s^*} p^* \frac{\partial h^*}{\partial x^*} dx^* dz^* \right\} \end{array} \right\} \quad (3.98)$$

$$\frac{2}{3} \left( \frac{\rho_b}{\rho_l} + C_{am} \right) \frac{dV^*}{dt^*} = \left\{ \begin{array}{l} -\frac{1}{3} \frac{Eo}{We} \cos(\theta) \cos(\alpha) - \frac{C_d Re_v V^*}{4Re} + \\ \frac{2}{\pi We} \left\{ \iint_{s^*} dx^* dz^* + \frac{1}{2} \left( \frac{hnd}{R} \right) \iint_{s^*} p^* dx^* dz^* \right\} \end{array} \right\} \quad (3.99)$$

$$\frac{2}{3} \left( \frac{\rho_b}{\rho_l} + C_{am} \right) \frac{dW^*}{dt^*} = \left\{ \begin{array}{l} \frac{1}{3} \frac{Eo}{We} \cos(\theta) \sin(\alpha) - \frac{C_d Re_v W^*}{4Re} - \\ \frac{2}{\pi We} \frac{hnd}{R} \left\{ \iint_{s^*} \frac{\partial h^*}{\partial z^*} dx^* dz^* + \frac{1}{2} \left( \frac{hnd}{R} \right) \iint_{s^*} p^* \frac{\partial h^*}{\partial z^*} dx^* dz^* \right\} \end{array} \right\} \quad (3.100)$$

$$C_1 \left\{ \frac{\partial h^*}{\partial t^*} + \frac{U^*}{2} \frac{\partial h^*}{\partial x^*} + \frac{W^*}{2} \frac{\partial h^*}{\partial z^*} \right\} = \left\{ \frac{\partial}{\partial x^*} \left( h^{*3} \frac{\partial p^*}{\partial x^*} \right) + \frac{\partial}{\partial z^*} \left( h^{*3} \frac{\partial p^*}{\partial z^*} \right) \right\} \quad (3.101)$$

$$p^* = - \left( \frac{\partial^2 h^*}{\partial x^{*2}} + \frac{\partial^2 h^*}{\partial z^{*2}} \right) \quad (3.102)$$

The dimensionless BCs and ICs are,

$$\begin{array}{l} \left. \begin{array}{l} Y_b^*(0) = \frac{h_\infty + R}{R}, Z_b^*(0) = 0, X_b^*(0) = 0 \\ U^*(0) = 1 \sin(\theta) \\ V^*(0) = -1 \cos(\theta) \cos(\alpha) \\ W^*(0) = 1 \cos(\theta) \sin(\alpha) \\ p^*(x^*, z^*, 0) = -2 \frac{R}{hnd} \\ h^*(x^*, z^*, 0) = \frac{h_\infty}{hnd} + \frac{R}{2hnd} (x^{*2} + z^{*2}) \end{array} \right\} \begin{array}{l} \text{initial conditions} \end{array} \end{array} \quad \begin{array}{l} \left. \begin{array}{l} \left. \frac{\partial h^*}{\partial t^*} \right|_{\text{boundary } S^*} = \frac{R}{hnd} V^* = \frac{R}{hnd} \frac{dY_b^*}{dt^*} \\ \left. p^* \right|_{\text{boundary } S^*} = -2 \frac{R}{hnd} \end{array} \right\} \begin{array}{l} \text{boundary conditions} \end{array} \end{array} \quad (3.103)$$

Using lubrication approximation and a reliable excess pressure model we have proposed an equations system for one , two , and three-dimensional bubble-wall interactions,

to describe the dynamic behavior of a bubble during the bouncing phenomena. In the following chapter, the numerical techniques used to solve the equations proposed in sections (3.2), (3.3), and (3.4) are described.

## 4. NUMERICAL SOLUTION OF THE BWI MODEL

### 4.1 OVERVIEW

This chapter describes in detail the numerical method used to solve the bubble-wall interaction problem. A model for the BWI problem that considers the effect of the wall on a deformable bubble was proposed in chapter 3. This model is complex in its one, two or three-dimensional forms, because the bubble motion and film drainage equations are non-linear and must be solved as a coupled system. Furthermore, the domain of excess pressure is variable with time and it is difficult to determine a boundary shape at each time. Hence, no analytical techniques to solve the proposed system of equations exist. In consequence, it must be solved numerically using methods based on Finite Difference techniques.

The process in which a differential equation is approximated by a finite difference equation (FDE) is called *discretization*. The discretization both in space and in time of the system of equations derived in previous chapters is also explained in detail.

For the problem of a bubble interacting with a horizontal wall, the 1D-BWI model from section 3.2 is used and for the problem of a bubble interacting with an inclined wall, the 3D-BWI model from section 3.4 is used. Note that the 3D-BWI model is sufficiently general because it can be reduced to two dimensions when one angle is zero and to one dimension when the two angles are zero (see Fig. 3.1).

## 4.2 INTERACTION OF A BUBBLE WITH A HORIZONTAL WALL

### 4.2.1 Problem statement

For the interaction of a bubble with a horizontal plane wall the dimensionless system of equations and their respective ICs and BCs from section 3.2 (Eqs. (3.65-3.67) and (3.70)) are solved numerically. Replacing Eq. (3.67) in Eq. (3.66), the system of equations is reduced to two equations, a non-linear Ordinary Differential Equation (ODE) and a non-linear Partial Differential Equation (PDE) for the bubble velocity  $V^*(t^*)$  and the film height  $h^*(r^*, t^*)$ .

The problem statement can be written as follows,

*Non-dimensional bubble motion equation (ODE)*

$$\frac{2}{3} \left( \frac{\rho_b}{\rho_l} + C_{am} \right) \frac{dV^*}{dt^*} = -\frac{1}{3} \frac{Eo}{We} - \frac{C_d Re_V V^*}{4Re} + \frac{2}{We} (r_{max}^*)^2 + \frac{2}{We} \frac{hnd}{R} \int_0^{r_{max}^*} p^* r^* dr^* \quad (4.1)$$

with the initial conditions

$$at \ t^* = 0 \quad \left\{ \begin{array}{l} V^*(0) = -1 \\ p^*(r^*, 0) = -2 \frac{R}{hnd} \end{array} \right. \quad (4.2)$$

*Non-dimensional film drainage equation (PDE)*

$$C_1 \frac{\partial h^*}{\partial t^*} = -\frac{h^{*2}}{r^{*3}} \left\{ \begin{array}{l} h^* \frac{\partial h^*}{\partial r^*} - h^* \hat{r} \frac{\partial^2 h^*}{\partial r^{*2}} + 2h^* r^{*2} \frac{\partial^3 h^*}{\partial r^{*3}} - 3r^* \left( \frac{\partial h^*}{\partial r^*} \right)^2 + \\ 3r^{*2} \frac{\partial h^*}{\partial r^*} \frac{\partial^2 h^*}{\partial r^{*2}} + 3r^{*3} \frac{\partial h^*}{\partial r^*} \frac{\partial^3 h^*}{\partial r^{*3}} + h^* r^{*3} \frac{\partial^4 h^*}{\partial r^{*4}} \end{array} \right. \quad (4.3)$$

with the initial condition

$$at \ t^* = 0 \quad \left\{ h^*(r^*, 0) = \frac{h_\infty}{hnd} + \frac{1}{2} \frac{R}{hnd} r^{*2} \right. \quad (4.4)$$

and boundary conditions

$$\text{at } t^* > 0 \left\{ \begin{array}{l} \left. \frac{\partial h^*}{\partial r^*} \right|_{r^*=0} = 0 \quad \text{symmetry condition} \\ \left. \frac{\partial p^*}{\partial r^*} \right|_{r^*=0} = 0 \quad \text{symmetry condition} \\ \left. \frac{\partial h^*}{\partial t^*} \right|_{r^*=r_{\max}^*} = \frac{R}{hnd} V^* = \frac{R}{hnd} \frac{dY_b^*}{dt^*} \\ \left. p^* \right|_{r^*=r_{\max}^*} = -2 \frac{R}{hnd} \end{array} \right. \quad (4.5)$$

Equation (4.3) is obtained by replacing Eq. (3.67) in Eq. (3.66) and expanding the derivatives. Since the deformation axisymmetrical as described in section 3.2, the spatial domain of the excess pressure is bounded by a circle of radius  $r^* = r_{\max}^*$ . The  $r_{\max}^*$  value varies with time. For the numerical solution we chose a constant value of  $r_{\max}^*$ , which is assumed that includes any domain of excess pressure during the bouncing process. The values of  $r_{\max}^*$  are approximated to the equivalent radius  $R$  of the bubble.

After solving for the velocity  $V^*$  we can easily determine the bubble centroid position with the following equation:

$$Y_b^*(t^*) = Y_b^*(0) + \int_0^{t^*} V^* dt^* \quad (4.6)$$

with initial condition  $Y_b^*(0) = \frac{h_\infty + R}{R}$

#### 4.2.2 Discretization of the film drainage equation

The discretization by the finite difference method approximates the derivatives to differences based on the truncation of Taylor series expansion. The approximation can be of any order. It is clear that if we take a higher order of approximation the error is reduced but the number of operations to solve the problem increases. In the present thesis, we have used

the approximation of derivatives with a Taylor series of second-order accuracy. In order to derive the difference expressions, a uniform *grid* is placed over the space coordinate  $r^*$  and time coordinate  $t^*$ . Thus, the spatial domain is divided into small grids in which the film height is assumed constant. Each small grid is represented by its central point called the *node* as shown in Fig. 4.1. Also, the time domain is divided in small grids known as *time steps*. Therefore, the discretization process produces a finite difference equation for each node and time step within the spatial and temporal domains respectively.

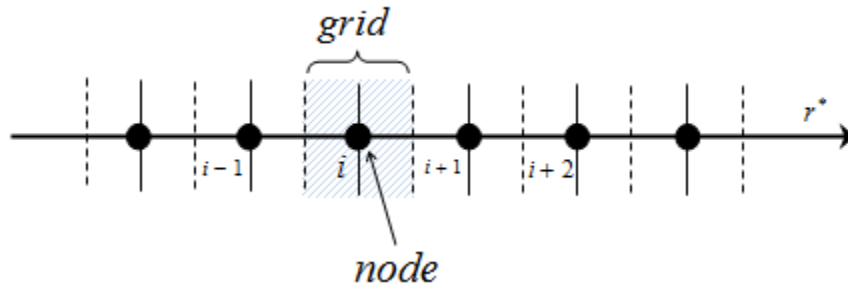


**Figure 4.1:** Discretization of spatial domain

Figure 4.2 shows the numerical domain used to numerically solve the PDE Eq. (4.3) with its respective ICs and BCs from Eqs. (4.4) and (4.5). In this figure  $\Delta r^*$  and  $\Delta t^*$  are the spatial and temporal grid sizes respectively,  $i$  represent the spatial node,  $n$  represents the time step, the total nodes in the space domain is represented by  $nr$  and the total time steps (nodes in time) is represented by  $nt$ .

The spatial discretization of the film drainage equation can be performed by the explicit or implicit method, as described below.

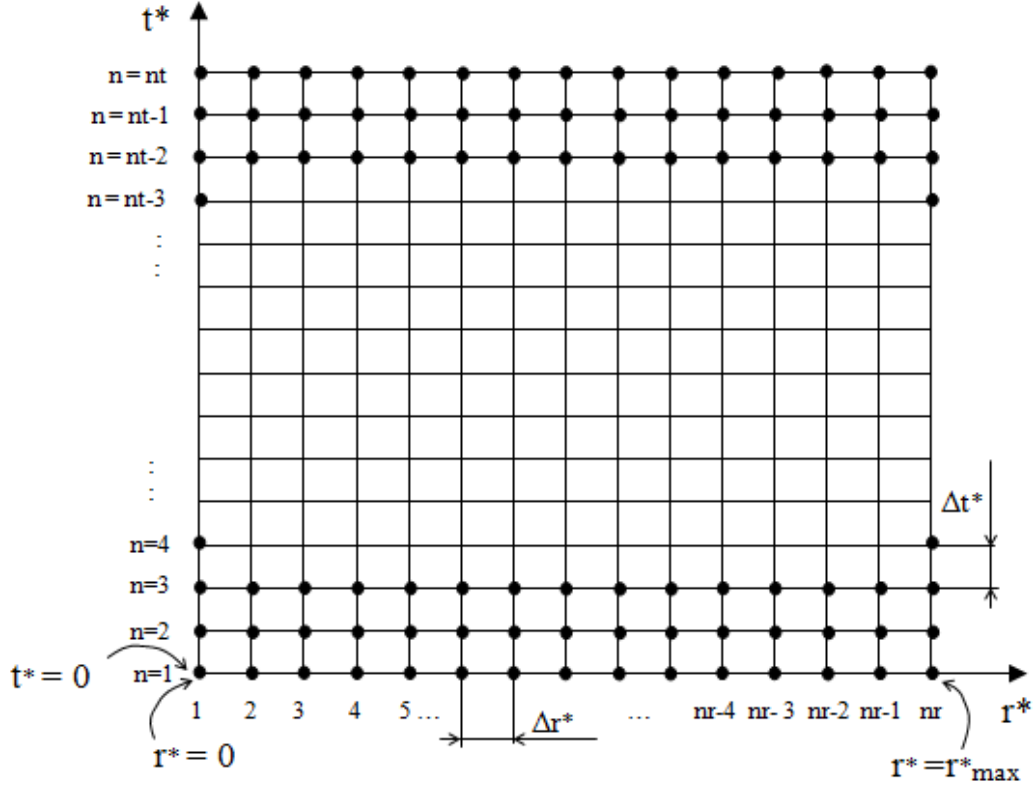
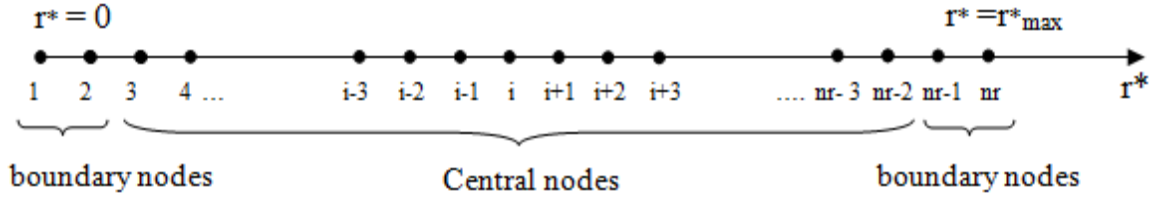


Figure 4.2: Numerical domain for 1D-BWI

#### 4.2.2.1 Explicit discretization

The central, forward and backward derivatives approximation of second-order accuracy listed in appendix B are used in the present section. The spatial derivatives in Eq. (4.3) are approximated using central derivatives. In accordance with the high order derivative in Eq. (4.3), we need a five-node stencil to derive the FDE (i.e. we need the node in question and four neighboring nodes). This implies that Eq. (4.3) can be applied only at the spatial nodes from  $i = 3$  to  $i = nr - 2$ , such nodes are called *central nodes*. The FDEs for the first two nodes and last two nodes in the spatial domain are determined using the boundary conditions Eq. (4.5). These nodes are called *boundary nodes*. Fig. 4.3 shows the central and boundary nodes.



**Figure 4.3:** Central and boundary nodes for 1D-BWI

The *explicit discretization* consists in approximating the time derivative with a backward difference in time  $n$  and the spatial derivatives with central differences in time  $n-1$ . Hence, the explicit discretization of Eq. (4.3) gives the following expression for  $h_{i,n}^*$ , which indicates the value of fluid film height  $h^*$  in the node  $i$  and time step  $n$ :

$$h_{i,n}^* = \frac{b(i-1, i-2, i, i+1, i+2, n-1, n-2)}{a}, \quad \text{for } \begin{cases} i = 3, 4, \dots, nr-2 \\ n > 2 \end{cases} \quad (4.7)$$

with  $a = \frac{3}{2} \frac{C_1}{\Delta t^*}$

Since the expression for  $b$  is large, it is shown in Eq. (C.1a) in appendix C. the constant  $b$  (Eq. (4.7)) for the node  $i$  depends on the value of  $h^*$  at four neighboring nodes at time  $n-1$  and at the node  $i$  at time  $n-2$ . This dependence is shown in Fig. 4.4.

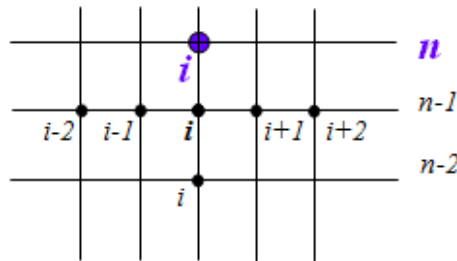


**Figure 4.4:** Explicit scheme for 1D-BWI

Applying explicit discretization to the boundary conditions (Eq. (4.5)), we obtain the following relationships for the boundary nodes (see Fig. 4.3):

$$h_{1,n}^* = \frac{9}{5}h_{3,n}^* - \frac{4}{5}h_{4,n}^* \quad (4.8)$$

$$h_{2,n}^* = \frac{8}{5}h_{3,n}^* - \frac{3}{5}h_{4,n}^* \quad (4.9)$$

$$h_{nr,n}^* = -\frac{1}{3} \frac{h_{nr,n-2}^* hnd - 4h_{nr,n-1}^* hnd - 2RV_n^* \Delta t^*}{hnd} \quad (4.10)$$

$$h_{nr-1,n}^* = -\frac{1}{6(5nr-3)} \left\{ \begin{array}{l} (4nr-1)h_{nr,n-2}^* - 4(4nr-1)h_{nr,n-1}^* - (8nr-2) \frac{RV_n^* \Delta t^*}{hnd} - \\ (24nr-21)h_{nr-2,n}^* + (6nr-6)h_{nr-3,n}^* + 12(nr-1) \frac{R\Delta r^{*2}}{hnd} \end{array} \right\} \quad (4.11)$$

Note that in Eqs. (4.10) and (4.11) the value of the bubble velocity must be known at time  $n$  to compute the fluid film height at same time in nodes  $nr$  and  $nr-1$ .

Equations (4.7), (4.10) and (4.11) required known values of film height at two previous time steps. Hence, at  $n=2$  these equations cannot be used. In order to compute the film height at the second time step, time derivative approximation of first-order accuracy is used. Therefore, we obtain similarly equations for central and boundary nodes as follows,

$$h_{i,n}^* = \frac{b(i-1, i-2, i, i+1, i+2, n-1)}{a}, \quad \text{for } \begin{cases} i = 3, 4, \dots, nr-2 \\ n = 2 \end{cases} \quad (4.12)$$

$$h_{nr,2}^* = \frac{h_{nr,1}^* hnd + RV_{n=2}^* \Delta t^*}{hnd} \quad (4.13)$$

$$h_{nr-1,2}^* = \frac{1}{2(5nr-3)} \left\{ \begin{array}{l} (4nr-1)h_{nr,1}^* + (4nr-1) \frac{RV_{n=2}^* \Delta t^*}{hnd} + (8nr-7)h_{nr-2,2}^* + \\ 2(nr-1)h_{nr-3,2}^* + 4(nr-1) \frac{R\Delta r^{*2}}{hnd} \end{array} \right\} \quad (4.14)$$

The discretization of the initial condition is straightforward, that is,

$$at t^* = 0, n = 1 \left\{ h_{i,1}^* = \frac{h_\infty}{hnd} + \frac{1}{2} \frac{R}{hnd} ((i-1)\Delta r^*)^2 \quad for i = 1,2,3...nr \quad (4.15) \right.$$

Equations (4.7-4.15) are independent i.e., each equation is fully solved at time  $n$ . The number of equations to independently solve each time step is the same as the number of spatial nodes. The advantage of the explicit method is that the algebraic effort required is minimal (Hoffmann, 2000). However, a disadvantage is that the solution is conditionally stable. Based on the code used by Moraga et al. (2005), we determined that the temporal step must be less than or equal to  $10^{-10}$  in order to obtain a stable algorithm.

#### **4.2.2.2 Implicit discretization**

The *implicit discretization* consists in approximating the time derivative with a backward difference and the spatial derivatives with central differences in time  $n$ . The central and boundary nodes as shown in Fig. 4.3 are also used for the explicit discretization.

Because of the non-linearities in Eq. (4.3), non-linear finite difference equations are obtained by the discretization process. Consequently, the linearization method based on the Taylor series expansion is used to approximate the non-linear differential equation, Eq. (4.3), to a linear differential equation.

Let a general function  $f(x_1, x_2, \dots, x_n)$  evaluated at the point  $\vec{x}_0 = (x_{10}, x_{20}, \dots, x_{n0})$ . The linearization of  $f(\vec{x})$  by Taylor series expansion around the point  $\vec{x}_0$  is expressed as follows (Hoffmann, 2000):

$$f(x_1, \dots, x_n) \approx f(x_{10}, \dots, x_{n0}) + \left. \frac{\partial f}{\partial x_1} \right|_0 (x_1 - x_{10}) + \left. \frac{\partial f}{\partial x_2} \right|_0 (x_2 - x_{20}) + \dots + \left. \frac{\partial f}{\partial x_n} \right|_0 (x_n - x_{n0}) \quad (4.16)$$

To simplify the notation, the following linear operators are defined:

$$L_p = \frac{\partial^p h^*}{\partial r^{*p}} \quad L_{p0} = \frac{\partial^p h0^*}{\partial r^{*p}} \quad \text{for } p = 1, 2, 3, 4 \quad (4.17)$$

where  $h0^*$  is a know film height profile and we use the film height at the previous time step as  $h0^*$ . Using these linear operators, Eq. (4.3) can be rewritten as,

$$C_1 \frac{\partial h^*}{\partial t^*} = \left\{ \begin{array}{l} -\frac{h^{*3}}{r^{*3}} L_1 + \frac{h^{*3}}{r^{*2}} L_2 - 2\frac{h^{*3}}{r^*} L_3 + 3\frac{h^{*2}}{r^{*2}} (L_1)^2 - \\ 3\frac{h^{*2}}{r^*} L_1 L_2 - 3h^{*2} L_1 L_3 - h^{*3} L_4 \end{array} \right\} \quad (4.18)$$

We use a function  $\Phi$  to represent the right hand side of Eq. (4.18), which is non-linear.

$$\Phi(h^*, L_1, L_2, L_3, L_4) = \left\{ \begin{array}{l} -\frac{h^{*3}}{r^{*3}} L_1 + \frac{h^{*3}}{r^{*2}} L_2 - 2\frac{h^{*3}}{r^*} L_3 + 3\frac{h^{*2}}{r^{*2}} (L_1)^2 - \\ 3\frac{h^{*2}}{r^*} L_1 L_2 - 3h^{*2} L_1 L_3 - h^{*3} L_4 \end{array} \right\} \quad (4.19)$$

Applying Eq. (4.16) to Eq. (4.19), we obtain:

$$\Phi(h^*, L_1, L_2, L_3, L_4) \approx \left\{ \begin{array}{l} \Phi(h0^*, L_{10}, L_{20}, L_{30}, L_{40}) + \left. \frac{\partial \Phi}{\partial h^*} \right|_0 (h^* - h0^*) + \left. \frac{\partial \Phi}{\partial L_1} \right|_0 (L_1 - L_{10}) \\ + \left. \frac{\partial \Phi}{\partial L_2} \right|_0 (L_2 - L_{20}) + \left. \frac{\partial \Phi}{\partial L_3} \right|_0 (L_3 - L_{30}) + \left. \frac{\partial \Phi}{\partial L_4} \right|_0 (L_4 - L_{40}) \end{array} \right\} \quad (4.20)$$

Solving the linear approximation of  $\Phi$  in last equation and replacing it in Eq. (4.18), we obtain a linear approximation of the original non-linear PDE Eq. (4.3). The expression is

presented in appendix C (Eq. (C.2)). The linear approximation of Eq. (4.3) is valid only around a known film height profile denoted by  $h_0^*$ .

Equation (C.2) is discretized by the implicit method and using second order accuracy approximation for the derivatives and it can be written as,

$$A_i h_{i-2,n}^* + B_i h_{i-1,n}^* + C_i h_{i,n}^* + D_i h_{i+1,n}^* + E_i h_{i+2,n}^* = F_i \quad \text{with, } i = 3, 4, \dots, nr - 2 \quad (4.21)$$

Eq. (4.21) applies to the central nodes shown in Fig. (4.3). The film drainage equation for each central node is represented by a FDE of the form presented by Eq. (4.21) using a five-node stencil (Fig. 4.5(a)). The constants A, B, C, D, E, and F have different values for each node and for each time step; these are shown in appendix C (Eqs. (C.3-C.7)). Fig. 4.5(b) shows that the fluid film height for a generic node  $i$  and time step  $n$  depends on the unknown fluid film height of the four neighboring nodes at the same time  $n$  and on known fluid film height of the same node  $i$  during the two previous time steps.

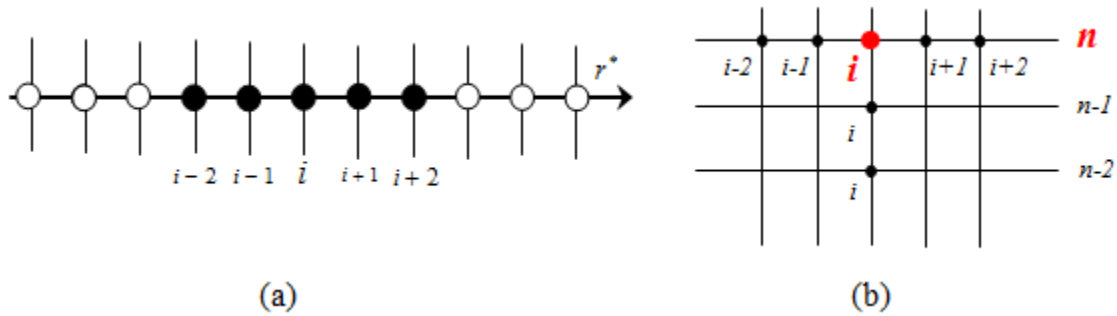


**Figure 4.5:** (a) Five point stencil represented by the filled nodes; (b) Implicit scheme for 1D-BWI

Implicit discretization of the BCs, Eq. (4.5), at  $r^* = 0$  and  $r^* = r_{\max}^*$ , gives the following equations:

Node  $i = 1$ , BCs at  $r^* = 0$  (Fig. 4.3)

$$C_1 h_{1,n}^* + D_1 h_{2,n}^* + E_1 h_{3,n}^* = 0 \quad (4.22)$$

Node  $i = 2$  , BCs at  $r^* = 0$  (Fig. 4.3)

$$B_2 h_{1,n}^* + C_2 h_{2,n}^* + D_2 h_{3,n}^* + E_2 h_{4,n}^* = 0 \quad (4.23)$$

Node  $i = nr - 1$  , BCs at  $r^* = r_{\max}^*$  (Fig. 4.3)

$$A_{nr-1} h_{nr-3,n}^* + B_{nr-1} h_{nr-2,n}^* + C_{nr-1} h_{nr-1,n}^* + D_{nr-1} h_{nr,n}^* = \frac{2R}{hnd} (\Delta r^*)^2 \quad (4.24)$$

Node  $i = nr$  , BCs at  $r^* = r_{\max}^*$  (Fig. 4.3)

$$C_{nr} h_{nr,n}^* = 2h_{nr,n-1}^* - \frac{1}{2} h_{nr,n-2}^* + \frac{R}{hnd} V_n^* \Delta t^* \quad (4.25)$$

where:

$$C_1 = -3 \quad , \quad D_1 = 4 \quad , \quad E_1 = -1 \quad , \quad C_{nr} = 3/2$$

$$B_2 = -2 \quad , \quad C_2 = 1 \quad , \quad D_2 = 2 \quad , \quad E_2 = -1$$

$$A_{nr-1} = -1 \quad , \quad B_{nr-1} = \left( 4 + \frac{1}{2(nr-1)} \right) \quad , \quad C_{nr-1} = \left( -5 - \frac{2}{nr-1} \right) \quad , \quad D_{nr-1} = \left( 2 + \frac{3}{2(nr-1)} \right)$$

Unlike the explicit method, in the implicit method, each node is represented by a FDE with more than one unknown. The computation of the unknowns requires a set of  $nr$  coupled FDEs which need to be solved simultaneously. These equations can be put in a linear system of equations. Since each equation depends on the values of  $h^*$  at 5 different nodes, the coefficients of the FDEs are organized in a pentadiagonal band matrix. A schematic form of this linear system is expressed as follows,

$$\begin{bmatrix}
C_1 & D_1 & E_1 & & & \dots & 0 & 0 \\
B_2 & C_2 & D_2 & E_2 & & & & 0 \\
A_3 & B_3 & C_3 & \ddots & \ddots & & & \vdots \\
& A_4 & \ddots & \ddots & & & & \\
& & \ddots & & & & & \\
& & & \ddots & \ddots & & E_{nr-3} & \\
\vdots & & & \ddots & \ddots & C_{nr-2} & D_{nr-2} & E_{nr-2} \\
0 & & & A_{nr-1} & B_{nr-1} & C_{nr-1} & D_{nr-1} & \\
0 & 0 & \dots & & A_{nr} & B_{nr} & C_{nr} & \\
\end{bmatrix}
\begin{bmatrix}
h_{1,n}^* \\
h_{2,n}^* \\
\vdots \\
h_{nr-2,n}^* \\
h_{nr-1,n}^* \\
h_{nr,n}^*
\end{bmatrix}
=
\begin{bmatrix}
F_1 \\
F_2 \\
\vdots \\
F_{nr-2} \\
F_{nr-1} \\
F_{nr}
\end{bmatrix}
\tag{4.26}$$

The discretized initial condition in this case is equal to Eq. (4.15)

A disadvantage of the implicit discretization is that it requires more computation time per time step (Hoffman, 2001). The great advantage that it offers is the stability of the linear system obtained, since it is unconditionally stable; which implies that use of a larger time step is permitted. However, the choice of a larger time step is limited due to the required accuracy, because if the time step increases the error made on the approximation of the time derivative increases.

### 4.2.3 Discretization of the bubble motion equation

The ordinary differential equation that governs the bubble motion (Eq. (4.1)) is non-linear. Since the  $Re_V$  depends on the instantaneous bubble velocity  $V^*$ , the non-dimensional drag force represented by the second term on the right hand side of Eq. (4.1) is non-linear. The non-dimensional buoyancy force which does not depend on  $V^*$  is represented by the first term of right hand side and, the non-dimensional wall force corresponds to the two last terms.

To compute these last two terms the instantaneous film thickness profile  $h^*$  needs to be known. In order to numerically solve this equation, two discretization methods based on second-order accuracy derivative approximation are used. These methods are the explicit and implicit discretization as described below.

#### 4.2.3.1 Explicit discretization

The explicit discretization of Eq. (4.1) is based on the explicit computation of drag and BWI forces as follows,

$$F_d^* = -\frac{C_d \text{Re}_{V_{n-1}} V_{n-1}^*}{4 \text{Re}} \quad (4.27)$$

$$F_w^* = \frac{2}{We} (r_{\max}^*)^2 + \frac{2}{We} \frac{hnd}{R} \int_0^{r_{\max}^*} p_{n-1}^* r^* dr^* \quad (4.28)$$

where both the drag and BWI forces are evaluated in the previous time step  $n-1$ . Hence, using the backward time derivative (see appendix B) and Eqs. (4.27) and (4.28), the discretized Eq. (4.1) can be written as,

$$V_n^* = \frac{2 \text{independent}}{3 \text{aux}} + \frac{4}{3} V_{n-1}^* - \frac{1}{3} V_{n-2}^* \quad \text{for } n = 3, 4, \dots, nt \quad (4.29)$$

With

$$\text{aux} = \frac{1}{\Delta t^*} \frac{2}{3} \left( \frac{\rho_b}{\rho_l} + C_{am} \right)$$

$$FP = \int_0^{r_{\max}^*} p_{n-1}^* r^* dr^*$$

$$\text{independent} = -\frac{1}{3} \frac{Eo}{We} - \frac{C_d \text{Re}_{V_{n-1}} V_{n-1}^*}{4 \text{Re}} + \frac{2}{We} \left( (nr-1) \Delta r^* \right)^2 + \frac{2}{We} \frac{hnd}{R} FP$$

Then, the bubble centroid velocity can be directly computed from Eq. (4.29) which has only one unknown. Since we used second-order accuracy to approximate the derivatives, Eq.

(4.29) needs the velocity values at two previous time steps to solve for the velocity at the present step. Therefore, it is strictly valid from  $n = 3, 4, \dots, nt$ . For the first temporal step, the initial condition is used. Since the bubble initially moves at a terminal velocity,  $V_{n=1}^* = -1 = V_{n=2}^*$  is used.

In order to solve for the expression FP, trapezoidal rule for integration is used (Nakamura, 1992),

$$FP := \int_0^{r_{\max}^*} p^* r^* dr^* = \sum_{i=1}^{i=nr-1} \left\{ \frac{p_{i,n-1}^* r_{i,n-1}^* + p_{i+1,n-1}^* r_{i+1,n-1}^*}{2} \Delta r^* \right\} \quad (4.30)$$

with  $i = 1, 2, \dots, nr - 1$  and  $r_i^* = (i - 1)\Delta r^*$

where the discretized non-dimensional excess pressure  $p$  is given by,

$$\left. \begin{aligned} p_{i,n}^* &= -\frac{h_{i+1,n}^* - h_{i-1,n}^*}{2(i-1)\Delta r^{*2}} - \frac{h_{i+1,n}^* - 2h_{i,n}^* + h_{i-1,n}^*}{\Delta r^{*2}} & \text{for } i = 2, 3, \dots, nr - 1 \\ p_{1,n}^* &= \frac{4}{3} p_{2,n}^* - \frac{1}{3} p_{3,n}^* & \text{for } i = 1 \quad \text{BC at } r^* = 0 \\ p_{nr,n}^* &= -2 \frac{R}{hnd} & \text{for } i = nr \quad \text{BC at } r^* = r_{\max}^* \end{aligned} \right\} \quad (4.31)$$

#### 4.2.3.2 Implicit discretization

In our case, the implicit discretization of Eq. (4.1) is based on an explicit computation of the wall force but an implicit computation of the drag force. The BWI force is still evaluated using Eq. (4.28), but the implicit treatment of the drag force yields

$$F_d^* = -\frac{C_d Re_v V_n^*}{4Re} \quad (4.32)$$

$$\text{with, } Re_v = Re |V_n^*| \quad (4.33)$$

Hence, the discretized Eq. (4.1) is written as,

$$V_n^* = \frac{aux(2V_{n-1}^* - 0.5V_{n-2}^*) + independent1}{denom} \quad \text{for } n = 3, 4, \dots, nt \quad (4.34)$$

where:

$$denom := \frac{3}{2}aux + \frac{C_d Re_v}{4Re}$$

$$independent1 := -\frac{1}{3} \frac{Eo}{We} + \frac{2}{We} ((nr-1)\Delta r^*)^2 + \frac{2}{We} \frac{hnd}{R} FP$$

As the instantaneous Reynolds number  $Re_v$  depends on  $V^*$  at time  $n$ , Eq. (4.34) is solved using an iterative method. An initial guess for the bubble velocity denoted by  $V_p^*$  is assumed and the Reynolds number is computed as,

$$Re_v = Re|V_p^*| \quad (4.35)$$

We have chosen the known value of velocity in previous time  $n-1$  as the initial guess. Replacing Eq. (4.35) in Eq. (4.34) gives a new value for bubble velocity,  $V^*$ . The procedure is repeated substituting the bubble velocity guess for the new value of bubble velocity until a tolerance of  $10^{-13}$  is reached.

#### 4.2.4 Computational algorithms

In order to solve the one-dimensional bubble-wall interaction model in numerical form as described in sections 4.2.2 and 4.2.3, two computational codes have been developed using FORTRAN 90 computer language. The first code, called the *explicit code*, solves the bubble motion and the fluid film drainage equations using explicit discretization as detailed in sections 4.2.2.1 and 4.2.3.1. The second code, called the *implicit code*, solves the bubble motion and the fluid film drainage equations using implicit discretization as detailed in sections 4.2.2.2 and 4.2.3.2.

*Explicit coupling* is used to couple the system of equations in both codes. The bubble centroid velocity at a particular time step is computed using the excess pressure at a previous time step.

In this section, we have described the general steps of the explicit and implicit codes. The programming details can be found in the flowcharts and the codes presented in appendix D.

#### **4.2.4.1 Algorithm of the explicit 1D-BWI code**

The general steps of this algorithm are the following:

- I. At the initial time  $t = 0$  ( $n = 1$ ) or for the first time step, the initial conditions such as the bubble velocity  $\vec{V} = \vec{V}_T$  ( $V_{n=1}^* = -1$ ) and the excess pressure  $p = 0$  ( $p^* = -2R/hnd$ ) from Eq. (4.2) and the parabolic film height profile  $h_{i,n=1}^*$  from Eq. (4.15) are used.
- II. At time  $t = 1\Delta t$  ( $n = 2$ ) or for the second time step:
  - a) Compute FP and the BWIF ( $F_w^*$ ), using the excess pressure established in I. Use Eq. (4.30).
  - b) As the bubble at the second time step is still not deformed, the result of (a) will be zero. Hence, at  $n=2$   $V_{n=2}^* = -1$  is used.
  - c) The fluid film height profile in the second time step,  $h_{i,n=2}^*$ , is determined with the result of (b) for using the discretized PDE (Eq. 4.12) and its respective BCs (Eqs. (4.8), (4.9), (4.13) and (4.14)).
- III. At time  $t = 2\Delta t$  ( $n = 3$ ) or for the third time step:

- a) With the fluid film height profile determined at the previous time step (i.e.,  $h_{i,n=2}^*$ ) we compute the excess pressure using Eq. (4.31).
  - b) With the results of (a), we compute the part of the film force expressed by FP in Eq. (4.30).
  - c) With the result of (b) we solve for the bubble velocity at the present time step (i.e.,  $V_{n=3}^*$ ) using the discretized ODE (Eq. 4.29).
  - d) With the result of (c) for the present velocity, the fluid film height profile at the present time step (i.e.,  $h_{i,n=3}^*$ ) using the discretized PDE, Eq. (4.7), and its respective BCs (Eqs. (4.8-4.11)) is determined.
- IV. Steps (a), (b), (c) and (d) as described in item III are repeated in the same order for all the remaining time steps until the final time step  $n = nt$  is reached.

The computer code uses two modules, the *physical module* and the *numerical module*, in which the used global variables are defined. The structure of the main program called *Exp\_ID\_BWI* is shown Fig. 4.6 as well as the structure of three principal subroutines shown in Fig. D1-D4.

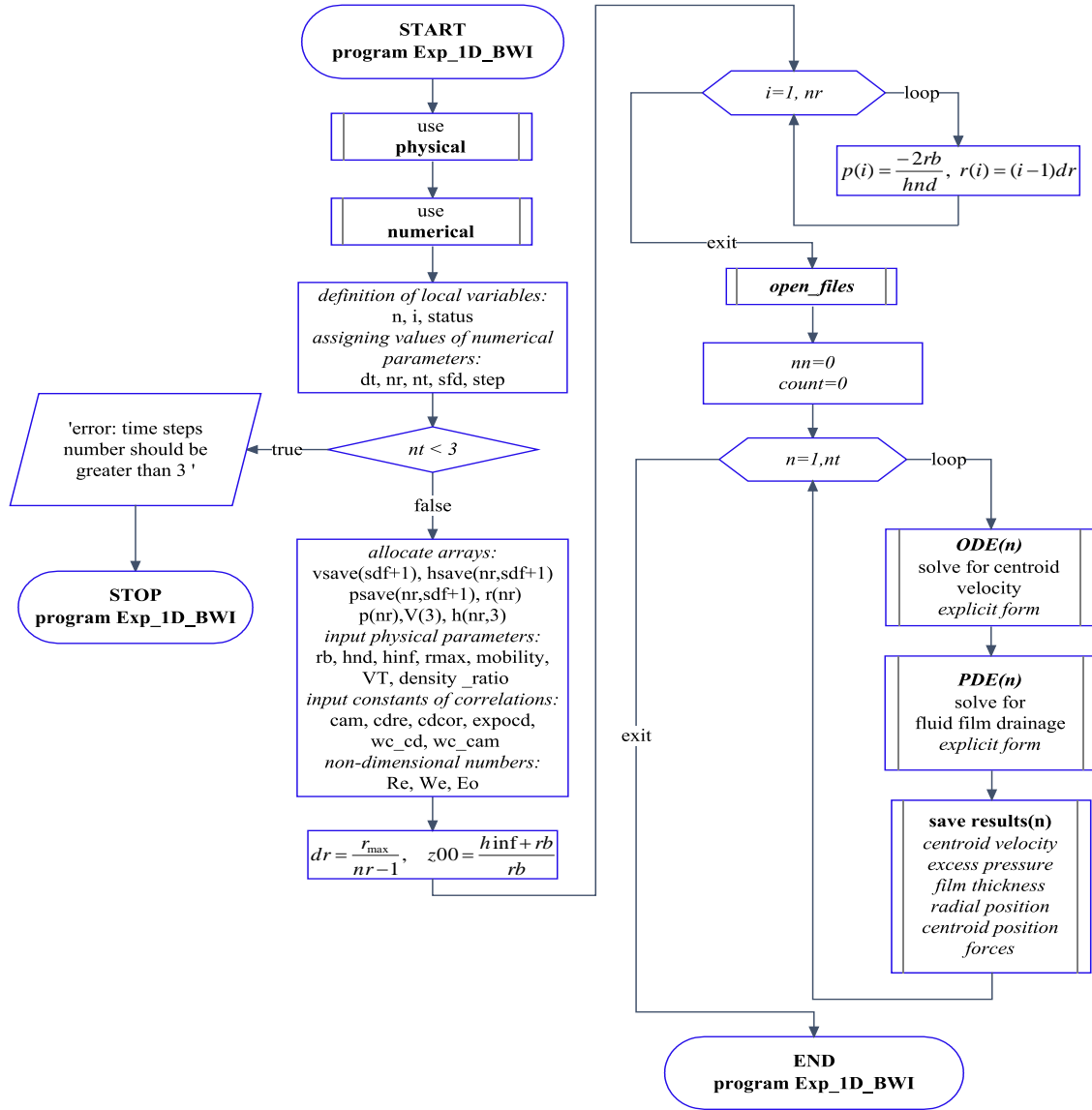


Figure 4.6: Structure of the main program *Exp\_1D\_BWI*

#### 4.2.4.2 Algorithm of the implicit 1D-BWI code

The general steps of this algorithm are the following:

- I. At the initial time  $t = 0$  ( $n = 1$ ) or for the first time step, the initial conditions such as bubble velocity  $\vec{V} = \vec{V}_T$  ( $V_{n=1}^* = -1$ ) and excess pressure  $p = 0$  ( $p^* = -2R/hnd$ )

from Eq. (4.2) and parabolic film height profile  $h_{i,n=1}^*$  from Eq. (4.15) are established.

- II. At time  $t = 1\Delta t$  ( $n = 2$ ) or for the second time step, the bubble terminal velocity,  $\vec{V} = \vec{V}_T$  ( $V_{n=2}^* = -1$ ) and zero excess pressure  $p = 0$  ( $p^* = -2R/hnd$ ) are still used. It is reasonable to use the terminal velocity in the second time step because the bubble is still without significant deformation. In consequence, the fluid film height profile  $h_{i,n=2}^* = h_{i,n=1}^* + V_{n=1}^* \Delta t^* R / hnd$  is used at  $n=2$ .
- III. At time  $t = 2\Delta t$  ( $n = 3$ ) or for the third time step:
- a) With the fluid film height profile determined in the previous time step (i.e.,  $h_{i,n=2}^*$ ), the excess pressure is computed using Eq. (4.31).
  - b) The results of (a) are used to compute the part of the film force expressed by FP in Eq. (4.30).
  - c) We solve for bubble velocity at the present time step (i.e.,  $V_{n=3}^*$ ) with the result from (b) using the discretized ODE (Eq. (4.34)). This equation is solved via iteration until an established tolerance is reached.
  - d) With the results from (c) for the present velocity, the fluid film height profile at the present time step (i.e.,  $h_{i,n=3}^*$ ) is determined by solving the linear system of FDEs Eq. (4.26). To solve this linear system, an equilibrium value of fluid film height,  $h0^*$ , is required. We use  $h0^* = h_{i,n=1}^*$ , and after solving the linear system, the present and previous film height profile are compared. The  $h0^*$  is updated, the system of equations is solved to determine the new film profile,

and again the comparison is performed. The procedure is continued until an accuracy of  $10^{-10}$  is reached.

IV. The steps (a), (b), (c) and (d) as described in item III are repeated in the same order until the final time step  $n = nt$  is reached.

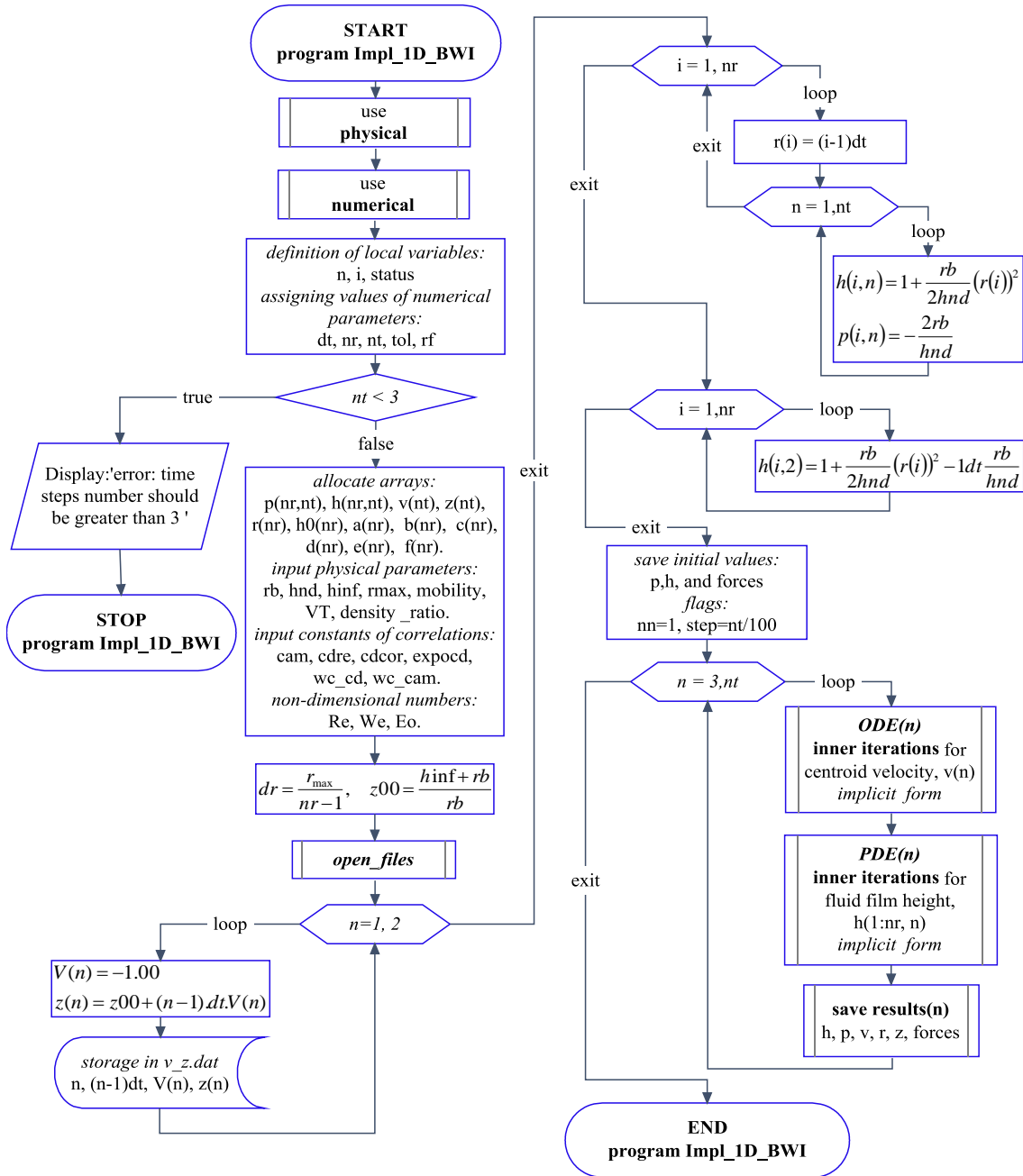


Figure 4.7: Structure of the main program *Impl\_1D\_BWI*

The implicit computer code uses two modules, the *physical module* and the *numerical module*, in which the used global variables are defined. The structure of the main program called *Impl\_1D\_BWI* is shown in Fig. 4.7. The structure of the two principal subroutines of the ODE and the PDE (see Fig. 4.7) are presented in appendix D in Figs. D5 and D6 respectively.

### 4.3 INTERACTION OF A BUBBLE WITH AN INCLINED WALL

#### 4.3.1 Problem statement

In section 3.4 we developed the 3D-BWI model in Cartesian coordinates that considers two inclinations as shown in Fig. 3.1 and Fig. 3.2. This model can be reduced to 2D-BWI (as in section 3.3) and 1D-BWI (as in section 3.2). In accordance with the work of Klaseboer et al. (2001) and Moraga et al. (2005), the 1D-BWI model in cylindrical coordinates has been solved using the discretization detailed in section 4.2. The bubble tangential velocities that appear in two or three dimensions affect the deformation in the tangential directions; thereby, the axisymmetric deformation assumption is no longer valid. Therefore, the use of cylindrical coordinates in these cases is not appropriate because the excess pressure variation in the  $\gamma$  direction is no longer constant and because establishing the boundary of the excess pressure domain is not straightforward. Therefore, we discretized the equation system of 3D-BWI model in Cartesian coordinates in which a square boundary interface is defined as:  $|x| = r_{\max}$  ,  $|z| = r_{\max}$  with  $r_{\max} \approx R$ . We expect the excess pressure variations to be significant only near the very top part of the bubble facing the wall; therefore, the exact boundary for the excess pressure domain should be irrelevant. This

assumption must be verified a posteriori. Hence, considering a square spatial domain of width  $2r_{\max}$  the 3D-BWI model derived in section 3.4 (Eqs. (3.98-3.103)) is solved numerically.

Replacing Eq. (3.96) in Eq. (3.95) the system of equations is reduced to five equations: three non-linear Ordinary Differential Equations (ODEs) a non-linear Partial Differential Equation (PDE) for the bubble velocity  $\vec{V}^* = U^*(t^*)\hat{i} + V^*(t^*)\hat{j} + W^*(t^*)\hat{k}$ , and the film height  $h^*(x^*, z^*, t^*)$  respectively. Therefore, the statement of the problem can be written as follows:

*Non-dimensional bubble motion equations (ODEs)*

$$\frac{2}{3} \left( \frac{\rho_b}{\rho_l} + C_{am} \right) \frac{d\vec{V}^*}{dt^*} = \frac{1}{3} \frac{Eo}{We} \hat{e}_b - \frac{C_d \text{Re}_V \vec{V}^*}{4 \text{Re}} + \vec{F}_w^* \quad (4.36)$$

with the initial conditions,

$$at \ t^* = 0 \quad \left\{ \begin{array}{l} \vec{V}^*(0) = \vec{V}_T^* = 1\hat{e}_b \\ p^*(x^*, z^*, 0) = -2 \frac{R}{hnd} \end{array} \right. \quad (4.37)$$

*Non-dimensional film drainage equation (PDE)*

$$C_1 \left\{ \frac{\partial h^*}{\partial t^*} + \frac{U^*}{2} \frac{\partial h^*}{\partial x^*} + \frac{W^*}{2} \frac{\partial h^*}{\partial z^*} \right\} = - \left\{ \begin{array}{l} 3h^{*2} \frac{\partial h^*}{\partial x^*} \frac{\partial^3 h^*}{\partial x^{*3}} + h^{*3} \frac{\partial^4 h^*}{\partial x^{*4}} + 3h^{*2} \frac{\partial h^*}{\partial x^*} \frac{\partial^3 h^*}{\partial x^* \partial z^{*2}} + \\ 2h^{*3} \frac{\partial^4 h^*}{\partial x^{*2} \partial z^{*2}} + 3h^{*2} \frac{\partial h^*}{\partial z^*} \frac{\partial^3 h^*}{\partial z^* \partial x^{*2}} + \\ 3h^{*2} \frac{\partial h^*}{\partial z^*} \frac{\partial^3 h^*}{\partial z^{*3}} + h^{*3} \frac{\partial^4 h^*}{\partial z^{*4}} \end{array} \right\} \quad (4.38)$$

with ICs and BCs

$$\text{at } t^* = 0 \left\{ h^*(x^*, z^*, 0) = \frac{h_\infty}{hnd} + \frac{1}{2} \frac{R}{hnd} (x^{*2} + z^{*2}) \right. \quad (4.39)$$

$$\text{at } t^* > 0 \left\{ \begin{aligned} \left. \frac{\partial h^*}{\partial t^*} \right|_{\text{squareboundary } S^*} &= \frac{R}{hnd} V^* = \frac{R}{hnd} \frac{dY_b^*}{dt^*} \\ p^* \Big|_{\text{squareboundary } S^*} &= -2 \frac{R}{hnd} \end{aligned} \right. \quad (4.40)$$

where

$$P^* = - \left( \frac{\partial^2 h^*}{\partial x^{*2}} + \frac{\partial^2 h^*}{\partial z^{*2}} \right) \quad (4.41)$$

$$\vec{V}^* = \begin{bmatrix} U^* \\ V^* \\ W^* \end{bmatrix} \quad (4.42)$$

$$\hat{e}_b = \begin{bmatrix} \sin(\theta) \\ -\cos(\theta) \cos(\alpha) \\ \cos(\theta) \sin(\alpha) \end{bmatrix} \quad (4.43)$$

$$\vec{F}_w^* = \left[ \begin{aligned} & - \frac{2}{\pi We} \frac{hnd}{R} \left\{ \int_{-z_{\max}^*}^{z_{\max}^*} \int_{-x_{\max}^*}^{x_{\max}^*} \frac{\partial h^*}{\partial x^*} dx^* dz^* + \left( \frac{hnd}{2R} \right) \int_{-z_{\max}^*}^{z_{\max}^*} \int_{-x_{\max}^*}^{x_{\max}^*} p^* \frac{\partial h^*}{\partial x^*} dx^* dz^* \right\} \\ & + \frac{2}{\pi We} \left\{ 4(r_{\max}^*)^2 + \left( \frac{hnd}{2R} \right) \int_{-z_{\max}^*}^{z_{\max}^*} \int_{-x_{\max}^*}^{x_{\max}^*} p^* dx^* dz^* \right\} \\ & - \frac{2}{\pi R We} \left\{ \int_{-z_{\max}^*}^{z_{\max}^*} \int_{-x_{\max}^*}^{x_{\max}^*} \frac{\partial h^*}{\partial z^*} dx^* dz^* + \left( \frac{hnd}{2R} \right) \int_{-z_{\max}^*}^{z_{\max}^*} \int_{-x_{\max}^*}^{x_{\max}^*} p^* \frac{\partial h^*}{\partial z^*} dx^* dz^* \right\} \end{aligned} \right] \quad (4.44)$$

$$x_{\max}^* = z_{\max}^* = r_{\max}^* \quad (4.45)$$

After solving for the bubble velocity,  $\vec{V}^*$ , we can determine easily the bubble centroid

position,  $\chi_b^*(t^*)$ , using the following equation,

$$\chi_b^*(t^*) = \chi_b^*(0) + \int_0^{t^*} \vec{V}^* dt^* \quad (4.46)$$

with

$$\chi_b^* = \begin{bmatrix} X_b^* \\ Y_b^* \\ Z_b^* \end{bmatrix} \quad (4.47)$$

$$\chi_b^*(0) = \begin{bmatrix} 0 \\ \frac{h_\infty + R}{R} \\ 0 \end{bmatrix} \quad (4.48)$$

### 4.3.2 Discretization of the film drainage equation

In order to numerically solve the film drainage equation, Eq. (4.38), in Cartesian coordinates, the implicit method is used. Eq. (4.38) needs to be linearized. To simplify the notation the following linear operators are defined:

$$LX_p := \frac{\partial^p h^*}{\partial x^{*p}} \quad , \quad LX_{p0} := \frac{\partial^p h0^*}{\partial r^{*p}} \quad \text{for } p = 1, 2, 3, 4 \quad (4.49)$$

$$LZ_p := \frac{\partial^p h^*}{\partial z^{*p}} \quad , \quad LZ_{p0} := \frac{\partial^p h0^*}{\partial z^{*p}} \quad \text{for } p = 1, 2, 3, 4 \quad (4.50)$$

$$LA := \frac{\partial^3 h^*}{\partial x^* \partial z^{*2}} \quad , \quad LA_0 := \frac{\partial^3 h0^*}{\partial x^* \partial z^{*2}} \quad (4.51)$$

$$LB := \frac{\partial^3 h^*}{\partial z^* \partial x^{*2}} \quad , \quad LB_0 := \frac{\partial^3 h0^*}{\partial z^* \partial x^{*2}} \quad (4.52)$$

$$LXZ := \frac{\partial^4 h^*}{\partial x^{*2} \partial z^{*2}} \quad , \quad LXZ_0 := \frac{\partial^4 h0^*}{\partial x^{*2} \partial z^{*2}} \quad (4.53)$$

where  $h0^*$  is a known film height profile. Using these linear operators, Eq. (4.38) can be rewritten as,

$$C_1 \left\{ \frac{\partial h^*}{\partial t^*} + \frac{U^*}{2} LX_1 + \frac{W^*}{2} LZ_1 \right\} = - \left\{ \begin{array}{l} 3h^{*2} LX_1 LX_3 + h^{*3} LX_4 + 3h^{*2} LX_1 LA + \\ 2h^{*3} LXZ + 3h^{*2} LZ_1 LB + \\ 3h^{*2} LZ_1 LZ_3 + h^{*3} LZ_4 \end{array} \right\} \quad (4.54)$$

The right hand side of Eq. (4.54) contains all the non-linear terms with respect to the dependent variable  $h^*$ . These terms are linearized using the function  $\varphi$ , where  $\varphi$  can be written as,

$$\varphi = \left\{ \begin{array}{l} 3h^{*2} LX_1 LX_3 + h^{*3} LX_4 + 3h^{*2} LX_1 LA + 2h^{*3} LXZ + \\ 3h^{*2} LZ_1 LB + 3h^{*2} LZ_1 LZ_3 + h^{*3} LZ_4 \end{array} \right\} \quad (4.55)$$

Applying Eq. (4.16) to Eq. (4.55), we obtain:

$$\varphi \approx \left\{ \begin{array}{l} \left. \varphi|_0 + \frac{\partial \varphi}{\partial h^*} \Big|_0 (h^* - h0^*) + \frac{\partial \varphi}{\partial LX_1} \Big|_0 (LX_1 - LX_{10}) + \frac{\partial \varphi}{\partial LX_3} \Big|_0 (LX_3 - LX_{30}) + \right. \\ \left. \frac{\partial \varphi}{\partial LX_4} \Big|_0 (LX_4 - LX_{40}) + \frac{\partial \varphi}{\partial LZ_1} \Big|_0 (LZ_1 - LZ_{10}) + \frac{\partial \varphi}{\partial LZ_3} \Big|_0 (LZ_3 - LZ_{30}) + \right. \\ \left. \frac{\partial \varphi}{\partial LZ_4} \Big|_0 (LZ_4 - LZ_{40}) + \frac{\partial \varphi}{\partial LA} \Big|_0 (LA - LA_0) + \frac{\partial \varphi}{\partial LB} \Big|_0 (LB - LB_0) + \right. \\ \left. \frac{\partial \varphi}{\partial LXZ} \Big|_0 (LXZ - LXZ_0) \right\} \quad (4.56)$$

Replacing the linear approximation of  $\varphi$  (Eq. (4.56)) in Eq. (4.54) we obtain a linear approximation of the original non-linear PDE Eq. (4.38). The final expression is presented in appendix B (Eq. (B.9)). The linear approximation of Eq. (4.38) is valid only around of a known film height profile denoted by  $h0^*$ .

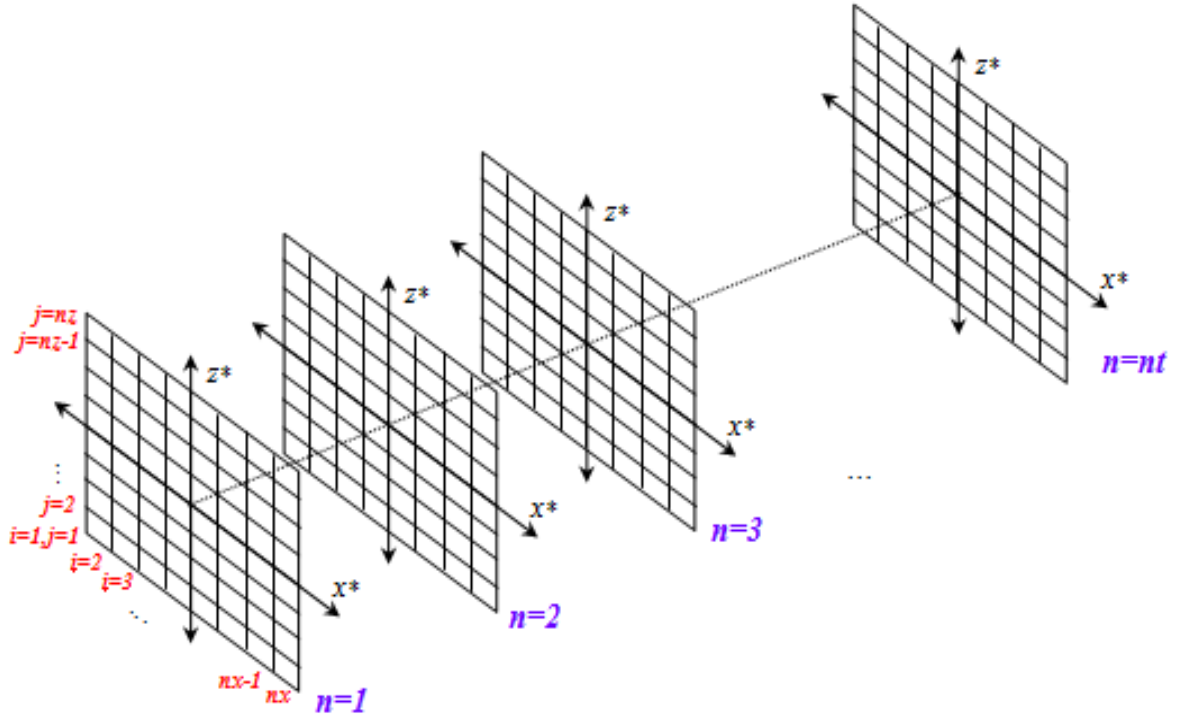


**Figure 4.8:** Numerical domain for BWI in Cartesian coordinates

The discrete numerical domain for 3D-BWI (the same discretization is used for 2D-BWI and 1D-BWI in Cartesian coordinates) is sketched in Fig. 4.8 in which  $nx$  and  $nz$  represent the total nodes in  $x$ -direction and  $z$ -direction respectively and  $nt$  represents the total nodes in time (total time steps). Fig. 4.9 provides a sketch of the spatial domain at any time, where the grid size is  $\Delta x^* \Delta z^*$  and the total number of nodes in the square domain is given by  $nd = nxnz$ . The spatial nodes are denoted by  $i$  and then it can take values from 1 to  $nd$ . The time steps are denoted by  $n$ .

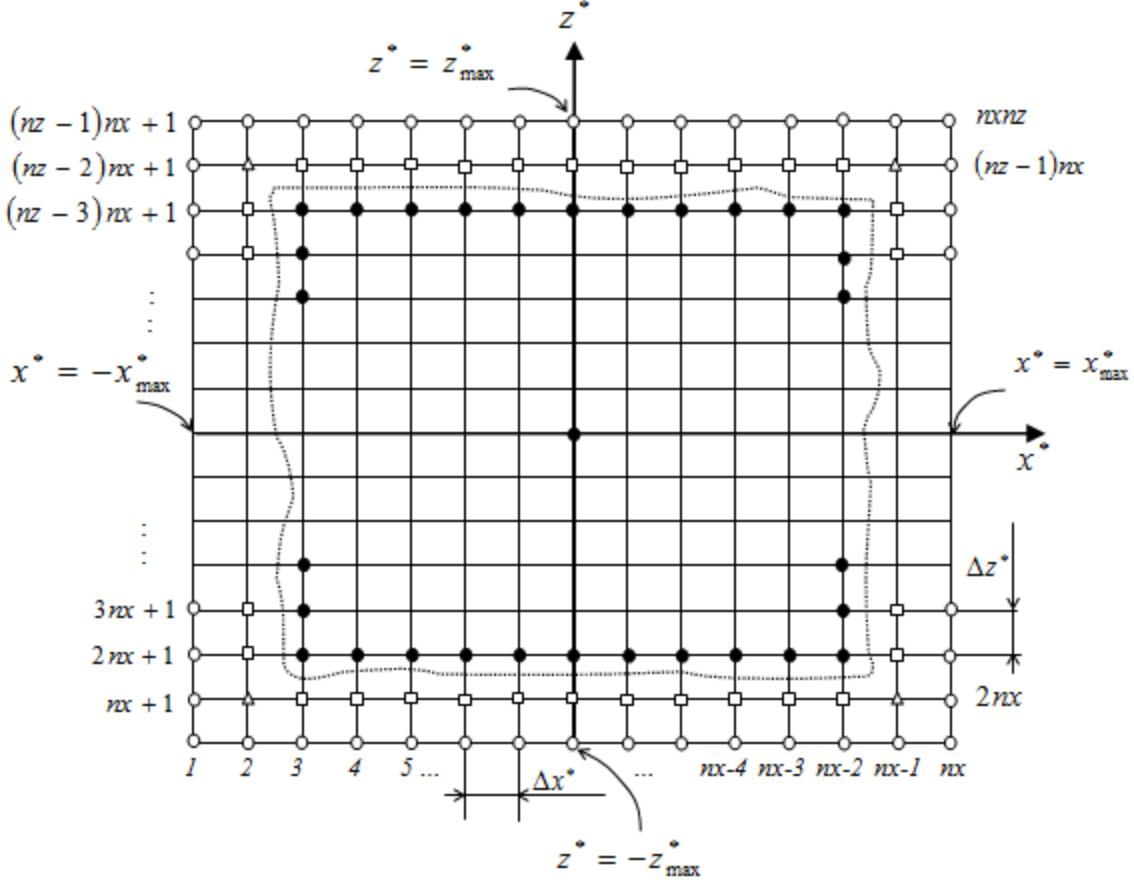


**Figure 4.9:** Discrete spatial domain for BWI in Cartesian coordinates: Open symbols as the square, circle and triangle are called *boundary nodes* and the closed circles within the discontinuous closed line are called *central nodes*.

Equation (C.9) (from appendix C) discretized by the implicit method using derivatives approximation of second-order accuracy (approximations of high order and mixed derivatives are shown in appendix B) can be written as,

$$\left\{ \begin{aligned} &D_1 h_{i-2nx,n}^* + D_2 h_{i-nx-1,n}^* + D_3 h_{i-nx,n}^* + D_4 h_{i-nx+1,n}^* + D_5 h_{i-2,n}^* + D_6 h_{i-1,n}^* + D_7 h_{i,n}^* \\ &+ D_8 h_{i+1,n}^* + D_9 h_{i+1,n}^* + D_{10} h_{i+2,n}^* + D_{11} h_{i+nx-1,n}^* + D_{12} h_{i+nx+1,n}^* + D_{13} h_{i+2nx,n}^* \end{aligned} \right\} = f \quad (4.57)$$

Eq. (4.57) applies only for the central nodes shown in Fig. 4.9. The film drainage equation for each central node is represented by a FDE as Eq. (4.57) using a thirteen-node stencil as shown at time  $n$  in Fig. 4.10. The constants  $D_m$  (with  $m=1,2,..13$ ) and  $f$  (see Eq. (4.57)) have

different values for each node and for each time step as presented in Appendix C (Eqs. (C.10-C.25)).

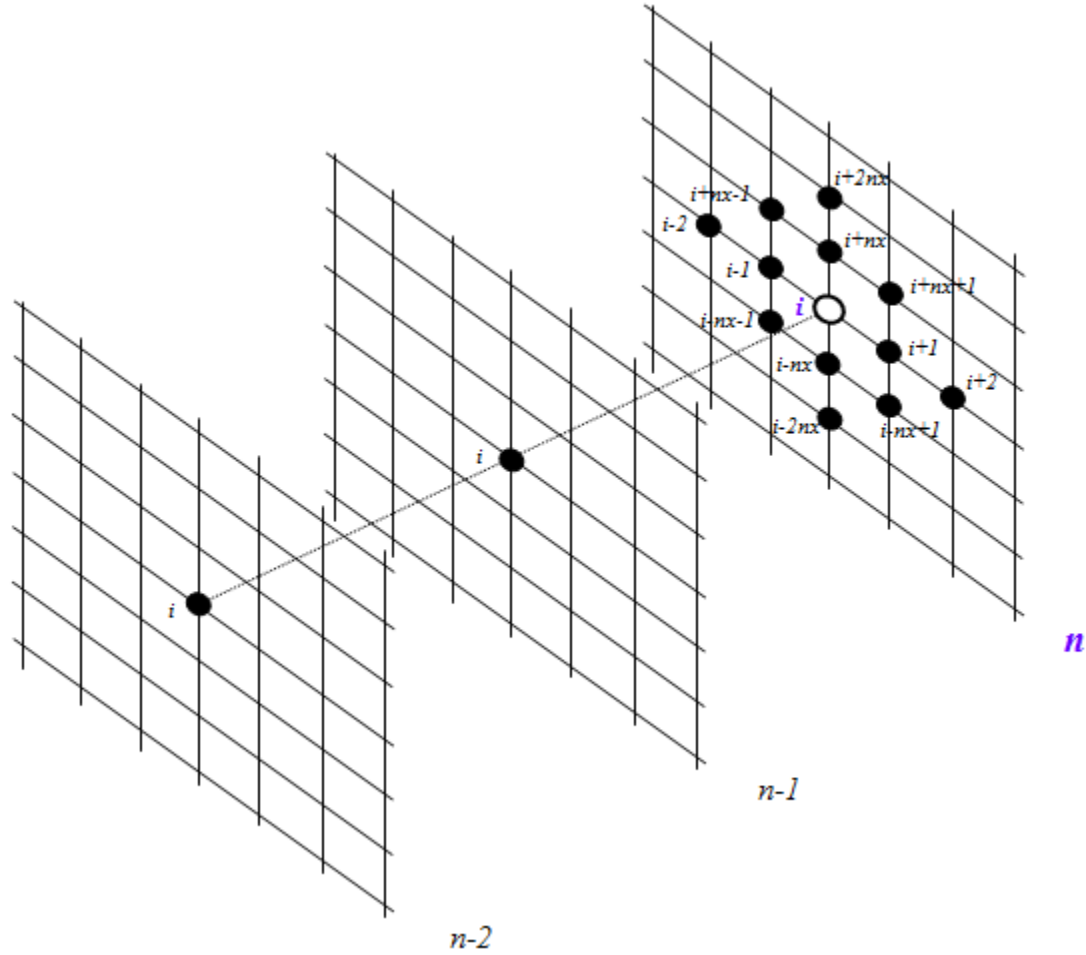


**Figure 4.10:** Implicit scheme for film drainage equation in Cartesian coordinates

Figure 4.10 shows that the fluid film height for a generic node  $i$  and time step  $n$  depends on the unknown fluid film height of the twelve neighboring nodes at the same time  $n$  and on the known fluid film height of the same node  $i$  at two previous time steps.

At the boundary nodes as shown in Fig. 4.9, Eq. (4.40) is applied. Thus, applying the

boundary condition  $\left. \frac{\partial h^*}{\partial t^*} \right|_{\text{square boundary of } S^*} = \frac{R}{hnd} V^*$  from Eq. (4.40), we obtain

$$\frac{3}{2}h_{i,n}^* = 2h_{i,n-1}^* - \frac{1}{2}h_{i,n-2}^* + \frac{R}{hnd}V_n^*\Delta t^* \quad \text{for } i = \begin{cases} 1, nx \\ (nz-1)nx+1, nxnz \\ nx+1, (nz-2)nx+1, nx \\ 2nx, (nz-1)nx, nx \end{cases} \quad (4.58)$$

Applying the condition  $p^* \Big|_{\text{square boundary of } S^*} = -2\frac{R}{hnd}$  from Eq. (4.40), the following equations

are obtained:

$$\begin{aligned} 5h_{i,n}^* - h_{i-nx-1,n}^* - h_{i-nx+1,n}^* - 4h_{i+nx,n}^* + h_{i+2nx,n}^* &= -\frac{2R}{hnd}\Delta x^{*2} \quad \text{for } i = nx+3, 2nx-2 \\ 5h_{i,n}^* - h_{i+nx-1,n}^* - h_{i+nx+1,n}^* - 4h_{i-nx,n}^* + h_{i-2nx,n}^* &= -\frac{2R}{hnd}\Delta x^{*2} \quad \text{for } i = (nz-2)nx+3, (nz-1)nx-2 \\ 5h_{i,n}^* - h_{i+nx-1,n}^* - h_{i-nx-1,n}^* - 4h_{i+1,n}^* + h_{i+2nx,n}^* &= -\frac{2R}{hnd}\Delta x^{*2} \quad \text{for } i = 2nx+2, (nz-3)nx+2, nx \\ 5h_{i,n}^* - h_{i+nx+1,n}^* - h_{i-nx+1,n}^* - 4h_{i-1,n}^* + h_{i-2,n}^* &= -\frac{2R}{hnd}\Delta x^{*2} \quad \text{for } i = 3nx-1, (nz-2)nx-1, nx \end{aligned} \quad (4.59)$$

for the node  $i=nx+2$

$$10h_{i,n}^* - 2h_{i-nx-1,n}^* - h_{i-nx+1,n}^* - h_{i+nx-1,n}^* - 4h_{i+nx,n}^* - 4h_{i+1,n}^* + h_{i+2nx,n}^* + h_{i+2,n}^* = -\frac{4R}{hnd}\Delta x^{*2} \quad (4.60)$$

for the node  $i=2nx-1$

$$10h_{i,n}^* - 2h_{i-nx+1,n}^* - h_{i-nx-1,n}^* - h_{i+nx-1,n}^* - 4h_{i-1,n}^* - 4h_{i+nx,n}^* + h_{i+2nx,n}^* + h_{i-2,n}^* = -\frac{4R}{hnd}\Delta x^{*2} \quad (4.61)$$

for the node  $i=(nz-2)nx+2$

$$10h_{i,n}^* - 2h_{i+nx-1,n}^* - h_{i+nx+1,n}^* - h_{i-nx-1,n}^* - 4h_{i+1,n}^* - 4h_{i-nx,n}^* + h_{i-2nx,n}^* + h_{i+2,n}^* = -\frac{4R}{hnd}\Delta x^{*2} \quad (4.62)$$

and finally for the node  $i=(nz-1)nx-1$

$$10h_{i,n}^* - 2h_{i+nx+1,n}^* - h_{i+nx-1,n}^* - h_{i-nx+1,n}^* - 4h_{i-nx,n}^* - 4h_{i-1,n}^* + h_{i-2,n}^* + h_{i-2nx,n}^* = -\frac{4R}{hnd} \Delta x^{*2} \quad (4.63)$$

In Eqs. (4.58) and (4.59) the expressions such as  $i = 1, nx$  mean that  $i$  takes values from 1 to  $nx$  with increments of 1 and the expressions such as  $i = 2nx, (nz-1)nx, nx$  mean that  $i$  takes values from  $2nx$  to  $(nz-1)nx$  with increments of  $nx$ .

Coupling the FDEs from Eq. (4.57) to Eq. (4.63) a linear system is obtained. In this linear system the matrix coefficients are no longer pentadiagonal as in 1D-BWI, but instead have thirteen non-zero diagonals over a lower and upper bandwidth of  $2nx$ . The system can be represented by

$$\begin{bmatrix} A \end{bmatrix}_{nd \times nd} \begin{bmatrix} h^* \end{bmatrix}_{nd \times 1} = \begin{bmatrix} f \end{bmatrix}_{nd \times 1} \quad (4.64)$$

From the linear system equation, Eq. (4.64), the film height profile  $h^*$  is obtained using a known profile  $h0^*$  and information from the two previous time steps. The profile  $h0^*$  is not arbitrary, but it will be close in value to  $h^*$  such that the linearization is valid. In our case, we have chosen a  $h0^*$  at a time step  $n$  equal to the profile  $h^*$  at time step  $n-1$ . Thus, the applied linearization makes sense at any time step.

### 4.3.3 Discretization of the bubble motion equation

Implicit discretization as detailed in section 4.2.3.2 is used to numerically solve Eq. (4.34). Hence, the drag force is treated implicitly while the BWI force is treated explicitly. The implicit drag force can be written as,

$$\vec{F}_d^* = -\frac{C_d Re_{V_n} \vec{V}_n^*}{4Re} \quad (4.65)$$

with,

$$Re_{V_n} = Re \sqrt{(U^*)^2 + (V^*)^2 + (W^*)^2} \quad (4.66)$$

Hence, the discretized Eq. (4.36) is written as,

$$\vec{V}_n^* = \frac{aux(2\vec{V}_{n-1}^* - 0.5\vec{V}_{n-2}^*) + \vec{\Gamma}}{denom} \quad \text{for } n = 3, 4, \dots, nt \quad (4.67)$$

where,

$$aux = \frac{1}{\Delta t^*} \frac{2}{3} \left( \frac{\rho_b}{\rho_l} + C_{am} \right)$$

$$denom = \frac{3}{2} aux + \frac{C_d Re_{V_n}}{4Re}$$

$$\vec{\Gamma} = \frac{1}{3} \frac{Eo}{We} \hat{e}_b + \vec{F}_w$$

As the instantaneous Reynolds number,  $Re_{V_n}$ , in *denom* depends of  $\vec{V}_n$ , Eq. (4.67) is solved iteratively. As an initial guess for the bubble velocity, the value at the previous time step ( $\vec{V}_{n-1}$ ) is used and the Reynolds number is computed as,

$$Re_{V_{guess}} = Re \sqrt{(U_{n-1}^*)^2 + (V_{n-1}^*)^2 + (W_{n-1}^*)^2} \quad (4.68)$$

Replacing Eq. (4.68) in Eq. (4.67), a new value for bubble velocity,  $\vec{V}_n^*$ , is obtained. The procedure is repeated substituting the bubble velocity guess for the new value of bubble velocity until a tolerance of  $10^{-8}$  is reached.

The independent term in Eq. (4.67),  $\vec{\Gamma}$ , is extended as:

$$\vec{\Gamma} = \begin{bmatrix} \frac{1}{3} \frac{Eo}{We} \sin(\theta) - \frac{2}{\pi We} \frac{hnd}{R} \left\{ \int_{-z_{\max}^*}^{z_{\max}^*} \int_{-x_{\max}^*}^{x_{\max}^*} \frac{\partial h^*}{\partial x^*} dx^* dz^* + \left( \frac{hnd}{2R} \right) \int_{-z_{\max}^*}^{z_{\max}^*} \int_{-x_{\max}^*}^{x_{\max}^*} p^* \frac{\partial h^*}{\partial x^*} dx^* dz^* \right\} \\ \frac{1}{3} \frac{Eo}{We} - \cos(\theta) \cos(\alpha) + \frac{2}{\pi We} \left\{ 4(r_{\max}^*)^2 + \left( \frac{hnd}{2R} \right) \int_{-z_{\max}^*}^{z_{\max}^*} \int_{-x_{\max}^*}^{x_{\max}^*} p^* dx^* dz^* \right\} \\ \frac{1}{3} \frac{Eo}{We} \cos(\theta) \sin(\alpha) - \frac{2}{\pi R We} \frac{hnd}{We} \left\{ \int_{-z_{\max}^*}^{z_{\max}^*} \int_{-x_{\max}^*}^{x_{\max}^*} \frac{\partial h^*}{\partial z^*} dx^* dz^* + \left( \frac{hnd}{2R} \right) \int_{-z_{\max}^*}^{z_{\max}^*} \int_{-x_{\max}^*}^{x_{\max}^*} p^* \frac{\partial h^*}{\partial z^*} dx^* dz^* \right\} \end{bmatrix} \quad (4.69)$$

The vector  $\vec{\Gamma}$  is computed explicitly. Hence, all the term in Eq. (4.69) are computed at the previous time step, i.e. at  $n-1$ . The buoyancy force in Eq. (4.69) does not depend on time but only on the wall inclinations. Given a wall inclination, the buoyancy force in each direction is constant during the entire bouncing process. The excess pressure  $p^*$  and the double integrals in Eq. (4.69) are numerically computed as follows,

From Eq. (4.41), using central second-order accuracy for the approximation of the derivatives, the excess pressure is computed as,

$$p^* = - \left( \frac{h_{i+1,n-1}^* - 2h_{i,n-1}^* + h_{i-1,n-1}^*}{(\Delta x^*)^2} + \frac{h_{i+nx,n-1}^* - 2h_{i,n-1}^* + h_{i-nx,n-1}^*}{(\Delta z^*)^2} \right) \quad (4.70)$$

Eq. (4.70) cannot be applied to the boundary nodes (denoted by open circles in Fig. 4.9). At

these boundary nodes the equation  $p^* = -\frac{2R}{hnd}$  is used.

With the results of the excess pressure obtained for all nodes in the spatial domain, the integral terms in Eq. (4.69) are computed using the trapezoid rule (Hoffman, 2001).

The normal part in  $y$ -direction

$$\int_{-z_{\max}^*}^{z_{\max}^*} \int_{-x_{\max}^*}^{x_{\max}^*} p^* dx^* dz^* \approx \sum_{i=(j-1)nx+1}^{i=jnx-1} \left( \frac{p_i^* + p_{i+1}^* + p_{i+nx}^* + p_{i+nx+1}^*}{4} \right) \Delta x^* \Delta z^* \quad \text{where}$$

$$j = 1, 2, 3, \dots, nz - 1 \quad (4.71)$$

The tangential part in  $x$ -direction

$$\int_{-z_{\max}^*}^{z_{\max}^*} \int_{-x_{\max}^*}^{x_{\max}^*} p^* \frac{\partial h^*}{\partial x^*} dx^* dz^* = \int_{-z_{\max}^*}^{z_{\max}^*} \int_{-x_{\max}^*}^{x_{\max}^*} \Theta dx^* dz^* \approx \sum_{i=(j-1)nx+1}^{i=jnx-1} \left( \frac{\Theta_i + \Theta_{i+1} + \Theta_{i+nx} + \Theta_{i+nx+1}}{4} \right) \Delta x^* \Delta z^* \quad (4.72)$$

for  $j = 1, 2, 3, \dots, nz - 1$

$$\text{with } \Theta = p^* \frac{\partial h^*}{\partial x^*} \quad (4.73)$$

The last function is discretized as,

$$\Theta_i \approx p_i^* \frac{h_{i+1,n-1}^* - h_{i-1,n-1}^*}{2\Delta x^*} \quad \text{for } \begin{cases} j = 1, nz \\ i = (j-1)nx + 2, jnx - 1 \end{cases} \quad (4.74)$$

And using the forward derivative approximation, we obtain

$$\Theta_i \approx p_i^* \frac{-3h_{i,n-1}^* + 4h_{i+1,n-1}^* - h_{i+2,n-1}^*}{2\Delta x^*} \quad \text{for } i = 1, (nz - 1)nx + 1, nx \quad (4.75)$$

Finally, using the backward derivative approximation, it gives

$$\Theta_i \approx p_i^* \frac{3h_{i,n-1}^* - 4h_{i-1,n-1}^* + h_{i-2,n-1}^*}{2\Delta x^*} \quad \text{for } i = nx, nd, nx \quad (4.76)$$

The tangential part in  $z$ -direction

$$\int_{-z_{\max}^*}^{z_{\max}^*} \int_{-x_{\max}^*}^{x_{\max}^*} p^* \frac{\partial h^*}{\partial z^*} dx^* dz^* = \int_{-z_{\max}^*}^{z_{\max}^*} \int_{-x_{\max}^*}^{x_{\max}^*} \Omega dx^* dz^* \approx \sum_{i=(j-1)nx+1}^{i=jnx-1} \left( \frac{\Omega_i + \Omega_{i+1} + \Omega_{i+nx} + \Omega_{i+nx+1}}{4} \right) \Delta x^* \Delta z^* \quad (4.77)$$

for  $j = 1, 2, 3, \dots, nz - 1$

$$\text{with } \Omega = p^* \frac{\partial h^*}{\partial z^*} \quad (4.78)$$

Eq. (4.76) is discretized as,

$$\Omega_i \approx p_i^* \frac{h_{i+nx,n-1}^* - h_{i-nx,n-1}^*}{2\Delta z^*} \quad \text{for } \begin{cases} j = 1, nx \\ i = nx + j, (nz - 2)nx + j, nx \end{cases} \quad (4.79)$$

And using the forward derivative approximation, we obtain

$$\Omega_i \approx p_i^* \frac{-3h_{i,n-1}^* + 4h_{i+nx,n-1}^* - h_{i+2nx,n-1}^*}{2\Delta z^*} \quad \text{for } i = 1, nx \quad (4.80)$$

Finally using the backward derivative approximation, gives

$$\Omega_i \approx p_i^* \frac{3h_{i,n-1}^* - 4h_{i-nx,n-1}^* + h_{i-2nx,n-1}^*}{2\Delta z^*} \quad \text{for } i = (nz - 1)nx + 1, nd \quad (4.81)$$

The terms which correspond at the components of the normal vector are computed as,

$$\int_{-z_{\max}^*}^{z_{\max}^*} \int_{-x_{\max}^*}^{x_{\max}^*} \frac{\partial h^*}{\partial x^*} dx^* dz^* \approx \sum_{i=1}^{i=nz-1} \left( \frac{h_{inx,n-1}^* + h_{(i+1)nx,n-1}^* - h_{(i-1)nx+1,n-1}^* - h_{inx+1,n-1}^*}{2} \right) \Delta z^* \quad (4.82)$$

$$\int_{-z_{\max}^*}^{z_{\max}^*} \int_{-x_{\max}^*}^{x_{\max}^*} \frac{\partial h^*}{\partial z^*} dx^* dz^* \approx \sum_{i=1}^{i=nx-1} \left( \frac{h_{(nz-1)nx+i,n-1}^* + h_{(nz-1)nx+i+1,n-1}^* - h_{i,n-1}^* - h_{i+1,n-1}^*}{2} \right) \Delta x^* \quad (4.83)$$

### 4.3.4 Computational algorithm

In order to solve the 3D-BWI model in numerical form as described in sections 4.3.2 and 4.3.3, a computational code using FORTRAN 90 computer language was developed. This code is sufficiently general to solve the BWI when the wall is horizontal or when the wall has one or two inclinations.

*Explicit coupling* is used to couple the system of equations in the present code as described in section 4.2.4.

The computer code of 3D-BWI is similar to the implicit code of 1D-BWI. The difference lies in the extensive calculations that must be made in 3D-BWI due to Cartesian coordinates and no symmetry conditions. The details of the code can be found in the flowchart of the Fig. 4.11. The principal subroutines in this figure and the full 3D-BWI code are presented in appendix D.

The general steps of the computational algorithm of the 3D-BWI code are the following:

- I. At the initial time  $t = 0$  ( $n = 1$ ) or for the first time step, the initial conditions such as the bubble velocity  $\vec{V} = \vec{V}_T$  ( $\vec{V}_{n=1}^* = 1\hat{e}_b$ ) and excess pressure  $p = 0$  ( $p^* = -2R/hnd$ ) from Eq. (4.37) and parabolic film height profile  $h_{i,n=1}^*$  from Eq. (4.39) are used.
- II. At time  $t = 1\Delta t$  ( $n = 2$ ) or for the second time step, the bubble terminal velocity,  $\vec{V} = \vec{V}_T$  ( $\vec{V}_{n=1}^* = 1\hat{e}_b$ ) and zero pressure  $p = 0$  ( $p^* = -2R/hnd$ ) are still used. It is again reasonable to use the terminal velocity in the second time step because the bubble is still without significant deformation. As a consequence, the fluid film height profile  $h_{i,n=2}^* = h_{i,n=1}^* + V_{n=1}^* \Delta t^* R / hnd$  is used at  $n=2$ .
- III. At time  $t = 2\Delta t$  ( $n = 3$ ) or for the third time step:
  - a) The excess pressure is computed with the fluid film height profile determined in the previous time step (i.e.,  $h_{i,n=2}^*$ ) using Eq. (4.70).
  - b) We use the results of (a) to compute the integral terms of  $\vec{\Gamma}$  (Eq. 4.69) discretized as Eqs. (4.71-4.83).

- c) With the results from (b) we solve for the bubble velocity at the present time step (i.e.,  $\vec{V}_{n=3}^*$ ) using the discretized ODE Eq. (4.67). This equation is solved via iteration until an established tolerance is reached.
- d) With the results of (c) for the present velocity, the fluid film height profile at the present time step (i.e.,  $h_{i,n=3}^*$ ) is determined by solving the linear system of FDEs Eq. (4.64). To solve this linear system, an equilibrium value of fluid film height,  $h0^*$  is required. We use  $h0^* = h_{i,n-1}^*$ , and after solving the linear system, the present and previous film height profile are compared. The  $h0^*$  is updated, the system of equations is solved to determine a new film profile, and again the comparison is performed. The procedure is continued until certain accuracy is reached.

- IV. Steps (a), (b), (c) and (d) as described in item III are repeated in the same order for the next time steps until the final time step  $n = nt$  is reached.

The 3D-BWI code uses two modules, the *physical module* and the *numerical module* (see Fig. 4.11), in which the used global variables are defined. The structure of the main program called *main3D\_BWI* is presented in Fig. 4.11. The structure of two principal subroutines as the ODE and the PDE are presented in Appendix D in the Figs. D7-D8 and D9-D10 respectively.

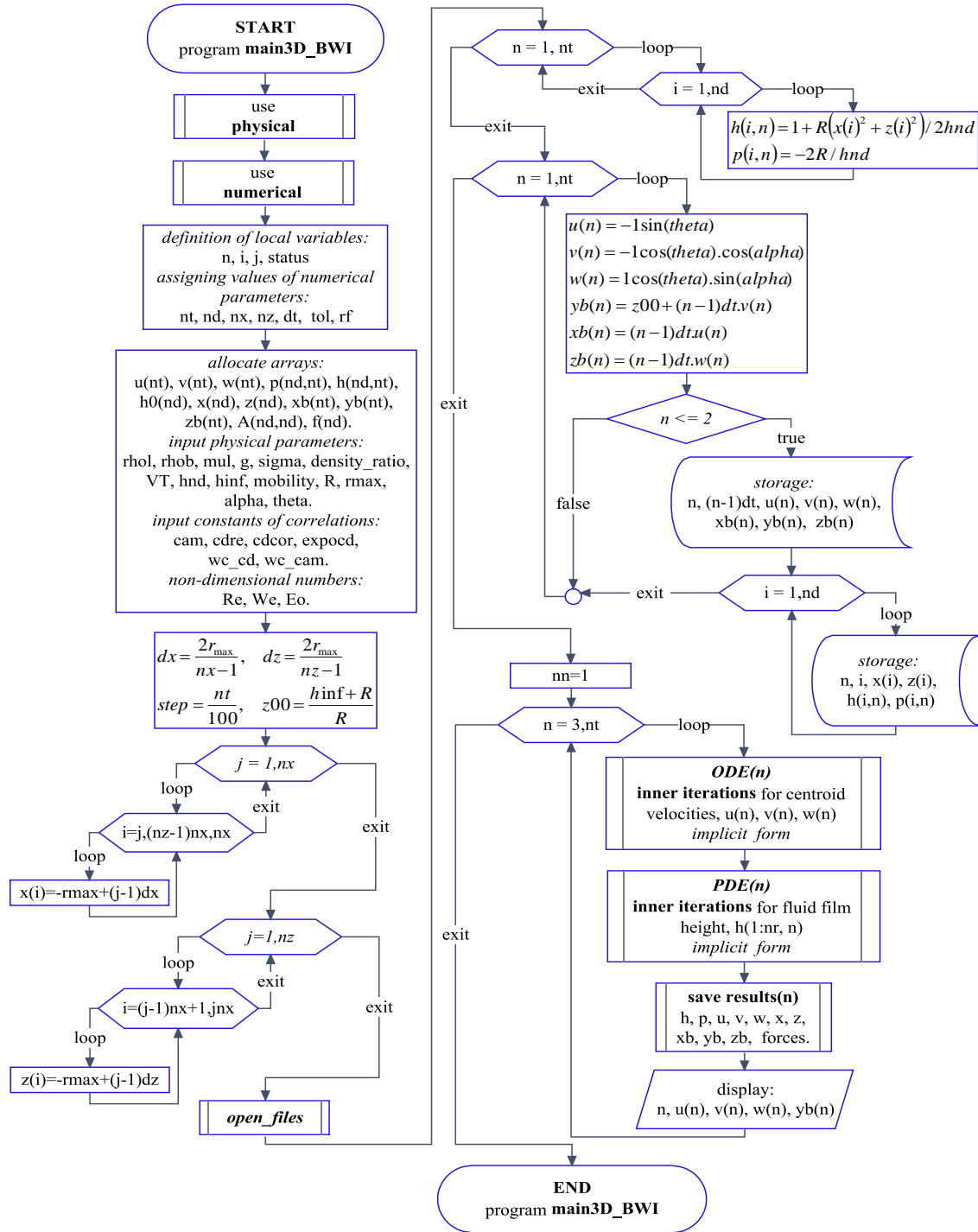


Figure 4.11: Structure of the main program *main3D\_BWI*

## 5. BWI RESULTS AND ANALYSIS

In this chapter the results of the numerical simulations performed to study the bubble-wall interaction process using the numerical model described in chapter 3 are presented and discussed. These results are divided in two sections, first the interaction of a bubble with a horizontal wall and secondly the interaction of a bubble with an inclined wall. In both sections a grid resolution study is first presented to justify the grid used in order to obtain the velocity and position of a bubble predicted by the model derived in the present thesis. In order to validate the present model, comparisons with available experimental data are also presented in both sections.

Air bubbles of diameters ranging from 0.3-2.0 mm in contaminated and purified water were considered. The Reynolds ( $Re$ ) and Weber ( $We$ ) numbers as defined in Eq. (3.31) range from 8 to 600 and from 0.003 to 1.7 respectively. A variety of correlations were used to represent the drag and the added mass coefficients. From correlations listed in Tables 1 and 2 those that have better agreement with experimental data were chosen. These correlations are mentioned following:

For an equivalent bubble diameter  $d_e < 1\text{mm}$  (see Fig. 2.5(a)) the air bubble presents small deformations and basically retains its spherical shape when it is rising in water. Since the drag coefficients are sensitive to the presence of contaminants at the surface the correlations used to compute this coefficient are specified for each simulation. For a *contaminated system* the following drag correlation was used:

$$C_d = \frac{24}{Re_v} C(y) (1 + 0.15 Re_v^{0.687}) \quad (\text{see Table 2, \#2}) \quad (5.1)$$

$$\text{with } C(y) = \left( 1 - \left( \frac{R}{2y} \right)^3 \right)^{-2} \quad (5.2)$$

$C(y)$  is used to consider the wall proximity (see Fig. 2.2). Considering the bubble deformations in the wall proximity, the added mass coefficient varies with respect to a full spherical shape ( $C_{am}=0.5$ ) and is computed with the following equation (see Table 2 for references):

$$C_{am} = \frac{3}{2} (C(y))^{1/2} - 1 \quad (\text{Table 2, \#4}) \quad (5.3)$$

For a *purified system* the following drag correlation was used (see Table 1):

$$C_d(Re_v, k) = \frac{2-k}{2} C_D(Re_v, 0) + \frac{4k}{6+k} C_D(Re_v, 2) \quad (\text{Table 1, \#7}) \quad (5.4)$$

where

$$C_d(Re_v, 0) = \frac{48}{Re} \left( 1 + \frac{2.21}{Re_v^{1/2}} - \frac{2.14}{Re_v} \right),$$

$$C_d(Re_v, 2) = 17.0 Re_v^{-2/3}$$

The added mass coefficient is not affected by the water purity (Klaseboer et al. 2001). Then, for a clean system, Eq. (5.3) is still used to compute the added mass coefficient.

For an equivalent bubble diameter between 1 and 2 mm the air bubbles in water are non-spherical. In this case an ellipsoidal shape is observed for bubbles ranging from 1mm to 10mm (see Fig. 2.5(a)). Hence, the large deformation of the bubble affects significantly the drag and added mass coefficients. For a *purified system* the following drag correlation was considered (see Table 2):

$$C_d = \frac{48}{Re_v} G(\chi) \left( 1 + \frac{H(\chi)}{Re_v^{1/2}} \right) \quad (\text{Table 2, \#3}) \quad (5.5)$$

$$\text{with } G(\chi) = \frac{1}{3} \chi^{4/3} (\chi^2 - 1)^{3/2} \frac{\left( \sqrt{\chi^2 - 1} - (2 - \chi^2) \cos^{-1}\left(\frac{1}{\chi}\right) \right)}{\left( \chi^2 \cos^{-1}\left(\frac{1}{\chi}\right) - \sqrt{\chi^2 - 1} \right)^2} \quad (5.6)$$

$$H(\chi) = 0.0195\chi^4 - 0.2134\chi^3 + 1.7026\chi^2 - 2.1461\chi - 1.5732 \quad (5.7)$$

Another drag correlation used is the one proposed by Bozzano & Dente, (2009) Eq. (2.11).

The added mass correlation is affected by the bubble shape. For an aspect ratio  $\chi < 2.5$  the added mass coefficient used was (Klaseboer et al. 2001)

$$C_{am} = 0.62\chi - 0.12 \quad (5.8)$$

Air bubbles of diameter  $d_e > 1\text{mm}$  in a contaminated system were not evaluated in the present thesis. In order to evaluate this case the drag correlation from Eq. (2.11) can be used.

## 5.1 INTERACTION WITH A HORIZONTAL WALL

### 5.1.1 Computer codes analysis

The first study performed was to compare the simulation results between the explicit and implicit codes developed in chapter 4 to solve the 1D-BWI model. Fig. 5.1 shows the velocity variation of an air bubble with  $Re=407$  and  $We = 0.566$  impinging on a horizontal rigid wall obtained with the explicit and implicit code. The number of nodes used in  $r$  direction was  $nr = 50$  for both codes. The implicit simulation was performed using the following non-dimensional temporal steps:  $10^{-3}$ ,  $10^{-4}$ ,  $10^{-5}$ , and  $10^{-6}$ ; the explicit code is stable for non-dimensional time steps less than or equal to  $10^{-9}$  causing a large computational time

to obtain results comparable with results of the implicit code. The implicit code has a slight variation in maximum values of velocity with respect to the explicit code; the maximum difference observed was about 7% (see Fig. 5.1 (b) and (c)). The implicit code with different time steps values had no significantly variations in velocity results, but it was observed that the computational time increased as the time step decreased. Fig. 5.2 shows the comparison of the bubble centroid position between explicit and implicit code results for the same data used in Fig. 5.1. A maximum difference of about 3% was obtained for the first rebound.

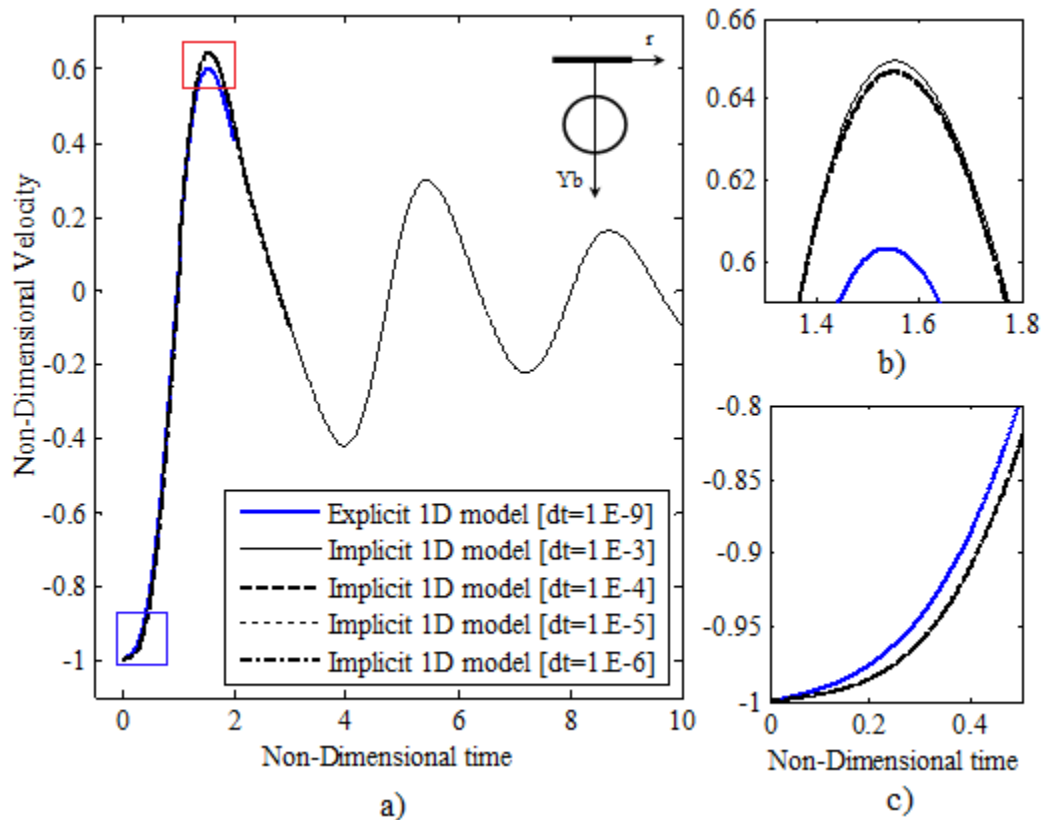


**Figure 5.1:** Comparison results from implicit and explicit codes: (a) Non-dimensional normal velocity vs Non-dimensional time for a bubble of  $R=1$  mm,  $Re=407$  and  $We=0.566$ ; (b) Amplified view, time range 1.3-1.8; (c) Amplified view, time range 0-0.5

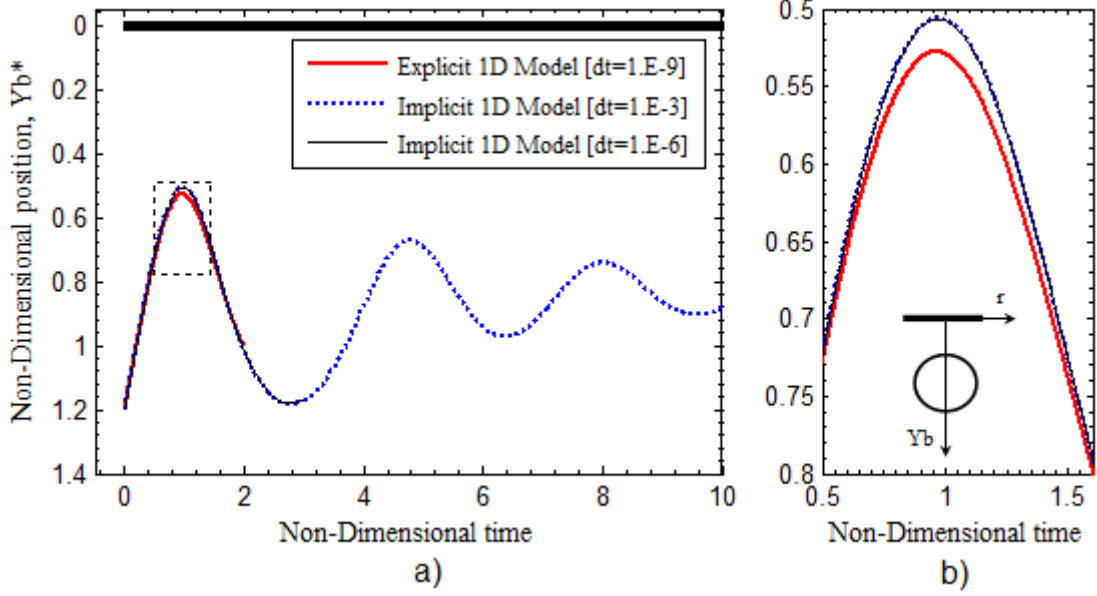
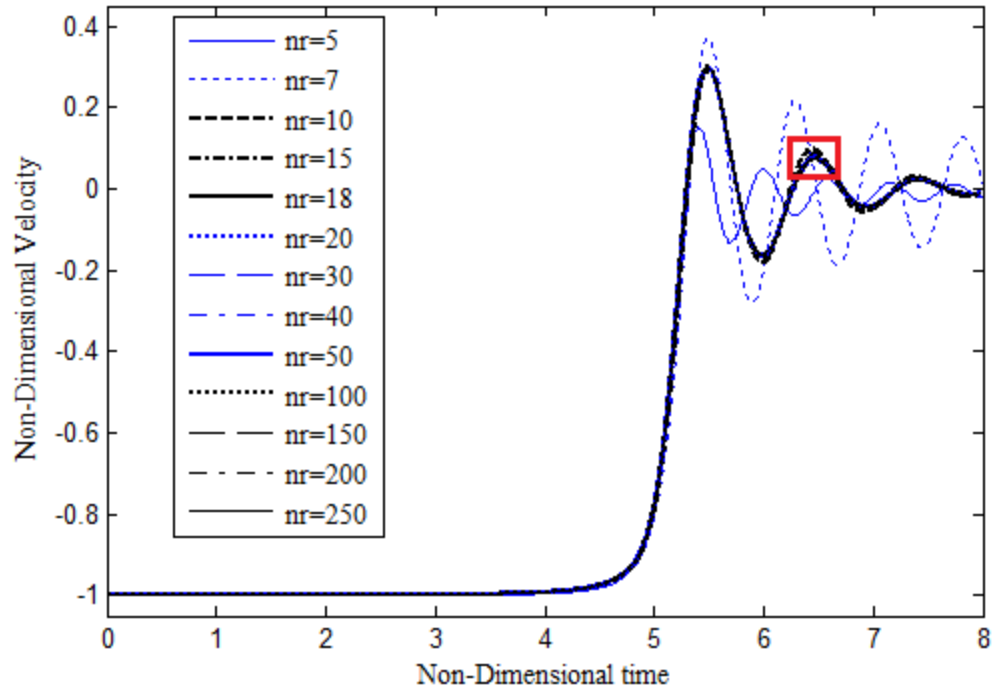


**Figure 5.2:** Comparison results from implicit and explicit codes: (a) Non-dimensional position vs Non-dimensional time for a bubble of  $R=1$  mm ,  $Re=407$  and  $We=0.566$ ; (b) Amplified view of the first rebound

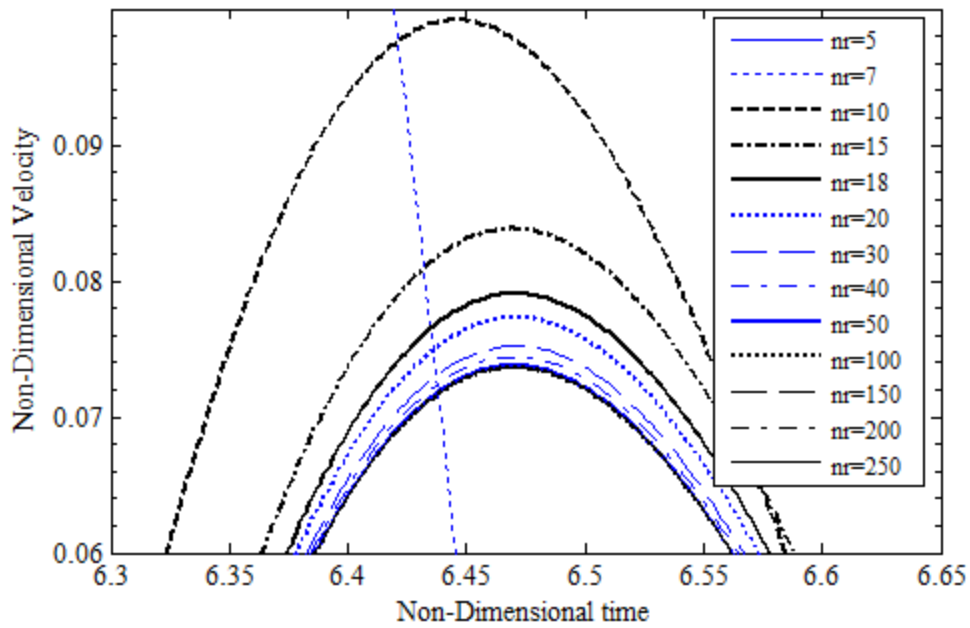
We have run the explicit code only for one case (see Fig. 5.1), in which a temporal time step less than or equal to  $10^{-9}$  is needed. Hence, the number of time steps required to obtain results comparables with those obtained with the implicit code is very large (of order  $O(10^9)$ ). In addition, a lot of computational time is required. Therefore, we have used only the implicit code for our future simulations.

To determine the proper grid resolution required in order to obtain reliable results, a grid resolution study of the implicit code was performed. Fig. 5.3 shows simulations for a bubble of radius  $R=0.4$ mm,  $Re=72.543$ ,  $We=0.0888$ ,  $Eo=0.0847$ , and  $\Delta t^* = 0.002$  using the implicit code at different levels of spatial resolution. In these simulations the water is considered contaminated. Hence, Eqs. (5.1) and (5.3) were used to compute the drag and added mass coefficients respectively. The terminal velocity  $V_T = 9.07$  cm/s was obtained from the balance between the drag and buoyancy forces. In this figure, as the number of

radial nodes is increased, the solution converges to a determinate value of velocity in each time. For  $nr > 20$  the maximum difference is less than to 4% compared to  $nr=250$ . Fig. 5.4 shows a temporal grid resolution study for the same data used in Fig. 5.3. In this case the spatial grid was kept constant ( $nr= 200$ ) and the temporal grid was changed. From Fig. 5.4(b) it can be observed that for  $\Delta t^* \leq 0.002$  the results don't have a noticeable difference (difference  $\ll 1\%$ ).

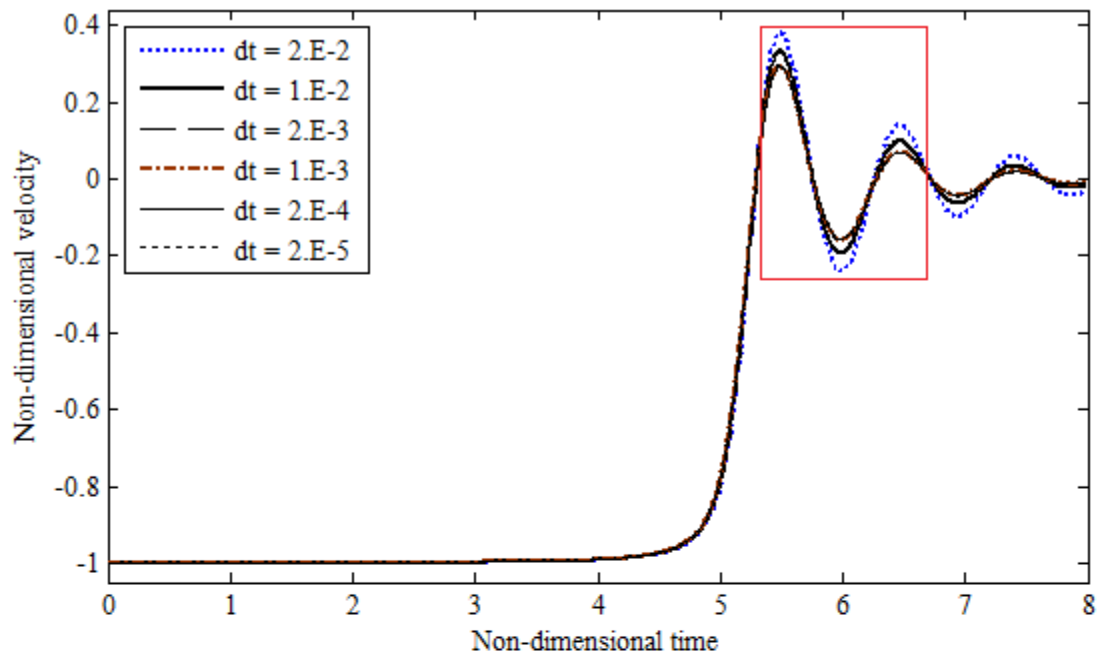


a)

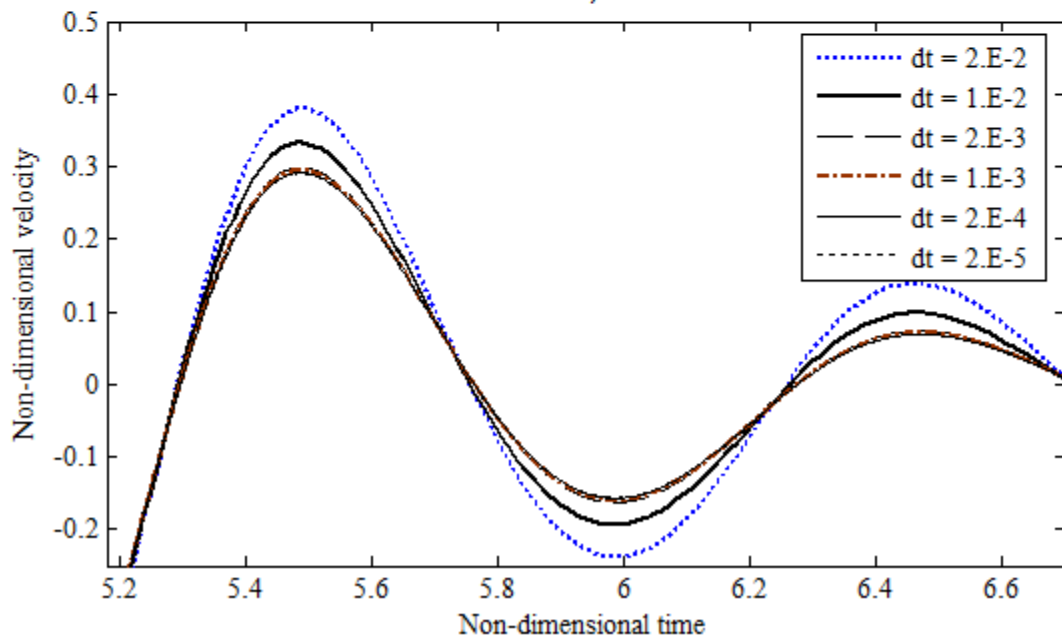


b)

**Figure 5.3:** Non-dimensional velocity vs non-dimensional time for a bubble for different values of spatial grid resolution: (a) Non- dimensional time range:0-8; (b) Amplified view about the second maximum value of velocity



a)



b)

**Figure 5.4:** Non-dimensional velocity vs non-dimensional time for a bubble for different values of spatial grid resolution: (a) Non- dimensional time range:0-8; (b) Amplified view non- dimensional time range:5.2-6.7

### 5.1.2 Bouncing Prediction of a bubble using the 1D-BWI model

Based on the results of section 5.1.1 for all simulations presented in this section and in sections 5.1.3 and 5.1.4 we used the implicit code with a uniform spatial grid  $nr = 200$  and a non-dimensional time step  $\Delta t^* = 0.001$ .

Predictions of the behavior of a bubble with radius  $R=0.4\text{mm}$  interacting with a horizontal wall and for the cases of contaminated and uncontaminated system, are presented here.

a) *Bubble position and velocity in a clean system*

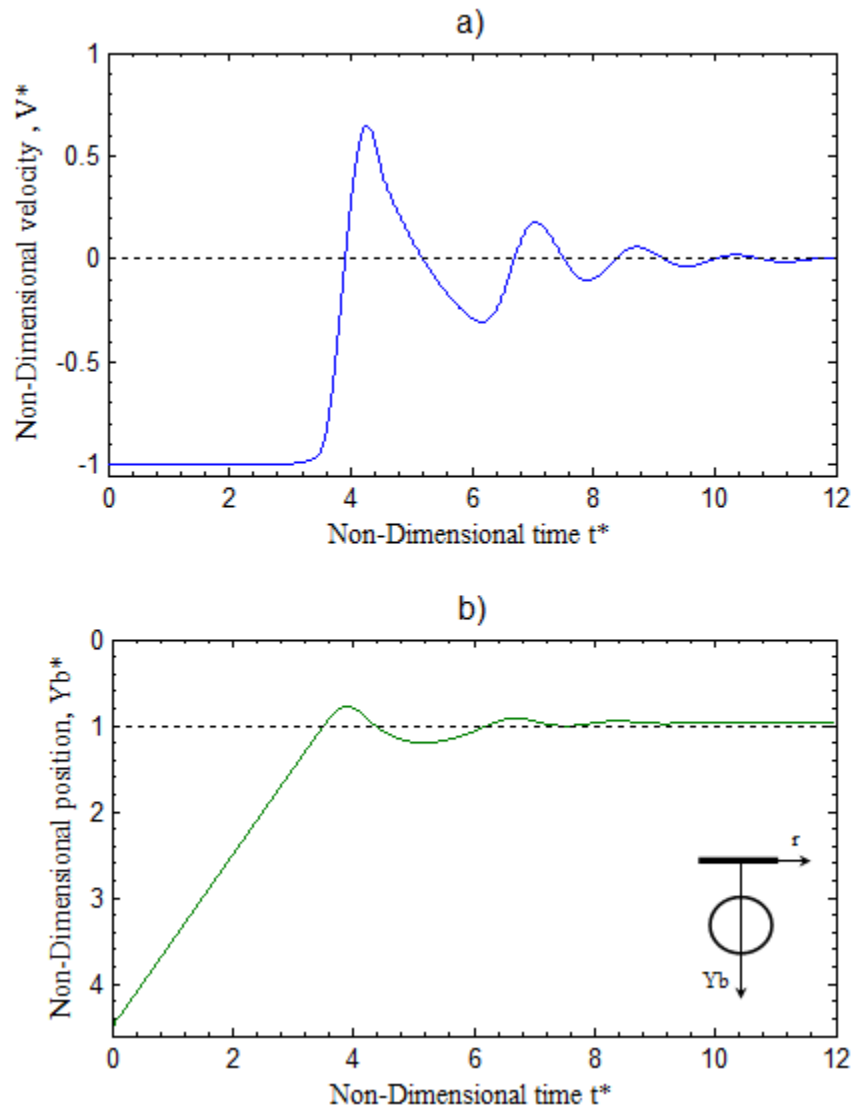


**Figure 5.5:** Non-dimensional velocity (a) and position (b) vs non-dimensional time for a bubble of radius  $R=0.4$  mm,  $Re=92$   $We=0.143$  and  $Eo=0.08476$  immersed in purified water and interacting with a horizontal wall.

Figure 5.5 shows the bubble velocity and position predicted by the present 1D-BWI model for an air bubble in purified water. As the terminal velocity is sensitive to the degree of purity we used the terminal velocity read from Fig. 2.5(a). This value was  $V_T = 11.5$  cm/s for  $R=0.4$ mm, which is less than the terminal velocity  $V_T = 14$  cm/s (approx. 18% variation respect to the  $V_T$  in contaminated system) computed using the Eq.2.10 with drag coefficient from correlation of Feng & Michaelides, (2001). We used experimental terminal velocity to obtain results for future experimental verification. The non-dimensional numbers were  $Re=92$   $We=0.143$  and  $Eo= 0.08476$ . Eqs. (5.3) and (5.4) were used to compute the added mass and drag coefficients respectively. The lubrication equation solved in this case was using the slip condition at the bubble surface. Hence, the value of  $M$  in Eq. (3.36) was 3. The drag coefficient was corrected by a factor of 1.25 such that far from the wall the buoyancy and drag force were balanced, this factor was obtained because an experimental value of terminal velocity was used from Fig. 2.5(a). In some cases this factor is attributed to the effect of a small concentration of contaminants which were still present in the liquid after the purification process (Klaseboer et al. 2001). The maximum non-dimensional radius used was  $r_{\max}^* = 1.00$ . From Fig. 5.5(a) we can observe that the bubble velocity decreases as it approaches the wall, owing to a favorable pressure gradient taking place at the top of the bubble which produces a wall force on the bubble in opposite direction of the bubble velocity producing the deceleration of the bubble. The first rebound occurs at the non-dimensional time 3.91 (13.61 ms). During the first rebound, part of the kinetic energy of the bubble is dissipated into the fluid film. The kinetic energy before and after the rebound is computed using the minimum and maximum velocity value around the instant of rebound respectively (for instance for the first rebound in Fig. 5.5(a) the non-dimensional velocities -1 and 0.65 is

used). Hence, only 42% of the initial kinetic energy is restored after the first rebound. Three rebounds occur until the kinetic energy restored is zero. The non-dimensional bubble position is scaled by the bubble radius; consequently, a non-dimensional position  $Y_b^* < 1$  indicates that the bubble is deformed. In Fig. 5.5(b) we can observe that at the first rebound the bubble has a deformation higher than at the second rebound, and this higher than at the third rebound. After the third rebound the bubble is stopped permanently on the wall with a small deformation ( $Y_b^* \cong 0.95$ ). Before the first rebound, the bubble is instantaneously stopped and the kinetic energy is zero, therefore, the kinetic energy is converted in dissipation energy and deformation energy. After the first rebound the deformation energy is converted to kinetic energy.

*b) Fluid film thickness in a clean system*

Figures 5.6 and 5.7 show the fluid film thickness profile on the top of the bubble at the first and second rebound respectively. These figures correspond to the data used to obtain the Fig. 5.5. In both figures the maximum bubble deformation occurs when the film thickness is around  $5\mu\text{m}$ ; this is approximately  $1/100$  of the bubble radius. These results are in agreement with results from Canot et al. (2003). Therefore, the assumption  $h/R \ll 1$  is satisfied. A dimple is produced around  $r = 0$ , since the maximum excess pressure is produced at this position (see Figs. 5.8 and 5.9). It is clearly observable that the dimple is more pronounced in the first rebound than in the second, as an example, just before the first rebound ( $t=13.57\text{ms}$ ) the dimple depth is of  $2\mu\text{m}$  and just before the second rebound ( $22.96\text{ms}$ ) the dimple depth is zero.

The bubble deformation occurs only for  $r$  less than 0.2mm, which is less than  $R$  and justifies a posteriori the assumption made for the deformation domain when deriving and solving the model in chapters 3 and 4.

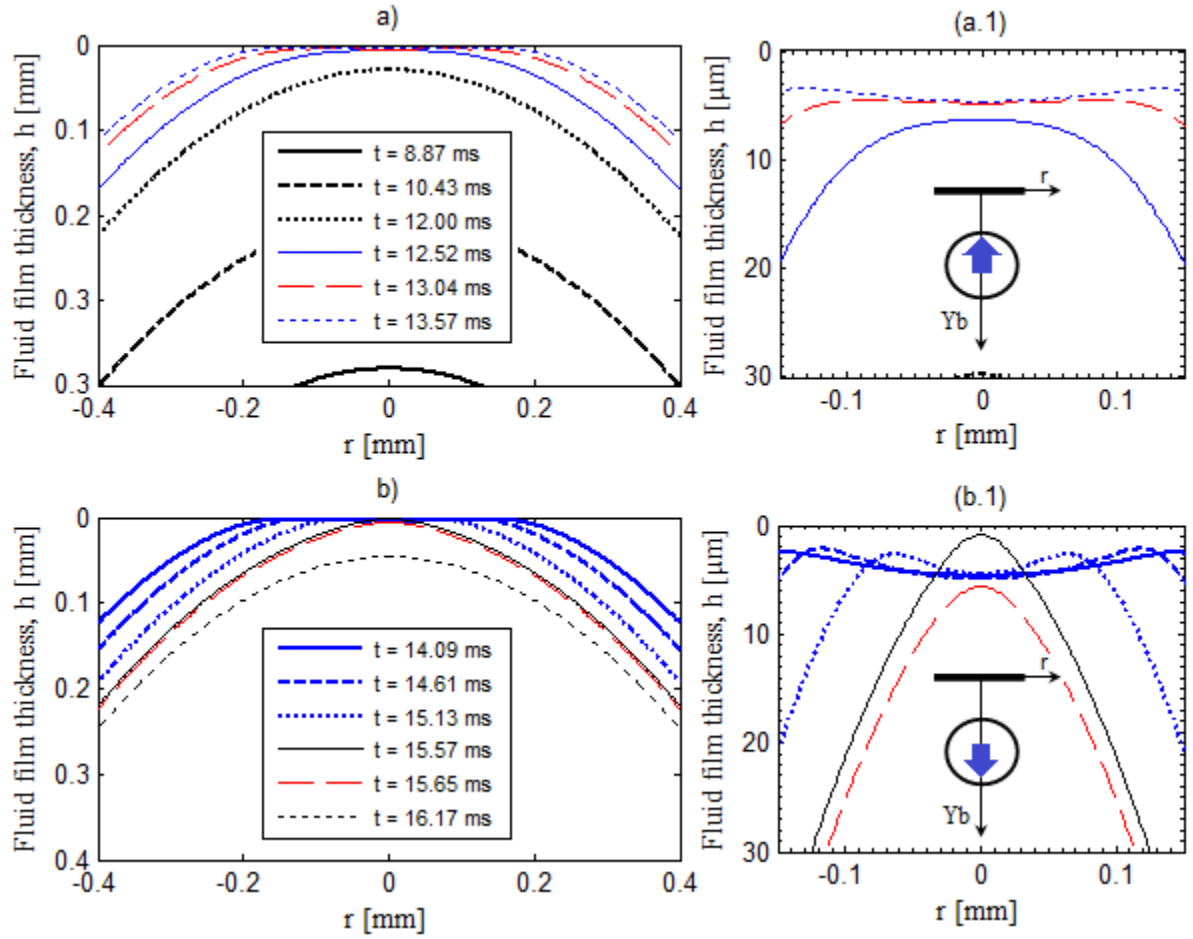


**Figure 5.6:** Evolution of the fluid film thickness profile during the first rebound for a bubble of radius  $R=0.4$  mm,  $Re=92$ ,  $We=0.143$  and  $Eo=0.08476$  immersed in purified water and interacting with a horizontal wall: (a) Before the first rebound; (a.1) amplified view of (a) around  $r=0$ ; (b) After the first rebound; (b.1) amplified view of (b) around  $r=0$ . The first rebound occur at 13.61ms

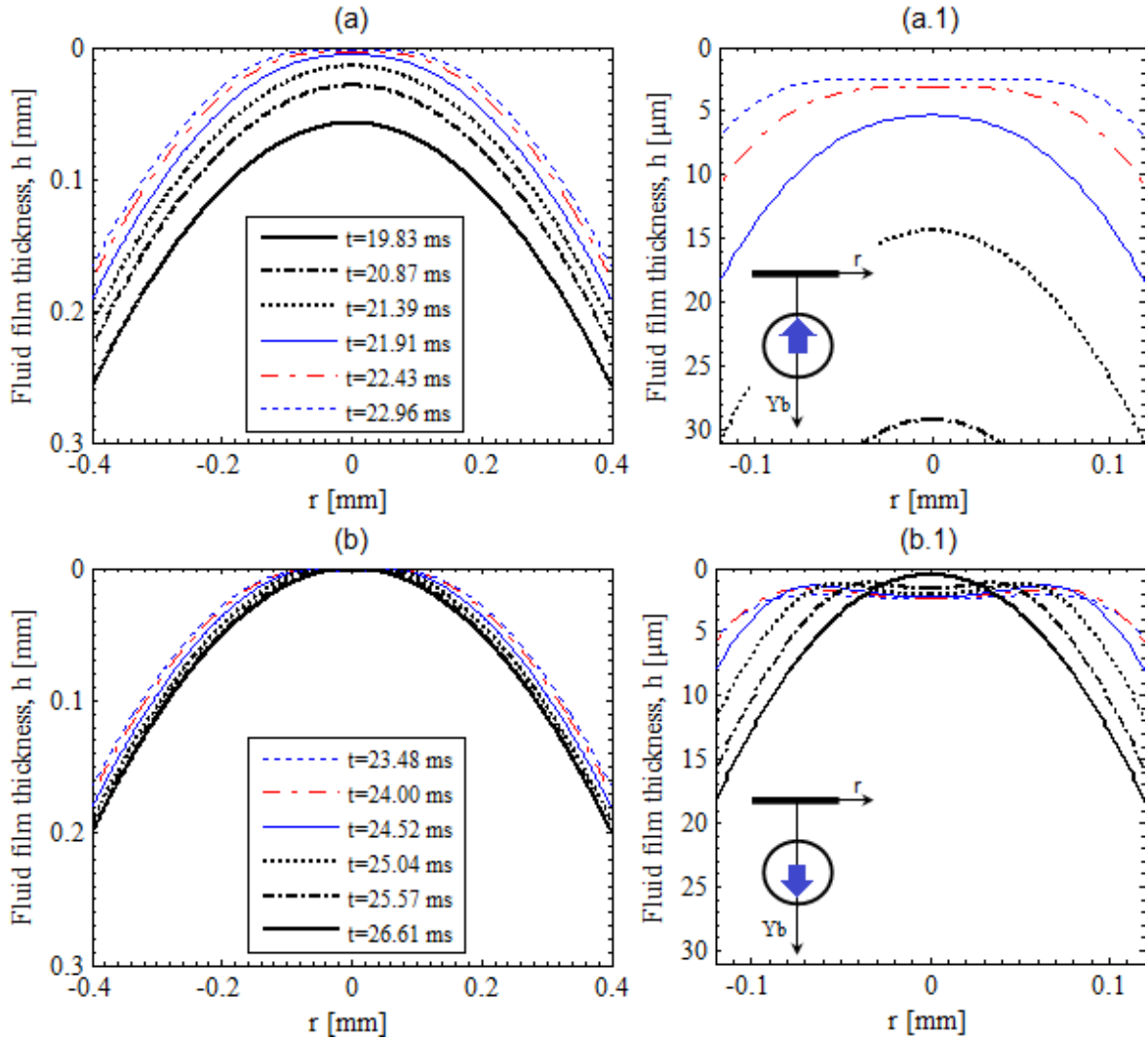


**Figure 5.7:** Evolution of the fluid film thickness profile during the second rebound for a bubble of radius  $R=0.4$  mm,  $Re=92$ ,  $We=0.143$  and  $Eo=0.08476$  immersed in purified water and interacting with a horizontal wall: (a) Before the second rebound; (a.1) amplified view of (a) around  $r=0$ ; (b) After the second rebound; (b.1) amplified view of (b) around  $r=0$ . The second rebound occur at 23.31ms

*c) Excess pressure profile in a clean system*

Figures 5.8 and 5.9 show the excess pressure profile on the top of the bubble at the first and second rebound respectively. Far from the wall the excess pressure is zero and starts to increase as the bubble approaches the wall. From the figure it can be observed that for  $r > 0.3\text{mm}$  the value of the excess pressure is zero. This validates the assumption previously made when solving numerically the model in chapter 4 when it was assumed that pressure

variations occurred over a circle of radius less than the bubble radius. Before the first rebound (Fig. 5.8(a)) the excess pressure profile is positive over all  $r$ -coordinate.

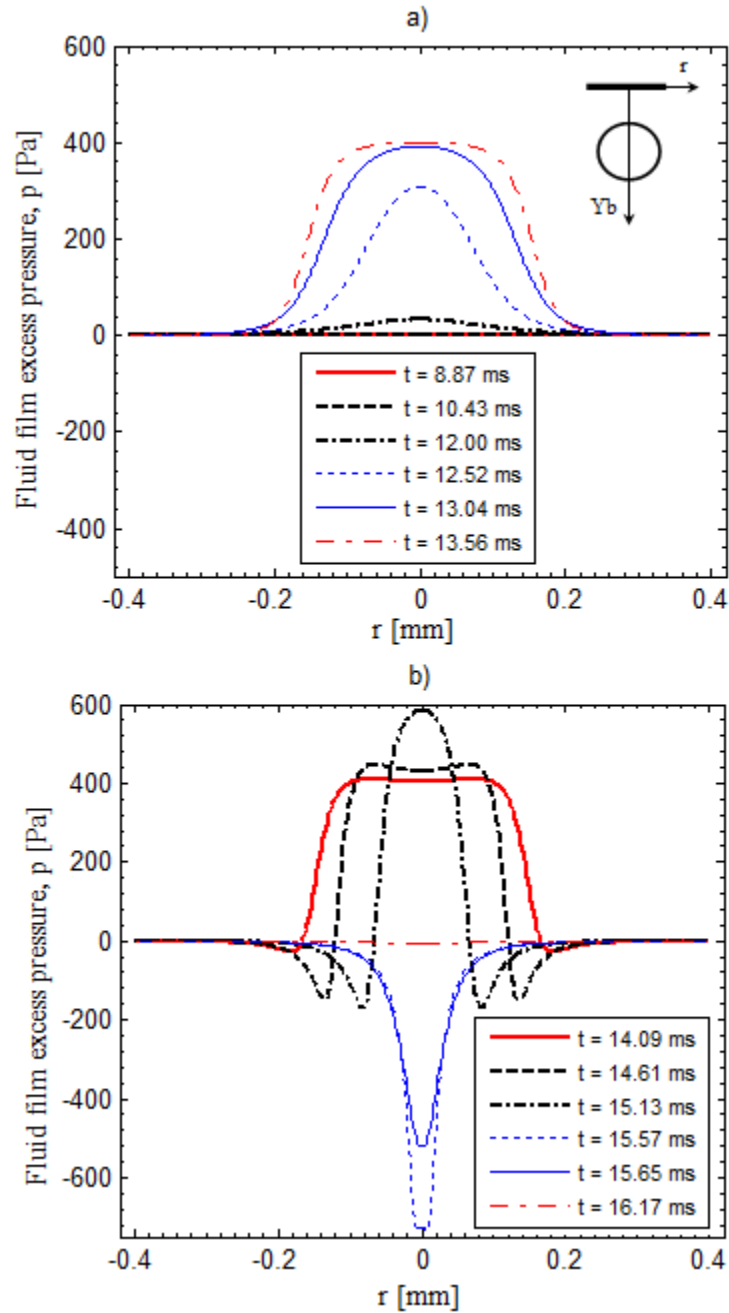


**Figure 5.8:** Evolution of the excess pressure profile during the first rebound for a bubble of radius  $R=0.4$  mm,  $Re=92$ ,  $We=0.143$  and  $Eo=0.08476$  immersed in purified water and interacting with a horizontal wall: (a) Before the first rebound; (b) After the first rebound;. The first rebound occur at 13.61ms

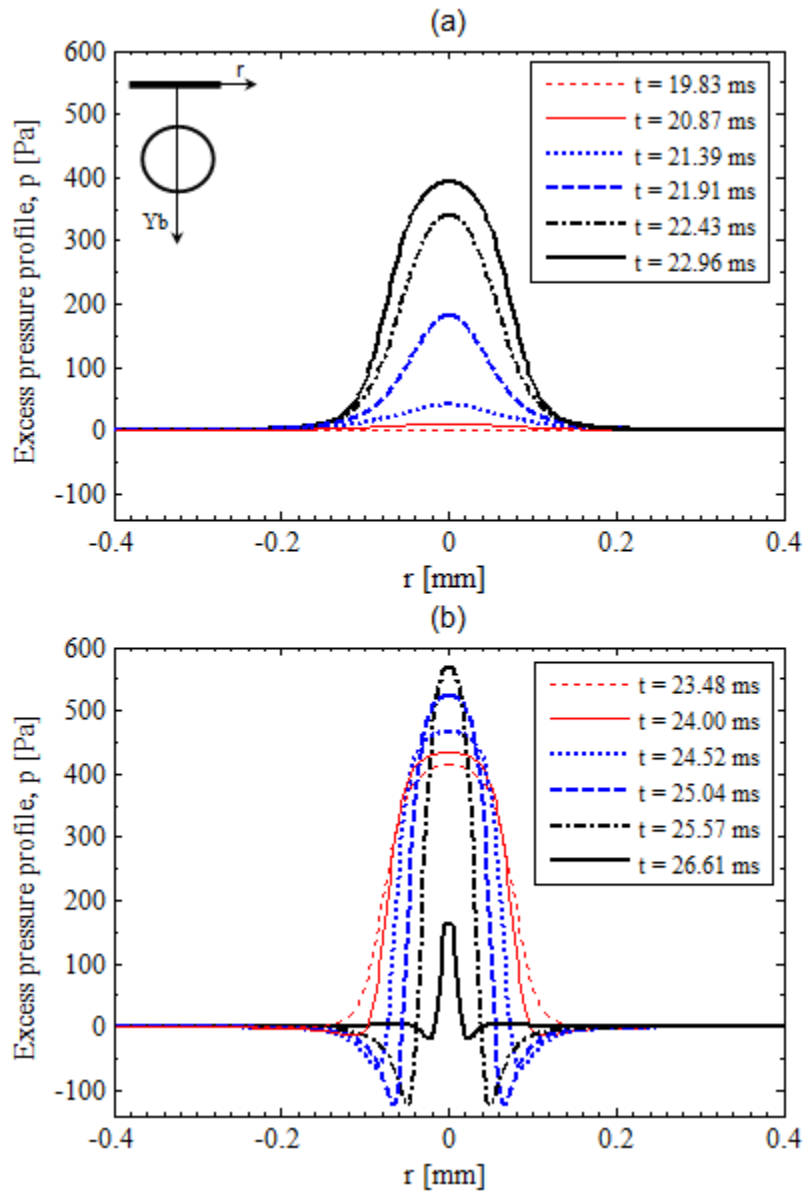


**Figure 5.9:** Evolution of the excess pressure profile during the second rebound for a bubble of radius  $R= 0.4$  mm,  $Re= 92$ ,  $We=0.143$  and  $Eo= 0.08476$  immersed in purified water and interacting with a horizontal wall: (a) Before the second rebound; (b) After the second rebound. The second rebound occur at 23.31ms

After the first rebound a negative excess pressure appears which is responsible of a more pronounced dimple (see Fig. 5.6(b.1)). This negative pressure acts over the film as a suction effect toward the wall, therefore, the fluid film thickness decrease by this action after the first rebound (see Fig. 5.6(b.1)). Similar effects to first rebound occur at the second rebound (Fig.

5.9) with the difference that the excess pressure domain is reduced. Therefore, the film force computed in the second rebound must be less than for the first rebound.

*d) Forces in a clean system*

Time evolution of the forces acting on the bubble is shown in Fig. 5.10. The data used is the same mentioned in (a). Before the time  $t = 10\text{ms}$  the buoyancy force is balanced by the drag force, and the net force is zero, therefore, the bubble moves upward at the constant terminal velocity. At  $t = 13.61\text{ms}$  the bubble velocity is reduced to zero, consequently the drag force, which is proportional to velocity, is also zero at the instant in time. As the film thickness decrease the excess pressure increases, therefore the wall force increases. As the velocity decreases the absolute value of acceleration increases, hence the added mass force decreases. The buoyancy force in accordance with its definition is constant during all the bubble-wall interaction process since a constant volume was assumed in the derivation of the model (chapter 3). At the instant of the first rebound ( $t=13.61\text{ms}$ ) the drag force is zero and the wall force and the added mass force reach its maximum absolute values.

After the first rebound the velocity changes its direction and the bubble is moving away from the wall and the magnitude of the wall force and added mass force decrease. During the following rebound the kinetic energy restored decreases, which produces a reduction on the magnitudes of the wall force and added mass force. Finally, the buoyancy force is balanced by the wall force and the bubble stoppes on the wall.

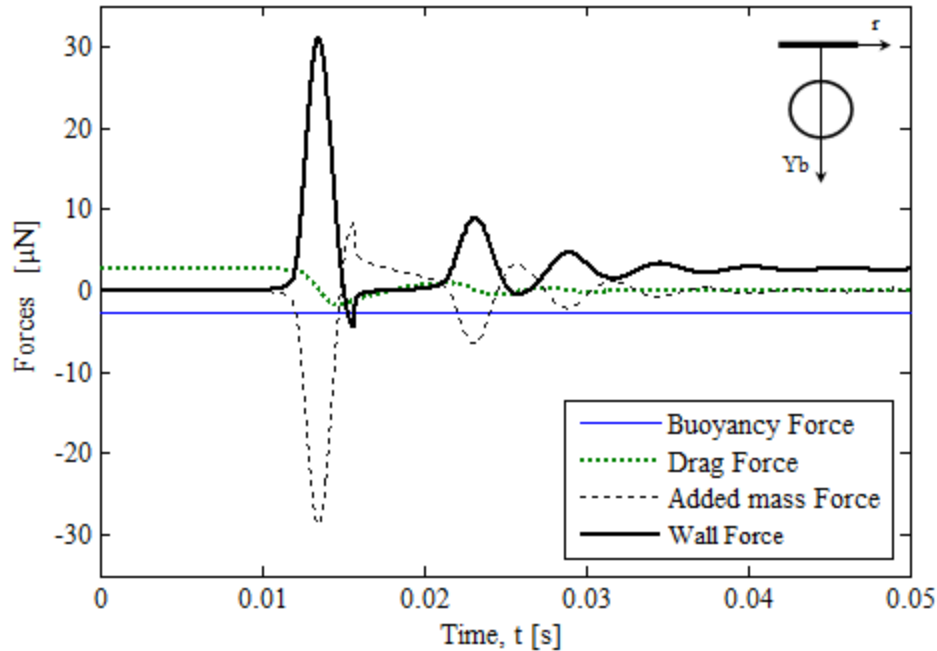


**Figure 5.10:** Time evolution of the forces exerted on a bubble of radius  $R= 0.4$  mm,  $Re= 92$ ,  $We=0.143$  and  $Eo= 0.08476$  immersed in purified water and interacting with a horizontal wall.

e) *Bubble rising in a contaminated and a clean system*

A comparison between the bubble velocity and position obtained for a bubble of  $R=0.4$ mm immersed in a clean system and in a contaminated system is presented in Fig. 5.11. In the case of the bubble immersed in a clean system the results used are the same used for the Fig. 5.5. For the bubble in a contaminated system, the terminal velocity was  $V_T= 8.6$  cm/s which was obtained from Fig. 2.5(a). The non-dimensional numbers in this case were:  $Re = 68.8$ ,  $Eo = 0.08476$  and  $We = 0.080$ . Eqs. (5.1) and (5.3) were used to evaluate the drag and added mass coefficients respectively. Since an experimental terminal velocity was used, the drag coefficient was corrected by a factor of 1.08 such that away from the wall the buoyancy and drag forces were balanced. The lubrication equation solved in this case was the one that

corresponded to a no slip condition at the bubble surface. Hence, the value of  $M$  in Eq. (3.36) was 12.

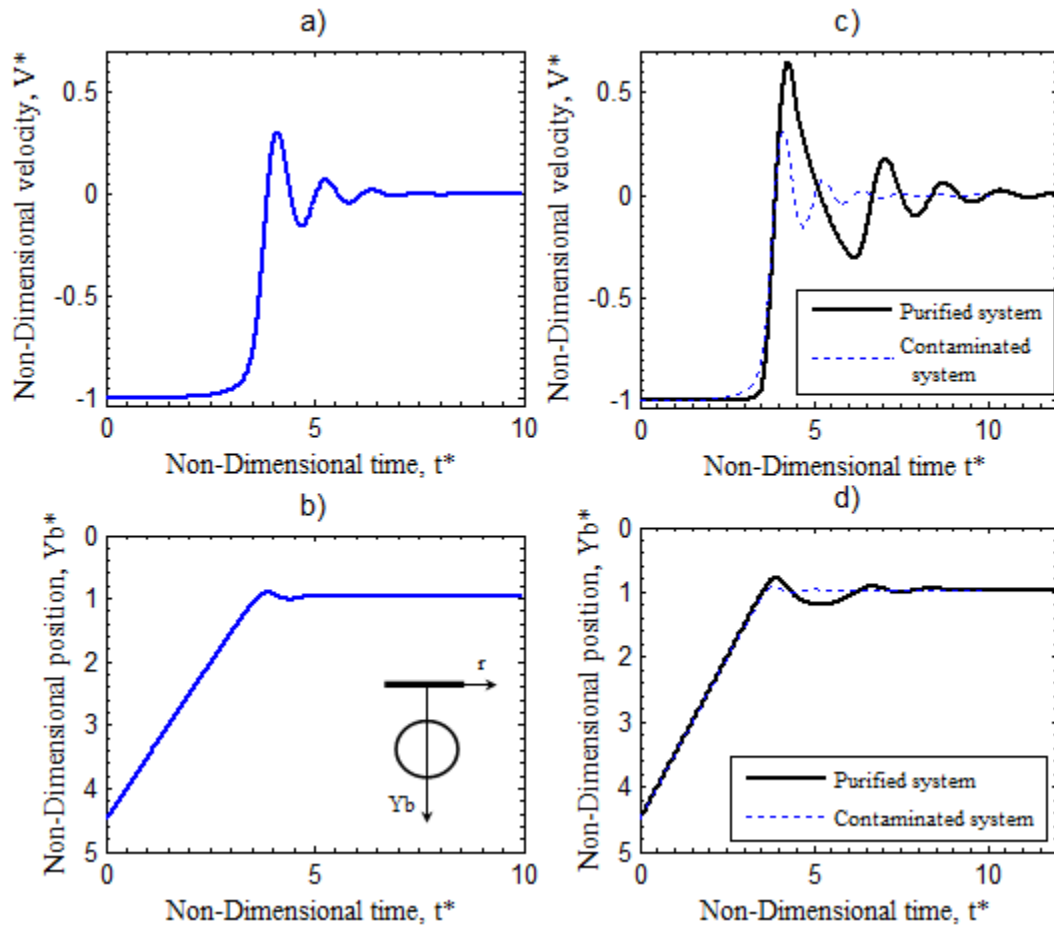


**Figure 5.11:** Non-dimensional velocity and position vs non-dimensional time for a bubble of radius  $R= 0.4$  mm. (a) and (b) bubble immersed in contaminated water ; (c) and (d) velocity and position comparison for a bubble immersed in a contaminated and a purified system.

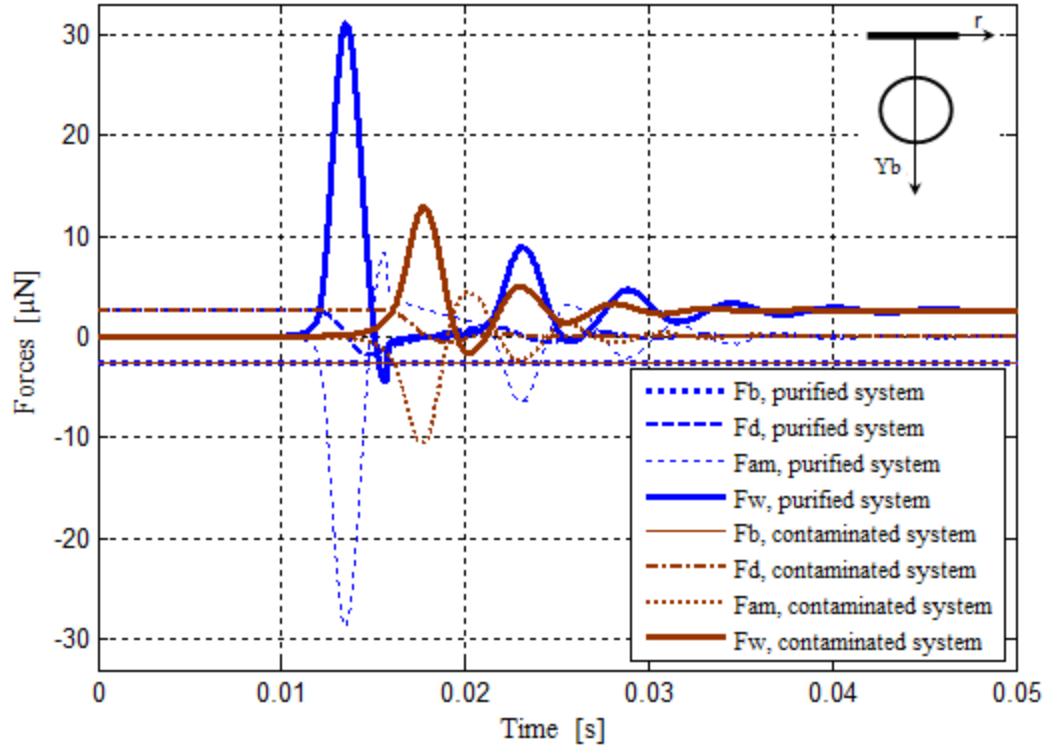


**Figure 5.12:** Time evolution of the forces exerted on a bubble of radius  $R=0.4\text{mm}$  immersed in purified and contaminated system and interacting with a horizontal wall.

The initial kinetic energy of the bubble determines the amplitude and amount of bounces during the bubble-wall interaction. The bubble in clean system has a terminal velocity greater than that of a bubble of equal radius in contaminated system. Therefore, the initial kinetic energy of a bubble immersed in a clean system is greater than for a bubble immersed in a contaminated system. As a consequence, the amplitude and the characteristic time scale of the rebound are greatly diminished for a bubble in contaminated system in comparison with the same bubble in a purified system (see Figs. 5.11(c) and 5.11(d)). Also, as a consequence of the smaller kinetic energy of the bubble immersed in contaminated water, the added mass and wall force are reduced by 50% in comparison with a bubble in clean water (Fig. 5.12).

### 5.1.3 Comparison with previous results

#### a) Comparison with experimental data

A validation of the 1D-BWI model proposed in the present thesis is shown in Fig. 5.13 in which the bubble position obtained with the present model is compared with the experimental data obtained by Tsao & Koch (1997). The experimental data was obtained for an air bubble immersed in purified water and interacting with a horizontal wall. The bubble radius was  $R = 0.79\text{mm}$ ,  $V_T = 26\text{cm/s}$ , the non-dimensional numbers were:  $Re = 410$ ,  $We = 1.463$  and  $Eo = 0.3283$ . In this case the bubble is no longer spherical; then, the correlations used for the drag and added mass coefficients were those that take into account the bubble deformation. Eqs. (2.11) and (5.5) were used for the drag coefficient. The values of functions  $G(\chi)$  and  $H(\chi)$  in Eq. (5.5) were computed using  $\chi = 1.8$  (Tsao & Koch (1997)). The added mass coefficient was constant,  $C_{am}=1.0$  and it was computed using Eq. (5.8) also with  $\chi = 1.8$ . The drag obtained with Eqs. (2.11) and (5.5) were corrected by the factors 1.57 and 1.15 respectively. The  $r_{\max}^*$  used in the simulation was 1.2. In Fig. 5.13(b), it can be observed that the numerical simulations using the correlations from Moore (1965) Eq. (5.5) and Bozzano & Dente (2009) Eq. (2.11) capture the correct instant of the rebounds. However, there is a difference in the amplitude of the rebounds that decreases over time. From Fig. 5.14 it can be seen that the maximum difference occur between  $t=20\text{ms}$  and  $55\text{ms}$  and they are always less than 15% . We attribute this difference to the constant aspect ratio  $\chi$  used during the simulations, which assumes a constant ellipsoidal bubble shape during all the bouncing process.

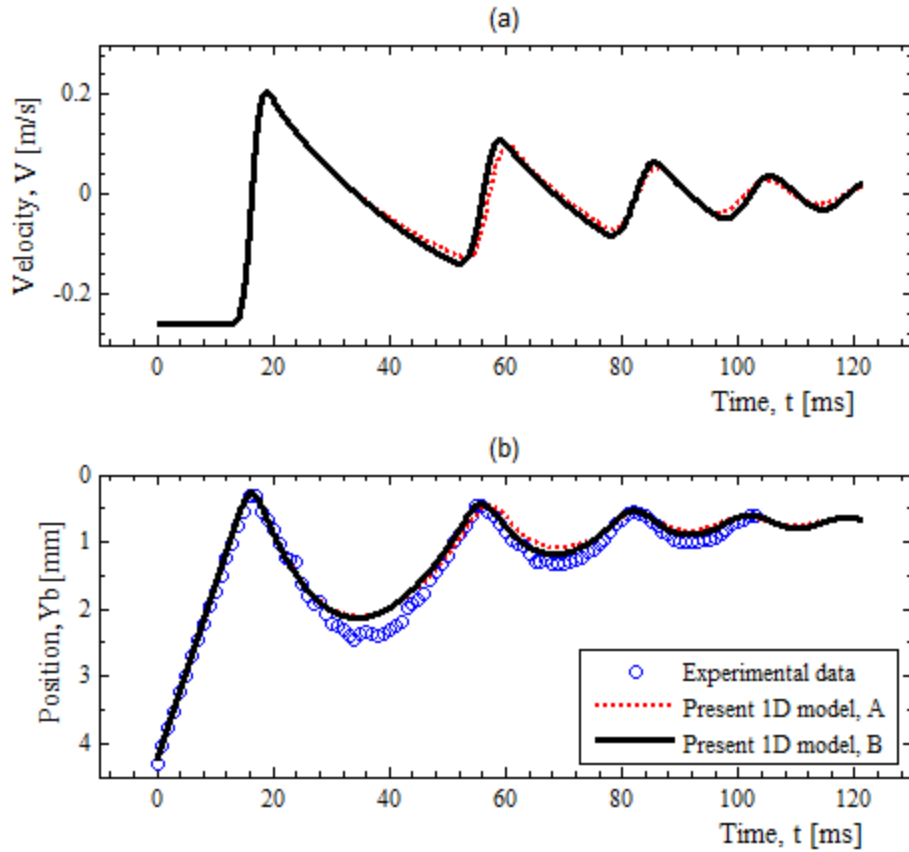


**Figure 5.13:** Centroid velocity (a) and centroid position (b) of a bubble of radius  $R=0.79\text{mm}$ ,  $Re=410$ ,  $We=1.463$  and  $Eo=0.3283$ . Discontinuous line: Present 1D-BWI model with Moore's Correlation. Continuous line: Present 1D-BWI model with Bozzano & Dente's Correlation. Circles: Experimental data from Tsao & Koch (1997).

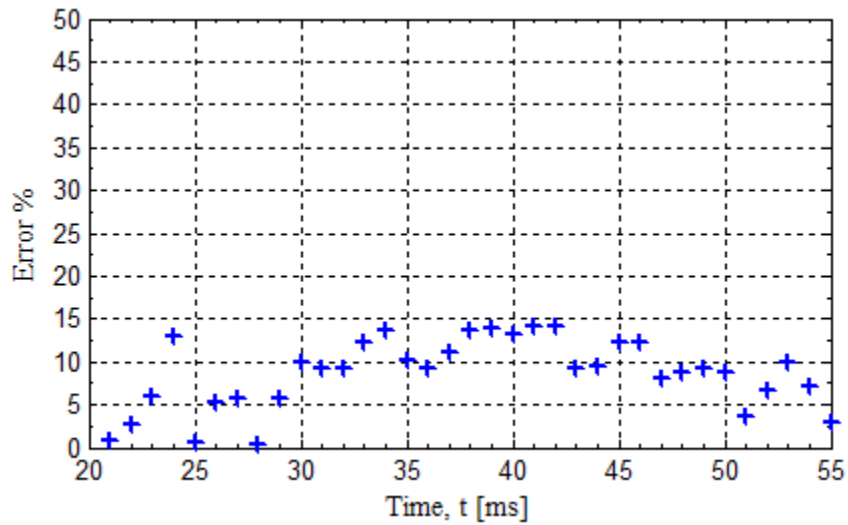


**Figure 5.14:** Difference between the present 1D model B (drag correlation from Bozzano & Dente, (2009)) specified in Fig. 5.13 and the experimental data from Tsao & Koch, (1997).

The fluid film thickness and excess pressure are shown in Fig. 5.15. The deformation is relatively large compared to the results presented in section 5.1.2 (see Fig. 5.6). This is due to two factors: (1) the terminal velocity is large and consequently, the initial kinetic energy of the bubble is also greater; (2) the Weber number ( $We=1.463$ ) is greater than one, then the bubble has a better ability to deform (Canot et al. 2003). In this case it was necessary a  $r_{\max}^* > 1$  to capture all the deformed top surface of the bubble. After the first bounce the necessary radius  $r_{\max}^*$  will be less than 1 since the kinetic energy is dissipated and the deformation is less than during the first rebound. The percentage of the initial kinetic energy restored after the first rebound was 59% ( $R= 0.79\text{mm}$ ,  $We > 1$ ), which is larger than the kinetic energy restored (42%) for  $R=0.4\text{mm}$  with  $We < 1$  (see Fig. 5.5 and Fig. 5.13). Five rebounds were observed (Fig. 5.13) until the initial energy was totally dissipated.

The fluid film thickness in the first rebound was between 10 and 15  $\mu\text{m}$  and in the following rebounds this range was reduced. These values are approximately 1/100 of the bubble radius(0.79mm) and the assumption  $h / R \ll 1$  is satisfied.

Figure 5.16 shows the time evolution of the forces for the bubble considered in Fig. 5.13 with the drag correlation from Bozzano & Dente, (2009). As it was observed for smaller bubbles, in this case, we can observe that the wall force is balanced by the added mass force.

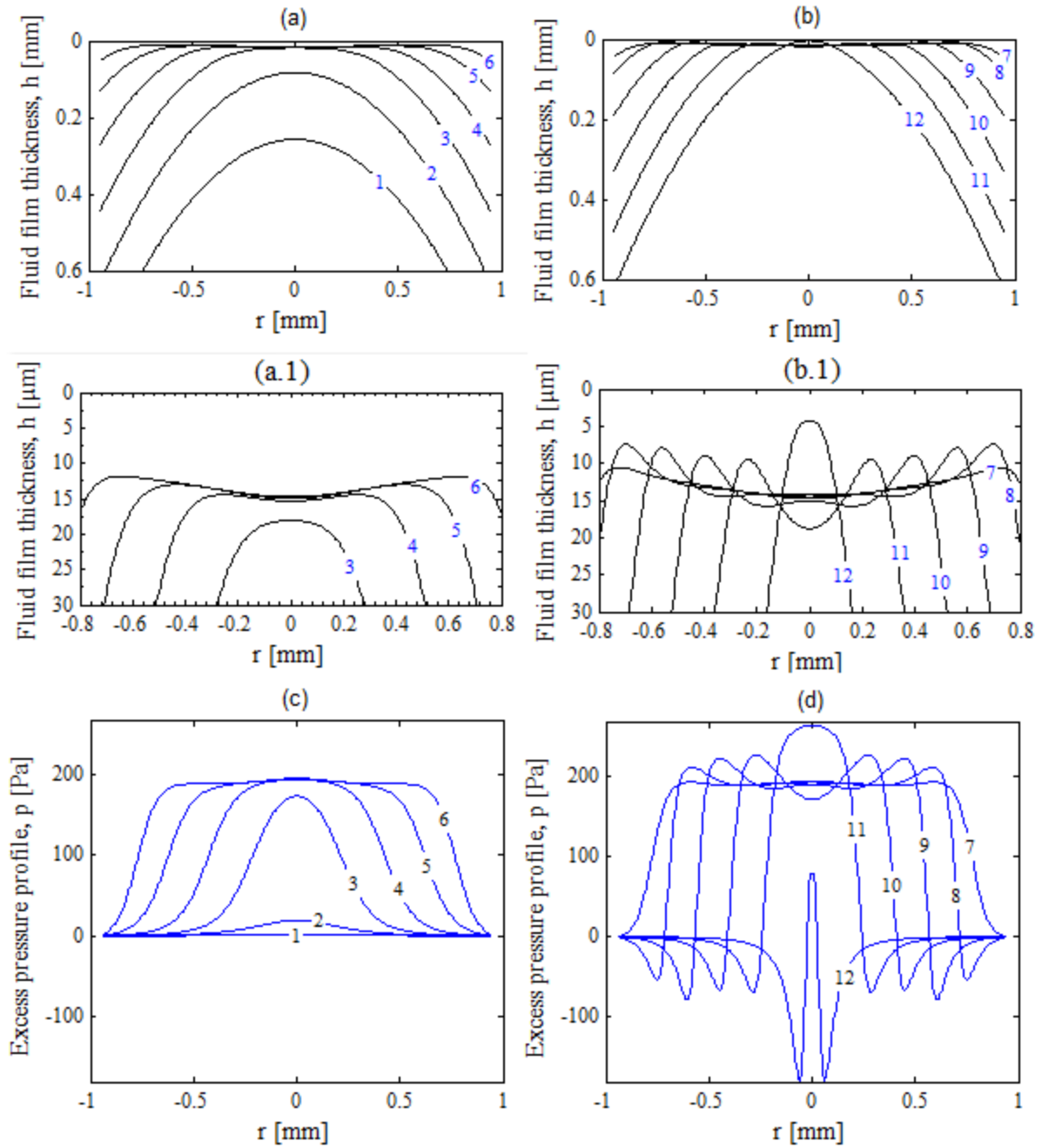


**Figure 5.15:** Excess pressure and film thickness profiles of a bubble of radius  $R=0.79\text{mm}$ ,  $Re=410$ ,  $We=1.463$ ,  $Eo=0.3283$  during the first rebound. (a) and (c) are the fluid film thickness and excess pressure profile before the 1<sup>st</sup> rebound at 12.4 ms (1), 13.12ms (2), 13.90ms (3), 14.58ms (4), 15.31ms (5), and 16.04ms (6). (b) and (d) are the fluid film thickness and excess pressure profile after 1<sup>st</sup> rebound at 16.35 ms (7), 17.08ms (8), 17.81ms (9), 18.53 ms (10), 19.26ms (11), and 20.00ms (12). (a.1) and (b.1) are amplified view of (a) and (b) respectively. The 1<sup>st</sup> rebound occur at  $t = 16.346\text{ms}$ .

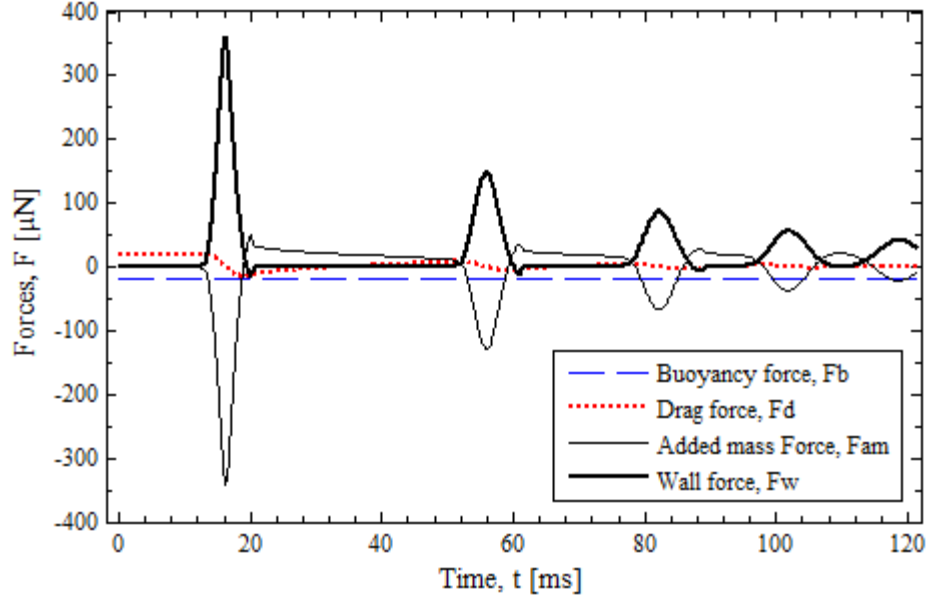


**Figure 5.16:** Time evolution of the forces exerted on a bubble of radius  $R=0.79$  mm,  $Re=410$  and  $We=1.463$  immersed in purified system and interacting with a horizontal wall.

*b) Comparison with previous 1D-BWI model results*

Figure 5.17 shows a comparison between the solution obtained with the present 1D model, the solution obtained by Moraga et al. (2005) and the experimental data for the same data used in (a). We can see that the solution of the present 1D model has a better agreement with the experimental data than the solution reported by Moraga et al. (2005). The amplitude of the rebound from the previous model is similar to the present model but the instants of rebounds are out of phase by a maximum of 10 ms for the third rebound (Fig. 5.17). The methodology used for the 1D-BWI model in the present thesis is the same used by Moraga et al. (2005) but an error in the derivation of the equations in non-dimensional form was detected. They used a Weber number based on bubble diameter ( $We = \rho_f |\vec{V}_T|^2 2R / \sigma$ ) in the film drainage equation and based on the bubble radius ( $We = \rho_f |\vec{V}_T|^2 R / \sigma$ ) in the bubble motion equation. We used a Weber number based on bubble diameter to derive all equations for 1D, 2D and 3D versions of the BWI-model. Also, the terms multiplied by  $h^* - h0^*$  in Eq.

(C.2) (Appendix C) have been neglected by Moraga et al. (2005). We have used these terms, however we checked the effect of neglecting these terms and no appreciable variation in the results was observed. Moraga et al. (2005) have used a  $\Delta t^* = 0.002$  and we have used a  $\Delta t^* = 0.001$ ; but also in this case the solution was not affected. Therefore, the principal discrepancy in the results respect to the work of Moraga et al. (2005) is attributed to the error committed on the definition of the  $We$  number.

The results of the equations of the present 1D-BWI model using the Moore's correlation and the correlation recently published by Bozzano & Dente, (2009) for the drag coefficient were nearly superposed (Fig. 5.17). This confirmed that the equations used by Moraga et al. (2005) needed to be corrected despite that they have used the Moore's correlation for the drag coefficient.

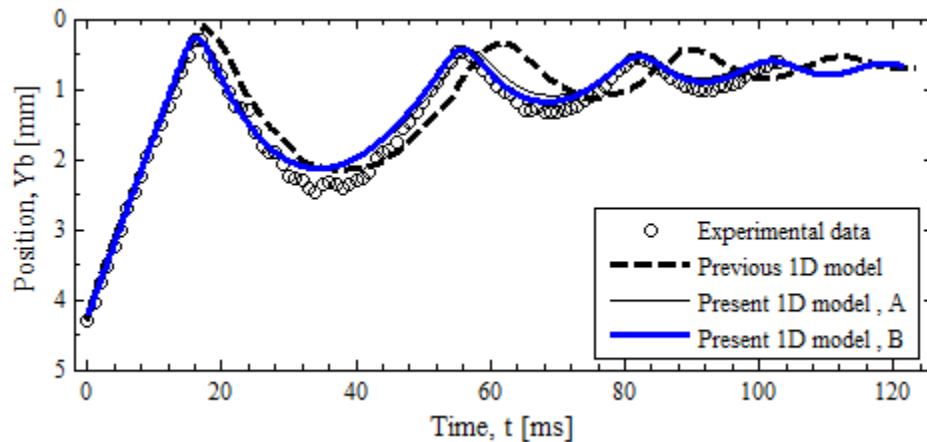


**Figure 5.17:** Centroid position of a bubble of  $R=0.79\text{mm}$ ,  $Re=410$  and  $We=1.463$ . Continuous line: present 1Dmodel A with drag correlation from Moore (1965); Continuous bold line: present 1D model B with drag correlation from Bozzano & Dente, (2009); Discontinuous bold line: Previous model 1D from Moraga et al. (2005); Circles: experimental data from Tsao & Koch, (1997).

#### 5.1.4 Critical radius for the rebound of an air bubble in water

Simulations using the parameters shown in Table 3 to investigate the critical radius for the rebound of an air bubble immersed in water and interacting with a wall have been made. The water is considered contaminated, hence, the bubble surface is considered immobile and Eq. (5.1) and Eq. (5.3) are used to obtain the drag coefficient and the added mass coefficient respectively. In this case the terminal velocities were calculated from the force balance between the drag and buoyancy forces away from the wall.

**Table 3:** Data used for runs

R [ $\mu\text{m}$ ]	VT [cm/s]	Re	We	Eo
150	2.94	8.809	0.0034956	0.011919
200	4.25	16.995	0.0097577	0.02119
210	4.51	18.929	0.0115282	0.023362
230	5.02	23.080	0.0156495	0.028023
240	5.27	25.296	0.0180145	0.030513
250	5.52	27.602	0.0205916	0.033109
300	6.74	40.466	0.0368811	0.047677
350	7.92	55.462	0.0593837	0.064893
400	9.06	72.495	0.0887751	0.084758

In Figs. 5.18, 5.19 and 5.20 the bubble velocity, position and wall force for several bubble radii are presented. In these figures as the bubble radius decreases the kinetic energy restored decreases. The amplitude and number of oscillations of the wall force also decrease. A bubble is considered not to rebound when bubble velocity oscillations are not observed. According to this criterion, a bubble immersed in contaminated water with radius  $R \leq 200 \mu\text{m}$  does not bounce on a horizontal wall. Air bubbles of  $R < 250 \mu\text{m}$  immersed in

water are not affected by the contamination at the surface (Fig. 2.5(a)), and their terminal velocities are equal in a clean and a contaminated system. Therefore, the critical diameter determined is valid for an air bubble in clean and contaminated water.

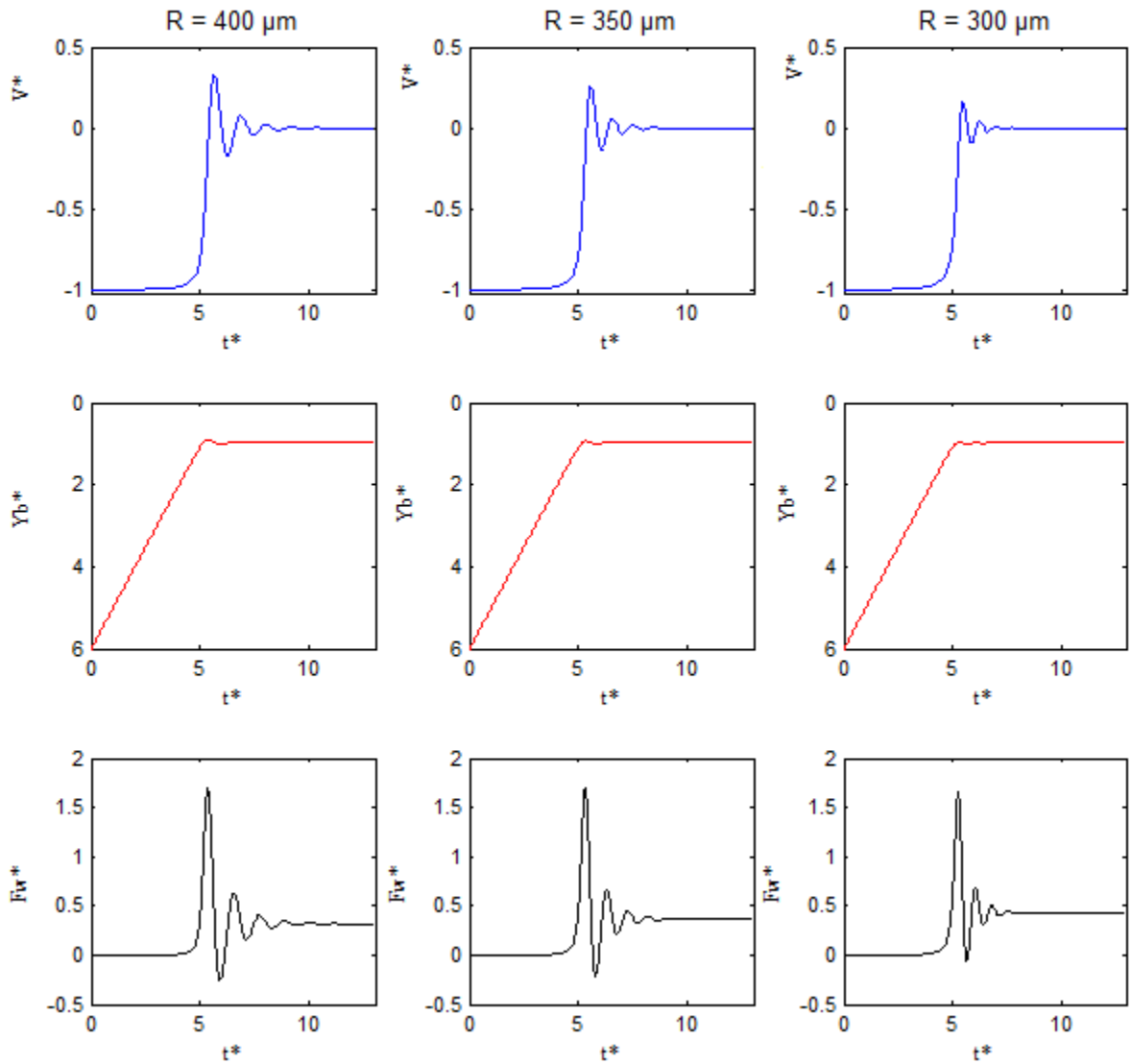


**Figure 5.18:** Non-dimensional velocity, position and wall force vs non-dimensional time for bubble radius  $R=400\mu\text{m}$ ,  $R=350\mu\text{m}$  and  $R=300\mu\text{m}$ .

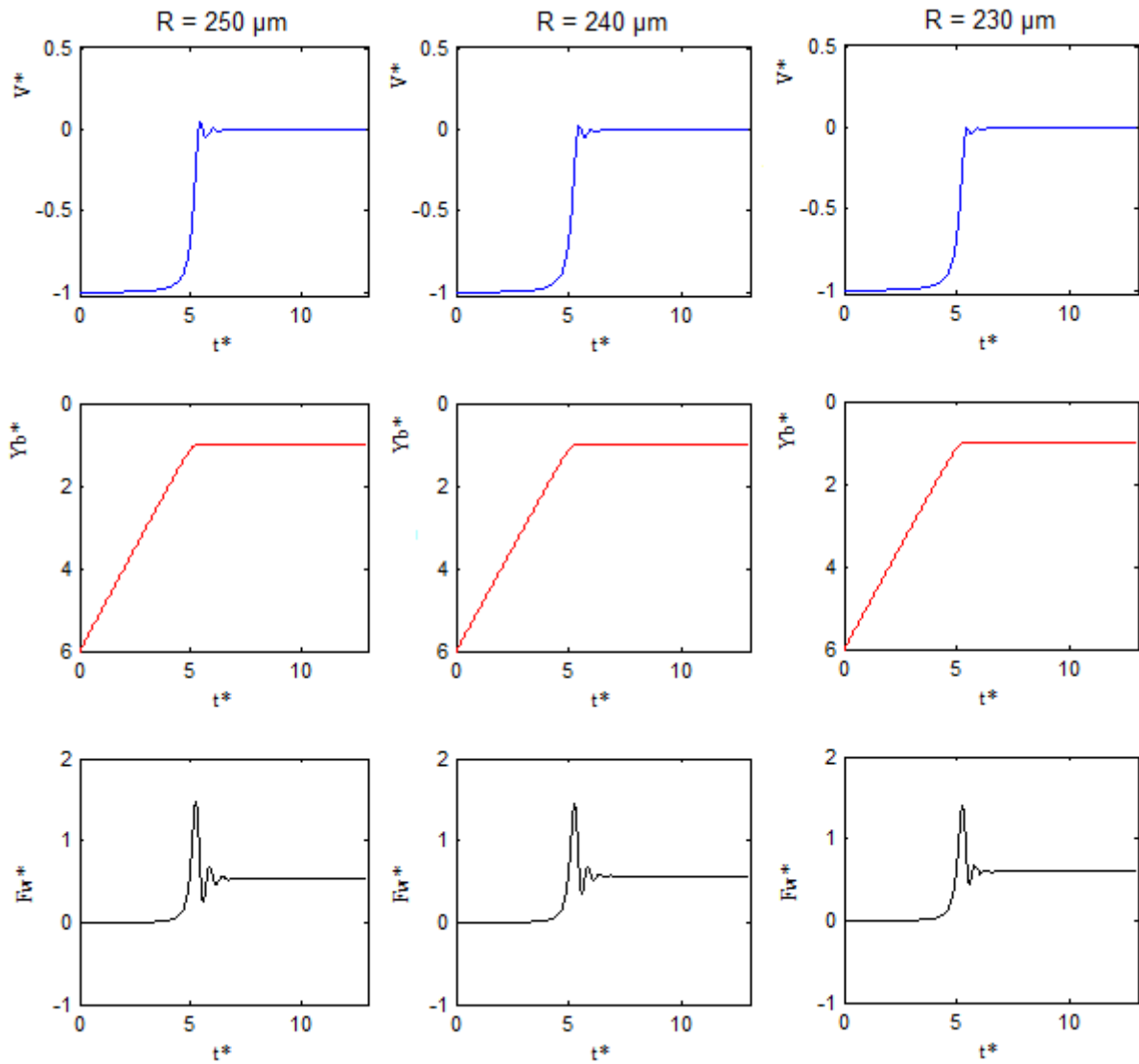


**Figure 5.19:** Non-dimensional velocity, position and wall force vs non-dimensional time for bubble radius  $R=250\mu\text{m}$ ,  $R=240\mu\text{m}$  and  $R=230\mu\text{m}$ .

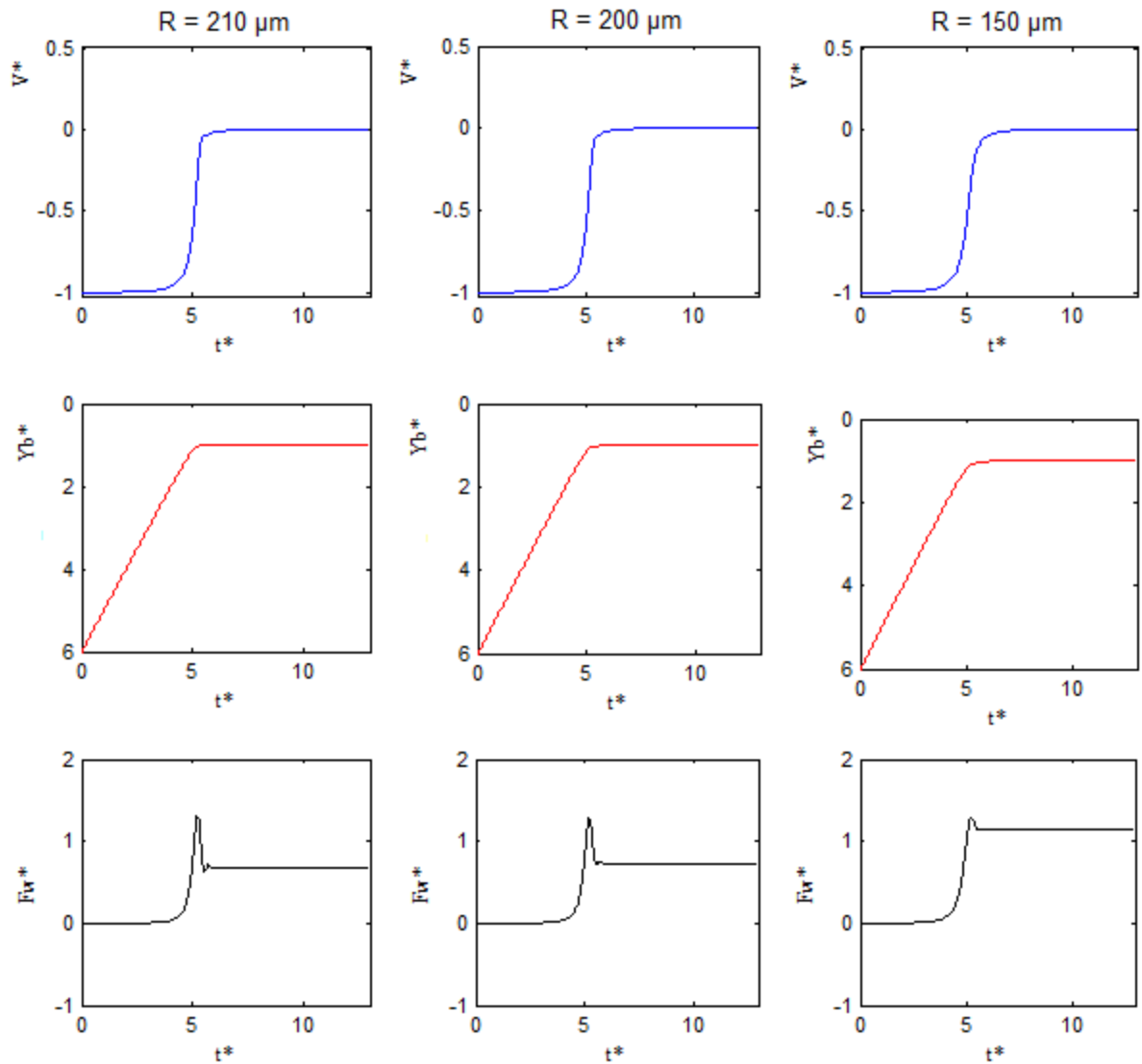


**Figure 5.20:** Non-dimensional velocity, position and wall force vs non-dimensional time for bubble radius  $R=210\mu\text{m}$ ,  $R=200\mu\text{m}$  and  $R=150\mu\text{m}$ .

## 5.2 INTERACTION WITH AN INCLINED WALL

The solution of the 3D-BWI model (simulations made with the 3D-BWI CODE) to predict the dynamic behavior of a bubble interacting with a horizontal and inclined wall are presented in this section.

### 5.2.1 Computer code analysis

A computational code was developed to solve in Cartesian coordinates the 3D version of the bubble-wall interaction model proposed in chapter 3. This implementation is justified since the axial symmetry of the cylindrical coordinate 1D version is no longer valid for a bubble interacting with a wall with one or two inclinations. A large computational time was required to solve the thirteen diagonal band matrix necessary to solve the lubrication equation for the fluid film thickness. Therefore, several algorithms to solve the linear system (Eq. (4.62)) were implemented and a comparison was made to determine which algorithm was more efficient in terms of the computational time needed to solve the linear system. The algorithms implemented were the following: Gauss elimination (direct method), Gauss Jordan elimination (direct method), LU decomposition with backward and forward substitution (direct method), Jacobi method (iterative method) and Successive Over-Relaxation method (Iterative method) (Press et al. 2001; Hoffman, 2001; Nakamura, 1992). The LU decomposition with backward and forward substitution was chosen because it was much faster in solving the linear system with respect to the other methods. The bubble motion and film drainage equations were solved with a tolerance of  $10^{-8}$ , the non-dimensional time step was between 0.001 and 0.002 in most of the simulations.

A spatial grid study analysis was performed to determine the proper grid resolution required in order to obtain reliable results. Fig. 5.21 shows the normal distance between the bubble and the wall over time for several levels of spatial grid resolution using the 3D-BWI code and compared with results of 1D-BWI code (solution of the 1D-BWI model) for a bubble rising in a clean system and towards a horizontal wall ( $\theta = 0^\circ$ , and  $\alpha = 0^\circ$ ). The bubble characteristics are given by  $R=0.79\text{mm}$ ,  $V_T = 0.26\text{m/s}$ ,  $r_{\max}^* = 1.2$ ,  $Re = 410$ ,  $We = 1.463$  and  $EO = 0.3283$ . The non-dimensional time used was 0.002. The drag and added mass coefficients used were the same used to obtain Fig. 5.13. The results of the grid resolutions 30x30 (the first value represents the number of nodes in  $x$ -direction, the second represents the number of nodes in  $y$ -direction), 32x32 and 40x40 are almost superposed with the results from the 1D-BWI code which was run with 200 radial nodes (see Fig. 5.21). Fig. 5.22 shows that as the grid resolution increases the bubble position converges to the results obtained by the 1D-BWI code for time  $t=35\text{ms}$ .

Based on results shown in Figs. 5.21 and 5.22 grid resolutions between 30x30 and 40x40 and non-dimensional time between 0.001 and 0.002 were used in all the following simulations. Based on the results of the 1D-BWI model we used time steps between 0.001 and 0.002 because it was observed (Fig. 5.4), that for smaller time steps the difference in the results was negligible.

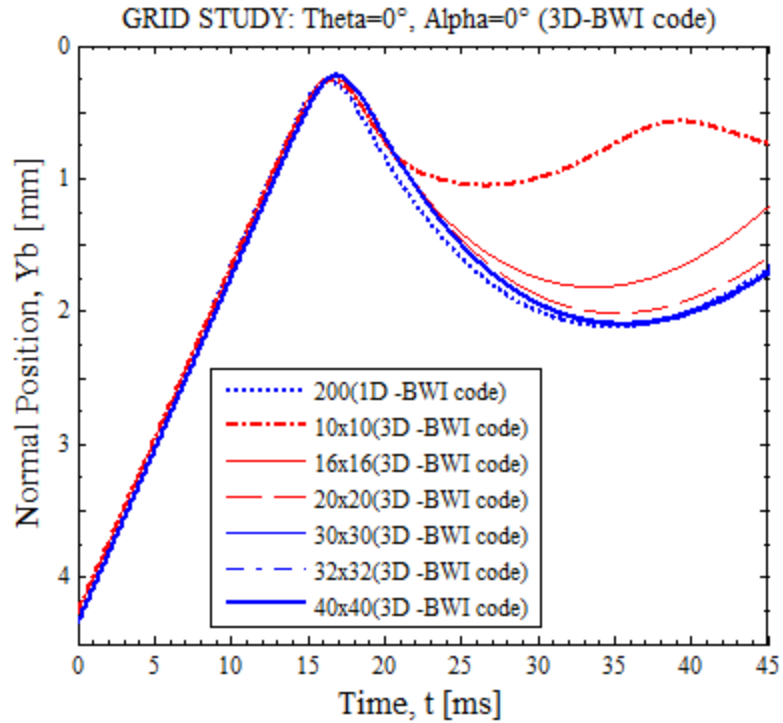


**Figure 5.21:** Normal position of a Bubble respect to a horizontal wall for different values of spatial grid resolution using 3D-BWI and 1D-BWI codes. Bubble in clean system with characteristics given by  $R=0.79\text{mm}$ ,  $Re=410$ ,  $We=1.463$  and  $EO=0.3283$ . In 3D-BWI code, the angles  $\theta = 0^\circ$  and  $\alpha = 0^\circ$  were used.

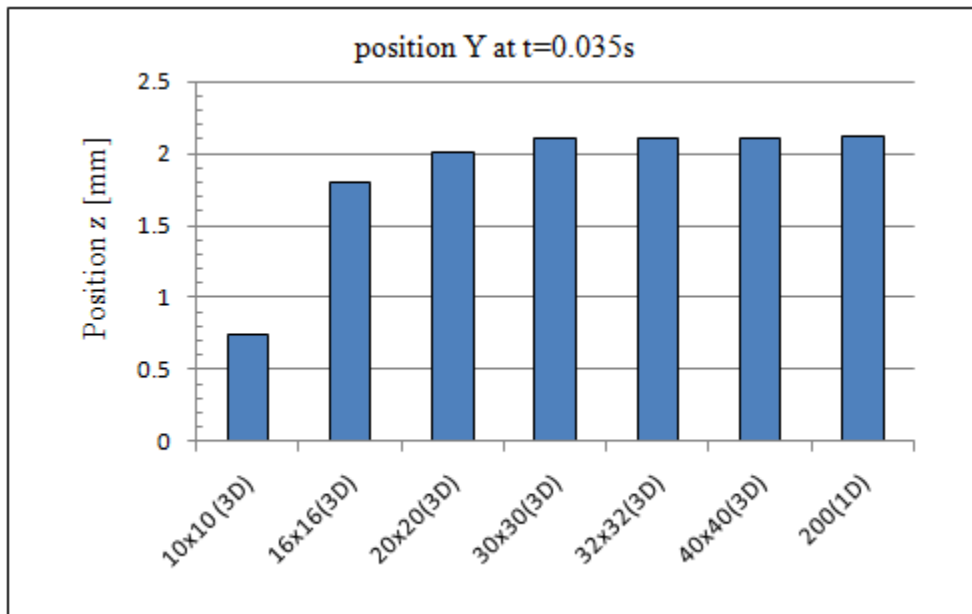


**Figure 5.22:** Position vs Grid Resolution at time  $t = 0.035\text{s}$  (35ms) from Fig. 5.21

## 5.2.2 Comparison with the 1D-Model

Figure 5.23 shows a comparison between the experimental data and simulation results using the 1D-BWI code and the 3D-BWI code for a bubble immersed in a clean system and interacting with a horizontal wall. The bubble characteristics were the same used to perform the grid study in Fig. 5.21. The grid resolution and non-dimensional time step used were  $31 \times 31$  and 0.001 respectively. As we can see, the solution obtained with the 1D-BWI model in cylindrical coordinates which directly accounts for the axisymmetry of the problem, is superposed with the solution of the 3D-BWI model in Cartesian coordinates which does not assume the axisymmetrical condition. Our 3D-BWI model predicts that the bubble impacts on the horizontal wall and rebounds five times from the wall (see Fig. 5.23) with a maximum amplitude difference in the first rebound of 15% with respect to the experimental data.

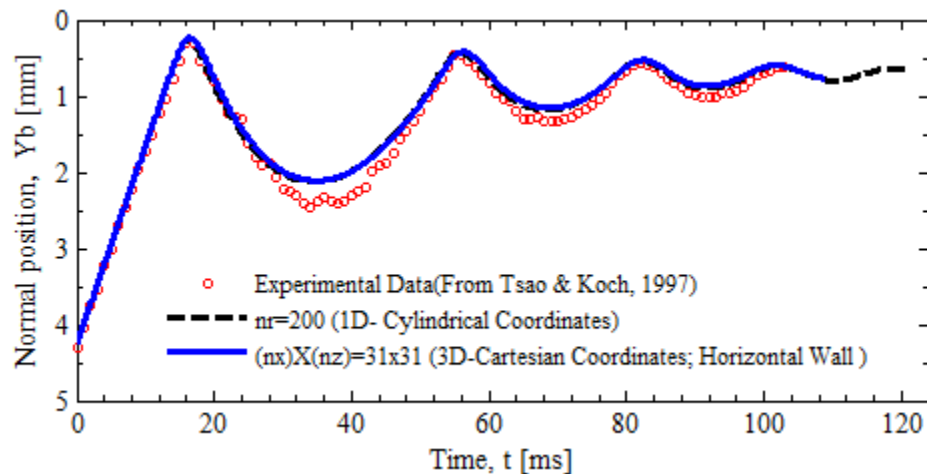


**Figure 5.23:** Centroid position of a bubble of  $R=0.79\text{mm}$ ,  $Re=410$  and  $We=1.463$  immersed in a clean system and interacting with a horizontal wall; Continuous bold line: present Cartesian coordinates 3D-BWI model; Discontinuous bold line: Present cylindrical coordinates 1D-BWI model; Circles: experimental data from Tsao & Koch, (1997).

Figure 5.24 shows the evolution of the fluid film thickness as the bubble approaches the horizontal wall during the first rebound. This figure was constructed using the results

obtained with the 3D-BWI code. The time  $t = 15.8ms$  was just before the first rebound and time  $t = 17.01ms$  was just after the first rebound. The first rebound occurs at  $t = 17.346ms$ . As observed in the results obtained in Figs. 5.24-5.26 we can observe that the 3D-BWI model predicts the axisymmetrical deformation in the case of a bubble interacting with a horizontal wall.

Figures 5.25 and 5.26 show the non-dimensional excess pressure profile obtained with the 3D-BWI code in which again the axisymmetric condition of the excess pressure profile is obtained.

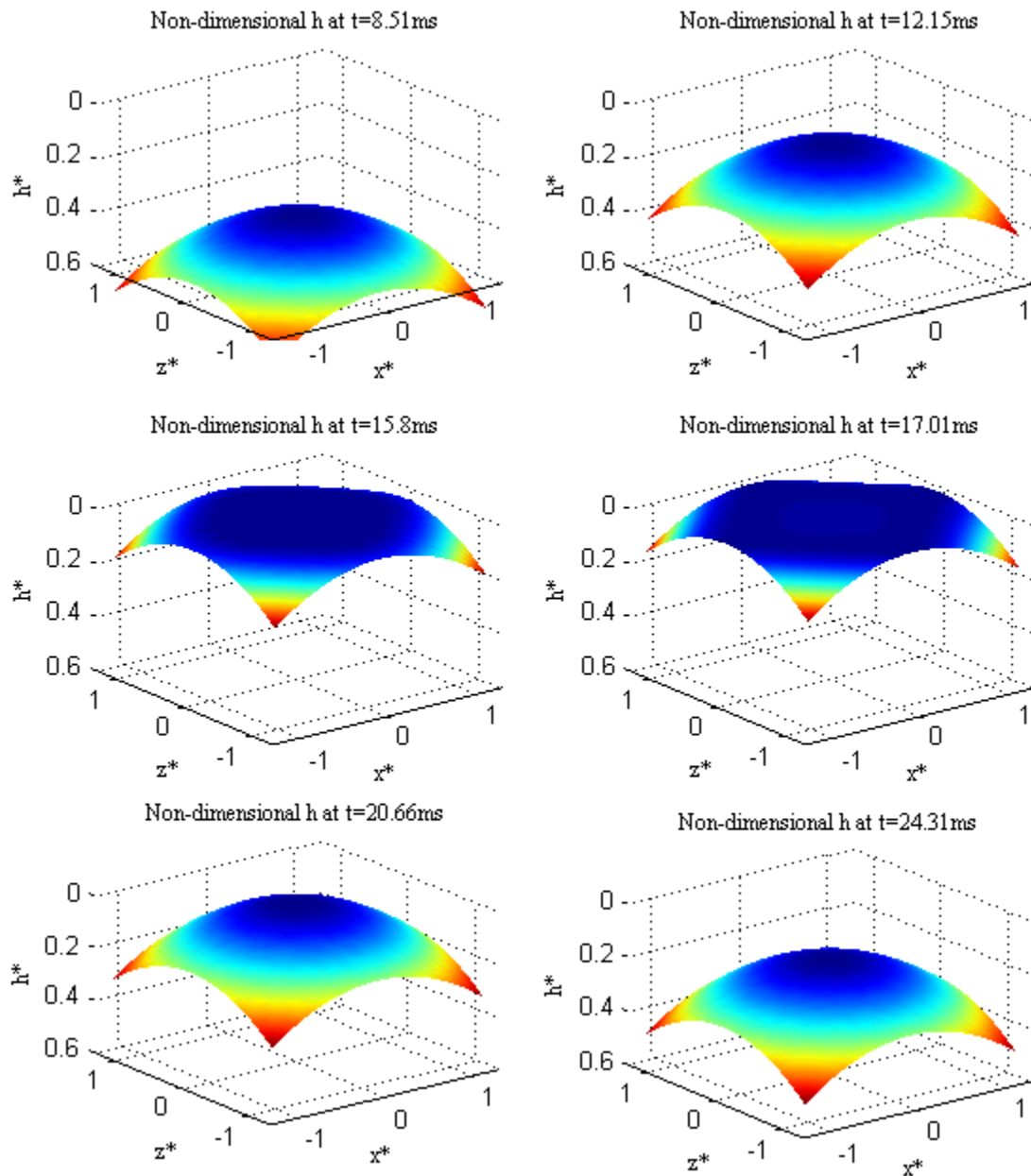


**Figure 5.24:** Time evolution of the non-dimensional fluid film thickness during the first rebound of a bubble of  $R=0.79$ mm,  $Re=410$  and  $We=1.463$  immersed in a clean system and interacting with a horizontal wall. The first rebound occur at  $t = 16.346$  ms .

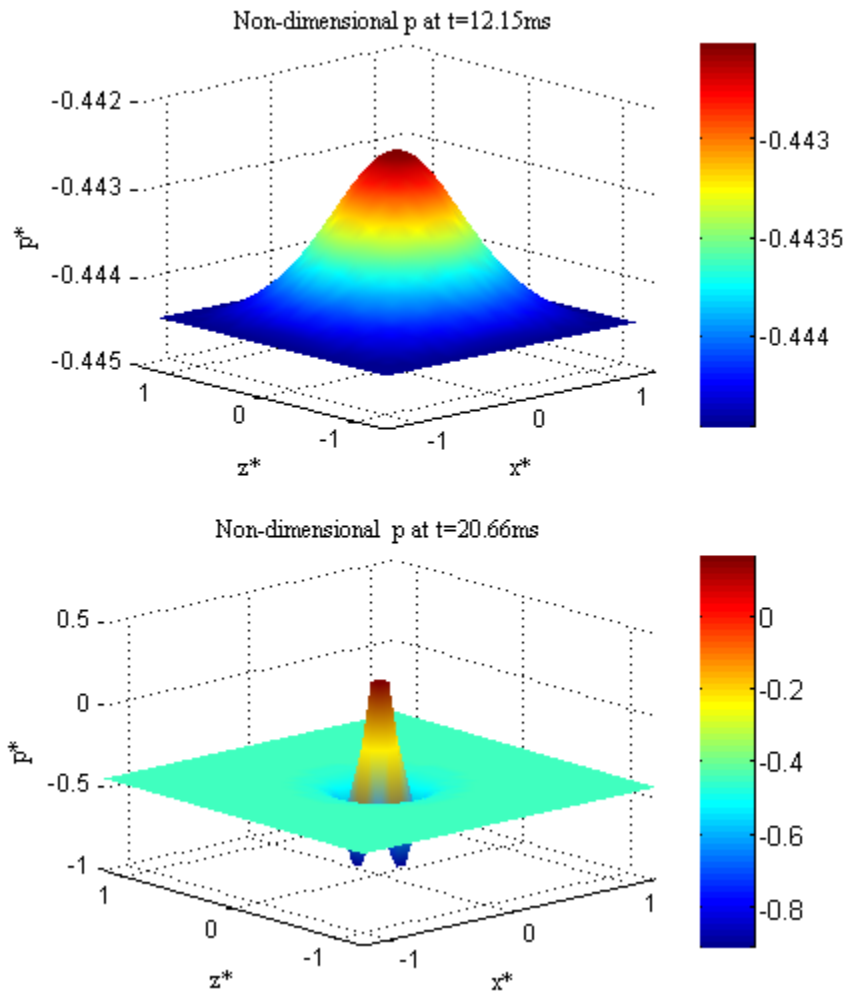


**Figure 5.25:** Non-dimensional excess pressure profile of a bubble before the first rebound ( $t=12.15\text{ms}$ ) and after the first rebound ( $t=20.66\text{ms}$ ). Bubble immersed in clean system with characteristics given by  $R=0.79\text{mm}$ ,  $Re=410$  and  $We=1.463$ . The first rebound occur at  $t = 16.346 \text{ ms}$ .

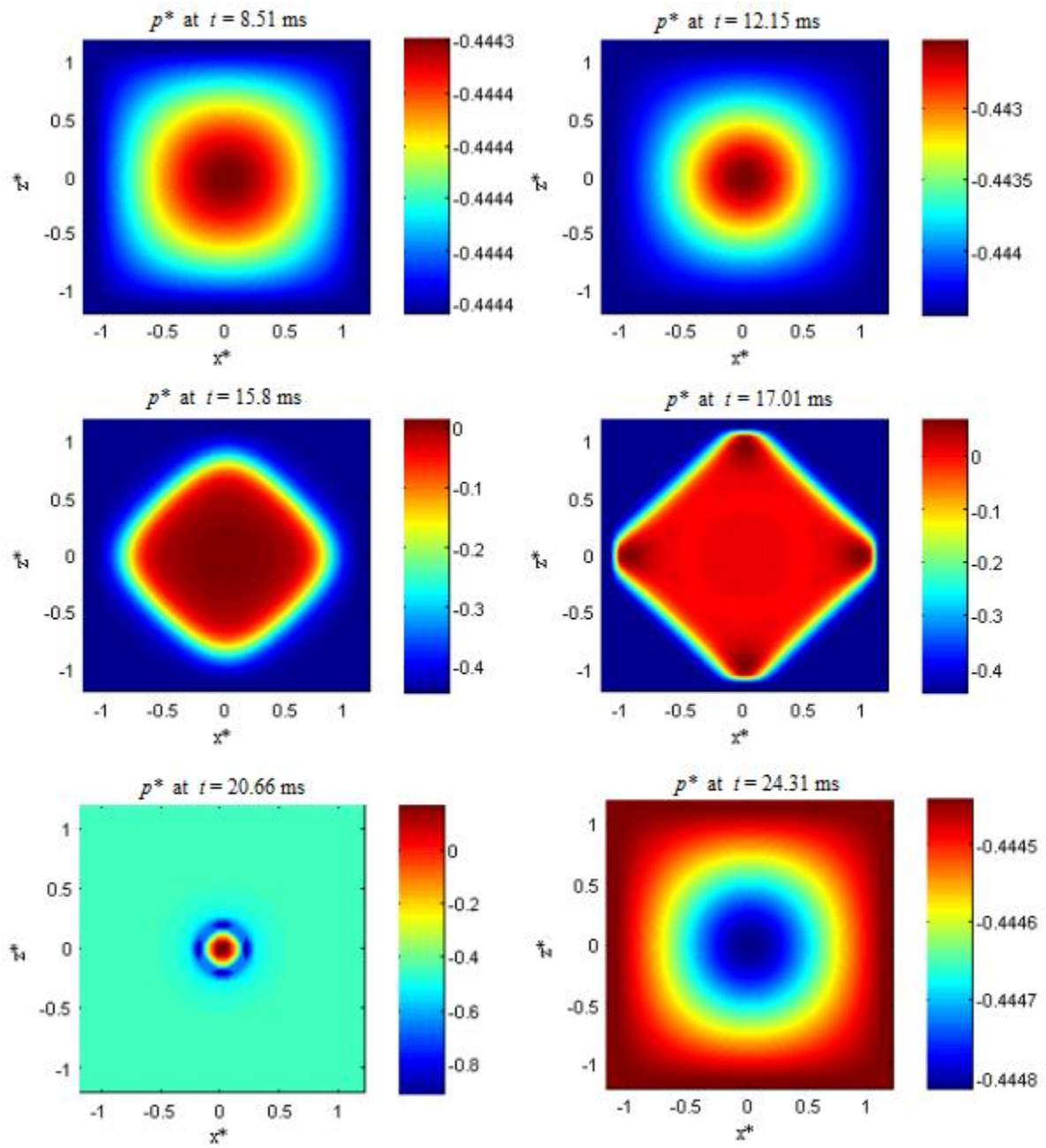
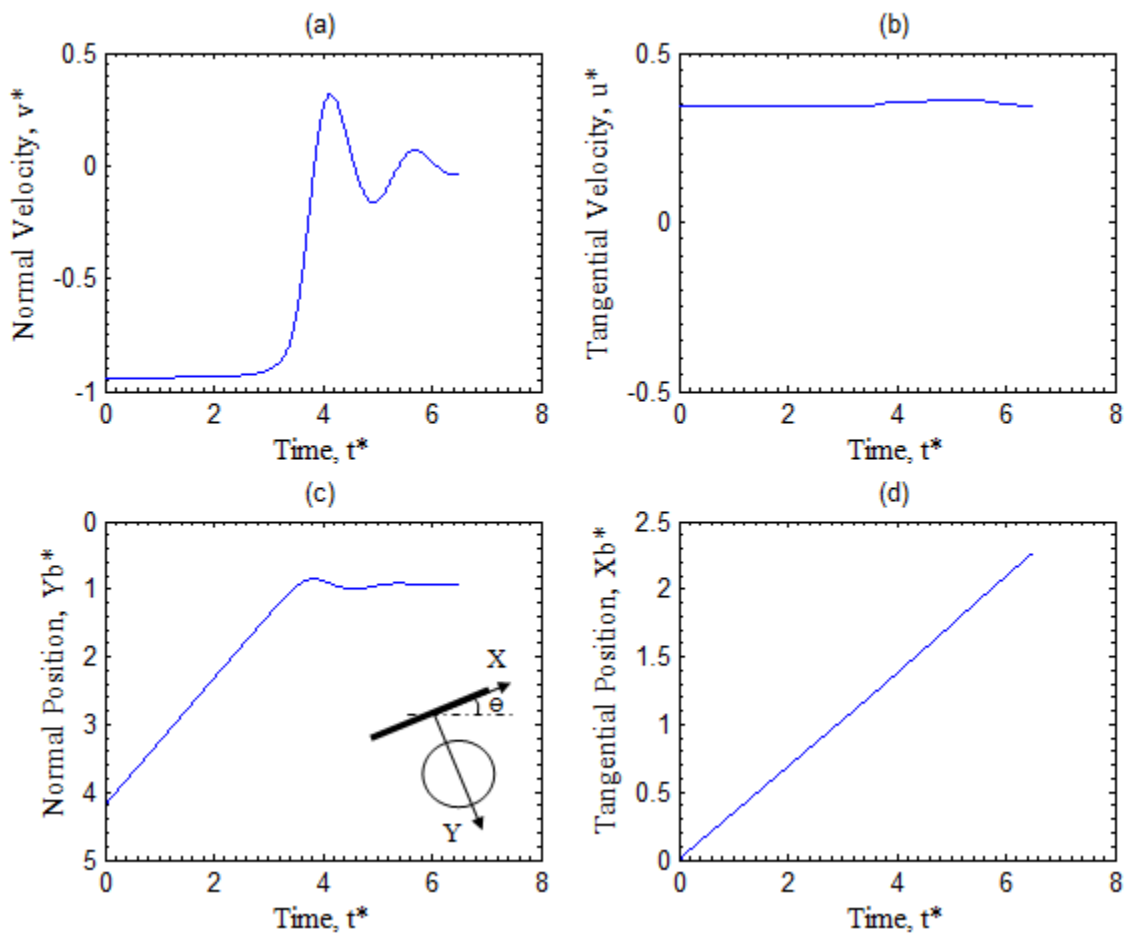


**Figure 5.26:** Non-dimensional excess pressure profile on a bubble during the first rebound. Bubble characteristics are given by  $R=0.79\text{mm}$ ,  $Re=410$  and  $We=1.463$ . The first rebound occur at  $t = 16.346$  ms.

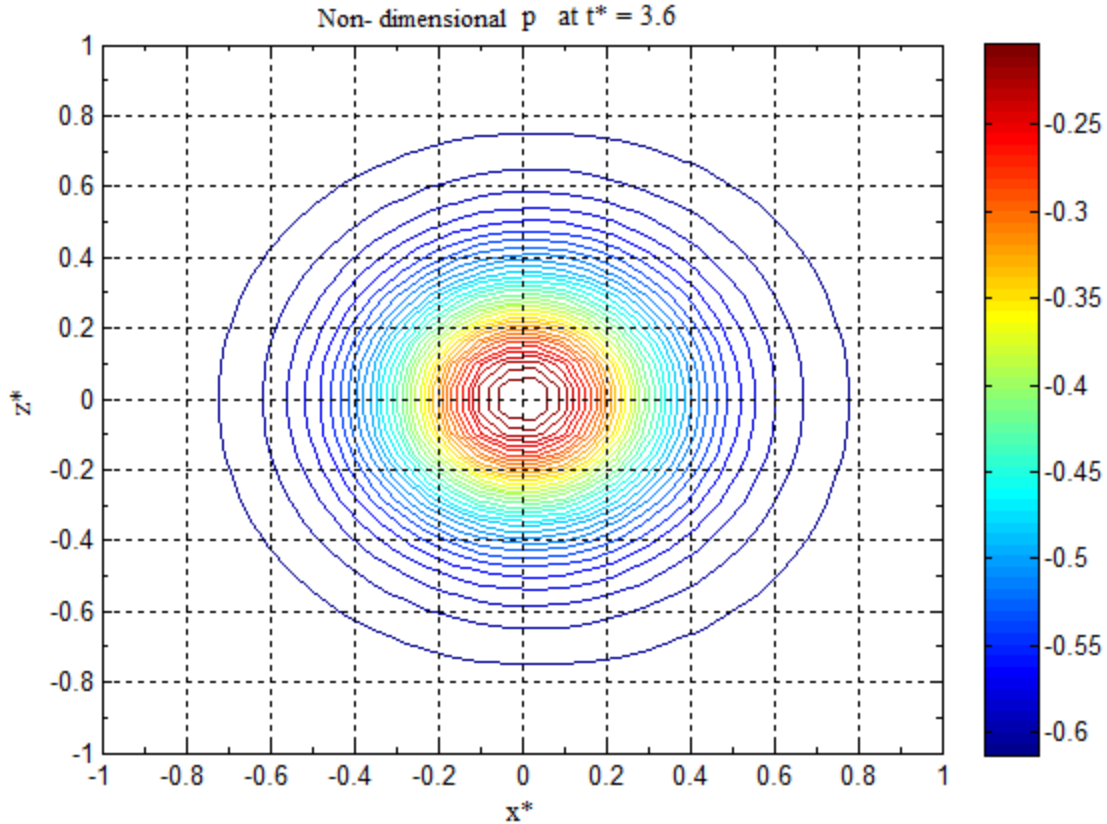
### 5.2.3 Prediction of bubble motion when interacting with a wall with one inclination

Figure 5.27 shows the velocities and positions of a bubble rising in a contaminated system and interacting with a wall at  $\theta = 20^\circ$ . The bubble characteristics are given by  $R=0.51\text{mm}$ ,  $r_{\max}^* = 1.0$ ,  $Re=103$ ,  $We= 0.24$  and  $Eo=0.1938$ . The grid and non dimensional time step used were  $32 \times 32$  and  $0.002$ . The drag and added mass correlations used were those from the Eqs. (5.1) and (5.3) respectively. The bubble rebound in the direction normal to the wall ( $Y$ ) (Fig. 5.27(c)) has the same behavior observed in the 1D-BWI model, but in this case, the bubble is also moving in the tangential wall direction ( $X$ ) (Fig. 5.27(d)) with a tangential velocity almost constant throughout the time (Fig. 5.27(b)). The normal wall velocity (Fig. 5.27(a)) is oscillatory after the first rebound and is damped to zero, the same behavior was observed in results of simulations conducted for a bubble interacting with a horizontal wall. Unlike in the normal direction, in the tangential direction, the velocity oscillations are not appreciable, however, a small disturbance is observed around the time in which the bubbles bounce in the normal direction.

In Fig. 5.28 an excess pressure distribution at non-dimensional time  $t = 3.6$  is presented. The time  $t=3.6$  is just before the first rebound. The first rebound occurs at  $t=3.844$  (non-dimensional). In this figure we can observe the non symmetrical distribution of the excess pressure profile in the  $x$ -direction due to fact that the wall is inclined at  $\theta = 20^\circ$ . In the  $z$ -direction the excess pressure profile is symmetric; this symmetry condition is verified a posteriori, unlike what was done in the 2D-BWI model in which the symmetry in  $z$ -direction was imposed a priori.



**Figure 5.27:** Normal Velocity (a), Tangential velocity (b), Normal position (c) and Tangential position (d) of a bubble immersed in a contaminated system and rising towards a wall inclined at  $\theta = 20^\circ$ . The bubble characteristics are given by  $R=0.51\text{mm}$ ,  $Re=103$ ,  $We=0.24$  and  $Eo=0.1938$ .



**Figure 5.28:** Excess pressure profile time  $t=3.6$  (non-dimensional) of a bubble immersed in a contaminated system and rising towards a wall inclined at  $\theta = 20^\circ$ . The bubble characteristics are given by  $R=0.51\text{mm}$ ,  $Re=103$ ,  $We= 0.24$  and  $Eo=0.1938$ . The first rebound occur at non-dimensional time  $t = 3.844$ . The non-dimensional excess pressure  $p^*=0.625$  is zero in dimensional form.

Another important observation is that the wall force is reduced as the wall inclination increases. This effect can be observed in Figs. 5.29 and 5.30, in which the normal velocity (Fig. 5.29(a)), normal position (Fig. 5.29(b)) and normal wall force (Fig. 5.30) are plotted over time. All magnitudes plotted here were in non-dimensional form. The bubble characteristics were given by  $R=0.4\text{mm}$ ,  $r_{\max}^* = 1.0$ ,  $V_T = 0.086\text{m/s}$ ,  $Re= 68.8$ ,  $We = 0.08$  and  $Eo=0.08476$ . The system was assumed contaminated. The grid and non-dimensional time were  $31 \times 31$  and  $0.001$ . As the wall inclination increases the initial normal velocity decreases (Fig. 5.29(a)) which originates a decrease on the kinetic energy before the first impact on the

wall. This decrease causes an appreciable reduction on the maximum normal wall force obtained in the first rebound (see Fig. 5.30).

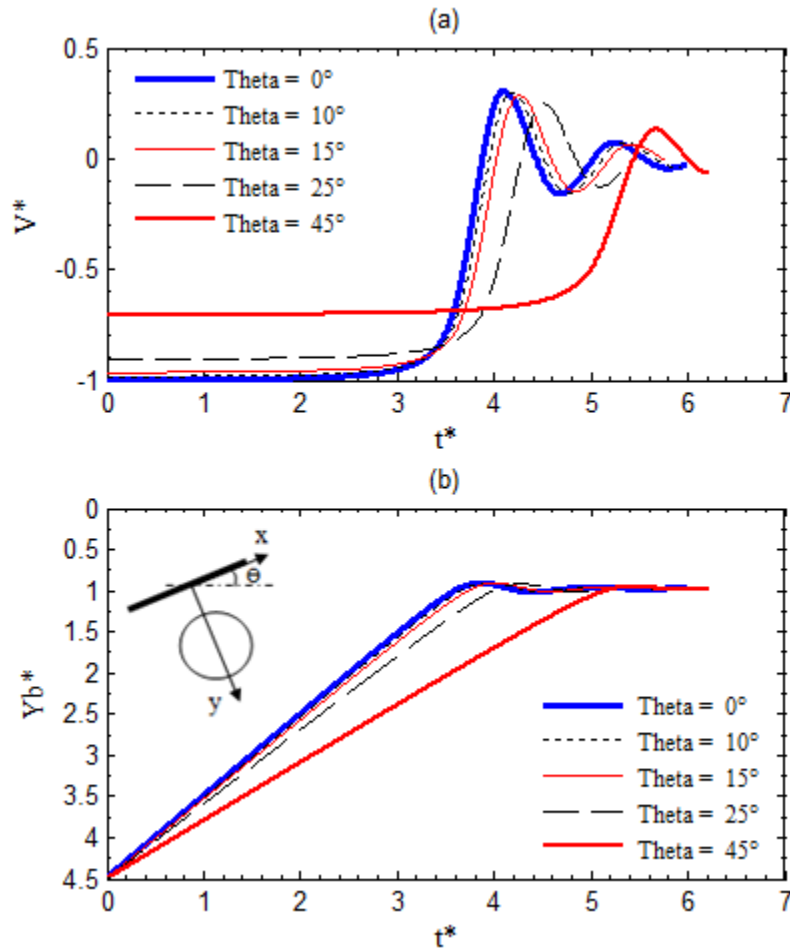


**Figure 5.29:** Normal velocities (a) and normal positions (b) of a bubble immersed in a contaminated system and rising towards a wall with several inclinations. The bubble characteristics are given by  $R=0.4\text{mm}$ ,  $V_T=0.086\text{m/s}$ ,  $Re=68.8$ ,  $We=0.08$  and  $Eo=0.08476$

For the bubble radius used ( $R=0.4\text{mm}$ ), we can observe that the normal wall force is reduced by about 50% when the inclination is  $\theta = 45^\circ$  with respect to the normal wall force obtained with a horizontal wall ( $\theta = 0^\circ$ ) (see Fig. 5.30). In the case ( $\theta = 45^\circ$ ), the bubble no longer bounces off the wall, as observed in Fig. 5.29(b).

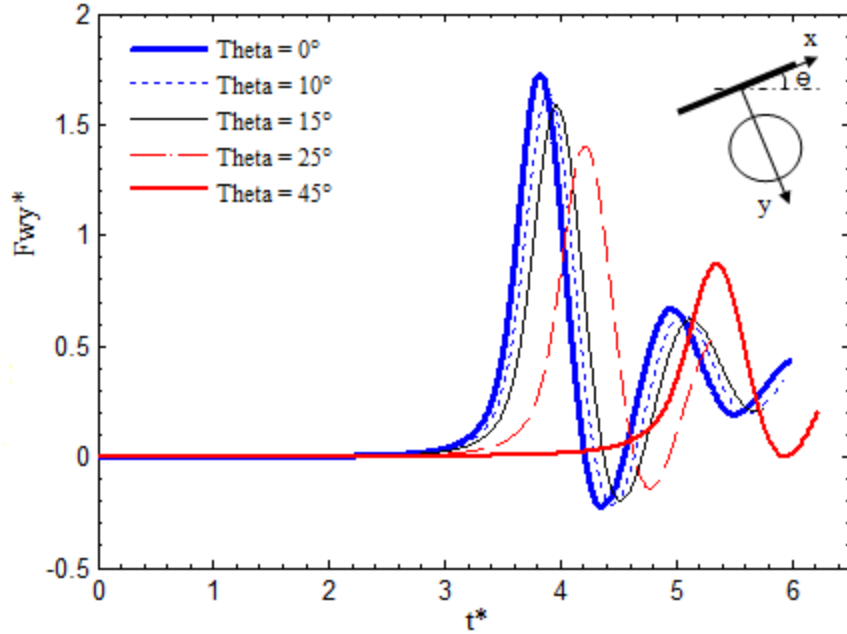


**Figure 5.30:** Normal wall forces on a bubble immersed in a contaminated system and rising towards a wall with several angles of inclination. The bubble characteristics are given by  $R=0.4\text{mm}$ ,  $V_T=0.086\text{m/s}$ ,  $Re=68.8$ ,  $We=0.08$  and  $Eo=0.08476$ .

#### 5.2.4 Prediction of bubble motion when interacting with a wall with two inclinations.

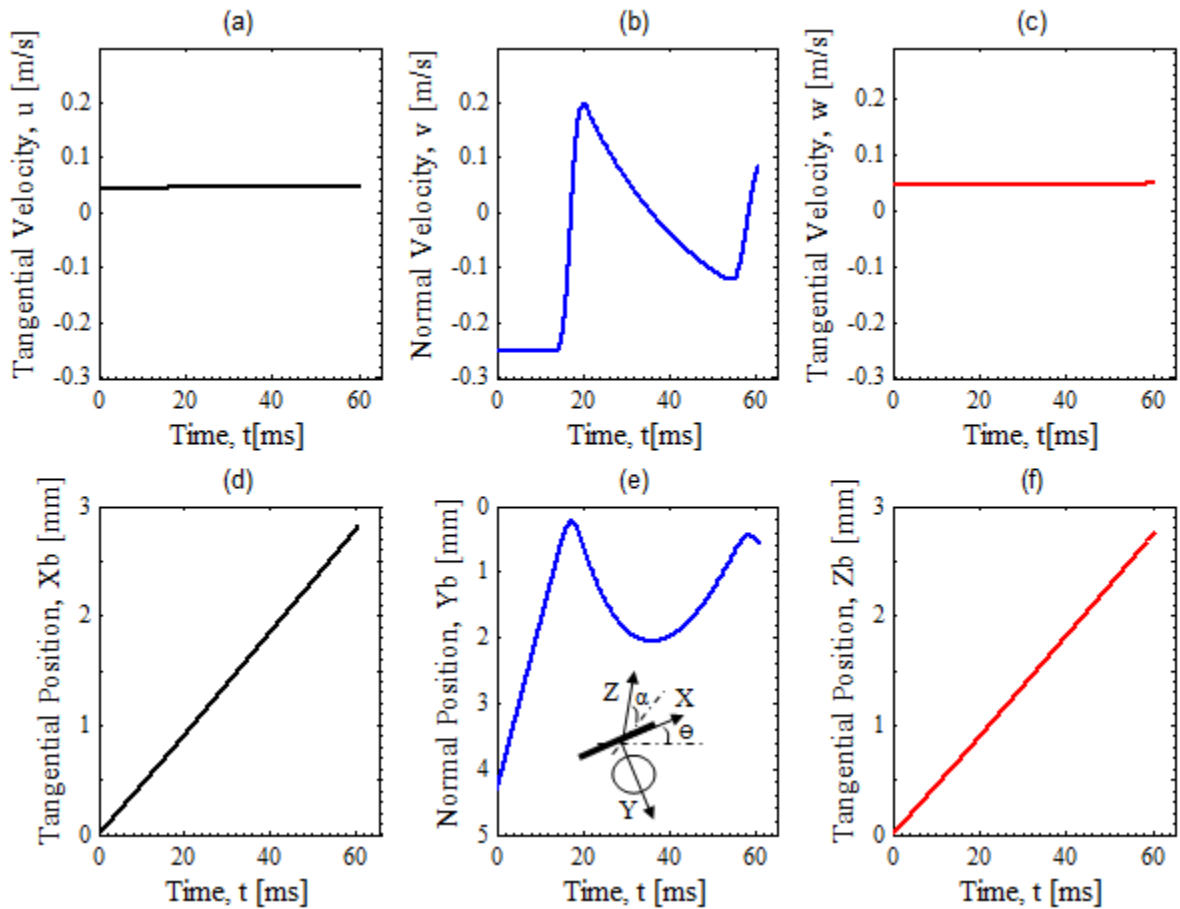
The behavior of a bubble rising in a clean system and interacting with a wall inclined in two directions is presented in this section. We use clean system to obtain results comparables with results of simulations obtained for the case of a horizontal wall (section 5.1.3)

Figure 5.31 shows the normal velocity,  $V$  (b); tangential velocity in  $x$ -direction,  $U$  (a); tangential velocity in  $z$ -direction,  $W$  (c); normal positions,  $Yb$  (e); tangential positions in  $x$ -direction,  $Xb$  (d); and tangential positions in  $z$ -direction,  $Zb$  (f) of a bubble of  $R=0.79\text{mm}$ ,  $Re=410$ ,  $We=1.463$  and  $Eo=0.3283$ . The inclinations were  $\theta=10^\circ$  and  $\alpha=10^\circ$  (see sketch in Fig. 5.31(e)). In this figure the two first rebounds were plotted. The data used for this simulations were chosen to obtain results comparables with data obtained when the wall was

horizontal (Fig. 5.23). The initial velocities  $U(t=0)$ ,  $V(t=0)$ , and  $W(t=0)$ , in this case were 0.0451m/s, 0.252m/s, and 0.0446m/s respectively ( $U(t=0)=|V_T|\sin\theta$ ,  $V(t=0)=|V_T|\cos\theta\cos\alpha$ , and  $W(t=0)=|V_T|\cos\theta\sin\alpha$ ). The tangential velocities are generally constant over time (Fig. 5.31(a) and 5.31(c)) but contribute to a decrease of the rebound amplitude (Fig. 5.31(e)); since as the inclination increases the bubble normal velocity decreases (this result was observed in Fig. 5.29(a)) and then the reduced normal velocity implies a kinetic energy in the normal direction (computed as  $m_b[V(t=0)]^2/2$ ) less than the initial kinetic energy computed for the same bubble interacting with a horizontal wall (computed as  $m_b|\vec{V}_T|^2/2$ ). Therefore, the wall force in an inclined wall is less than in a horizontal wall which produces lower amplitude of the first rebound as observed in Fig. 5.31(e) with respect to the Fig. 5.23. The time of the first two rebounds in this case increases about 2ms due to fact that the initial normal velocity is reduced (see Fig. 5.31(e) and Fig. 5.23).

In Fig. 5.32 the normal and tangential forces were plotted. In this figure we can observe two cases: *First*, as observed for a bubble interacting with a horizontal wall before the first rebound, in the normal direction the buoyancy force is balanced by the drag force. As the bubble approaches the wall, the dominant forces are the wall and added mass forces which are of higher values respect to the buoyancy and drag forces, therefore the added mass and wall force almost compensate each other (see Fig. 5.32(b)). As the bubble moves away from the wall after the first rebound the wall force is turned to zero and the force balance is between the added mass and buoyancy force, since the drag force is almost zero. The same behavior is observed in the next rebounds. *Second*, in tangential x and z directions slightly variations of the drag, added mass and wall forces are observed (Figs. 5.32 (a) and 5.32(c)) and the force balance is basically between the drag and buoyancy force almost at all times.

When the initial kinetic energy is completely dissipated on the film, the bubble normal velocity must be turned to zero and a sliding motion tangential to the wall is predicted, since the tangential velocities are generally constant. In this case the buoyancy force is compensated by the wall force in the normal direction and by the drag force in the tangential direction. This last fact predicted by the model in 2D and 3D for a wall with one or two inclinations respectively does not occur for a bubble interacting with a horizontal wall because in this case the bubble is stopped on the wall (see Fig. 5.23).



**Figure 5.31:** Velocities (a), (b) and (c) and positions (d), (e), and (f) of a bubble immersed in a clean system and rising towards a wall inclined at  $\theta=10^\circ$  and  $\alpha=10^\circ$ . The bubble characteristics are given by  $R=0.79\text{mm}$ ,  $Re=410$  and  $We=1.463$ .

In Fig. 5.33 the time evolution of the film thickness profile is shown before [(a), (b) and (c)] and after [(d), (e), and (f)] the first bubble rebound. The first rebound occurs at time  $t=17.48\text{ms}$ . Large deformations are presented as the bubble approaches the wall. These deformations are observed in the fluid film thickness profile just before [5.32(c)] and after [5.32(d)] the first rebound. Away from the wall [5.32 (a), (b), (e) and (f)] the bubble is not deformed. For inclination angles less than  $28^\circ$  for a wall with one inclination Podvin et al. (2008) obtained that the fluid film thickness is slightly asymmetric with respect to the bubble normal axis. In our case, for a bubble interacting with a wall inclined at two small angles, the fluid film profile is also slightly asymmetric (Figs. 5.33 and 5.34).

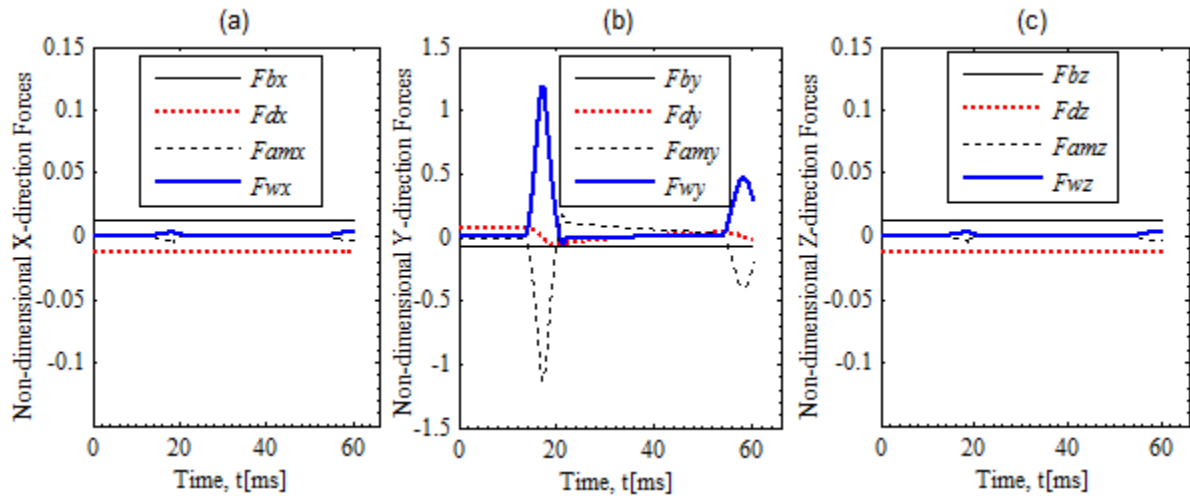


**Figure 5.32:** Tangential forces in x-direction (a), Normal forces in y-direction (b) and tangential forces in z-direction(c) of a bubble immersed in a clean system and rising towards a wall inclined at  $\theta=10^\circ$  and  $\alpha=10^\circ$ . The bubble characteristics are given by  $R=0.79\text{mm}$ ,  $Re=410$  and  $We=1.463$ . One unit of non-dimensional force corresponds to about  $264.6 \mu\text{N}$ .

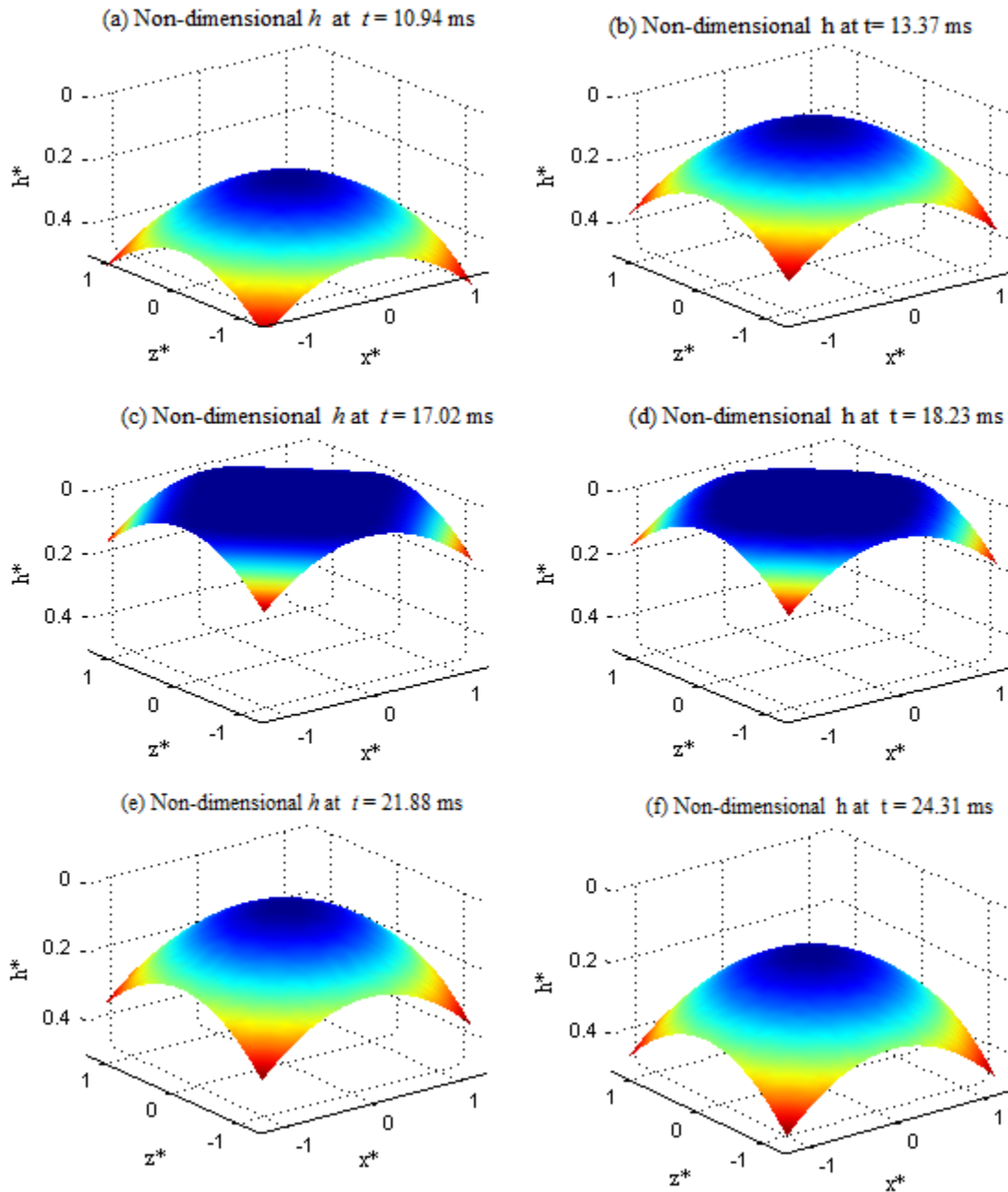


**Figure 5.33:** Fluid film thickness during the first rebound of a bubble immersed in a clean system and rising towards a wall inclined at  $\theta = 10^\circ$  and  $\alpha = 10^\circ$ . The bubble characteristics are given by  $R=0.79\text{mm}$ ,  $Re=410$  and  $We=1.463$ . The first rebound occur at  $t=17.48\text{ms}$

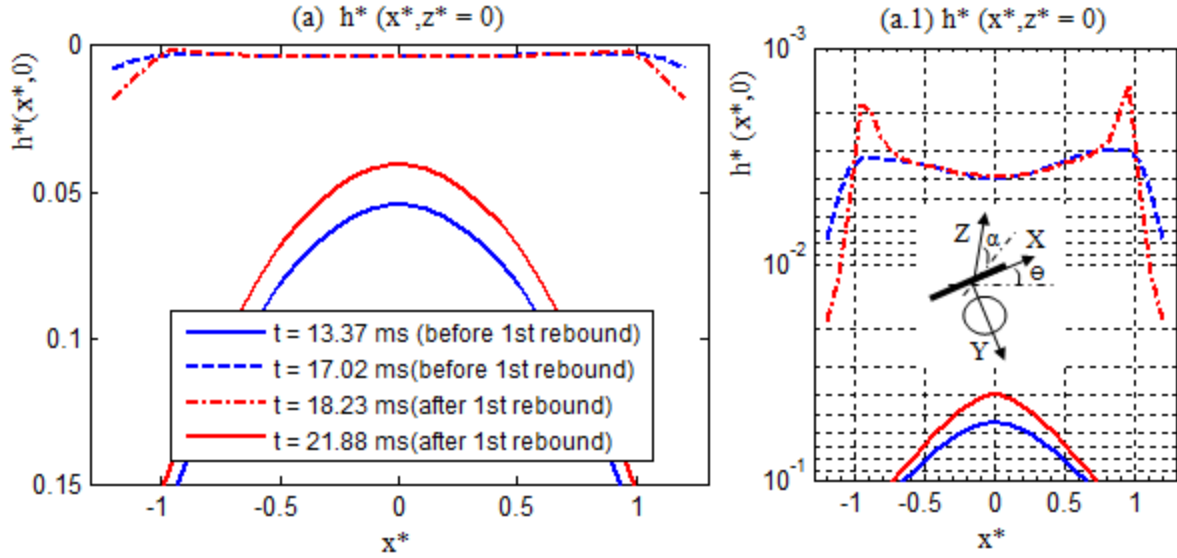


**Figure 5.34:** Non-dimensional film thickness during the first rebound of a bubble immersed in a clean system and rising towards a wall inclined at  $\theta = 10^\circ$  and  $\alpha = 10^\circ$ . (a)  $h^*(x^*, 0)$  before and after the first rebound; (a.1) Amplified view of (a) around  $x^* = 0$ . The bubble characteristics are given by  $R=0.79\text{mm}$ ,  $Re=410$  and  $We=1.463$ . The first rebound occur at 17.48ms

The asymmetric deformation is caused by an asymmetric excess pressure profile which is shown in Figs. 5.35-5.37. In these figures we can observe that away from the wall the excess pressure profile can be considered generally symmetric but in the wall proximity the asymmetric excess pressure profile is observed (just before the rebound  $t = 17.02\text{ms}$  and just after the rebound at  $t=18.23\text{ms}$ ). The asymmetric excess pressure profile is observed in  $x$ - and  $z$ - directions and is shown clearly in Figs. 5.37(b) and 5.37(c).

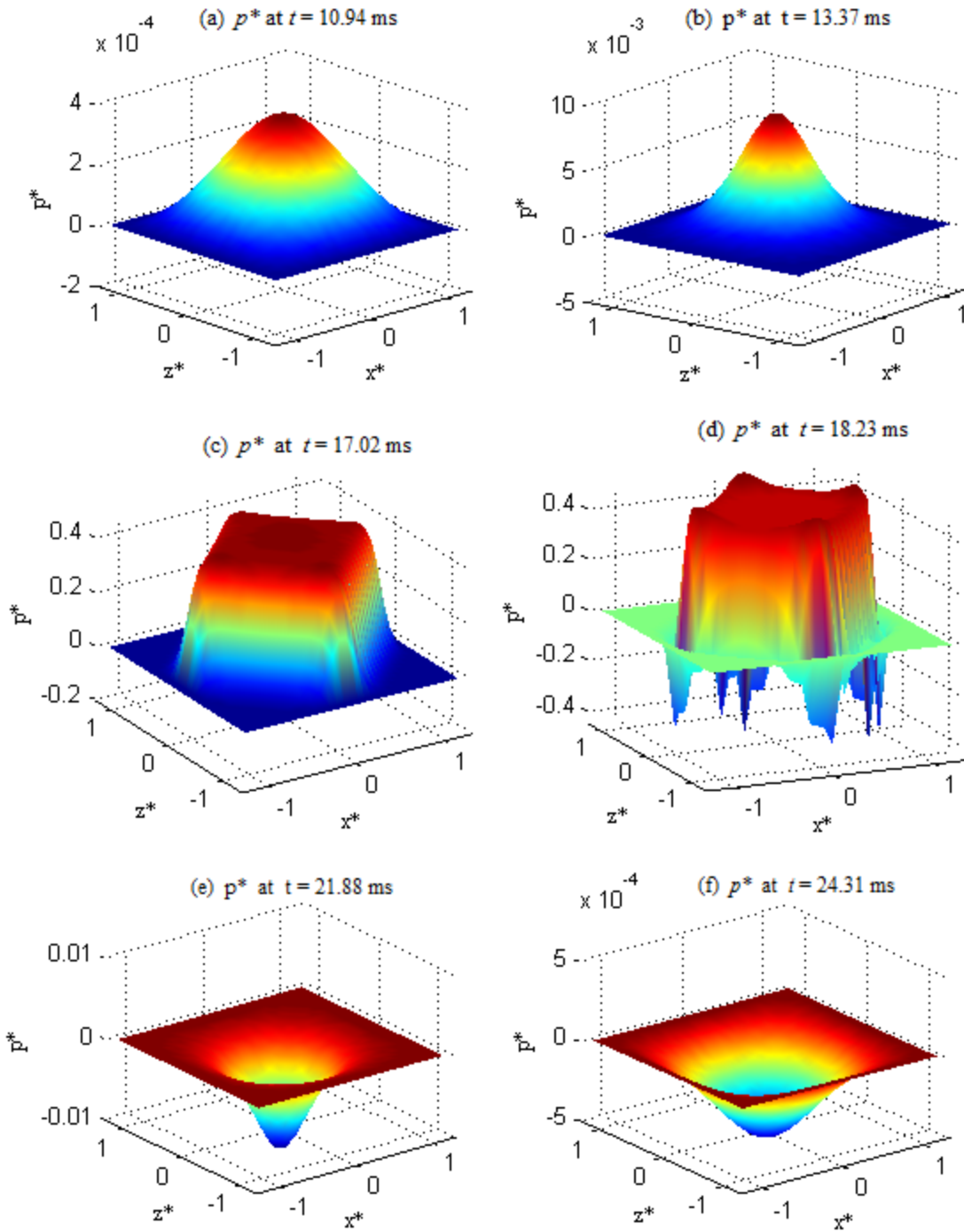


**Figure 5.35:** Excess pressure profile (surface) during the first rebound of a bubble immersed in a clean system and rising towards a wall inclined at  $\theta = 10^\circ$  and  $\alpha = 10^\circ$ . The bubble characteristics are given by  $R=0.79\text{mm}$ ,  $Re=410$  and  $We=1.463$ . The first rebound occur at 17.48ms

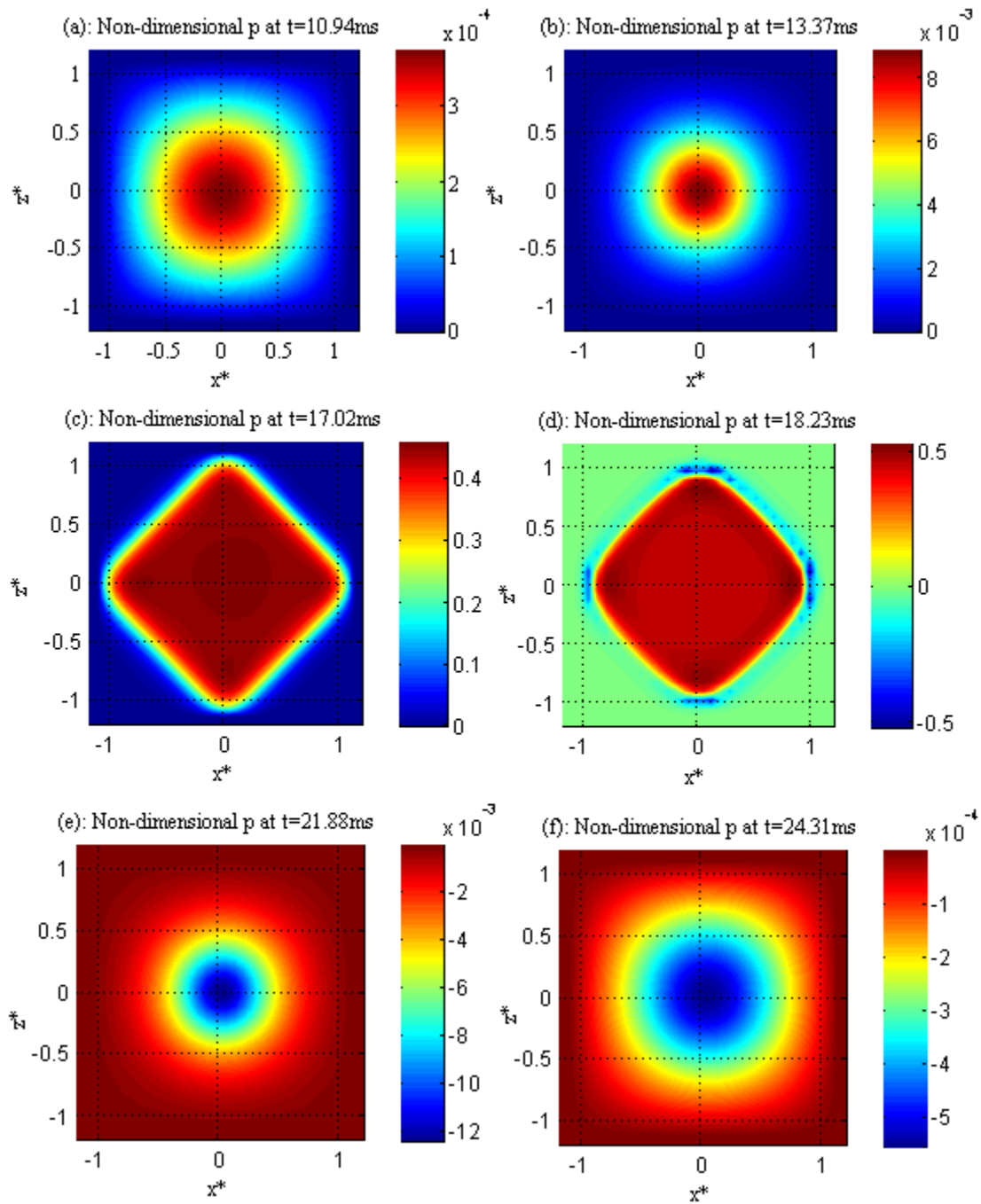


**Figure 5.36:** Excess pressure profile (contour fill) during the first rebound of a bubble immersed in a clean system and rising towards a wall inclined at  $\theta = 10^\circ$  and  $\alpha = 10^\circ$ . The bubble characteristics are given by  $R=0.79\text{mm}$ ,  $Re=410$  and  $We=1.463$ . The first rebound occur at 17.48ms

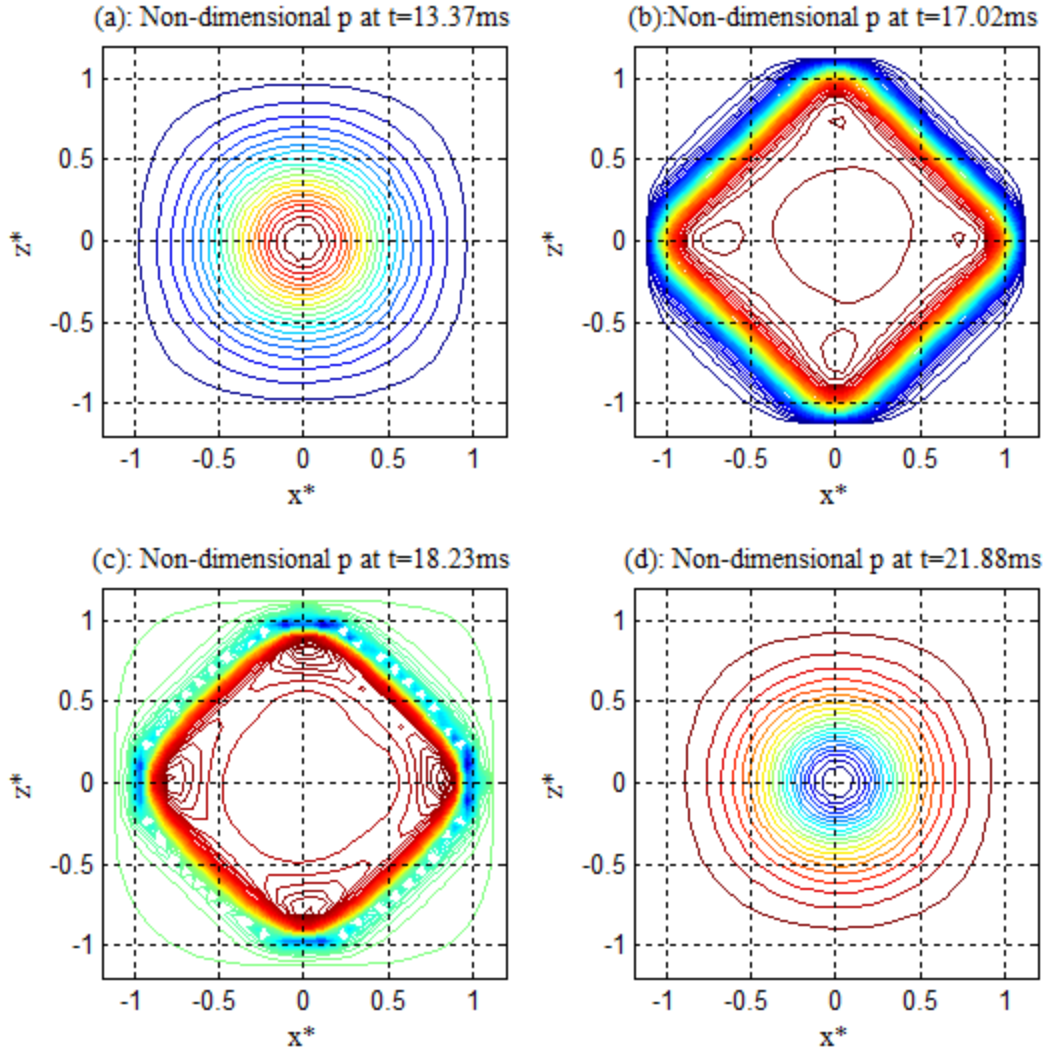


**Figure 5.37:** Excess pressure profile (contour lines) during the first rebound of a bubble immersed in a clean system and rising towards a wall inclined at  $\theta = 10^\circ$  and  $\alpha = 10^\circ$ . The bubble characteristics are given by  $R=0.79\text{mm}$ ,  $Re=410$  and  $We=1.463$ . The first rebound occur at 17.48ms

Our 3D-BWI model, in Cartesian coordinates, was able to predict with good agreement the bubble position in the bouncing process compared with experimental data (Fig. 5.23). The hypothesis made for the validity of the lubrication equation ( $h/R \ll 1$ ) was verified in all simulations (Figs. 5.6-5.9, 5.15 and 5.34). Also the bubble deformation and the excess pressure domain were observed to occur at a  $r < r_{\max} \approx R$ . The deformed bubble

interface was observed nearly parallel with the wall (Figs. 5.6, 5.7, 5.15 and 5.34), hence,

$$\frac{\partial h}{\partial x} \ll 1 \text{ and } \frac{\partial h}{\partial z} \ll 1 \text{ were generally satisfied.}$$

An additional and very important inequality that needs to be verified is the relation between the  $Re$  and  $h$ . As it was mentioned in section (2.6), the lubrication equation is valid as long as

$$Re \left( \frac{h}{R} \right)^2 \ll 1 \quad (5.9)$$

Applying Eq. (5.9) at the case of a bubble of  $R=0.4\text{mm}$  interacting with a horizontal wall, in which case  $Re = 92, h \approx 5\mu\text{m}$  (Fig. 5.6) the inequality (5.9) is satisfied. Applying this inequality to the bubble of  $R=0.79\text{mm}$  interacting with a horizontal wall with  $Re = 410, h \approx 15\mu\text{m}$  (Fig. 5.15) the inequality is still satisfied ( $Re(h/R)^2 = 0.15 \ll 1$ ); but after few times steps the film thickness decreases and the inequality is better satisfied (as example for  $h \approx 10\mu\text{m}, Re(h/R)^2 = 0.06 \ll 1$ ). Also the Eq. (5.9) is applied to the bubble of  $R=0.79\text{mm}$  interacting with a wall with two inclinations with Reynolds number related to the initial component of the terminal velocity in the normal direction ( $V(0) = 0.252\text{m/s}$ )  $Re = 397, hnd = (4.5)R, h = h^*hnd \approx (0.004)hnd \approx 14\mu\text{m}$  (Fig. 5.34) the inequality is satisfied.

As the  $We$  number increases the ability of the bubble to deform increases, consequently we expect to see one increase in the excess pressure domain. This was the case in our results (Fig. 5.6 and Fig. 5.24). For bubbles radius  $R=0.4\text{mm}$   $r_{\text{max}}^* = 1.0$  was used, and for  $R=0.79\text{mm}$   $r_{\text{max}}^* = 1.2$  was used in order to capture the largest deformation which was observed during the first rebound. In the following rebound the value of  $r_{\text{max}}^*$  was less than

first rebound (Figs. 5.6-5.9). Our 3D-BWI code was not adaptive to variations of  $r_{\max}^*$  because a constant  $r_{\max}^*$  was used during the simulations. It can be an important improvement of our present code to consider an adaptive  $r_{\max}^*$  or a changeable grid size in the spatial domain such that we consider a refined grid in the wall proximity and a large grid size away to wall.

The 3D-BWI code developed in this research predicted typically two or three bubble rebounds on the wall for inclination angles less than  $45^\circ$ , after the second or third rebound the convergence failed with tolerances of  $10^{-8}$  for the film thickness using a number of iterations less than 10000, a temporal step of 0.001 and grid size between 30x30 and 40x40. In order to improve our code, need to use a smaller or adaptive grid size or a large number of iterations, however this analysis would require a large computational time.

Our present model predicted satisfactorily the bouncing process, unlike previous numerical studies made by Canot et al. (2003) in which their 3D model was not capable of predicting the bouncing process on a horizontal wall.

## 6. CONCLUSIONS AND FUTURE WORKS

### 6.1 Conclusions

A three dimensional model to describe the bouncing process of a bubble immersed in a stagnant viscous fluid interacting with an immersed inclined solid wall has been developed. This model is an extension of the 2D model developed by Podvin et. al. (2008).

Three equations of motion for the bubble centroid, one for each special dimension, were solved. These equations were coupled with the three dimensional film drainage equation to obtain the bubble centroid velocities ( $U(t)$ ,  $V(t)$ , and  $W(t)$ ) and the fluid film thickness,  $h(x, z, t)$ . A reduction to two dimensions in Cartesian coordinates and one-dimension in cylindrical coordinates with adequate assumptions was carried out to compare with previous numerical models presented in the literature.

Owing to the strongly non-linearity of the system of equations and the difficulty in establishing the exact excess pressure domain; a numerical method was implemented to solve the proposed system of equations. The equation of motion was solved using an iterative method. In the case of the film drainage equation, implicit and explicit methods were implemented. Both methods produced good results but the explicit method was unstable for time steps greater than  $10^{-9}$ . Despite that the explicit method was easier to implement it required large computational time. Therefore, the implicit method, that was stable even for large time steps ( $O(10^{-3})$ ), was used in all simulations conducted in this research.

The results of the simulations using the 1D-BWI model in cylindrical coordinates and 3D-BWI model in Cartesian coordinates were validated with experimental data available in

the literature for a bubble immersed in a clean system and interacting with a horizontal wall. Moreover, the present model predicts the bubble rebounds with a higher accuracy than the previous 1D model developed by Moraga et al. (2005).

From the results obtained with the numerical simulations we verified that the excess pressure domain in general is less than the bubble radius and no error is committed by using an excess pressure domain of the same order of magnitude as the bubble radius. The hypothesis of small bubble deformation on the top surface of the bubble was also verified. Also, for bubbles in the range 0.3-2mm of diameter the lubrication approximation was satisfactory verified.

Simulation results have predicted that the bouncing process of a bubble rising in a viscous fluid and interacting with a wall depends principally on the Reynolds and Weber numbers calculated with the equivalent bubble radius as well as on the wall inclinations  $\theta$  and  $\alpha$ . A large  $Re$  can cause rebounds with large amplitude in comparison with a small  $Re$ . The  $Re$  is strongly affected by the system purity. In a clean system, the rebound amplitude was larger than for the same bubble in a contaminated system ( $Re$  in contaminated system smaller than  $Re$  in clean system). A small deformation was observed with  $We < 1$  and a large deformation with  $We > 1$ . Therefore, for bubbles with  $We > 1$  a large part of initial kinetic energy was converted to deformation energy during the impact such that after the impact this energy was restored as kinetic energy. Hence a large amplitude rebound was observed in comparison with bubbles with  $We < 1$ . It was also observed that the wall inclinations contribute to a reduction of the component of the initial terminal velocity in the direction normal to the wall and consequently the kinetic energy in the normal direction was reduced, causing a reduction on the amplitude of the rebound.

The critical diameter for the rebound of an air bubble in water on a horizontal wall does not depend on the water purity (see section 5.1.4). In the case of an inclined wall, the critical diameter for the rebound strongly depended of the wall inclination (see Fig. 5.29).

From the simulation results it can also be observed that the normal wall force decreases as the wall inclination increases. This observation was important to predict that a bubble that rebounds in a horizontal wall might not rebound from an inclined wall, since the initial kinetic energy available for the rebound is greatly reduced with the wall inclination. The wall inclinations for which the bubble does not rebound depends of the bubble radius and the contamination of the fluid. This is due to the reduction of the wall force such that the net force cannot produce a change in the bubble velocity after the first rebound, in other words, all kinetic energy is dissipated totally in the first rebound.

Unlike previous numerical studies (Canot et al. 2003; Shopov et al, 1990) performed in 3D, our 3D model reproduces the results of the 1D-BWI model when inclination angles of  $0^\circ$  were used. Asymmetrical surface deformation and asymmetrical excess pressure profile on a bubble immersed in a contaminated or clean system and interacting with a wall with one or two inclinations has been predicted by the 3D-BWI model. This conclusion was also made by Podvin et al. (2008) in their 2D model for a bubble interacting with a wall with only one inclination.

The 3D-BWI code developed to solve the 3D-BWI model in Cartesian coordinates was unable to simulate the bouncing process typically after the third rebound for angles less than  $45^\circ$  and after the first rebound for angles greater than  $45^\circ$ . In the case of a horizontal wall the code simulated the complete bouncing process. The problem was observed as deterioration in convergence. It is likely that a smaller grid or a greater number of iterations

was required, considering a smaller grid the solution obtained will be more accuracy and less information of velocity and excess pressure will be lost. However, due to the large computational resources required we have not been able to adequately evaluate this hypothesis.

Numerical predictions in the present study for bubbles of radii less than 0.8mm interacting with a horizontal or inclined wall in a clean or contaminated system could not be verified with experimental data because it is not available in the literature.

A potential application of this model is to determine the sliding, stopping or bouncing of a bubble interacting with a rigid wall, conditions that could be included in a two-phase flow code.

## **6.2 Future works**

The following recommendations are proposed, as future work, in order to improve the present numerical model and to expand the scope of this study.

An experimental study should be performed to measure the instantaneous bubble position and bubble deformation as it approaches an inclined wall. The motion of bubbles in a contaminated or in a clean system could be recorded with high-speed imaging to capture the bubble trajectory and its deformation during the bouncing process. The video images can be analyzed to determine the aspect ratio and the bubble velocity. The bubble velocity and the bubble position should be compared with the numerical predictions presented in the present thesis.

Improvements of the predictions of the present model can be studied by using drag and added mass coefficients as a function of the bubble aspect ratio during the bouncing process.

The complete form of the bubble top mean curvature (Eq. 2.3) could be implemented in present computer codes to verify if there is a significant improvement.

A non-uniform grid can be used in the present numerical method, such that, a fine grid is used in areas of high excess pressure and a large grid in areas where the excess pressure is small. Another more complex implementation could use an adaptive grid that is refined as the bubble approaches the wall. These implementations are justified because we have concluded that away from the wall the excess pressure reduces to zero and in the wall proximity the excess pressure domain is smaller than the constant domain assigned.

Other methods for solving the linear system could be studied and implemented in the present 3D-BWI code, in an attempt to solve the numerical convergence without modifying the current grid.

For a bubble approaching a wall with large inclinations an additional force term should be implemented to account for the lift effect, which is not present in the current lubrication model.

## REFERENCES

- Adamson, A. W., (1982). *Physical Chemistry of Surfaces*. Wiley, NY.
- Basset, A. B. (1888). *A treatise on hydrodynamics: with numerous examples*. Deighton, Bell and Co, LDN.
- Benitez, J., (2002). *Principles and Modern Applications of Mass Transfer Operations*. Wiley-Interscience, NY.
- Bird, R. B., Stewart, W. E. & Lightfoot, E. N., (2006). *Transport Phenomena*. Revised 2nd Edition., John Wiley & Sons, Inc, NY.
- Bozzano, G. & Dente, M., (2009). "Single bubble and drop motion modeling", *Chemical Engineering Transactions*, Vol. 17, pp. 567-572.
- Brennen, C. E. (2005). *Fundamentals of multiphase flow*. Cambridge Univ. Press, NY.
- Brennen, C. E., (1982). "A review of added mass and fluid inertial forces". *Department of the Navy*, Port Hueneme, CA, USA.
- Canot, E., Davoust, L., El Hammoumi, M. & Lachkar, D., (2003). "Numerical simulation of the Buoyancy-driven bouncing of a 2-D bubble at a horizontal wall", *Theoretical and computational fluid dynamics*, Vol. 17, No. 1, pp. 51–72.
- Clift, R., Grace, J. R., Weber, M. E. & Clift, R., (1978). *Bubbles, drops, and particles*. Academic press, NY.
- Do Carmo, M. P., (1976). *Differential geometry of curves and surfaces*. Prentice-Hall Englewood Cliffs, NJ.
- Domgin, J. F., Huilier, D. G. F., Karl, J. J., Gardin, P. & Burnage, H., (1998). "Experimental and numerical study of rigid particles, droplets and bubbles motion in quiescent and turbulent flows-influence of the history force". *Proceeding of Third international conference on Multiphase Flow, ICFM-98*, Lyon, France.
- Feng, Z. G. & Michaelides E. E., (2001). "Drag Coefficients of Viscous Spheres at Intermediate and High Reynolds Numbers". *Journal of Fluids Engineering*, Vol. 123, No. 4, pp. 841-849.

- Gondret, P., Lance, M. & Petit, L., (2002). "Bouncing motion of spherical particles in fluids", *Physics of Fluids*, Vol. 14, No. 2, pp. 643-653.
- Haberman, W. L. & Morton, R. K., (1953). " An experimental investigation of the drag and shape of air bubbles rising in various liquids". *David Taylor model Basin Rep.* No. 802.
- Hamrock, B. J., Schmid, S. R. & Jacobson, B. O., (2004). *Fundamentals of fluid film lubrication*. 2nd edition, Marcel Dekker, Inc., NY.
- Happel, J. & Brenner, H., (1991). *Low Reynolds number hydrodynamics: with special applications to particulate media*. Kluwer Academic.
- Harper, J. F. & Moore, D. W., (1968). "The motion of a spherical liquid drop at high Reynolds number". *Journal of Fluid Mechanics*, Vol. 32, No. 02, pp. 367–391.
- Hoffman, J. D., (2001). *Numerical Methods for Engineers and Scientists*. 2nd edition, Marcel Dekker, Inc., NY.
- Hoffmann, K. A., (2000). *Computational Fluid Dynamics*, 4th edition, Engineering Education System, KS.
- Hori, Y., (2006). *Hydrodynamic lubrication*. Springer Verlag, Tokyo.
- Klaseboer, E., Chevaillier, J. P., Maté, A., Masbernat, O. & Gourdon, C., (2001). "Model and experiments of a drop impinging on an immersed wall". *Physics of Fluids*, vol. 13, No. 1 pp. 45-57.
- Kodama Y., Kakugawa A., Takahashi T., Nagaya S. & Kawamura T., (2004). "Drag Reduction of Ships by Microbubbles". *National Maritime Research Institute of Japan and Tokyo University*.
- Leal, L. G., (2007). *Advanced transport phenomena: fluid mechanics and convective transport processes*. Cambridge University Press, NY.
- Levich, V. G., (1962). "Physicochemical hydrodynamics". Prentice Hall, New York.
- Lovalenti, P. M. & Brady, J. F., (1993). "The force on a bubble, drop, or particle in arbitrary time-dependent motion at small Reynolds number", *Physics of Fluids A: Fluid Dynamics*, Vol. 5, pp. 2104-2116.
- Michaelides, E. E., (2006). *Particles, Bubbles & Drops: Their Motion, Heat And Mass Transfer*. World Scientific Publishing Company.

- Michaelides, E. E., (2003). "Hydrodynamic force and heat/mass transfer from particles, bubbles, and drops—The Freeman Scholar Lecture", *Journal of fluids engineering*, Vol. 125, pp. 209-238.
- Michaelides, E. E., (1997). "Review—the transient equation of motion for particles, bubbles, and droplets", *Journal of fluids engineering*, Vol. 119, pp. 233-247.
- Moore, D. W., (1965). "The velocity of rise of distorted gas bubbles in a liquid of small viscosity", *Journal of Fluid Mechanics*, Vol. 23, No. 04, pp. 749–766.
- Moore, D. W., (1963). "The boundary layer on a spherical gas bubble", *Journal of fluid mechanics*, vol. 16, No. 02, pp. 161–176.
- Moraga, F. J., Cancelos, S. & Lahey Jr, R. T., (2005). "Modeling wall-induced forces on bubbles for inclined walls". *Multiphase Science and Technology*, Vol. 17, No. 4, pp. 483-505.
- Nakamura, S., (1992). *Applied Numerical Methods in C*. Prentice Hall, NJ.
- Podvin, B., Khoja, S., Moraga, F. & Attinger, D., (2008). "Model and experimental visualizations of the interaction of a bubble with an inclined wall". *Chemical Engineering Science*, Vol. 63, No. 7, pp. 1914–1928.
- Press, W. H., Teukolsky, S. A., Vetterling, W. T. & Flannery, B. P., (2001). *Numerical recipes in Fortran 77: the art of scientific computing*. Cambridge University Press, Cambridge, UK.
- Reddy, J. N. & Corporation, E., (2007). *An introduction to continuum mechanics*. Cambridge University Press, NY.
- Reynolds, O., (1886). "On the Theory of Lubrication and Its Application to Mr. Beauchamp Tower's Experiments, Including an Experimental Determination of the Viscosity of Olive Oil". *Proceedings of the Royal Society of London*, Vol. 40, pp. 191-203.
- Ruiz, O. E., (2002). "Evaporation of water droplets placed on a heated horizontal surface", *Journal of heat transfer*, Vol. 124, No. 5, pp. 854-864.
- Shames, I. H., (2003). *Mechanics of fluids*. McGraw-Hill Science/Engineering/Math, NY.
- Shopov, P. J., Minev, P. D., Bazhlevkov, I. B. & Zapryanov, Z. D., (1990). "Interaction of a deformable bubble with a rigid wall at moderate Reynolds numbers". *Journal of Fluid Mechanics*, Vol. 219, pp. 241–271.

- Sondergaard, R., Chaney, K. & Brennen, C. E., (1990). "Measurements of solid spheres bouncing off flat plates". *Journal of Applied Mechanics*, Vol. 112, No. 3, pp. 694–699.
- Tsao, H. K. & Koch, D. L., (1997). "Observations of high Reynolds number bubbles interacting with a rigid wall". *Physics of Fluids*, Vol. 9, No. 1, pp. 44-56.
- Van Der Geld, C. W. M., (2002). "On the motion of a spherical bubble deforming near a plane wall". *Journal of engineering mathematics*, Vol. 42, No. 2, pp. 91–118.

# APPENDIX A

## DRAG AND ADDED MASS FORCES

### *Added mass force*

The simplest view of the added mass phenomenon is that *it determines the necessary work done to change the kinetic energy associated with the change of fluid motion*. The fluid motion caused by the motion of a body immersed in it, implies a certain positive non-zero amount of kinetic energy associated with the fluid motion.

The fluid kinetic energy,  $E_k$ , can be represented as (Brennen, 1982),

$$E_k = \frac{\rho_f}{2} \int_{\mathcal{G}} (u^2 + v^2 + w^2) d\mathcal{G} \quad (\text{A.1})$$

Where  $\rho_f$  is the fluid density;  $u$ ,  $v$ , and  $w$  are the fluid velocity around the body; and  $\mathcal{G}$  is the fluid volume. Far from the body, the fluid velocity is uniform and represented by  $U_\infty$  (see Fig. A1). Hence, Eq. (A.1) can be rewritten as,

$$E_k = \frac{\rho_f I U_\infty^2}{2} \quad \text{with} \quad I = \int_{\mathcal{G}} \left( \left( \frac{u}{U_\infty} \right)^2 + \left( \frac{v}{U_\infty} \right)^2 + \left( \frac{w}{U_\infty} \right)^2 \right) d\mathcal{G} \quad (\text{A.2})$$

From Eq. (A.2) we can observe that the kinetic energy is proportional to the fluid velocity far from the body. If the kinetic energy of the fluid increases, an additional work must be done over the body, and this rate of additional work is simply the rate of change of  $E_k$  with respect to time,  $dE_k/dt$ . This additional work ( $FU_\infty$ ) is experienced by the body as an additional force,  $F$  done. Hence,

$$FU_\infty = \frac{dE_k}{dt} \rightarrow F = \frac{1}{U_\infty} \frac{dE_k}{dt} = \rho_f I \frac{dU_\infty}{dt} \quad (\text{A.3})$$

The force  $F$  is applied over the body and  $\rho_f I = M_f$  is the fluid mass. Consequently, it is often convenient to visualize  $\rho_f I = M_f$  as an “added mass” of fluid which is being accelerated with the body. Hence the force is called the added mass force  $F_{am}$  and expressed as,

$$F_{am} = M_f \frac{dU_\infty}{dt} \quad (\text{A.4})$$

We can observe that if  $U_\infty = \text{const}$  then  $F_{am} = 0$ . Values of  $M_f$  are computed according with the body geometry. For a spherical rigid body immersed on an inviscid fluid  $M_f = \frac{2}{3} \pi R^3 \rho_f$  computed as follow:

The potential flow velocities of a fluid moving over a rigid sphere (see Fig. A1)

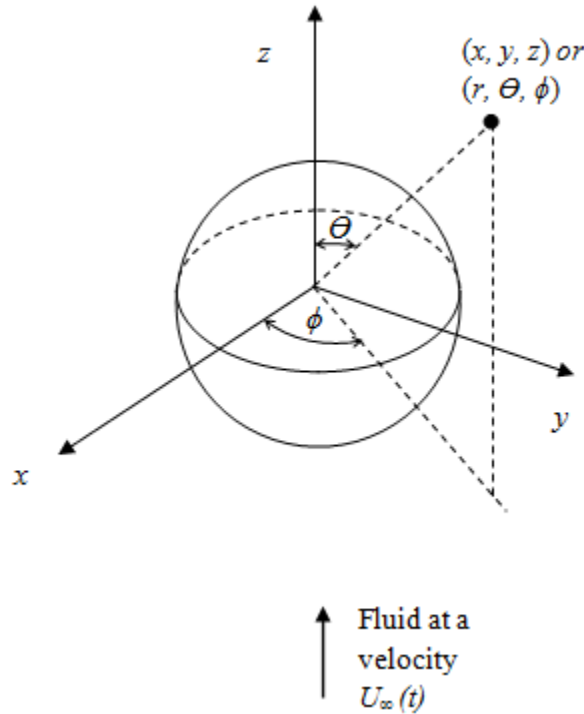


**Figure A 1:** Coordinate system to describe the flow around a rigid sphere

Can be expressed as (Brennen, 1982):

$$u_r = \frac{\partial \Psi}{\partial r}, \quad u_\theta = \frac{1}{r} \frac{\partial \Psi}{\partial \theta}, \quad \text{with } \Psi = -U_\infty \frac{R^3}{2r^2} \cos \theta \quad (\text{A.5})$$

Hence,

$$M_f = \rho_f I = \rho_f \int_R^\infty \int_0^{2\pi} \int_0^\pi \left\{ \left( \frac{1}{U_\infty} \frac{\partial \Psi}{\partial r} \right)^2 + \left( \frac{1}{U_\infty r} \frac{\partial \Psi}{\partial \theta} \right)^2 \right\} r^2 \sin \theta d\theta d\phi dr = \rho_f \frac{2}{3} \pi R^3 \quad (\text{A.6})$$

Replacing Eq. (A.6) in Eq. (A.4) we obtain,

$$F_{am} = \frac{2}{3} \pi R^3 \rho_f \frac{dU_\infty}{dt} \quad (\text{A.7})$$

Doing the following change

$$F_{am} = \frac{1}{2} \frac{4}{3} \pi R^3 \rho_f \frac{dU_\infty}{dt} = C_{am} m_f \frac{dU_\infty}{dt} \quad (\text{A.8})$$

Where  $C_{am}$  is called the added mass coefficient ( $C_{am}=1/2$  for a sphere) and  $m_f$  is the mass of fluid occupying the same volume of the rigid sphere.

If the rigid sphere moves at a velocity  $V(t)$  and the fluid at a velocity  $U_\infty(t)$ , hence, the added mass over the sphere can be written as,

$$F_{am} = C_{am} m_f \frac{d(V(t) - U_\infty(t))}{dt} \quad (\text{A.9})$$

### ***Drag force***

When a fluid with a viscosity  $\mu_f$  moves at very slow constant uniform velocity (*creeping flow*), over a fixed rigid sphere of radius  $R$  the force due to the fluid viscosity is determined integrating the normal and tangential stresses on the solid particle. We consider the motion shown in Fig. A1 and the fluid at constant uniform velocity,  $U_\infty$  far from the sphere in the  $z$ -direction. With no slip condition at sphere surface; the shear stress, pressure and velocity fields are provided (Bird et al. 2006, Chapter 4) as,

$$\tau_{r\theta} = \frac{3}{2} \frac{\mu_f U_\infty}{R} \left( \frac{R}{r} \right)^4 \sin \theta \quad (\text{A.10})$$

$$p = p_0 - \rho_f g z - \frac{3}{2} \frac{\mu_f U_\infty}{R} \left( \frac{R}{r} \right)^2 \cos \theta \quad (\text{A.11})$$

$$v_r = U_\infty \left( 1 - \frac{3}{2} \left( \frac{R}{r} \right) + \frac{1}{2} \left( \frac{R}{r} \right)^3 \right) \cos \theta \quad (\text{A.12})$$

$$v_\theta = -U_\infty \left( 1 - \frac{3}{4} \left( \frac{R}{r} \right) - \frac{1}{4} \left( \frac{R}{r} \right)^3 \right) \sin \theta \quad (\text{A.13})$$

In each point of the spherical surface there is a normal stress ( $p$ ) and a shear stress ( $\tau_{r\theta}$ ). The total hydrodynamics force must be the total sum of these shear and normal stresses.

The resultant force in  $z$ -direction caused by the pressure (normal stress) is,

$$Fp = \int_0^{2\pi} \int_0^\pi \left( -p \Big|_{r=R} \cos \theta \right) R^2 \sin \theta d\theta d\phi = \int_0^\pi \left( p_0 - \rho_f g R \cos \theta - \frac{3}{2} \frac{\mu_f U_\infty}{R} \cos \theta \right) \cos \theta 2\pi R^2 \sin \theta d\theta \quad (\text{A.14})$$

$$Fp = \frac{4}{3} \pi R^3 \rho_f g + 2\pi \mu_f R U_\infty \quad (\text{A.15})$$

The resultant force in  $z$ -direction caused by the shear stresses (tangential to surface) is,

$$F\tau = \int_0^{2\pi} \int_0^\pi \left( \tau_{r\theta} \Big|_{r=R} \sin \theta \right) R^2 \sin \theta d\theta d\phi = \int_0^\pi \left( \frac{3}{2} \frac{\mu_f U_\infty}{R} \sin^2 \theta \right) 2\pi R^2 \sin \theta d\theta \quad (\text{A.16})$$

$$F\tau = 4\pi \mu_f R U_\infty \quad (\text{A.17})$$

It can be easily proven that the total force on the plane perpendicular to the direction of motion is zero. Therefore, the total force on the sphere is (from Eqs. (A.15) and (A.17)),

$$F_T = F\tau + Fp = \frac{4}{3} \pi R^3 \rho_f g + 6\pi \mu_f R U_\infty \quad (\text{A.18})$$

The first term of the right hand side in Eq. (A.18) is called the *buoyancy force* and the second term is the *drag force* or often called the *Stokes Law*, and is denoted as

$$F_d = 6\pi \mu_f R U_\infty \quad (\text{A.19})$$

## APPENDIX B

### DERIVATIVES APPROXIMATION

Derivatives approximation using Taylor series are listed in the following tables:

**Table B.1:** Forward difference representations of  $O(\Delta x)$

	$f_i$	$f_{i+1}$	$f_{i+2}$	$f_{i+3}$	$f_{i+4}$
$(\Delta x)\partial f/\partial x$	-1	1			
$(\Delta x)^2\partial^2 f/\partial x^2$	1	-2	1		
$(\Delta x)^3\partial^3 f/\partial x^3$	-1	3	-3	1	
$(\Delta x)^4\partial^4 f/\partial x^4$	1	-4	6	-4	1

**Table B.2:** Backward difference representations of  $O(\Delta x)$

	$f_{i-4}$	$f_{i-3}$	$f_{i-2}$	$f_{i-1}$	$f_i$
$(\Delta x)\partial f/\partial x$				-1	1
$(\Delta x)^2\partial^2 f/\partial x^2$			1	-2	1
$(\Delta x)^3\partial^3 f/\partial x^3$		-1	3	-3	1
$(\Delta x)^4\partial^4 f/\partial x^4$	1	-4	6	-4	1

**Table B.3:** Central difference representations of  $O(\Delta x)^2$

	$f_{i-2}$	$f_{i-1}$	$f_i$	$f_{i+1}$	$f_{i+2}$
$2(\Delta x)\partial f/\partial x$		-1	0	1	
$(\Delta x)^2\partial^2 f/\partial x^2$		1	-2	1	
$2(\Delta x)^3\partial^3 f/\partial x^3$	-1	2	0	-2	1
$(\Delta x)^4\partial^4 f/\partial x^4$	1	-4	6	-4	1

**Table B.4:** Forward difference representations of  $O(\Delta x)^2$

	$f_i$	$f_{i+1}$	$f_{i+2}$	$f_{i+3}$	$f_{i+4}$	$f_{i+5}$
$2(\Delta x)\partial f/\partial x$	-3	4	-1			
$(\Delta x)^2\partial^2 f/\partial x^2$	2	-5	4	-1		
$2(\Delta x)^3\partial^3 f/\partial x^3$	-5	18	-24	14	-3	
$(\Delta x)^4\partial^4 f/\partial x^4$	3	-14	26	-24	11	-2

**Table B.5:** Backward difference representations of  $O(\Delta x)^2$

	$f_{i-5}$	$f_{i-4}$	$f_{i-3}$	$f_{i-2}$	$f_{i-1}$	$f_i$
$2(\Delta x)\partial f/\partial x$				1	-4	3
$(\Delta x)^2\partial^2 f/\partial x^2$			-1	4	-5	2
$2(\Delta x)^3\partial^3 f/\partial x^3$		3	-14	24	-18	5
$(\Delta x)^4\partial^4 f/\partial x^4$	-2	11	-24	26	-14	3

**Table B.6:** Central-mixed derivatives of  $O((\Delta x)^2, (\Delta z)^2)$

	$f_{i-1,j-1}$	$f_{i,j-1}$	$f_{i+1,j-1}$	$f_{i-1,j}$	$f_{i,j}$	$f_{i+1,j}$	$f_{i-1,j+1}$	$f_{i,j+1}$	$f_{i+1,j+1}$
$4(\Delta x)(\Delta z)\partial f/\partial x\partial z$	1		-1				-1		1
$2(\Delta x)^2(\Delta z)\partial^3 f/\partial x^2\partial z$	-1	2	-1				1	-2	1
$2(\Delta x)(\Delta z)^2\partial^3 f/\partial x\partial z^2$	-1		1	2		-2	-1		1
$(\Delta x)^2(\Delta z)^2\partial^4 f/\partial x^2\partial z^2$	1	-2	1	-2	4	-2	1	-2	1

where  $O(\Delta x)$  and  $O(\Delta x)^2$  represents the first and second order of accuracy of derivative approximations.

## APPENDIX C

### CONSTANTS OF EXPLICIT DISCRETIZATION OF 1D-BWI MODEL

In order to solve the 1D-BWI by explicit discretization the constant  $b$  in Eq. (4.6a) for  $n$  greater than or equal to 3 is obtained as follows,

$$b_{i,n} = \frac{1}{(i-1)^3 \Delta r^{*3}} \left\{ \begin{aligned} & -h_{i,n-1}^* \left[ \frac{-h_{i-1,n-1}^* + h_{i+1,n-1}^*}{2\Delta r^*} \right] + h_{i,n-1}^* \left[ \frac{h_{i-1,n-1}^* - 2h_{i,n-1}^* + h_{i+1,n-1}^*}{\Delta r^*} \right] (i-1) \\ & - 2h_{i,n-1}^* \left[ \frac{-0.5h_{i-2,n-1}^* + h_{i-1,n-1}^* - h_{i+1,n-1}^* + 0.5h_{i+2,n-1}^*}{\Delta r^*} \right] (i-1)^2 - \\ & h_{i,n-1}^* \left[ \frac{h_{i-2,n-1}^* - 4h_{i-1,n-1}^* + 6h_{i,n-1}^* - 4h_{i+1,n-1}^* + h_{i+2,n-1}^*}{\Delta r^*} \right] (i-1)^3 + \\ & 3h_{i,n-1}^* \left[ \frac{(-0.5h_{i-1,n-1}^* + 0.5h_{i+1,n-1}^*)^2}{\Delta r^*} \right] (i-1) - \\ & 3h_{i,n-1}^* \left[ \frac{-h_{i-1,n-1}^* + h_{i+1,n-1}^*}{2\Delta r^*} \right] (h_{i-1,n-1}^* - 2h_{i,n-1}^* + h_{i+1,n-1}^*) (i-1)^2 - \\ & 3h_{i,n-1}^* \left[ \frac{-h_{i-1,n-1}^* + h_{i+1,n-1}^*}{2\Delta r^*} \right] \left\{ \begin{aligned} & -\frac{1}{2}h_{i-2,n-1}^* + h_{i-1,n-1}^* - \\ & h_{i+1,n-1}^* + \frac{1}{2}h_{i+2,n-1}^* \end{aligned} \right\} (i-1)^3 \\ & - \frac{cons}{\Delta t^*} \left( \frac{1}{2}h_{i,n-2}^* - 2h_{i,n-1}^* \right) (i-1)^3 \Delta r^{*3} \end{aligned} \right\} \quad (C.1.a)$$

and for  $n = 2$  the constant  $b_{i,2}$  is,

$$b_{i,2} = \frac{1}{(i-1)^3 \Delta r^{*3}} \left\{ \begin{aligned} & -h_{i,1}^{*3} \left( \frac{-h_{i-1,1}^* + h_{i+1,1}^*}{2\Delta r^*} \right) + h_{i,1}^{*3} \left( \frac{h_{i-1,1}^* - 2h_{i,1}^* + h_{i+1,1}^*}{\Delta r^*} \right) (i-1) \\ & - 2h_{i,1}^{*3} \left( \frac{-0.5h_{i-2,1}^* + h_{i-1,1}^* - h_{i+1,1}^* + 0.5h_{i+2,1}^*}{\Delta r^*} \right) (i-1)^2 - \\ & h_{i,1}^{*3} \left( \frac{h_{i-2,1}^* - 4h_{i-1,1}^* + 6h_{i,1}^* - 4h_{i+1,1}^* + h_{i+2,1}^*}{\Delta r^*} \right) (i-1)^3 + \\ & 3h_{i,1}^{*2} \frac{(-0.5h_{i-1,1}^* + 0.5h_{i+1,1}^*)^2}{\Delta r^*} (i-1) - \\ & 3h_{i,1}^{*2} \left( \frac{-h_{i-1,1}^* + h_{i+1,1}^*}{2\Delta r^*} \right) (h_{i-1,1}^* - 2h_{i,1}^* + h_{i+1,1}^*) (i-1)^2 - \\ & 3h_{i,1}^{*2} \left( \frac{-h_{i-1,1}^* + h_{i+1,1}^*}{2\Delta r^*} \right) \left( -\frac{1}{2}h_{i-2,1}^* + h_{i-1,1}^* - h_{i+1,1}^* + \frac{1}{2}h_{i+2,1}^* \right) (i-1)^3 \\ & - \frac{cons}{\Delta t^*} h_{i,1}^* (i-1)^3 \Delta r^{*3} \end{aligned} \right\} \quad (C.1b)$$

CONSTANTS OF IMPLICIT DISCRETIZATION OF 1D-BWI MODEL

The linearized non-dimensional film drainage equation of the 1D-BWI model is,

$$C_1 \frac{\partial h^*}{\partial t^*} = \left\{ \begin{array}{l} \left( \frac{-h0^{*3} L_{10} + h0^{*3} L_{20} r^* - 2h0^{*3} L_{30} r^{*2} + 3h0^{*2} L_{10}^2 r^*}{r^{*3}} \right) + \\ \left( \frac{-3h0^{*2} L_{10} L_{20} r^{*2} - 3h0^{*2} L_{10} L_{30} r^{*3} - h0^{*3} L_{40} r^{*3}}{r^{*3}} \right) + \\ \left( \frac{-h0^{*3} - 3h0^{*2} L_{20} r^{*2} - 3h0^{*2} L_{30} r^{*3} + 6h0^{*2} L_{10} r^*}{r^{*3}} \right) (L_1 - L_{10}) + \\ \left( \frac{r^* h0^{*3} - 3h0^{*2} L_{10} r^{*2}}{r^{*3}} \right) (L_2 - L_{20}) + \\ \left( \frac{-2r^{*2} h0^{*3} - 3h0^{*2} L_{10} r^{*3}}{r^{*3}} \right) (L_3 - L_{30}) - h0^{*3} (L_4 - L_{40}) + \\ \left( \frac{-3h0^{*2} L_{10} + 3h0^{*2} L_{20} r^* - 6h0^{*2} L_{30} r^{*2} + 6h0^* L_{10}^2 r^*}{r^{*3}} \right) (h^* - h0^*) \\ \left( \frac{-6h0^* L_{10} L_{20} r^{*2} - 6h0^* L_{10} L_{30} r^{*3} - 3h0^{*2} L_{40} r^{*3}}{r^{*3}} \right) (h^* - h0^*) \end{array} \right\} \quad (C.2)$$

The constants of the linear system as shown in Eq. (4.22) for the central nodes ( $i = 3$  to  $i = nr - 2$ ) be expressed as follows:

$$A_{i,n} = \frac{h0_{i,n}^{*2}}{4(i-1)} \left\{ 8h0_{i,n}^* - 3h0_{i-1,n}^* i + 3h0_{i-1,n}^* + 3h0_{i+1,n}^* i - 3h0_{i+1,n}^* - 4h0_{i,n}^* i \right\} \quad (C.3)$$

$$B_{i,n} = \frac{h0_{i,n}^{*2}}{4(i-1)^3} \left\{ \begin{array}{l} -38h0_{i,n}^* + 92h0_{i,n}^* i - 68h0_{i,n}^* i^2 + 16h0_{i,n}^* i^3 - 6h0_{i-1,n}^* + 18h0_{i-1,n}^* i - \\ 24h0_{i-1,n}^* i^2 + 12h0_{i-1,n}^* i^3 + 18h0_{i+1,n}^* - 42h0_{i+1,n}^* i + 36h0_{i+1,n}^* i^2 - \\ 12h0_{i+1,n}^* i^3 + 3h0_{i-2,n}^* - 9h0_{i-2,n}^* i + 9h0_{i-2,n}^* i^2 - 3h0_{i-2,n}^* i^3 - 3h0_{i+2,n}^* + \\ 9h0_{i+2,n}^* i - 9h0_{i+2,n}^* i^2 + 3h0_{i+2,n}^* i^3 \end{array} \right\} \quad (C.4)$$

$$C_{i,n} = \frac{1}{2(i-1)^2} \left\{ \begin{aligned} &12h0_{i,n}^*{}^3 i^2 - 24h0_{i,n}^*{}^3 i + 16h0_{i,n}^*{}^3 - 6h0_{i,n}^*{}^2 h0_{i+1,n}^* (i-1) + \\ &6h0_{i,n}^*{}^2 h0_{i-1,n}^* (i-1) + 3 \frac{C_1}{\Delta t^*} \Delta r^*{}^4 (i-1)^4 + add_{i,n} \end{aligned} \right\} \quad (C.5)$$

$$D_{i,n} = \frac{h0_{i,n}^*{}^2}{4(i-1)^3} \left\{ \begin{aligned} &h0_{i,n}^* (-2+12i-28i^2+16i^3) + h0_{i-1,n}^* (-12i^3+36i^2-42i+18) + \\ &h0_{i-2,n}^* (3i^3-9i^2+9i-3) + h0_{i+2,n}^* (-3i^3+9i^2-9i+3) + \\ &h0_{i+1,n}^* (12i^3-48i^2+66i-30) \end{aligned} \right\} \quad (C.6)$$

$$E_{i,n} = \frac{1}{4(i-1)} \left\{ -4h0_{i,n}^*{}^3 - 3(i-1)h0_{i,n}^*{}^2 h0_{i+1,n}^* + 3(i-1)h0_{i,n}^*{}^2 h0_{i-1,n}^* \right\} \quad (C.7)$$

$$F_{i,n} = \left\{ \begin{aligned} &add_{i,n} + \frac{C_1}{\Delta t^*} \Delta r^*{}^4 (0.5h_{i,n-2}^* - 2h_{i,n-1}^*) + 3 \frac{h0_{i,n}^*{}^2}{(i-1)^2} \left( \frac{h0_{i+1,n}^* - h0_{i-1,n}^*}{2} \right)^2 + \\ &3 \frac{h0_{i,n}^*{}^2}{(i-1)} \left( \frac{h0_{i+1,n}^* - h0_{i-1,n}^*}{2} \right)^2 \left( \frac{h0_{i+1,n}^* - 2h0_{i,n}^* + h0_{i-1,n}^*}{2} \right) - \\ &3h0_{i,n}^*{}^2 \left( \frac{h0_{i+1,n}^* - h0_{i-1,n}^*}{2} \right)^2 \left( \frac{h0_{i+2,n}^* - 2h0_{i+1,n}^* + 2h0_{i-1,n}^* - h0_{i-2,n}^*}{2} \right) \end{aligned} \right\} \quad (C.8)$$

with,

$$add_{i,n} = -\frac{3}{4} \frac{h0_{i,n}^*{}^2}{(i-1)^3} \left\{ \begin{aligned} &2h0_{i+1,n}^* - 2h0_{i-1,n}^* - 4(i-1)(h0_{i+1,n}^* - 2h0_{i,n}^* + h0_{i-1,n}^*) + \\ &4(i-1)^2 (h0_{i+2,n}^* - 2h0_{i+1,n}^* + 2h0_{i-1,n}^* - h0_{i-2,n}^*) - 2(i-1) \frac{(h0_{i+1,n}^* - h0_{i-1,n}^*)^2}{h0_{i,n}^*} + \\ &4(i-1)^2 \frac{(h0_{i+1,n}^* - h0_{i-1,n}^*)}{h0_{i,n}^*} (h0_{i+1,n}^* - 2h0_{i,n}^* + h0_{i-1,n}^*) + \\ &2(i-1)^3 \frac{(h0_{i+1,n}^* - h0_{i-1,n}^*)}{h0_{i,n}^*} (h0_{i+2,n}^* - 2h0_{i+1,n}^* + 2h0_{i-1,n}^* - h0_{i-2,n}^*) + \\ &4(i-1)^3 (h0_{i+2,n}^* - 4h0_{i+1,n}^* + 6h0_{i,n}^* - 4h0_{i-1,n}^* + h0_{i-2,n}^*) \end{aligned} \right\}$$

CONSTANTS OF IMPLICIT DISCRETIZATION OF 3D-BWI MODEL

The linearized film drainage equation in Cartesian coordinate system for the 3D-BWI model is,

$$C_1 \left\{ \frac{\partial h^*}{\partial t^*} + \frac{u^*}{2} LX_1 + \frac{w^*}{2} LZ_1 \right\} = - \left\{ \begin{array}{l} \left[ \begin{array}{l} 6h0^* [(LX_{10})(LX_{30} + LA_0) + (LZ_{10})(LZ_{30} + LB_0)] + \\ 3h0^{*2} (LX_{40} + 2LXZ_0 + LZ_{40}) \end{array} \right] h^* \\ + 3h0^{*2} (LX_{30} + LA_0)(LX_1) + 3h0^{*2} (LX_{10})(LX_3 + LA) + \\ h0^{*3} (LX_4 + LZ_4) + (3h0^{*2})(LB_0 + LZ_{30})(LZ_1) + \\ 3h0^{*2} (LZ_{10})(LZ_3 + LB) + 2h0^{*3} LXZ - \\ \left[ \begin{array}{l} 6h0^* [(LX_{10})(LX_{30} + LA_0) + (LZ_{10})(LZ_{30} + LB_0)] + \\ 3h0^{*2} (LX_{40} + 2LXZ_0 + LZ_{40}) \end{array} \right] h0^* - \\ 3h0^{*2} [(LX_{10})(LX_{30} + LA_0) + (LZ_{10})(LZ_{30} + LB_0)] \end{array} \right\} \quad (C.9)$$

The diagonals obtained by discretization of Eq. (C.9) are written as,

$$D_{1\ i,n} = -\frac{3}{4} h0_{i,n}^{*2} \{ h0_{i+nx,n}^* - h0_{i-nx,n}^* \} + h0_{i,n}^{*3} \quad (C.10)$$

$$D_{2\ i,n} = -\frac{3}{4} h0_{i,n}^{*2} \{ h0_{i+1,n}^* - h0_{i-1,n}^* + h0_{i+nx,n}^* - h0_{i-nx,n}^* \} + 2h0_{i,n}^{*3} \quad (C.11)$$

$$D_{3\ i,n} = -\frac{w_n^*}{4} C_1 \Delta x^{*3} - 8h0_{i,n}^{*3} - \frac{3}{4} h0_{i,n}^{*2} \left\{ \begin{array}{l} h0_{i+2nx,n}^* - 8h0_{i+nx,n}^* + 8h0_{i-nx,n}^* - h0_{i-2nx,n}^* + \\ h0_{i+nx+1,n}^* - h0_{i-nx+1,n}^* + h0_{i+nx-1,n}^* - h0_{i-nx-1,n}^* \end{array} \right\} \quad (C.12)$$

$$D_{4\ i,n} = \frac{3}{4} h0_{i,n}^{*2} \{ h0_{i+1,n}^* - h0_{i-1,n}^* - h0_{i+nx,n}^* + h0_{i-nx,n}^* \} + 2h0_{i,n}^{*3} \quad (C.13)$$

$$D_{5\ i,n} = -\frac{3}{4}h0_{i,n}^{*2} \{h0_{i+1,n}^* - h0_{i-1,n}^*\} + h0_{i,n}^{*3} \quad (C.14)$$

$$D_{6\ i,n} = -\frac{u_n^*}{4}C_1\Delta x^{*3} - 8h0_{i,n}^{*3} - \frac{3}{4}h0_{i,n}^{*2} \left\{ \begin{array}{l} h0_{i+2,n}^* - 8h0_{i+1,n}^* + 8h0_{i-1,n}^* - h0_{i-2,n}^* + \\ h0_{i+nx+1,n}^* - h0_{i+nx-1,n}^* + h0_{i-nx+1,n}^* - h0_{i-nx-1,n}^* \end{array} \right\} \quad (C.15)$$

$$D_{7\ i,n} = \frac{3}{2}\frac{C_1}{\Delta t^*}\Delta x^{*4} + 3h0_{i,n}^{*2}s1_{i,n} + \frac{3}{2}h0_{i,n}^*s2_{i,n} + 20h0_{i,n}^{*3} \quad (C.16)$$

$$D_{8\ i,n} = \frac{u_n^*}{4}C_1\Delta x^{*3} - 8h0_{i,n}^{*3} + \frac{3}{4}h0_{i,n}^{*2} \left\{ \begin{array}{l} h0_{i+2,n}^* - 8h0_{i+1,n}^* + 8h0_{i-1,n}^* - h0_{i-2,n}^* + \\ h0_{i+nx+1,n}^* - h0_{i+nx-1,n}^* + h0_{i-nx+1,n}^* - h0_{i-nx-1,n}^* \end{array} \right\} \quad (C.17)$$

$$D_{9\ i,n} = \frac{3}{4}h0_{i,n}^{*2} \{h0_{i+1,n}^* - h0_{i-1,n}^*\} + h0_{i,n}^{*3} \quad (C.18)$$

$$D_{10\ i,n} = -\frac{3}{4}h0_{i,n}^{*2} \{h0_{i+1,n}^* - h0_{i-1,n}^* - h0_{i+nx,n}^* + h0_{i-nx,n}^*\} + 2h0_{i,n}^{*3} \quad (C.19)$$

$$D_{11\ i,n} = +\frac{w_n^*}{4}C_1\Delta x^{*3} - 8h0_{i,n}^{*3} + \frac{3}{4}h0_{i,n}^{*2} \left\{ \begin{array}{l} h0_{i+2nx,n}^* - 8h0_{i+nx,n}^* + 8h0_{i-nx,n}^* - h0_{i-2nx,n}^* + \\ h0_{i+nx+1,n}^* - h0_{i-nx+1,n}^* + h0_{i+nx-1,n}^* - h0_{i-nx-1,n}^* \end{array} \right\} \quad (C.20)$$

$$D_{12\ i,n} = \frac{3}{4}h0_{i,n}^{*2} \{h0_{i+1,n}^* - h0_{i-1,n}^* + h0_{i+nx,n}^* - h0_{i-nx,n}^*\} + 2h0_{i,n}^{*3} \quad (C.21)$$

$$D_{13\ i,n} = \frac{3}{4}h0_{i,n}^{*2} \{h0_{i+nx,n}^* - h0_{i-nx,n}^*\} + h0_{i,n}^{*3} \quad (C.22)$$

$$f_{i,n} = \frac{C_1}{\Delta t^*}\Delta x^{*4} (-0.5h_{i,n-2}^* + 2h_{i,n-1}^*) + 3h0_{i,n}^{*2} (h0_{i,n}^*s1_{i,n} + \frac{3}{4}s2_{i,n}) \quad (C.23)$$

with,

$$s1_{i,n} = \left\{ \begin{array}{l} h0_{i-2nx,n}^* + 2h0_{i-nx-1,n}^* - 8h0_{i-nx,n}^* + 2h0_{i-nx+1,n}^* + h0_{i-2,n}^* - 8h0_{i-1,n}^* + \\ 20h0_{i,n}^* - 8h0_{i+1,n}^* + h0_{i+2,n}^* + 2h0_{i+nx-1,n}^* - 8h0_{i+nx,n}^* + 2h0_{i+nx+1,n}^* + h0_{i+2nx,n}^* \end{array} \right\} \quad (C.24)$$

$$s2_{i,n} = \left\{ \begin{array}{l} (h0_{i+1,n}^* - h0_{i-1,n}^*) \left\{ \begin{array}{l} h0_{i+2,n}^* - 4h0_{i+1,n}^* + 4h0_{i-1,n}^* - h0_{i-2,n}^* + \\ h0_{i+nx+1,n}^* - h0_{i+nx-1,n}^* + h0_{i-nx+1,n}^* - h0_{i-nx-1,n}^* \end{array} \right\} + \\ (h0_{i+nx,n}^* - h0_{i-nx,n}^*) \left\{ \begin{array}{l} h0_{i+2nx,n}^* - 4h0_{i+nx,n}^* + 4h0_{i-nx,n}^* - h0_{i-2nx,n}^* + \\ h0_{i+nx+1,n}^* - h0_{i-nx+1,n}^* + h0_{i+nx-1,n}^* - h0_{i-nx-1,n}^* \end{array} \right\} \end{array} \right\} \quad (C.25)$$

## APPENDIX D

### FLOWCHARTS OF SUBROUTINES OF THE EXPLICIT 1D-BWI CODE

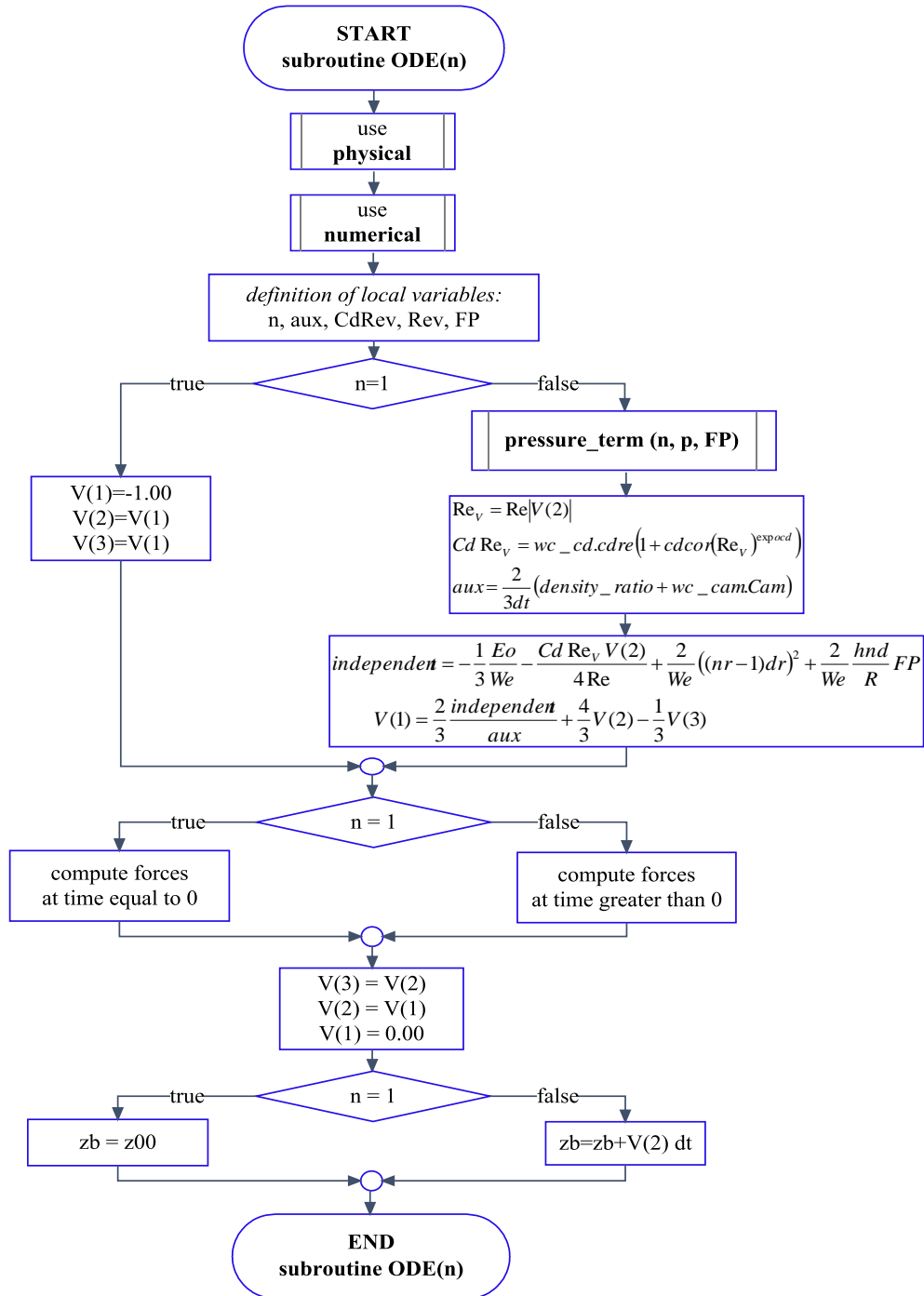


**Figure D1:** Structure of the subroutine ODE (n) specified in main program Exp\_1D\_BWI

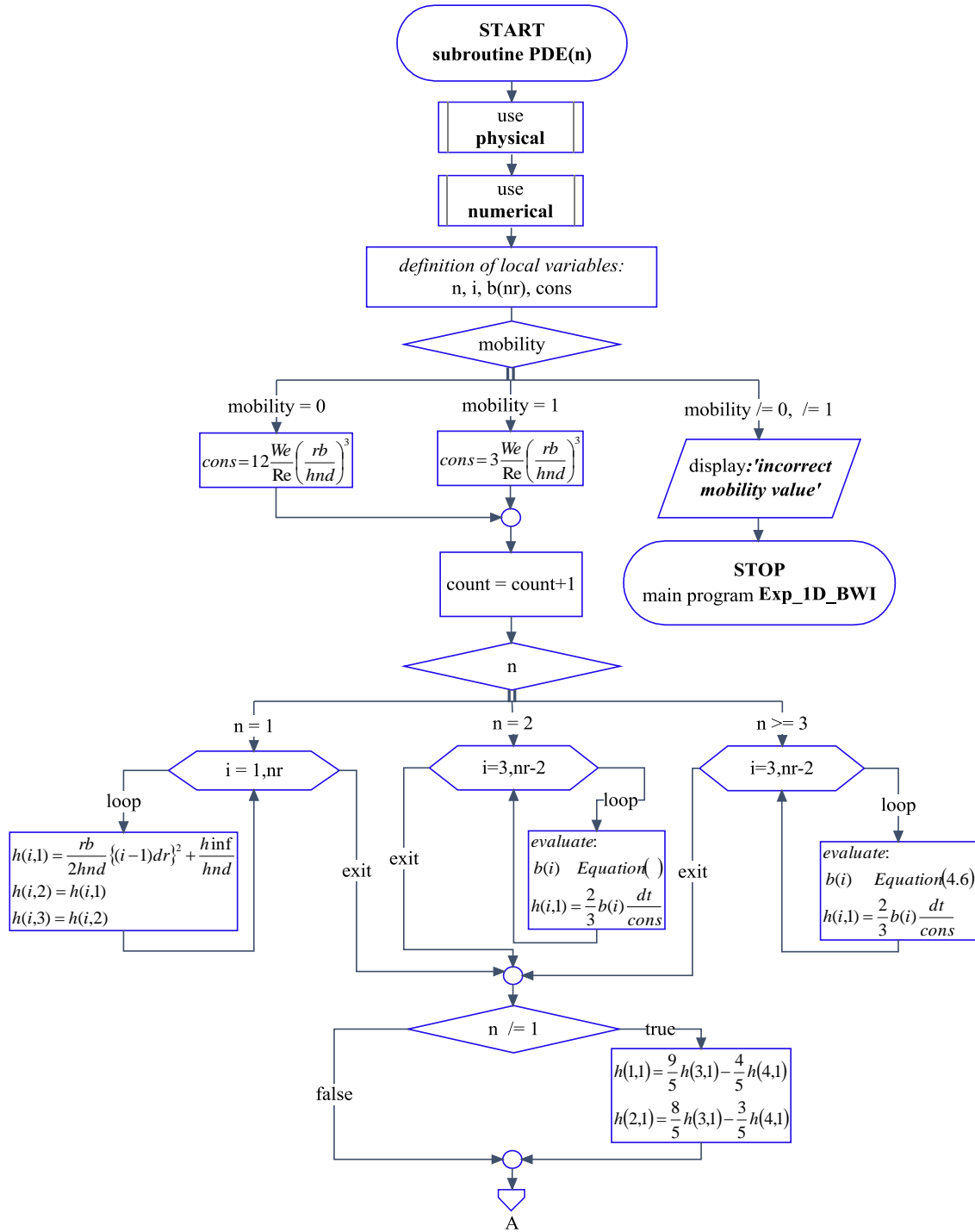


Figure D2: Structure of the subroutine PDE(n) specified in main program Exp\_1D\_BWI

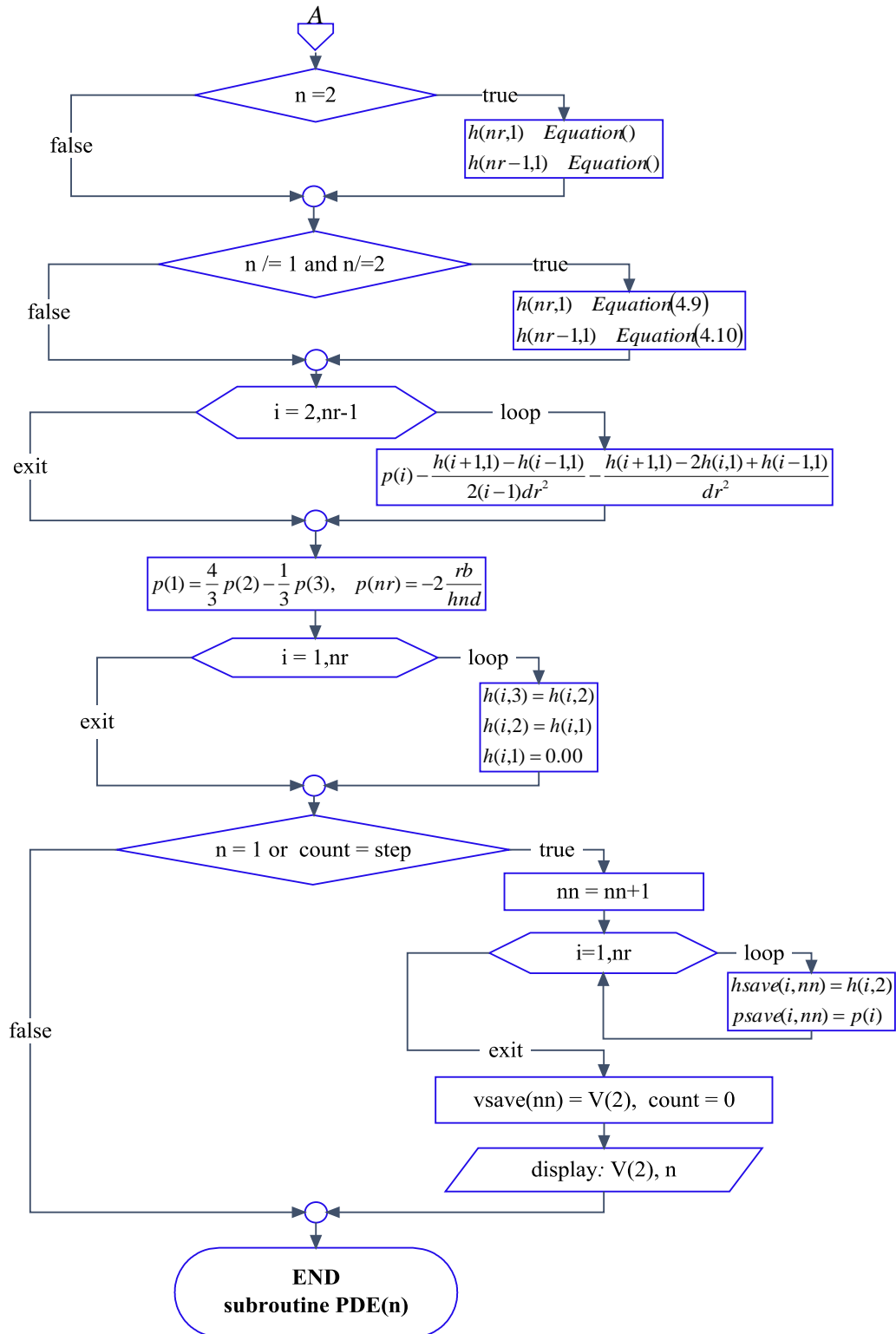
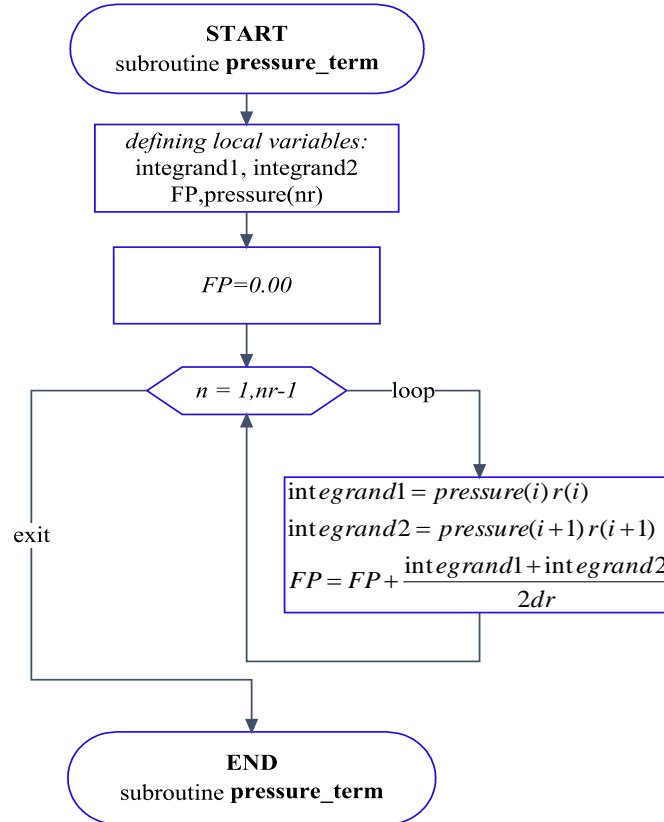


Figure D3: Structure of the subroutine PDE(n) specified in main program Exp\_1D\_BWI (continuation)



**Figure D4:** Structure of the subroutine pressure term specified in subroutine ODE (n) as shown in Fig. D1

### EXPLICIT 1D-BWI CODE

```

=====
! PROGRAM: Explicit one-dimensional Bubble-wall interaction
!
! PURPOSE: This program solve the one-dimensional bubble-wall interaction
! model, i.e. solves the trajectory and lubrication equations for
! an axisymmetrical bubble.
! The general algorithm is:
! 1st, using the h(i,n-1) we compute the pressure force.
! 2nd, using this pressure force the velocity for following time
! step is determined.
! finally, using the last velocity and explicit method we solve
! the lubrication equation for determine the h(i,n) that will be
! useful for determine the velocity for follow time step.
!
!
! RECORD OF REVISIONS:
! Date(mmddyyyy) Programmer Description of change
! =====
! 02/28/2011 R. De La Cruz Rev0
! ----- S. Cancelos, PhD. -----
=====

```



```

end module numerical

!!!!!!!!!!!!!!!!!!!!!!!!!!!!!!!!!!!!!!!!!!!!!!!!!!!!!!!!!!!!!!!!!!!!!!!!!!!!!!!!!!!!!!!!!!!!!!!!!!!!!!!!!!!!!!!!!!!!!!!!

program Exp_1D_BWI

use physical
use numerical
implicit none

!local variables
integer*8 :: n
integer    :: status,i

!input parameters
!Entering values of Numerical parameters.
dt = 1.d-11      !temporal step
nr = 100         !number of nodes
nt = 400000000001 !number of temporal steps
                  !(always + 1 if I want the last run to be saved)
sdf=100000      !save data frequency
step=nt/sdf     !every "step" steps is saving the solution in the matrix

if(nt.lt.3) then
  print *, 'error: time steps number should be greater than 3 '
  stop
endif

!allocate arrays
allocate(p(nr),STAT=status)
allocate(v(3),STAT=status)
allocate(h(nr,3),STAT=status)
allocate(psave(nr,sdf+1),STAT=status)
allocate(vsave(sdf+1),STAT=status)
allocate(hsave(nr,sdf+1),STAT=status)
allocate(r(nr),STAT=status)

!entering values of physical parameters
rb = 0.79d-3      ! [m]
hnd = 3.3d0*rb   ! [m]
hinf= hnd        ! [m]
rmax = 1.2d0     ! dimensionless
mobility = 0     ! integer:0=immobile,1=mobile(slip at bubble surface)
VT= 0.26d0      ! [m/s]
density_ratio = 0.001d0 !frequently 0.d0 is used

!input constants of correlations
!CdRev=wc_cd*cdre*(1+cdcor*Rev**expocd)
!Cam= wc_cam*Cam
Cam = 0.5d0      !0.5d0 for spherical bubble
cdre = 55.d0     !1.15*48 or 24 see Klaseboer's Paper
cdcor = -0.9596016d0 !From Klaseboer -0.9596016d0
expocd=-0.5d0    !-0.5d0 or 0.687d0
wc_cd= 2.3410767804d0
wc_cam=2.d0

Re = 410.d0      !for rb=.79e-3
We = 1.463d0     !calculated by 2rbrho1VT^2/sigma
!Eo = 0.547397d0 !calculated with g=9.81

!when no know liquid and bubble density the following equation can be used.
!This equetion results of drag and buoyancy forces balance for initial

```

```

!condition i.e. at V = VT.
Eo=3.d0/4.d0*cdre*(1.d0+cdc*Re**(expocd))*we/Re !for We=2Rrho1VT^2/sigma

!compute of grid space size
dr=rmax/float(nr-1)

!initialize: bubble far away moves at terminal velocity
z00= (hinf+rb)/rb !(hnd+rb)/rb

!p initialization
do i=1,nr
  p(i)=-2.d0*rb/hnd
  r(i)= float(i-1)*dr
end do

!open files
call open_files

nn = 0
count = 0
do n= 1,nt
  call ODE(n)           !solve trajectory equation
  call PDE(n)           !solve lubrication equation
  call save_results(n) !save results obtained
enddo
!close files
close (2)
close (3)
close (4)

end Program Exp_1D_BWI
!!!!!!!!!!!!!!!!!!!!!!!!!!!!!!!!!!!!!!!!!!!!!!!!!!!!!!!!!!!!!!!!!!!!!!!!!!!!!!!!!!!!!!!!!!!!!!!!!!!!!!!!!!!!!!!!!!!!!!!!

!=====
! name      : subroutine  ODE
! purpose   : solve the trajectory equation in explicit form. The trajectory
!             equation is a non linear non homogeneous partial differential
!             equation
! note      : the trajectory equation is a initial value problem
!=====
subroutine ODE(n)
use physical
use numerical
implicit none
integer*8 n

!local variables
real(kind=8) :: aux,CdRev,Rev
real(kind=8) :: FP

if (n.eq.1) then
  V(1)=-1.d0
  V(2)= V(1)
  V(3)= V(1)
else

  call Pressure_term(n,P,FP) !FP=Integral(r*p,{0,rmax})

  Rev=Re*abs(V(2)) ! should be Rev=Re*abs(V(1)),but V(1) is unknown now
  CdRev=wc_cd*cdre*(1.d0+cdc*Rev**(expocd))
  aux=2.d0/3.d0*(density_ratio+wc_cam*Cam)/dt
  !denominator=2.d0/3.d0*(density_ratio+wc_cam*Cam)

```

```

!Discretized trajectory equation considering V(n)=V(2) in drag force
V(1)=2.d0/3.d0*(-Eo/We/3.d0-CdRev*V(2)/4.d0/Re+2.D0/We*      &
(float(nr-1)*dr)**2 + 2.D0*hnd/rb/We*FP )/aux-              &
V(3)/3.d0+4.d0/3.d0*V(2)

!Discretized trajectory equation considering V(n)=V(1) in drag force
!V(1)=(-Eo/We/3.d0+2.D0/We*(float(nr-1)*dr)**2 +2.D0*hnd/rb  &
! /We*FP + denominator/dt*(2.D0*V(2)-0.5D0*V(3)))/          &
! (3.D0/2.D0*denominator/dt+CdRev/4.d0/Re)
endif

!compute non-dimensional forces. The dimensional forces are determined by
!multiply each forces by pi*mul*VT*rb*Re

if (n==1)then!P=-2rb/hnd
wallforce = 2.D0/We*(float(nr-1)*dr)**2 +2.D0*hnd/rb/We*(-rb*rmax**2/hnd)
buoyancy = -Eo/we/3.d0
addedmass = -2.d0/3.d0*wc_cam*cam*(1.5d0*V(1)-2.d0*V(2)+0.5d0*V(3))/dt
drag = -wc_cd*cdre*(1.d0+cdc*Re**expocd)*V(2)/4.d0/Re
else
buoyancy = -Eo/we/3.d0
addedmass = -2.d0/3.d0*wc_cam*cam*(1.5d0*V(1)-2.d0*V(2)+0.5d0*V(3))/dt
drag = -CdRev*V(2)/4.d0/Re
wallforce = 2.D0/We*(float(nr-1)*dr)**2 +2.D0*hnd/rb/We*FP
end if

!compute net force
netforce = buoyancy+addedmass+drag+wallforce

V(3)=V(2)
V(2)=V(1)
V(1)=0.d0
if (n==1) then
zb=z00
else
zb=zb+v(2)*dt
end if

end subroutine ODE

!=====
! name      :  subroutine PDE
! purpose   :  Solves the one-dimensional lubrication equation by the explicit
!              method using the second order approximation
!              finite differences scheme.
! note      :  the equation is converted to cylindrical coordinates, due that an
!              axisymmetrical bubble is considered.
!=====
subroutine PDE(n)
use physical
use numerical
implicit none
integer*8 n

!local variables
integer i
real(kind=8) :: b(nr),cons
real(kind=8) :: L1,L2,L3,L4,T,Tnd,Eq1,Eq2,Eqn !debug variables

if(mobility == 0)then
cons=12.d0*we/Re*(rb/hnd)**3 !for no slip at bubble surface
else if (mobility == 1)then

```

```

        cons=3.d0*we/Re*(rb/hnd)**3  !for slip at bubble surface
    else
        print*, ' incorrect mobility value'
        stop
    end if

count=count+1

!----- film thicknes at t=0 -----
if (n==1) then

    do i=1,nr
        h(i,1)=rb/(2.d0*hnd)*(float(i-1)*dr)**2+hinf/hnd !at n=1 i.e.,t=0
        h(i,2)=h(i,1)
        h(i,3)=h(i,2)
    end do
    !----- film thicknes at t > 0 -----
elseif (n==2) then
!use dh/dt=(h(i,n)-h(i,n-1))/dt
!For n=2 the second order time derivative operator can not be defined.
!Instead of defining h(i,n-1)=h(i,n) in the initial conditions
!I use a first order time derivative operator for the second iteration
!The second index in the matrix indicates the previous temporal step
!For example the true h(i-1,n-1) is the previous step to n and it is
!going to h(i-1,2)
!The second index = 1 mean the actual time (n)
!The second index = 2 means the previous step (n-1)
!The second index = 3 menans two previous steps (n-2)
!hence, dh/dt=(h(i,1)-h(i,2))/dt

do i = 3,nr-2
    b(i)=(-h(i,2)**3*(-h(i-1,2)/2.d0+h(i+1,2)/2.d0)/dr+h(i,2)**3* &
        (h(i-1,2)-2.d0 &
        *h(i,2)+h(i+1,2))/dr*float((i-1))-2.d0*h(i,2)**3*(-h(i-2,2)/2.d0+ &
        h(i-1,2)-h(i+1 &
        ,2)+h(i+2,2)/2.d0)/dr*(float(i-1))**2-h(i,2)**3*(h(i-2,2)-4.d0* &
        h(i-1,2)+6.d0*h(i,2 &
        )-4.d0*h(i+1,2)+h(i+2,2))/dr*(float(i-1))**3+3.d0*h(i,2)**2* &
        (-h(i-1,2)/2.d0+h(i+1, &
        2)/2.d0)**2/dr*float(i-1)-3.d0*h(i,2)**2*(-h(i-1,2)/2.d0+ &
        h(i+1,2)/2.d0)/dr*(h(i-1,2 &
        )-2.d0*h(i,2)+h(i+1,2))*(float(i-1))**2-3.d0*h(i,2)**2* &
        (-h(i-1,2)/2.d0+h(i+1,2)/2.d0) &
        /dr*(-h(i-2,2)/2.d0+h(i-1,2)-h(i+1,2)+h(i+2,2)/2.d0)*(float(i-1)) &
        **3+cons*h(i,2 &
        )/dt*(float(i-1))**3*dr**3)/(float(i-1))**3/dr**3

!therefore
    h(i,1)=b(i)*dt/cons  !using dh/dt=(h(i,1)-h(i,2))/dt
    !for debug
    L1 = (-h(i-1,2)/2+h(i+1,2)/2)/dr
    L2 = (h(i-1,2)-2*h(i,2)+h(i+1,2))/dr**2
    L3 = (-h(i-2,2)/2+h(i-1,2)-h(i+1,2)+h(i+2,2)/2)/dr**3
    L4 = (h(i-2,2)-4*h(i-1,2)+6*h(i,2)-4*h(i+1,2)+h(i+2,2))/dr**4
    T = (h(i,1)-h(i,2))/dt

end do

elseif (n .NE. 2 .and. n .NE. 1) then

do i = 3,nr-2

```

```

b(i)=- (h(i,2)**3*(-h(i-1,2)/2.d0+h(i+1,2)/2.d0)/dr-
h(i,2)**3*(h(i-1,2)-2.d0 &
*h(i,2)+h(i+1,2))/dr*float((i-1))+2.d0*h(i,2)**3*(-h(i-2,2)/2.d0 &
+h(i-1,2)-h(i+1,2)+h(i+2,2)/2.d0)/dr*(float(i-1))**2+h(i,2)**3*(h(i-2,2)-
4.d0*h(i-1,2)+6.d0*h(i,2 &
)-4.d0*h(i+1,2)+h(i+2,2))/dr*(float(i-1))**3-3.d0*h(i,2)**2*
(-h(i-1,2)/2.d0+h(i+1,2 &
)/2.d0)**2/dr*float(i-1)+3.d0*h(i,2)**2*(-h(i-1,2)/2.d0+
h(i+1,2)/2.d0)/dr*(h(i-1,2 &
)-2.d0*h(i,2)+h(i+1,2))*(float(i-1))**2+3.d0*h(i,2)**2*
(-h(i-1,2)/2.d0+h(i+1,2)/2.d0) &
/dr*(-h(i-2,2)/2.d0+h(i-1,2)-h(i+1,2)+h(i+2,2)/2.d0)*(float(i-1)) &
**3+cons*(h(i, &
3)/2.d0-2.d0*h(i,2))/dt*(float(i-1))**3*dr**3)/(float(i-1)) &
**3/dr**3

h(i,1)=2.d0/3.d0*b(i)*dt/cons

!This can be useful for debugging.
!L1, L2, L3, L4 and T are the derivative operators
!Eqn is the diferential equation that has to be equal zero to be satisfied

L1 = (-h(i-1,2)/2.d0+h(i+1,2)/2.d0)/dr
L2 = (h(i-1,2)-2*h(i,2)+h(i+1,2))/dr**2
L3 = (-h(i-2,2)/2.d0+h(i-1,2)-h(i+1,2)+h(i+2,2)/2.d0)/dr**3
L4 = (h(i-2,2)-4*h(i-1,2)+6*h(i,2)-4*h(i+1,2)+h(i+2,2))/dr**4
T = (h(i,3)/2.d0-2*h(i,2)+3.D0/2.D0*h(i,1))/dt

Eqn= -(h(i,1)**3*L1-h(i,1)**3*L2*(i-1)*dr+2*h(i,1)**3*L3*(i-1)**2* &
dr**2+h(i,1)**3*L4*(i-1)**3*dr**3-3*h(i,1)**2*L1**2*(i-1)*dr+3*h(i &
,1)**2*L1*L2*(i-1)**2*dr**2+3*h(i,1)**2*L1*L3*(i-1)**3*dr**3+cons* &
T*(i-1)**3*dr**3)/(i-1)**3/dr**3

end do
end if

!-----
! BOUNDARY CONDITIONS AT t > 0 (Ignore if n=1)
!-----
if (n .NE. 1) Then
h(1,1)=9.d0/5.d0*h(3,1)-4.d0/5.d0*h(4,1)
h(2,1)=8.d0/5.d0*h(3,1)-3.d0/5.d0*h(4,1)
end if

if (n == 2) then
!fortran(subs(n-1=2,n-2=3,n=1));
!using first backward derivative of time.

h(nr,1)=(hnd*h(nr,2)+rb*V(2)*dt)/hnd

h(nr-1,1)=0.5D0/(5.D0*float(nr)-3.D0)*((4.D0*float(nr)-1.D0)*h(nr,2)+ &
(4.D0*float(nr)-1.D0)*rb*V(2)*dt/hnd+(8.D0*float(nr)-7.D0)*h(nr-2,1)- &
2.d0*(float(nr)-1.D0)*h(nr-3,1)-4.d0*rb*(float(nr)-1.D0)/hnd*dr**2)

Tnd=(h(nr,1)-h(nr,2))/dt !variable for debug

end if

if (n .NE. 2 .and. n .NE. 1) then

```

```

!For whichever value of hnd
!fortran(subs(n-2=3,n-1=2,n=1,h[nr-1,n]));

h(nr-1,1)=- (12.d0*rb*dr**2*float(nr)-12.d0*rb*dr**2+
21.d0*hnd*h(nr-2,1)+4.d0*float(nr)*hnd*h(nr,3)+
6.d0*hnd*h(nr-3,1)*float(nr)-6.d0*hnd*h(nr-3,1)-
24.d0*hnd*h(nr-2,1)*float(nr)-hnd*h(nr,3)
+4.d0*hnd*h(nr,2)+2.d0*rb*V(2)*dt-
16.d0*float(nr)*hnd*h(nr,2)-
8.d0*float(nr)*rb*V(2)*dt)/hnd/(-3.d0+5.d0*float(nr))/6.d0

!fortran(subs(n-2=3,n-1=2,n=1,h[nr,n]));
h(nr,1)= -1.d0/hnd*(hnd*h(nr,3)-4.d0*hnd*h(nr,2)-2*rb*V(2)*dt)/3.d0

end if

!----- END BOUNDARY CONDITIONS -----

!-----
!
! PRESSURE CALCULUS
!-----

do i=2, nr-1
P(i)=- (h(i-1,1)-2.d0*h(i,1)+h(i+1,1))/dr**2-
(-h(i-1,1)/2.d0+h(i+1,1)/2.d0)/dr**2/(float(i-1))
end do

p(1)= 4.d0/3.d0*P(2)-1.d0/3.d0*P(3)
p(nr)=-2.d0*rb/hnd

!----- End Pressure calculus -----

!This moves the value of h one position up for the next time iteration
do i=1,nr
h(i,3)=h(i,2)
h(i,2)=h(i,1)
h(i,1)=0
end do
!.....
! algorithm for saving data in Psave,Vsave and hsave.
!.....
if (count==step .or. n==1) then
nn=nn+1
do i=1,nr
hsave(i,nn)=h(i,2)
psave(i,nn)=P(i)
end do
Vsave(nn)=V(2)
count=0
write(6,20) V(2), n !write in windows unit=6
20 format(' V =',E23.15, I22)
endif

end subroutine PDE

!=====
! name : subroutine open_files
! purpose : opens files to save data inputs and results obtained
! note : no has any variable for shared with main program, because this, is
! called only as 'call openfiles'

```

```

!=====
subroutine open_files
use physical
use numerical

open(unit=1,file='data.dat')
open(unit=2,file='h_p_solution.dat')
open(unit=3,file='z_v_solution.dat')
open(unit=4,file='save_forces.dat')

write(1,11) nt,nr,dt
write(1,21) rb,rmax,dr
!write(1,31) rho1,rhob,sigma,mul,g
write(1,41) hnd,hnd,z00 !use VT for reemplace z00
write(1,51) Re,We,Eo
write(1,61) Cam,cdre,cdcor,mobility
11 format('nt:',I12,'      nr:',I12,'      dt:',E10.3)
21 format('R[m]:',E14.6,'      rmax:',E14.6,'      dr :',E14.6)
!31 format('rho1:',E10.3,'rhob:',E10.3,'sigma:',E10.3,'mul:',E10.3,'g :',E10.3)
41 format('hinf[m]:',E14.6,'      hnd[m]:',E14.6,'      z00(initial): ',E14.6)
51 format('Re :',E14.6,'      We:',E14.6,'      Eo:',E14.6)
61 format('Cam :',E10.3,'      cdre:',E10.3,'      cdcor:',E10.3,'      mobility:',I5)
close (1)

write(2,30)
30 format('          n      ',' ',' ',' i      ',' ',' ','      h      ',' ',' ',' &
          '
          P      ')

write(2,31)
31 format('          ')

write(3,33)
33 format('          t      ',' ',' ','      v      ',' ',' ','      z[m] ')

write(4,14)
14 format('time-nondim      ',' ',' ' Fnet      ',' ',' ','      Fb      ',' ',' ' Fd      ',' &
          ' ',' '      Fam      ',' ',' '      Fwall')

end subroutine open_files

!=====
! name      :  subroutine save_results
! purpose   :  save results as n progresses
! note      :  the results are stored with a frequency defined
!            by sdf(see module numerical)
!=====
subroutine save_results(n)
use physical
use numerical
integer*8 n
integer i,check

!Write files
check=1+step*(nn-1)
if (check.eq.n) then
write(3,60) (check-1)*dt,Vsave(nn),zb*rb ! (n-1)*dt, nondimensional time
60 format(E23.15,' ',' ',E23.15,' ',E23.15)
write(4,24) (check-1)*dt,netforce,buoyancy,drag,addedmass,wallforce
24 format(E14.6,' ',' ',E16.8,' ',' ',E16.8,' ',' ',E16.8,' ',' ',E16.8,' ',' ',E16.8)
do i=1,nr
write(2,40) check,i, hsave(i,nn), Psave(i,nn)
40 format(I15,' ',' ',I5,' ',' ',E23.15,' ',' ',E23.15)
enddo
endif
end subroutine save_results

```

```

!.....
! name      :  subroutine pressure_term
! purpose   :  FP=Integral(p*r,{0,rmax}) where all variables and limits are
!             the non-dimensional variables.
! note      :  using trapezid rule
!.....
subroutine Pressure_term (n,Pressure,FP)
use physical
use numerical
implicit none
integer*8 n

!local variables
integer i
real(kind=8):: integrand1,integrand2,fp
real(kind=8):: pressure(nr)

fp=0.d0
do i=1,nr-1
  integrand1=Pressure(i)*r(i)      ! P*r(i)
  integrand2=Pressure(i+1)*r(i+1) ! P*r(i+1)
  FP=FP+(integrand1+integrand2)/2.d0*dr
end do

end subroutine Pressure_term
!!!!!!!!!!!!!!!!!!!!!!!!!!!!!!!!!!!!!!!!!!!!!!!!!!!!!!!!!!!!!!!!!!!!!!!!!!!!!!!!!!!!!!!!!!!!!!!!!!!!!!!!!!!!!!!!!!!!!!!!

```

**FLOWCHARTS OF THE SUBROUTINES IN IMPLICIT 1D-BWI CODE**

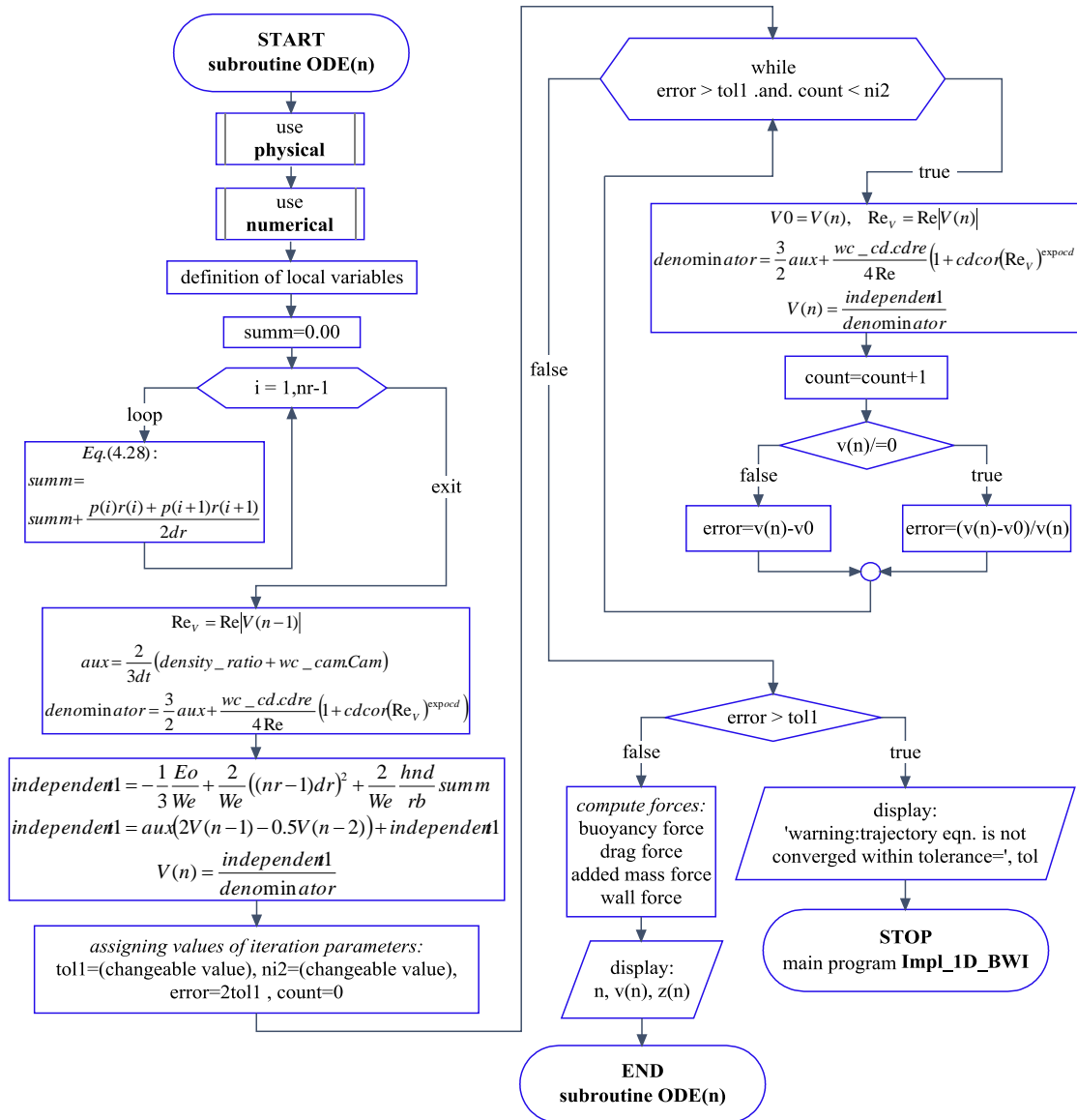


**Figure D5:** Structure of the subroutine ODE (n) specified in main program Impl\_1D\_BWI

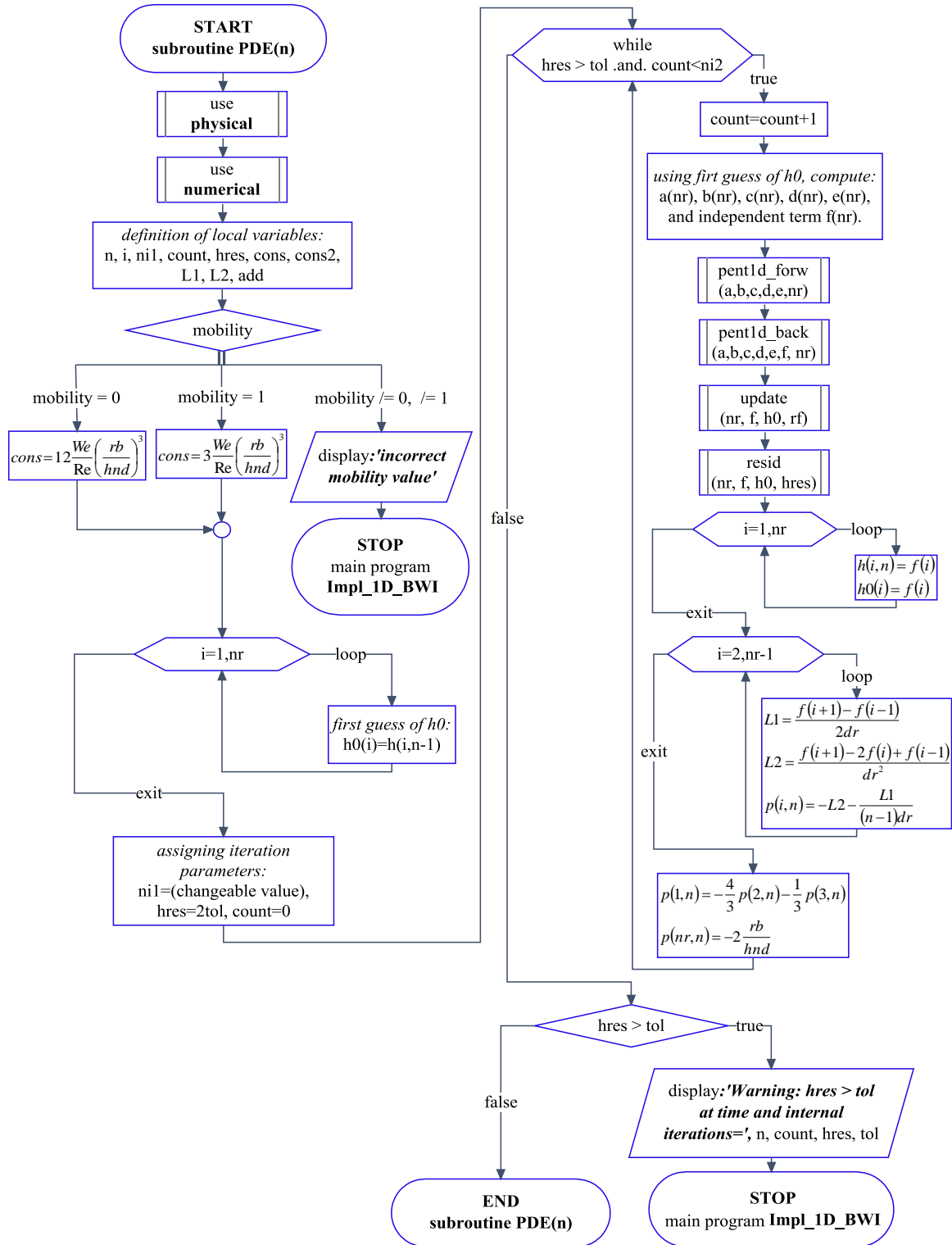


Figure D6: Structure of the subroutine  $PDE(n)$  which is called by the main program  $Impl\_1D\_BWI$

## IMPLICIT 1D-BWI CODE

```
=====
! PROGRAM: Implicit one-dimensional Bubble-wall interaction
!
! PURPOSE: This program solves the one-dimensional bubble-wall interaction
! model,i.e. solves the trajectory and lubrication equations for
! an axisymmetrical bubble.
! The general algorithm is:
! 1st, using the h(i,n-1) we compute the pressure force.
! 2nd, using this pressure force the velocity for following time
! step is determined.
! finally, using the last velocity and implicit method we solve
! the lubrication equation for determine the h(i,n) that will be
! useful for determine the velocity for the follow time step.
!
!
! RECORD OF REVISIONS:
! Date(mmddyyyy) Programmer Description of change
! =====
! 03/04/2011 R. De La Cruz Rev0
! 03/12/2011 R. De La Cruz Rev1, pressure p(1,n) L447
! ----- S. Cancelos,PhD. -----
=====
module physical

implicit none
save

integer, parameter :: single = 4
integer, parameter :: double = 8

!input parametrs

integer :: mobility ! switch for interface mobility: 0 = immobile, 1 = mobile
real(kind=double) :: density_ratio !bubble density/liquid density
real(kind=double) :: VT !terminal Velocity
real(kind=double) :: Re !terminal velocity based Reynolds number
real(kind=double) :: we !Diameter of bubble based Weber number
real(kind=double) :: Eo !eotvos number

real(kind=double) :: Cam !added mass coefficient
real(kind=double) :: cdre !main factor of cd*re
real(kind=double) :: cdcor !second constant in cd correlation
real(kind=double) :: expocd !exponent of grad correlation
real(kind=double) :: wc_cam !added mass wall correction
real(kind=double) :: wc_cd !drag wall correction

real(kind=double) :: z00 !initial bubble position
real(kind=double) :: hnd !characteristic film thickness
real(kind=double) :: hinf !initial film thickness at r=0
real(kind=double) :: rb !characteristic bubble radius
real(kind=double) :: rmax !maximum radius
real(kind=double) :: buoyancy, drag, wallforce, netforce, addedmass,history
!forces on the bubble, it is considered that are
!applied in the gravity center of this.

!Except r all the variables are non-dimensionals
```

```

real (kind=double), dimension(:) , allocatable :: v !bubble velocity
real (kind=double), dimension(:) , allocatable :: z !bubble position
real (kind=double), dimension(:) , allocatable :: r !radial coordinate
real (kind=double), dimension(:, :), allocatable :: h !film tickness
real (kind=double), dimension(:) , allocatable :: h0 !guess for film tickness
real (kind=double), dimension(:, :), allocatable :: p !excess pressure

end module physical
!!!!!!!!!!!!!!!!!!!!!!!!!!!!!!!!!!!!!!!!!!!!!!!!!!!!!!!!!!!!!!!!!!!!!!!!!!!!!!!!!!!!!!!!!!!!!!!!!!!!!!!!!!!!!!!!!!!!!!!!

module numerical

implicit none
save

integer, parameter :: single = 4
integer, parameter :: double = 8

!input parametrs
integer*8 :: nt !total numbers of nodes in time
integer :: nr !total numbers of nodes in space
integer :: nn !for saving data
integer*8 :: step !for saving data
real(kind=double) :: dt ! time step
real(kind=double) :: tol !tolerance for internal h iterations
real(kind=double) :: dr !spatial grid size
real(kind=double) :: rf !relaxation factor

real (kind=double), dimension(:) , allocatable :: a !i-2 diagonal
real (kind=double), dimension(:) , allocatable :: b !i-1 diagonal
real (kind=double), dimension(:) , allocatable :: c ! i diagonal
real (kind=double), dimension(:) , allocatable :: d !i+1 diagonal
real (kind=double), dimension(:) , allocatable :: e !i+2 diagonal
real (kind=double), dimension(:) , allocatable :: f ! independent term

end module numerical
!!!!!!!!!!!!!!!!!!!!!!!!!!!!!!!!!!!!!!!!!!!!!!!!!!!!!!!!!!!!!!!!!!!!!!!!!!!!!!!!!!!!!!!!!!!!!!!!!!!!!!!!!!!!!!!!!!!!!!!!

program Impl_1D_BWI
!declare variables
use physical
use numerical
implicit none

!local variables
integer :: status,i
integer*8 :: n

!changeable numerical parameters
!-----
nr=200 !total nodes in r direction
nt=600000 !total nodes in time
rf= 0.90d0
dt= 2.d-3 !dimensionless
tol= 1.d-10
!-----

if(nt.lt.3) then
print *, 'error: time steps number should be greater than 3 '
stop
endif

```

```

allocate(v(nt),STAT=status)
allocate(z(nt),STAT=status)
allocate(r(nr),STAT=status)
allocate(h(nr,nt),STAT=status)
allocate(h0(nr),STAT=status)
allocate(p(nr,nt),STAT=status)
allocate(a(nr),STAT=status)
allocate(b(nr),STAT=status)
allocate(c(nr),STAT=status)
allocate(d(nr),STAT=status)
allocate(e(nr),STAT=status)
allocate(f(nr),STAT=status)

!Changeable physical parameters
!-----

Cam = 0.5d0          !0.5d0 added mass coefficient
cdre = 24.d0         ! 0.864682d0*48.d0 ! see klaseboer's paper
cdcor = 0.15d0      !-0.9596016d0 !0.15d0 !
expocd= 0.687d0    !-0.5d0 for other cases cases
wc_cd= 1.d0
wc_cam= 1.d0

density_ratio = 0.001d0 !0.001d0!1.d-3 !bubble density/liquid density
VT = 0.0d0           !0.3266d0 !!0.0906787d0 ![m/s] write 0 if this is unknow
rb = 0.4d-3          !0.79d-3 !meters
hnd = 5.d0*rb        !0.01305271463d0*rb!0.0195d0*rb !meters
hinf= hnd            !can be use hinf=hnd if we change this condition
                    !all code will be revised
rmax = 0.80d0        !dimensionless
mobility = 0         !integer: 0 = immobile, 1 = mobile

Re = 72.543d0        !computed using VT
We = 0.0888          !1.46312329d0(for R=0.79mm) computed by 2RrholVT^2/sigma
!Eo=0.330610734d0    !calculated with g=9.81
!when no know liquid and bubble density the following equation can be used.
!This equation results of drag and bouyancy forces balance for initial
!condition i.e. at V = VT.
Eo=0.0847d0
!Eo=3.d0/4.d0*wc_cd*cdre*(1.d0+cdcor*(Re)**expocd)*we/Re !for We=2RrholVT^2/sigma
!-----

!initialize: bubble far away moves at terminal velocity
dr = rmax/float(nr-1)
z00 = (hnd+rb)/rb

!open files
call openfiles

do n=1,2
  v(n)=-1.d0
  z(n)=z00+v(n)*dt*float(n-1)
  !write(1,21) n, float(n-1)*dt*rb/VT ,v(n)*VT, z(n)*rb*1.d3
  write(1,21) n, float(n-1)*dt ,v(n), z(n)
  21 format(I8,' ',E23.15,' ',E23.15,' ',E23.15)
enddo

do i=1,nr
  r(i)=dr*float(i-1)
  do n=1,nt
    h(i,n)=1.d0+rb/2.d0/hnd*r(i)**2 !here hinf = hnd
    p(i,n)=-2.d0*rb/hnd
  enddo
enddo

```

```

        enddo
    enddo

do i=1,nr
    h(i,2)=1.d0+rb/2.d0/hnd*r(i)**2-1.d0*dt*rb/hnd
    !will be +v(2)*dt*rb/hnd but v(2)=-1.d0
    !h(i,3)=h(i,2)-1.d0*dt*rb/hnd
end do

!save initial conditions
do n=1,2
    do i=1,nr
        write(2,22) n,i,r(i),h(i,n),2.d0*rb/hnd+p(i,n)
        22 format(I8,' ',I5,' ',E14.6,' ',E14.6,' ',E14.6 )
    enddo
    buoyancy = -Eo/we/3.d0
    addedmass = 0.d0 !due that v(n-2)=v(n-1)=v(n)
    drag = -wc_cd*cdre/Re/4.d0*(1.d0+cdcor*Re**(expocd))*v(n)
    wallforce = 2.d0*rmax**2/we+2.d0*hnd/rb/we*(-rb*rmax**2/hnd)
    netforce = buoyancy+addedmass+drag+wallforce
    write(4,24) (n-1)*dt,netforce,buoyancy,drag,addedmass,wallforce
    24 format(E14.6,' ',E16.8,' ',E16.8,' ',E16.8,' ',E16.8,' ',E16.8,' ',E16.8)
enddo

nn = 1
step = nt/100 !every "step" is saving the solution in the h_p.dat file
!time loop
do n=3,nt
    call ODE(n) !advance trajectory equation
    call PDE(n) !solve film drainage equation
    call save_results(n) !save data
enddo

stop
end program Impl_1D_BWI

!!!!!!!!!!!!!!!!!!!!!!!!!!!!!!!!!!!!!!!!!!!!!!!!!!!!!!!!!!!!!!!!!!!!!!!!!!!!!!!!!!!!

!=====
! name : subroutine ODE(n)
! purpose : Solves the trajectory equation in explicit form. The trajectory
! equation is a non-linear non-homogeneous partial differential
! equation.
! note : the trajectory equation is a initial value problem
!=====
subroutine ODE(n)

!declare variables
use physical
use numerical
implicit none
integer*8 :: n
integer :: ni2,nh

!local variables
integer :: i,count,ninit,nfinal
real(kind=8) :: summ,independent1,aux,denominator,v0,rev,error,toll
real(kind=8) :: sumhis,fachis,aspr
real(kind=8), dimension(3) :: at ! time derivative coefficients SC

!second order time derivative approxiamtion:
at(1)= 1.5d0

```

```

at(2)=-2.d0
at(3)= 0.5d0
!Calculate pressure integral
summ=0.d0 !summ=integral {p*r,[0,rmax]}, Trapezoid rule
do i=1,nr-1
  summ=summ+(r(i+1)*p(i+1,n-1)+r(i)*p(i,n-1))/2.d0*dr
enddo

!from Dominique's paper(2005)for spherical drops
!wc_cam=1.d0+0.375d0*(1.d0/z(n-1))**3+3.d0/64.d0*(1.d0/z(n-1))**6+ &
  !9.d0/256.d0*(1.d0/z(n-1))**8+3.d0/512.d0*(1.d0/z(n-1))**9

!wc_cd=(1.d0/(1.d0-(0.5d0/z(n-1)+1.d-9)**3))**2
!cam= 1.5d0*(1.d0/(1.d0-(0.5d0/z(n-1)+1.d-10)**3))-1

!compute history term
sumhis=0.d0

!put limit on integration iujas con lasdo a que el kernel que estamos trabajando
parece
!que no aplica para burb
!segun hasta lo que he evaluado esta fuerza no mejora la aproximacioniar at(1) por
at(3)
!intercamb
! deb
if (n.gt.3.and.n.le.nt/2+3) then !(n.le.4003) (n.gt.3.and.n.le.4003)
  do nh=3, n-1 ! if nh=n you obtain inf#
    !sumhis=sumhis+(at(1)*v(nh)+at(2)*v(nh-1)+at(3)*v(nh-2))/sqrt(float(n-nh))
!esta es correcta
    sumhis=sumhis+(at(3)*v(nh)+at(2)*v(nh-1)+at(1)*v(nh-2))/sqrt(float(n-nh))
!segun Podvin 2d
  end do
else if (n==3) then
  sumhis=0.d0
else
  do nh=n-nt/2, n-1
    !sumhis=sumhis+(at(1)*v(nh)+at(2)*v(nh-1)+at(3)*v(nh-2))/sqrt(float(n-nh))!esta
es correcta
    sumhis=sumhis+(at(3)*v(nh)+at(2)*v(nh-1)+at(1)*v(nh-2))/sqrt(float(n-nh))
!segun Podvin 2d
  end do
endif

fachis=-3.0d0/sqrt(1.d0*3.141592d0*Re*dt) !modificado respecto al de Podvin
sumhis=sumhis*fachis

sumhis=0.0d0 ! Finally we not consider the history force because in bubbles it is
negligible
!print*, sumhis

!adding variable aspec_ratio, aspr.
!pero finamente no se uso porque la def aqui es debido a la superficie y esto
!no considera la correlacion de moore.
!ninit=nt !7310!4430
!nfinal=nt !9968
!if(n.gt.ninit.and.n.lt.nfinal) then
! aspr=0.0269d0*(we*v(n-1)**2)**4-0.1082d0*(we*v(n-1)**2)**3+0.1876d0*(we*v(n-
1)**2)**2&
! +0.0775d0*(we*v(n-1)**2)+1.d0

! wc_cd =0.33d0*aspr**(4.d0/3.d0)*(aspr**2-1.d0)**(1.5d0)*(sqrt(aspr**2-1)- &
! (2.d0-aspr**2)*acos(1.d0/aspr))/(aspr**2*acos(1.d0/aspr)-sqrt(aspr**2-1))**2

```

```

!cdcor=0.0195d0*aspr**4-0.2134d0*aspr**3+1.7026d0*aspr**2-2.1461d0*aspr-1.5732d0
!wc_cam= 0.62d0*aspr-0.12d0
!else
!wc_cd=2.3410767804d0
! cdcor=-0.9596016d0
! wc_cam=1.d0
!end if

independent1=-Eo/we/3.d0 +2.d0*rmax**2/we+2.d0*hnd/rb/we*summ +sumhis
aux=2.d0/3.d0*(density_ratio+wc_cam*Cam)/dt

independent1=independent1-(at(2)*v(n-1)+at(3)*v(n-2))*aux
Rev=Re*abs(v(n-1))
denominator=at(1)*aux+wc_cd*cdre/Re/4.d0*(1.d0+cdcor*(Rev)**(expocd))
v(n)=independent1/denominator
count=0
toll=1.d-13
error=2.d0*toll
ni2=10000
do while(error>toll.and.count<ni2)
  v0=v(n)
  Rev=Re*abs(v(n))
  denominator=at(1)*aux+wc_cd*cdre/Re/4.d0*(1.d0+cdcor*(Rev)**(expocd))
  v(n)=independent1/denominator
  count=count+1
  if(v(n).ne.0.d0) then
    error=abs(v(n)-v0)/v(n)
  else
    error=abs(v(n)-v0)
  endif
!print *, 'iteration, trajectory error,',count,error
enddo
if(error>toll) then
  print *, 'WARNING: TRAJECTORY EQN. IS NOT CONVERGED WITHIN TOLERANCE=',tol
  stop
endif

!Compute non-dimensional forces. The Dimensional forces are determined by
!multiply each forces by pi*mul*VT*rb*Re.
buoyancy = -Eo/we/3.d0
addedmass = -2.d0/3.d0*wc_cam*cam*(1.5d0*v(n)-2.d0*v(n-1)+0.5d0*v(n-2))/dt
drag = -wc_cd*cdre/Re/4.d0*(1.d0+cdcor*Rev**(expocd))*v(n)
wallforce = 2.d0*rmax**2/we+2.d0*hnd/rb/we*summ
history=sumhis

!compute the netforce dimensionless in all time history=0.00
netforce = buoyancy+addedmass+drag+wallforce+history

!z(n)=z(n-1)+(v(n-1)+v(n))/2.d0*dt*rb
z(n)=4.d0/3.d0*z(n-1)-1.d0/3.d0*z(n-2)+2.d0/3.d0*v(n)*dt
!z(n)=z(n-1)-v(n-1)*dt
print*, n, V(n), rb*z(n)
return
end subroutine ODE

```

```

=====
! name      :  subroutine PDE(n)
! purpose   :  Solves the one-dimensional lubrication equation by the implicit
!             method using the second order approximation
!             finite differences scheme.
! note      :  The equation is converted to cylindrical coordinates, due that an
!             axisymmetrical bubble is considered.
=====
subroutine PDE(n)
use physical
use numerical
implicit none
!local variables
integer :: nil
integer :: count
integer*8 :: n
integer :: i
real(kind=8) :: s1,hres,cons,l2,l1,cons2
real(kind=8), dimension(nr):: add

if(mobility == 0)then
  cons=12.d0*we/re*(rb/hnd)**3 !for no slip at bubble surface
else if (mobility == 1)then
  cons=3.d0*we/re*(rb/hnd)**3 !for slip at bubble surface
else
  print*, ' incorrect mobility value'
  stop
end if

cons2=cons*dr**4/dt

!copy h into h0
do i=1,nr
  h0(i)=h(i,n-1)
enddo

hres=2.d0*tol
nil=100000          !For debugging use small ni
count=0            !counter of internal iterations.
do while (hres.gt.tol.and.count.lt.nil)
  count=count+1
  !form matrix. Boundary conditions are enforced as part of matrix
  !bc
  !dh/dr=0 at r=0 with forward approximation of the derivatives
  a(1)= 0.d0
  b(1)= 0.d0
  c(1)=-3.0d0
  d(1)= 4.0d0
  e(1)=-1.0d0
  f(1)= 0.0d0
  !dp/dr=0 at r=0
  a(2)= 0.d0
  b(2)=-2.d0
  c(2)= 1.0d0
  d(2)= 2.0d0
  e(2)=-1.0d0
  f(2)= 0.0d0
  !dh/dr=v at r=rmax with forward approximation of the derivatives
  a(nr)=0.d0 !a(nr)= 0.5d0
  b(nr)=0.d0 !b(nr)=-2.d0
  c(nr)= 1.5d0
  d(nr)= 0.0d0
  e(nr)= 0.0d0

```

```

f(nr)=dt*rb/hnd*v(n)-0.5d0*h(nr,n-2)+2.d0*h(nr,n-1)
!f(nr)= dt*rb/hnd*v(n) !<--coupling of velocity and film thickness
!excess pressure=0 at r=rmax (p=-2rb/hnd)
a(nr-1)=-1.0d0
b(nr-1)= 4.0d0+0.5d0/float(nr-1)          !SC float
c(nr-1)=-5.0d0-2.0d0/float(nr-1)         !SC float
d(nr-1)= 2.0d0+1.5d0/float(nr-1)         !SC float
e(nr-1)= 0.0d0
f(nr-1)= 2.d0*rb/hnd*dr**2
!main body of matrix
add=0.d0
do i=3,nr-2

!see implicit.mws for derivation with SC modification
!AGREGADO ADD(i)
add(i)=-0.75d0*h0(i)**2*(2.d0*h0(i+1)-2.d0*h0(i-1)-4.d0*float(i-1)*
(h0(i+1)-2.d0*h0(i)+h0(i-1))+4.d0*(float(i-1))**2*(h0(i+2)-
2.d0*h0(i+1)+2.d0*h0(i-1)-h0(i-2))-2.d0*float(i-1)*(h0(i+1)-
h0(i-1))**2/h0(i)+4.d0*(float(i-1))**2*(h0(i+1)-h0(i-1))*
(h0(i+1)-2.d0*h0(i)+h0(i-1))/h0(i)+2.d0*(float(i-1))**3*
(h0(i+1)-h0(i-1))*(h0(i+2)-2.d0*h0(i+1)+2.d0*h0(i-1)-
h0(i-2))/h0(i)+4.d0*(float(i-1))**3*(h0(i+2)-4.d0*h0(i+1)+
6.d0*h0(i)-4.d0*h0(i-1)+h0(i-2)))/(float(i-1))**3

!fortran(a[i],precision=double);
a(i)= -h0(i)**2*(4.d0*h0(i)*float(i)-8.d0*h0(i)+3.d0*h0(i-1)*float(i)-
3.d0*h0(i-1)-3.d0*h0(i+1)*float(i)+3.d0*h0(i+1))/float(i-1)/4.d0

!fortran(b[i],precision=double);
b(i)= h0(i)**2*(-38.d0*h0(i)-3.d0*h0(i+2)-6.d0*h0(i-1)+18.d0*h0(i+1)+
3.d0*h0(i-2)+92.d0*h0(i)*float(i)+18.d0*h0(i-1)*float(i)-
42.d0*h0(i+1)*float(i)-24.d0*h0(i-1)*(float(i))**2-68.d0*h0(i)*
(float(i))**2 +36.d0*h0(i+1)*(float(i))**2-3.d0*h0(i-2)*(float(i))**3+
9.d0*h0(i-2)*(float(i))**2-9.d0*h0(i-2)*float(i)+12.d0*h0(i-1)*
(float(i))**3-12.d0*h0(i+1)*(float(i))**3+3.d0*h0(i+2)*(float(i))**3-
9.d0*h0(i+2)*(float(i))**2+9.d0*h0(i+2)*float(i)+
16.d0*h0(i)*(float(i))**3)/(float(i-1))**3/4.d0

!fortran(c[i],precision=double);
c(i)= -(3.d0*cons2*(float(i))**2-6.d0*cons2*float(i)+3.d0*cons2+
12.d0*h0(i)**3*(float(i))**2-24.d0*h0(i)**3*float(i)+16.d0*h0(i)**3+
6.d0*h0(i)**2*h0(i-1)*float(i)-6.d0*h0(i)**2*h0(i-1)-6.d0*h0(i)**2*
h0(i+1)*float(i)+6.d0*h0(i)**2*h0(i+1))/(float(i-1)**2)/2.d0 +add(i)
!AGREGADO ADD(i)

!fortran(d[i],precision=double);
d(i)= h0(i)**2*(-2.d0*h0(i)+3.d0*h0(i+2)+18.d0*h0(i-1)-30.d0*h0(i+1)-
3.d0*h0(i-2)+ 12.d0*h0(i)*float(i)-42.d0*h0(i-1)*float(i)+
66.d0*h0(i+1)*float(i)+36.d0*h0(i-1)*(float(i))**2-28.d0*h0(i)*
(float(i))**2 -48.d0*h0(i+1)*(float(i))**2+3.d0*h0(i-2)*(float(i))**3-
9.d0*h0(i-2)*(float(i))**2+9.d0*h0(i-2)*float(i)-12.d0*h0(i-1)*
(float(i))**3+12.d0*h0(i+1)*(float(i))**3-3.d0*h0(i+2)*(float(i))**3+
9.d0*h0(i+2)*(float(i))**2-9.d0*h0(i+2)*float(i)+
16.d0*h0(i)*(float(i))**3)/(float(i-1))**3/4.d0

!fortran(e[i],precision=double);
e(i)= -h0(i)**2*(4.d0*h0(i)*float(i)-3.d0*h0(i-1)*float(i)+
3.d0*h0(i-1)+3.d0*h0(i+1)*float(i)-3.d0*h0(i+1))/float(i-1)/4.d0

!fortran(f[i],precision=double);
f(i)= cons2*(h(i,n-2)/2.d0-2.d0*h(i,n-1))-(3.d0*h0(i)**2*
(-h0(i-2)/2.d0+h0(i-1)-h0(i+1)+h0(i+2)/2.d0)+3.d0*h0(i)**2/float(i-1)*
(h0(i-1)-2.d0*h0(i)+h0(i+1)))*(-h0(i-1)/2.d0+h0(i+1)/2.d0)+

```

```

        3.d0*h0(i)**2/(float(i-1))**2*(-h0(i-1)/2.d0+h0(i+1)/2.d0)**2+add(i)*h0(i)
        !AGREGADO ADD(i)
    enddo !matrix formation

!solve matrix
call pent1d_forw(a,b,c,d,e,nr)
call pent1d_back(a,b,c,d,e,f,nr)

!relax
call update(nr,f,h0,rf)

!calculate residual hres
call resid(nr,f,h0,hres)
!debug
!
!print *, n,count,hres !este debe imprimir casi siempre en la pantalla

do i=1,nr
    h(i,n)=f(i)
    h0(i)=f(i)
enddo

!update pressure
do i=2,nr-1
    l2=(f(i-1)-2.d0*f(i)+f(i+1))/dr**2 !centered 2nd derivative
    l1=(-f(i-1)+f(i+1))/2.0d0/dr !centered 1st derivative
    p(i,n)=-l2-l1/dr/float(i-1)
enddo
p(1,n)=4.d0/3.d0*p(2,n)-1.d0/3.d0*p(3,n)
p(nr,n)=-2.d0*rb/hnd

enddo !dowhile hres<tol

if(hres>tol) then
    print *, 'WARNING:hres>tol at time and internal iterations=',n,count
    print *, 'WARNING:hres and tol respectively=',hres,tol
    stop
endif

return
end subroutine PDE

!=====
! name      :  subroutine openfiles
! purpose   :  opens files to save data inputs and results obtained
! note      :  no has any variable for shared with main program, because this is
!              called only as 'call openfiles'
!=====
subroutine openfiles
use physical
use numerical

open(unit=1,file='v_z.dat',status='unknown')
open(unit=2,file='h_p.dat',status='unknown')
open(unit=3,file='data.dat',status='unknown')
open(unit=4,file='Implsave_forces.dat',status='unknown')

!saving data in 'data.dat'
write(3,13) nt,nr,dt
write(3,23) rb,rmax,dr
!write(3,33) rho1,rhob,sigma,mul,g
write(3,43) hnd,hnd,z00
write(3,53) Re,We,Eo

```



```

!-----
! name      : update
! purpose   : under-relax and update (n-1) time step values f0
! note      :
!-----
!
subroutine update(ntot,f,f0,rf)

! -- array/data declarations
implicit none
integer j,ntot
double precision f(ntot),f0(ntot),rf

do j=1,ntot
  if(abs(f(j)).le.1.0d-14) f(j)=0.0
  f(j)=f0(j)*(1.-rf)+f(j)*rf
! f(j)=f0(j)
enddo

return
end subroutine update
!-----
! name      : resid
! purpose   : calculate the L2-norm between two vectors
! note      :
!-----
subroutine resid(ntot,a,b,sum)

! -- array/data declarations
implicit none
integer :: j,ntot
real(kind=8):: a(ntot),b(ntot),sum

sum=0.0d0
do j=1,ntot
  sum=abs(a(j)-b(j))+sum
enddo

sum=sum/float(ntot)

return
end subroutine resid
!-----
! name      : pentld_forw
! purpose   : forward-sweep of penta diagonal solver
! note      : performs LU decomposition storing results in the original matrix
!           : Main diagonal of U (c array) is normalized to 1.
!           : Matches exactly formulas (6.7.7) to (6.7.12) for the particular
!           : case of a pentadiagonal matrix from "Applied numerical methods in
!           : C" by Schichiro Nakamura(source S. Cancelos)
!-----
subroutine pentld_forw(a,b,c,d,e,nx)

!penta diagonal solver.
implicit none

integer :: nx,i
real(kind=8):: a(nx),b(nx),c(nx),d(nx),e(nx)

! -- forward sweep.

```

```

c(1)=1./c(1)
d(1)=c(1)*d(1)
e(1)=c(1)*e(1)

c(2)=1./(c(2)-b(2)*d(1))
d(2)=c(2)*(d(2)-b(2)*e(1))
e(2)=c(2)*e(2)

do i=3,nx-2
  b(i)=b(i)-a(i)*d(i-2)
  c(i)=1./(c(i)-(a(i)*e(i-2)+b(i)*d(i-1)))
  d(i)=c(i)*(d(i)-b(i)*e(i-1))
  e(i)=c(i)*e(i)
enddo

b(nx-1)=b(nx-1)-a(nx-1)*d(nx-3)
c(nx-1)=1./(c(nx-1)-(a(nx-1)*e(nx-3)+b(nx-1)*d(nx-2)))
d(nx-1)=c(nx-1)*(d(nx-1)-b(nx-1)*e(nx-2))

b(nx)=b(nx)-a(nx)*d(nx-2)
c(nx)=1./(c(nx)-(a(nx)*e(nx-2)+b(nx)*d(nx-1)))

return
end subroutine pentld_forw

!-----
! name      : pentld_back
! purpose   : backward-sweep of penta diagonal solver
! note      : performs forward and backward substitution using LU decomposition
!             Verified it agrees with "Applied numerical methods in C" by
!             Schichiro Nakamura (source S. Cancelos)
!-----
subroutine pentld_back(a,b,c,d,e,f,nx)

!penta diagonal solver.
implicit none

integer nx,i
real(kind=8):: a(nx),b(nx),c(nx),d(nx),e(nx)
real(kind=8):: f(nx)

! -- backward sweep.

f(1)=c(1)*f(1)
f(2)=c(2)*(f(2)-b(2)*f(1))

do i=3,nx
  f(i)=c(i)*(f(i)-a(i)*f(i-2)-b(i)*f(i-1))
enddo

  f(nx-1)=f(nx-1)-d(nx-1)*f(nx)
do i=nx-2,1,-1
  f(i)=f(i)-(d(i)*f(i+1)+e(i)*f(i+2))
enddo

return
end subroutine pentld_back
!!!!!!!!!!!!!!!!!!!!!!!!!!!!!!!!!!!!!!!!!!!!!!!!!!!!!!!!!!!!!!!!!!!!!!!!!!!!!!!!!!!!

```

## FLOWCHARTS OF SUBROUTINES IN THE 3D-BWI CODE

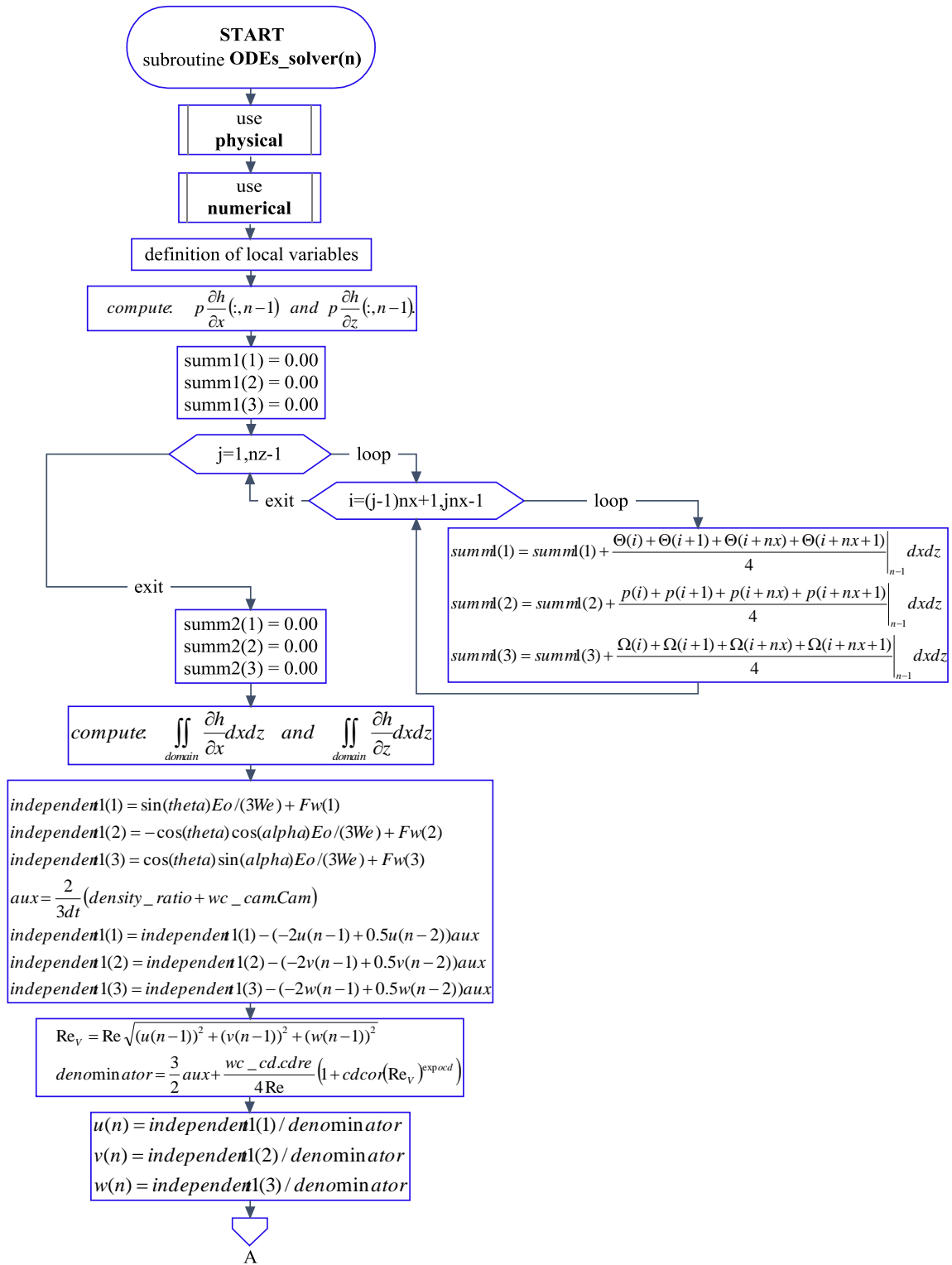


**Figure D7:** Structure of the subroutine ODEs\_solver called by the program main3D\_BWI

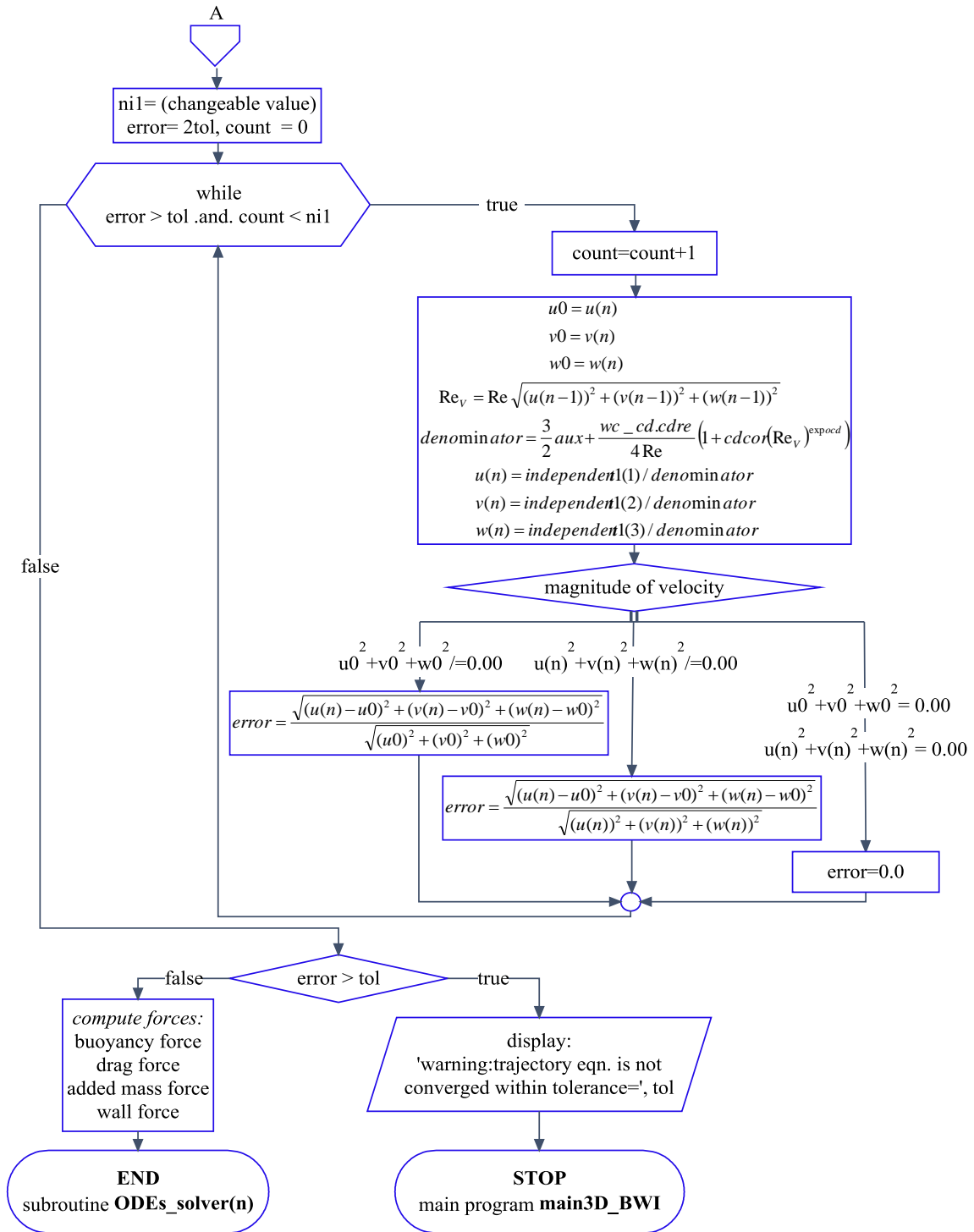


**Figure D8:** Structure of the subroutine ODEs\_solver called by the program main3D\_BWI (continuation)

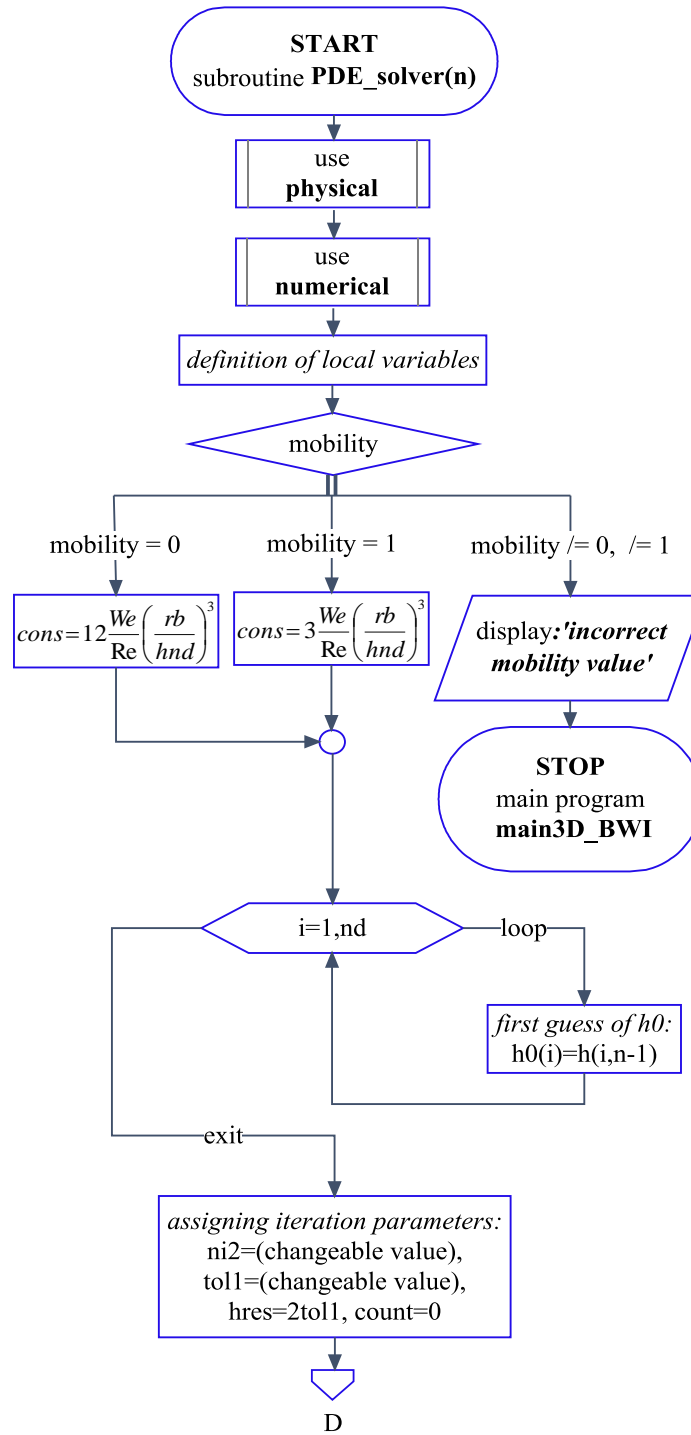


**Figure D9:** Structure of the subroutine PDE\_solver called by the program main3D\_BWI

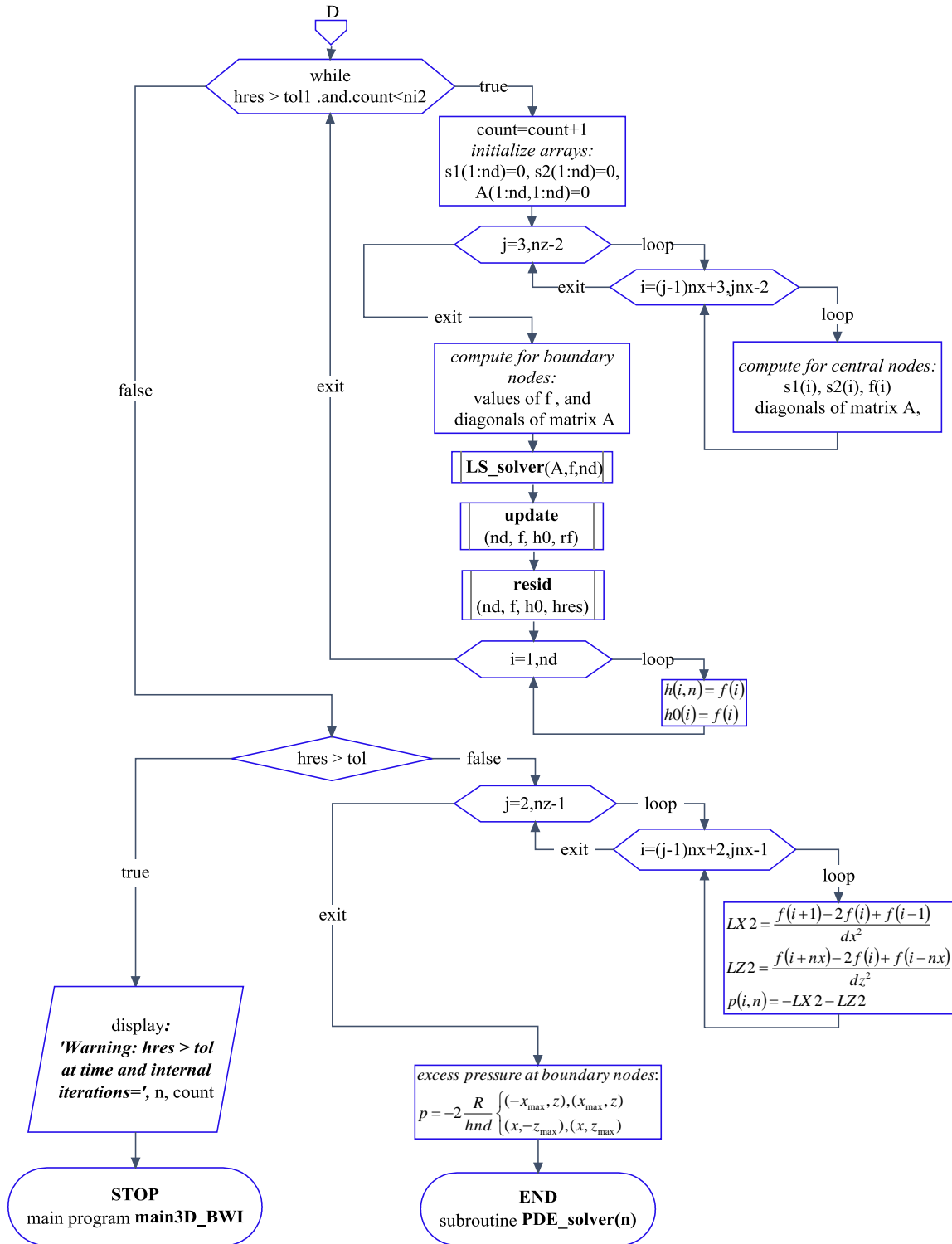


**Figure D10:** Structure of the subroutine *PDE\_solver* called by the program *main3D\_BWI* (continuation)

## 3D-BWI CODE

```
=====
! PROGRAM:  THREE-DIMENSIONAL Bubble-wall interaction
!
! PURPOSE:  This program solves the two-dimensional bubble-wall interaction
!           model,i.e. solves the two dimensional trajectory and three-
!           dimensional lubrication equations
!
!           The general algorithm is:
!           1st, using the h(i,n-1) we compute the pressure force.
!           2nd, using this pressure force the velocity for following time
!           step is determined.
!           finally, using the last velocity and implicit method we solve
!           the lubrication equation for determine the h(i,n) that will be
!           useful for determine the velocity for the follow time step.
!
!
! RECORD OF REVISIONS:
!           Date(mmddyyyy)      Programmer      Description of change
!           =====
!           03/28/2011          R. De La Cruz      REV0
!           -----
!           S. Cancelos,PhD.    -----
=====

!-----
! name      : module physical
! purpose   : Definition of physical properties of fluid,fluid flow, bubble,and
!           bubble motion. Also, the phenomenon variables are included.
!
! note      : These variables are used in all program.
!-----

module physical
implicit none
save

integer, parameter :: single = 4
integer, parameter :: double = 8
real(kind=8), parameter :: pi = 3.1416d0

!input parameters

real(kind=double) :: density_ratio !discontinuous density/continuous density
real(kind=double) :: mul          !liquid viscosity
real(kind=double) :: rhob        !Bubble density
real(kind=double) :: rhol        !liquid density
real(kind=double) :: g           !gravity acceleration
real(kind=double) :: sigma       !surface tension

real(kind=double) :: Re          !terminal velocity based Reynolds number
real(kind=double) :: we          !bubble diameter based Weber number
real(kind=double) :: Eo          !Eotvos number
real(kind=double) :: hnd         !characteristic film thickness
real(kind=double) :: hinf        !characteristic film thickness at (x,z)=0,0 and t=0
real(kind=double) :: R           !characteristic bubble radius
real(kind=double) :: VT          !bubble terminal velocity
real(kind=double) :: rmax        !maximum non-dimendional radius
real(kind=double) :: theta       !wall angle in degrees
real(kind=double) :: alpha       !wall angle in degrees
real(kind=double) :: z00         !initial bubble position related to y-coordinate
```

```

real(kind=double) :: cam      !added mass coefficient
real(kind=double) :: wc_cam  !added mass wall correction
real(kind=double) :: wc_cd   !drag wall correction
real(kind=double) :: cdre    !main factor of cd*re
real(kind=double) :: cdcor   !second factor of cd*re
real(kind=double) :: expocd  !cd correction exponent
integer :: mobility          !switch for interface mobility: 0=inmobile, 1= mobile
real(kind=double), dimension(3) :: buoyancy, drag, wallforce, netforce,      &
                                   addedmass,history
                                   !forces on the bubble, it is considered that are
                                   !applied in the center of gravity of this.

!variables
real (kind=double),dimension(:) ,allocatable :: u  !bubble velocity in x-coord
real (kind=double),dimension(:) ,allocatable :: v  !bubble velocity in y-coord
real (kind=double),dimension(:) ,allocatable :: w  !bubble velocity in y-coord
real (kind=double),dimension(:,) ,allocatable :: h  !film tickness,see geometry
real (kind=double),dimension(:) ,allocatable :: h0 !guess for film tickness
real (kind=double),dimension(:,) ,allocatable :: p  !excess pressure in film
real (kind=double),dimension(:) ,allocatable :: xb !bubble position in y-coord
real (kind=double),dimension(:) ,allocatable :: yb !bubble position in x-coord
real (kind=double),dimension(:) ,allocatable :: zb !bubble position in x-coord
real (kind=double), dimension(:) ,allocatable :: x  !non-dimensional x- coord.
real (kind=double), dimension(:) ,allocatable :: z  !non-dimensional z- coord.

end module physical

```

```

!-----
!  name      : module numerical
!  purpose   : definition of numerical parameters to be used throughout
!              the program, i.e. in main program and subroutines.
!  note      :
!-----

```

```

module numerical

implicit none
save

integer, parameter :: single = 4
integer, parameter :: double = 8

!input parametr

integer :: nx, nz, nt, nd      !nodes number in space and time
integer :: step, nn           !for saving data
real(kind=double) :: dt       !non-dimensional time step
real(kind=double) :: tol      !tolerance for internal h iterations
real(kind=double) :: dx,dz    !non-dimensional grid size
real(kind=double) :: rf       !relaxation factor
real(kind=double), dimension(:,), allocatable :: A    !coefficients matrix
real(kind=double), dimension(:) , allocatable :: f    !constants matrix
!real (kind=double), dimension(:) , allocatable :: LX10 !derivative operator
!real (kind=double), dimension(:) , allocatable :: LX30 !derivative operator
!real (kind=double), dimension(:) , allocatable :: LX40 !derivative operator
!real (kind=double), dimension(:) , allocatable :: LZ10 !derivative operator
!real (kind=double), dimension(:) , allocatable :: LZ30 !derivative operator
!real (kind=double), dimension(:) , allocatable :: LZ40 !derivative operator
!real (kind=double), dimension(:) , allocatable :: LA0 !derivative operator
!real (kind=double), dimension(:) , allocatable :: LB0 !derivative operator
!real (kind=double), dimension(:) , allocatable :: LXZ0 !derivative operator

```



```

density_ratio=0.001d0 !rhob/rhol
VT= 0.d0 !0.26d0 (R=0.79mm contaminated system)![m/s]
R = .4d-3 !0.79d-3 !bubble radius [m]
hnd=5.d0*R !characteristic lenght use hinf=hnd
hinf=hnd

mobility=0 !integer value 0(inmobile) or 1 (mobile)
rmax=1.0d0 !non-dimensional rmax = xmax = zmax
theta= 25.d0 !enter wall angle in degrees
alpha= 0.d0

!Drag and added mass correlation values
Cam=0.5d0 !added mass coefficient
wc_cd=1.d0 !2.3410767d0
wc_cam = 1.d0 !2.d0
expocd=0.687d0 !-0.5d0
cdre= 24.d0 !55.d0 !1.51d0*48.d0 !0.7997d0*48.d0
cdcdr=0.15d0 !-0.9596016d0

!compute non-dimensional numbers if is necessary
!Re=rhoL*2.D0*R*VT/mul
!Eo=g*(rhoL-rhob)*(2.D0*R)**2/sigma
!We=rhoL*VT**2*2.D0*R/(sigma)
Re= 72.543d0!410.d0 !410.d0
We= 0.0888 !1.463d0 !1.463d0 !
!when no know liquid and bubble density the following equation can be used.
!This equation results of drag and bouyancy forces balance for initial
!condition i.e. at V = VT.
Eo=0.0847d0
!Eo=3.d0/4.d0*wc_cd*cdre*(1.d0+cdcdr*(Re)**expocd)*we/Re !for We=2RrhoLVT^2/sigma
!print*, 'Eo=',Eo
!.....

!Additional Calculation and assignation of numerical values

dx=2.d0*rmax/float(nx-1)
dz=2.d0*rmax/float(nz-1)
step = nt/100 !every "step" is saving the solution in the matrix

!initialize: bubble far away moves at terminal velocity
theta=theta*pi/180.d0 !expressing in radians
alpha=alpha*pi/180.d0 !expressing in radians
u(1)=1.d0*sin(theta) !non-dimensional
v(1)=-1.d0*cos(theta)*cos(alpha) !non-dimensional
w(1)=1.d0*cos(theta)*sin(alpha) !non-dimensional
z00= (hnd+R)/R
!debug
print*,u(1),v(1),w(1)

!assigning coordinates to nodes i
do j=1,nx
do i=j,(nz-1)*nx+j,nx
x(i)=-rmax+dx*float(j-1)
enddo
enddo

do j=1,nz
do i=(j-1)*nx+1,j*nx
z(i)=-rmax+dz*float(j-1)
enddo
enddo

```



```

!           forces. No have analytical solution for this equation because the
!           equation is a non-linear non-homogeneous partial differential
!           equation.
! note     : the trajectory equation is a initial value problem
!=====
subroutine ODEs_Solver(n)
use physical
use numerical
implicit none
integer :: n

!local variables
integer :: i,count,j
integer :: nh,nil
real(kind=8) :: aux,denominator           !for simplify the algebra
real(kind=8) :: Rev                       !Instantaneous Reynolds number
real(kind=8) :: error                     !convergence variable
real(kind=8) :: fachis                    !constant of history force
real(kind=8) :: u0,v0,w0                  !old values of velocities for iterative process
real(kind=8), dimension(3) :: sumhis      !SC it was kind=double
real(kind=8), dimension(3) :: at         !coefficients of derivative
real(kind=8), dimension(3) :: independent1 !SC it was kind=double
real(kind=8), dimension(3) :: summl,summ2 ! parts of Fw
real(kind=8), dimension(nd) :: pdhdx     !integrand in x direction
real(kind=8), dimension(nd) :: pdhdz     !integrand in z direction

!coefficients of second order backward time derivative approximation:
at(1)= 1.5d0
at(2)=-2.d0
at(3)= 0.5d0

!compute pdhdx part
do j=1,nz
  do i=(j-1)*nx+2,j*nx-1
    !revisar esta division por dx
    pdhdx(i)=p(i,n-1)*0.5d0*(h(i+1,n-1)-h(i-1,n-1))/dx
  end do
end do
do i=1,(nz-1)*nx+1,nx
  !revisar el dx
  pdhdx(i)=(-3.d0*h(i,n-1)+4.d0*h(i+1,n-1)-h(i+2,n-1))*0.5d0*p(i,n-1)/dx
end do

do i=nx,nd,nx
  !revisar el dx
  pdhdx(i)=(3.d0*h(i,n-1)-4.d0*h(i-1,n-1)+h(i-2,n-1))*0.5*p(i,n-1)/dx
end do

!compute pdhdz part
do i=1,nx
  do j=nx+i,(nz-2)*nx+i,nx
    !revisar esta division por dx
    pdhdz(j)=p(j,n-1)*0.5d0*(h(j+nx,n-1)-h(j-nx,n-1))/dz
  end do
end do

do i=1,nx
  !revisar el dx
  pdhdz(i)=(-3.d0*h(i,n-1)+4.d0*h(i+nx,n-1)-h(i+2*nx,n-1))*0.5d0*p(i,n-1)/dz
end do

do i=(nz-1)*nx+1,nd

```

```

!revisar el dx
pdhdz(i)=(3.d0*h(i,n-1)-4.d0*h(i-nx,n-1)+h(i-2*nx,n-1))*0.5*p(i,n-1)/dz
end do

!integrate {pdh/dx and pdh/dz from -xmax to xmax and -zmax to zmax}
summ1(1)=0.d0
summ1(2)=0.d0
summ1(3)=0.d0
do j=1,nz-1
  do i=(j-1)*nx+1,j*nx-1
    summ1(1)=summ1(1)+0.25d0*(pdhdx(i)+pdhdx(i+1)+pdhdx(i+nx)+pdhdx(i+nx+1))*dx*dz
    summ1(2)=summ1(2)+0.25d0*(p(i,n-1)+p(i+1,n-1)+p(i+nx,n-1)+p(i+nx+1,n-1))*dx*dz
    summ1(3)=summ1(3)+0.25d0*(pdhdz(i)+pdhdz(i+1)+pdhdz(i+nx)+pdhdz(i+nx+1))*dx*dz
  enddo
enddo

!debug
!print*,summ(1),n

summ2(1)=0.d0
summ2(2)=0.d0 !we use this term when use normal n entire.
summ2(3)=0.d0

!compute dhdx part
do j=1, nz-1
  summ2(1)=summ2(1)+0.5d0*(h(j*nx,n-1)-h((j-1)*nx+1,n-1)+h((j+1)*nx,n-1)- &
    h(j*nx+1,n-1))*dz
end do

!compute dhdz part
do i=1, nx-1
  summ2(3)=summ2(3)+0.5d0*(h((nz-1)*nx+i,n-1)-h(i,n-1)+h((nz-1)*nx+1+i,n-1)- &
    h(i+1,n-1))*dx
end do

!debug
!print *, n,summ(1), summ(2), summ(3)

independent1(1)=sin(theta)*Eo/we/3.d0-hnd/(R*pi*we)*(2.d0*summ2(1)+hnd/R*summ1(1))
independent1(2)=-cos(theta)*cos(alpha)*Eo/we/3.d0
+(8.d0*rmax**2/pi+hnd/R*summ1(2)/pi)/we
independent1(3)=cos(theta)*sin(alpha)*Eo/we/3.d0-
hnd/(R*pi*we)*(2.d0*summ2(3)+hnd/R*summ1(3))
!debug
!write(*,*)independent(1), independent(2), u(n), w(n)
!call wall_correction(n)
!calculate corrections to drag and addedmass due to wall proximity

aux=2.d0/3.d0*(density_ratio+cam*wc_cam)/dt

independent1(1)=independent1(1)-(at(2)*u(n-1)+at(3)*u(n-2))*aux
independent1(2)=independent1(2)-(at(2)*v(n-1)+at(3)*v(n-2))*aux
independent1(3)=independent1(3)-(at(2)*w(n-1)+at(3)*w(n-2))*aux

!compute history term as for a rigid sphere
sumhis(1)=0.d0
sumhis(2)=0.d0
sumhis(3)=0.d0

!put limit on integration
!if (n.gt.3.and.n.le.4003) then !(n.le.4003)(n.gt.3.and.n.le.4003)
!do nh=3, n-1 ! if nh=n you obtain inf#

```

```

!sumhis(1)=sumhis(1)+(at(1)*u(nh)+at(2)*u(nh-1)+at(3)*u(nh-2))/sqrt(float(n-nh))
!sumhis(2)=sumhis(2)+(at(1)*v(nh)+at(2)*v(nh-1)+at(3)*v(nh-2))/sqrt(float(n-nh))
!sumhis(3)=sumhis(3)+(at(1)*w(nh)+at(2)*w(nh-1)+at(3)*w(nh-2))/sqrt(float(n-nh))
!end do
!else if (n==3)then
! sumhis(1)=0.d0
! sumhis(2)=0.d0
! sumhis(3)=0.d0
!else
!do nh=n-4000, n-1
!sumhis(1)=sumhis(1)+(at(1)*u(nh)+at(2)*u(nh-1)+at(3)*u(nh-2))/sqrt(float(n-nh))
!sumhis(2)=sumhis(2)+(at(1)*v(nh)+at(2)*v(nh-1)+at(3)*v(nh-2))/sqrt(float(n-nh))
!sumhis(3)=sumhis(3)+(at(1)*w(nh)+at(2)*w(nh-1)+at(3)*w(nh-2))/sqrt(float(n-nh))
!end do
!endif

!debug
!print*, 'sumhis(1)=', sumhis(1)
!fachis=-6.0d0/sqrt(2.d0*pi*Re*dt) !modificado respecto al de Moraga
fachis=0.d0
sumhis(1)=sumhis(1)*fachis
sumhis(2)=sumhis(2)*fachis
sumhis(3)=sumhis(3)*fachis
!print*, sumhis(1), sumhis(2)

independent1(1)=independent1(1)+sumhis(1)
independent1(2)=independent1(2)+sumhis(2)
independent1(3)=independent1(3)+sumhis(3)

Rev=Re*sqrt(u(n-1)**2+v(n-1)**2+w(n-1)**2)
denominator=at(1)*aux+wc_cd*cdre/Re/4.d0*(1.d0+cdc* (Rev+1.d-10)**expod)

u(n)=independent1(1)/denominator
v(n)=independent1(2)/denominator
w(n)=independent1(3)/denominator

count=0
error=2.d0*tol
nil=1000000
do while(error>tol.and.count<=nil)
count=count+1
u0=u(n)
v0=v(n)
w0=w(n)
Rev=Re*sqrt(u(n)**2+v(n)**2+w(n)**2)
denominator=at(1)*aux+wc_cd*cdre/Re/4.d0*(1.d0+cdc* (Rev+1.d-10)**expod)
u(n)=independent1(1)/denominator
v(n)=independent1(2)/denominator
w(n)=independent1(3)/denominator

!compute error
if (u(n)**2+v(n)**2+w(n)**2.ne.0.d0) then
!error=((u(n)-u0)**2+(v(n)-v0)**2+(w(n)-w0)**2)/(u(n)**2+v(n)**2+w(n)**2)
error=sqrt((u(n)-u0)**2+(v(n)-v0)**2+(w(n)-w0)**2)/
&
sqrt(u(n)**2+v(n)**2+w(n)**2)
elseif(u0**2+v0**2+w0**2.ne.0.d0) then
error=sqrt((u(n)-u0)**2+(v(n)-v0)**2+(w(n)-w0)**2)/sqrt(u0**2+v0**2+w0**2)
else
error=0.d0
endif
!print *, 'count=', count, 'error=', error, 'u(n)-u0=', u(n)-u0
!print*, 'v(n)-v0=', v(n)-v0, 'u(n)=', u(n), 'v(n)=', v(n)

```

```

enddo !dowhile error>tol

!print*, n, v(n),u(n)
if(error>tol) then
  print *, 'WARNING: TRAJECTORY EQN. IS NOT CONVERGED WITHIN TOLERANCE=',tol
  print *, 'n and error are',n,error
  stop
endif

!compute non-dimensional position

xb(n)=(-at(2)*xb(n-1)-at(3)*xb(n-2)+u(n-1)*dt)/at(1)
yb(n)=(-at(2)*yb(n-1)-at(3)*yb(n-2)+v(n-1)*dt)/at(1)
zb(n)=(-at(2)*zb(n-1)-at(3)*zb(n-2)+w(n-1)*dt)/at(1)

!compute non dimensional forces
buoyancy(1)=Eo/we/3.d0*sin(theta)
buoyancy(2)=-Eo/we/3.d0*cos(theta)*cos(alpha)
buoyancy(3)=Eo/we/3.d0*cos(theta)*sin(alpha)

!addedmass(2)=-aux*(at(1)*v(n)+at(2)*v(n-1)+at(3)*v(n-2))
addedmass(1)=-2.d0/3.d0*wc_cam*cam*(at(1)*u(n)+at(2)*u(n-1)+at(3)*u(n-2))/dt
addedmass(2)=-2.d0/3.d0*wc_cam*cam*(at(1)*v(n)+at(2)*v(n-1)+at(3)*v(n-2))/dt
addedmass(3)=-2.d0/3.d0*wc_cam*cam*(at(1)*w(n)+at(2)*w(n-1)+at(3)*w(n-2))/dt

drag(1)=-wc_cd*cdre/Re/4.d0*(1.d0+cdc*cor*(Rev)**expocd)*u(n)
drag(2)=-wc_cd*cdre/Re/4.d0*(1.d0+cdc*cor*(Rev)**expocd)*v(n)
drag(3)=-wc_cd*cdre/Re/4.d0*(1.d0+cdc*cor*(Rev)**expocd)*w(n)

wallforce(1)=-hnd/(R*pi*we)*(2.d0*summ2(1)+hnd/R*summ1(1))
wallforce(2)=(8.0*rmax**2+hnd/R*summ1(2))/(pi*we)
wallforce(3)=-hnd/(R*pi*we)*(2.d0*summ2(3)+hnd/R*summ1(3))

history(1)=sumhis(1)
history(2)=sumhis(2)
history(3)=sumhis(3)

!compute net force
do i=1,3
  netforce(i)=buoyancy(i)+addedmass(i)+drag(i)+wallforce(i)+history(i)
  ! print*,netforce(i)
  ! debug
  ! write(*,*)i,buoyancy(i), wallforce(i), summ(2)
end do

return
end subroutine ODEs_Solver

!=====
! name      : PDE_Solver
! purpose   : Solves the Three-dimensional lubrication equation by the implicit
!             method using the second-order finite differences scheme.
!             Due that the lubrication equation is a non-linear partial
!             differential equation we linearize this equation for each time n
!             around the time n-1.
! note      : The equation is solved in a square domain,due that axisymmetric
!             bubble is no longer considered.
!=====
subroutine PDE_Solver(n)
use physical
use numerical
implicit none

```

```

!local variables
integer :: n,i,count,ni2,j !status
real(kind=8) :: hres,cons,cons3,toll
real(kind=8),dimension(nd) :: s1,s2

!Mobility condition
if(mobility == 0)then
  !cons is c1 of model derivations
  cons=12.d0*we/Re*(R/hnd)**3 !for no slip at bubble surface
else if (mobility == 1)then
  cons=3.d0*we/Re*(R/hnd)**3 !for slip at bubble surface
else
  print*,' incorrect mobility value'
  stop
end if
!print*,cons
!copy h into h0
do i=1,nd
  h0(i)=h(i,n-1)
! print*, h0(i), i,n
end do

!cons3=(dx*dz)**2
toll=1.d-8
hres=2*toll
ni2=20000 !limit number of internal iterations.For debugging use small ni
count=0 !count the number of internal iterations.

do while(hres.gt.toll.and.count.lt.ni2)

  count=count+1
  !nz=nx
  !initialize
do j=1,nd
  s1(j)=0.d0
  s2(j)=0.d0
  do i=1,nd
    A(i,j)=0.d0
  end do
end do

!MATRIX FORMATION

do j=3,nz-2
  do i=(j-1)*nx+3,j*nx-2
    s1(i)=h0(i+2)-8.d0*h0(i+1)+20.d0*h0(i)-8.d0*h0(i-1)+h0(i-2)+ &
      2.d0*h0(i+nx+1)+2.d0*h0(i-nx+1)-8.d0*h0(i+nx)-8.d0*h0(i-nx)+ &
      2.d0*h0(i+nx-1)+2.d0*h0(i-nx-1)+h0(i+2*nx)+h0(i-2*nx)

    s2(i)= (h0(i+1)-h0(i-1))*(h0(i+2)-4.d0*h0(i+1)+4.d0*h0(i-1)-h0(i-2))+ &
      h0(i+nx+1)-h0(i+nx-1)+h0(i-nx+1)-h0(i-nx-1))+ (h0(i+nx)- &
      h0(i-nx))*(h0(i+2*nx)-4.d0*h0(i+nx)+4.d0*h0(i-nx)- &
      h0(i-2*nx)+h0(i+nx+1)-h0(i-nx+1)+h0(i+nx-1)-h0(i-nx-1))

    !Diag1
    A(i,i-2*nx)= -0.75d0*h0(i)**2*(h0(i+nx)-h0(i-nx))+h0(i)**3
    !Diag2
    A(i,i-nx-1)= -0.75d0*h0(i)**2*(h0(i+1)-h0(i-1)+h0(i+nx)-h0(i-nx))+ &
      2.d0*h0(i)**3
    !Diag3
    A(i,i-nx) = -0.75d0*h0(i)**2*(h0(i+2*nx)-8.d0*h0(i+nx)+8.d0*h0(i-nx)- &
      h0(i-2*nx)+h0(i+nx+1)-h0(i-nx+1)+h0(i+nx-1)-h0(i-nx-1))- &
      8.d0*h0(i)**3-0.25d0*w(n)*cons*(dx)**3
  end do
end do

```

```

!Diag4
A(i,i-nx+1)=0.75d0*h0(i)**2*(h0(i+1)-h0(i-1)-h0(i+nx)+h0(i-nx))+
      2.d0*h0(i)**3
!Diag5
A(i,i-2)=-0.75d0*h0(i)**2*(h0(i+1)-h0(i-1))+h0(i)**3

!Diag6
A(i,i-1)=-0.75d0*h0(i)**2*(h0(i+2)-8.d0*h0(i+1)+8.d0*h0(i-1)-
      h0(i-2)+h0(i+nx+1)+h0(i-nx+1)-h0(i+nx-1)-h0(i-nx-1))-
      0.25d0*u(n)*cons*(dx)**3-8.d0*h0(i)**3
!Diag7
A(i,i)=1.5d0*cons/dt*dx**4+3.d0*h0(i)**2*s1(i)+1.5d0*h0(i)*s2(i)+
      20.d0*h0(i)**3
!Diag8
A(i,i+1)=0.75d0*h0(i)**2*(h0(i+2)-8.d0*h0(i+1)+8.d0*h0(i-1)-
      h0(i-2)+h0(i+nx+1)+h0(i-nx+1)-h0(i+nx-1)-h0(i-nx-1))+
      0.25d0*u(n)*cons*(dx)**3-8.d0*h0(i)**3
!Diag9
A(i,i+2)=0.75d0*h0(i)**2*(h0(i+1)-h0(i-1))+h0(i)**3
!Diag10
A(i,i+nx-1)=-0.75d0*h0(i)**2*(h0(i+1)-h0(i-1)-h0(i+nx)+h0(i-nx))+
      2.d0*h0(i)**3
!Diag11
A(i,i+nx)=0.75d0*h0(i)**2*(h0(i+2*nx)-8.d0*h0(i+nx)+8.d0*h0(i-nx)-
      h0(i-2*nx)+h0(i+nx+1)-h0(i-nx+1)+h0(i+nx-1)-h0(i-nx-1))-
      8.d0*h0(i)**3+0.25d0*w(n)*cons*(dx)**3
!Diag12
A(i,i+nx+1)=0.75d0*h0(i)**2*(h0(i+1)-h0(i-1)+h0(i+nx)-h0(i-nx))+
      2.d0*h0(i)**3
!Diag13
A(i,i+2*nx)=0.75d0*h0(i)**2*(h0(i+nx)-h0(i-nx))+h0(i)**3

!entering the constants matrix f(nx*nz)=f(nd)
!FOR CENTRAL NODES
f(i)=3.d0*h0(i)**2*(h0(i)*s1(i)+0.75d0*s2(i))+
      cons/dt*dx**4*(2.d0*h(i,n-1)-0.5d0*h(i,n-2))

end do
end do

!boundary conditions p=-2R/hnd at boundary
do i=(nz-2)*nx+3,(nz-1)*nx-2
  A(i,i-2*nx)=-1.d0
  A(i,i-nx)=4.d0
  A(i,i)=-5.d0
  A(i,i+nx-1)=1.d0
  A(i,i+nx+1)=1.d0
end do
do i=nx+3,2*nx-2
  A(i,i-nx-1)=1.d0
  A(i,i-nx+1)=1.d0
  A(i,i)=-5.d0
  A(i,i+nx)=4.d0
  A(i,i+2*nx)=-1.d0
end do
do i=2*nx+2,(nz-3)*nx+2,nx
  A(i,i-nx-1)=1.d0
  A(i,i)=-5.d0
  A(i,i+1)=4.d0
  A(i,i+2)=-1.d0
  A(i,i+nx-1)=1.d0

```

```

end do

do i=3*nx-1, (nz-2)*nx-1, nx
  A(i, i-nx+1)=1.d0
  A(i, i-2)=-1.d0
  A(i, i-1)=4.d0
  A(i, i)=-5.d0
  A(i, i+nx+1)=1.d0
end do
!corner nodes.
i=nx+2
  A(i, i-nx-1)=2.d0
  A(i, i-nx+1)=1.d0
  A(i, i)=-10.d0
  A(i, i+1)=4.d0
  A(i, i+2)=-1.d0
  A(i, i+nx-1)=1.d0
  A(i, i+nx)=4.d0
  A(i, i+2*nx)=-1.d0

i=2*nx-1
  A(i, i-nx-1)=1.d0
  A(i, i-nx+1)=2.d0
  A(i, i-2)=-1.d0
  A(i, i-1)=4.d0
  A(i, i)=-10.d0
  A(i, i+nx)=4.d0
  A(i, i+nx+1)=1.d0
  A(i, i+2*nx)=-1.d0

i=(nz-2)*nx+2
  A(i, i-2*nx)=-1.d0
  A(i, i-nx-1)=1.d0
  A(i, i-nx)=4.d0
  A(i, i)=-10.d0
  A(i, i+1)=4.d0
  A(i, i+2)=-1.d0
  A(i, i+nx-1)=2.d0
  A(i, i+nx+1)=1.d0

i=(nz-1)*nx-1
  A(i, i-2*nx)=-1.d0
  A(i, i-nx)=4.d0
  A(i, i-nx+1)=1.d0
  A(i, i-2)=-1.d0
  A(i, i-1)=4.d0
  A(i, i)=-10.d0
  A(i, i+nx-1)=1.d0
  A(i, i+nx+1)=2.d0

!Para los nodos justo en el borde(en todo el borde cuadrado)
do i=1, nx
  A(i, i)=1.5d0*cons/dt
end do
do i=(nz-1)*nx+1, nd
  A(i, i)=1.5d0*cons/dt
end do

```

```

do i=nx+1, (nz-2)*nx+1, nx
    A(i,i)=1.5d0*cons/dt
end do
do i=2*nx, (nz-1)*nx, nx
    A(i,i)=1.5d0*cons/dt
end do

!FOR THE BOUNDARY NODES
do i=1, nx
    f(i)=(dt*v(n)*R/hnd+2.d0*h(i,n-1)-0.5d0*h(i,n-2))*cons/dt
end do
do i=(nz-1)*nx+1, nz*nx
    f(i)=(dt*v(n)*R/hnd+2.d0*h(i,n-1)-0.5d0*h(i,n-2))*cons/dt
end do
do i=nx+1, (nz-2)*nx+1, nx
    f(i)=(dt*v(n)*R/hnd+2.d0*h(i,n-1)-0.5d0*h(i,n-2))*cons/dt
end do
do i=2*nx, (nz-1)*nx, nx
    f(i)=(dt*v(n)*R/hnd+2.d0*h(i,n-1)-0.5d0*h(i,n-2))*cons/dt
end do
do i=nx+3, 2*nx-2
    f(i)=2.d0*R*dx**2/hnd
end do
do i=(nz-2)*nx+3, (nz-1)*nx-2
    f(i)=2.d0*R*dx**2/hnd
end do
do i=2*nx+2, (nz-3)*nx+2, nx
    f(i)=2.d0*R*dx**2/hnd
end do
do i=3*nx-1, (nz-2)*nx-1, nx
    f(i)=2.d0*R*dx**2/hnd
end do

f(nx+2)=4.d0*R*dx**2/hnd
f(2*nx-1)=4.d0*R*dx**2/hnd
f((nz-2)*nx+2)=4.d0*R*dx**2/hnd
f((nz-1)*nx-1)=4.d0*R*dx**2/hnd

call LS_solver(A,f,nd)
!relax
call update(nd,f,h0,rf)
!calculate residual hres
call resid(nd,f,h0,hres)
!print *, n,count,hres

!update h(i,n)
do i=1,nd
    h(i,n)=f(i)
    h0(i)=f(i)
end do
!print*, n, count, hres, h(1,n)

end do !dowhile hres<tol

!do i=1,nd
    !print*,n,'f(i)=' ,f(i)
!end do
!print*, count, h(1,n)
if(hres>tol1) then

```

```

    print *, 'WARNING:hres>tol at time and internal iterations=',n,count
    stop
endif

!compute non-dimensional excess pressure film
!using centered 2nd derivatives in x and z directions
do j=2,nz-1
  do i=(j-1)*nx+2,j*nx-1
    P(i,n)=-((f(i+1)+f(i-1))-2.d0*f(i))/dx**2-((f(i+nx)+f(i-nx))-2.d0*f(i))/dz**2
  end do
end do

!pressure at boundary nodes
do i=1,nx
  P(i,n)=-2.d0*R/hnd
end do
do i=(nz-1)*nx+1,nd
  P(i,n)=-2.d0*R/hnd
end do
do i=nx+1,(nz-2)*nx+1,nx
  P(i,n)=-2.d0*R/hnd
end do
do i=2*nx,(nz-1)*nx,nx
  P(i,n)=-2.d0*R/hnd
end do
!print*, n,count,P(20,n)

return
end subroutine PDE_Solver

!=====
! name      :  subroutine openfiles
! purpose   :  opens files to save data inputs and results obtained
! note      :  no has any variable for shared with main program, because this is
!              called only as 'call openfiles'
!=====
subroutine openfiles
use physical
use numerical

!open files
open(unit=1,file='velocities_3D.dat',status='unknown')
open(unit=2,file='xz_h3D.dat',status='unknown')
open(unit=3,file='data3D.dat',status='unknown')
open(unit=4,file='Xforces3D.dat',status='unknown')
open(unit=5,file='Yforces3D.dat',status='unknown')
open(unit=10,file='Zforces3D.dat',status='unknown')
open(unit=8,file='xz_p3D.dat',status='unknown')
open(unit=9,file='position_3D.dat',status='unknown')

!Saving data in 'data2D.dat'
write(3,9999) 'Code 3D_1. Numerical parameters'
write(3,8888) '===== '
write(3,1013) nt,nx,nd
write(3,1023) dt,dx,dz
write(3,1033) step,tol,rf
write(3,7777)
write(3,9999) 'Physical parameters      '
write(3,8888) '=====      '
write(3,1043) int(theta*180./pi),int(alpha*180./pi),mobility
write(3,1053) u(1),v(1),w(1)
write(3,1063) hnd,hinf,z00
write(3,1073) Re,We,Eo

```



```

use numerical
implicit none
integer :: n
!local variables
integer :: i,check
!save results in 'xz_h3D.dat' and 'xz_p3D.dat'
nn=nn+1
check=1+step*(nn-1)
if (check.eq.n) then
  do i=1,nd
    write(2,1032) n,i,x(i),z(i),h(i,n) !xz_h3D.dat
    write(8,1038) n,i,x(i),z(i),2*r/hnd+p(i,n) !xz_p3D.dat
1032 format(I10,' ',I5,' ',E14.6,' ',E14.6,' ',E14.8)
1038 format(I10,' ',I5,' ',E14.6,' ',E14.6,' ',E14.8)
  end do
else
  nn = nn-1
end if

!saving results in 'velocities_3D.dat'and position_3D.dat
!write(1,1031) n,float(n-1)*dt*R/VT,u(n)*VT,v(n)*VT,w(n)*VT
write(1,1031) n,float(n-1)*dt, u(n),v(n),w(n)
!write(9,1039) n,float(n-1)*dt*R/VT,xb(n)*R,yb(n)*R,zb(n)*R
write(9,1039) n,float(n-1)*dt, xb(n),yb(n),zb(n)
1031 format(I10,' ',E23.15,' ',E23.15,' ',E23.15,' ',E23.15,' ',E23.15)
1039 format(I10,' ',E23.15,' ',E23.15,' ',E23.15,' ',E23.15,' ',E23.15)

!netforce(i)=buoyancy(i)+addedmass(i)+drag(i)+wallforce(i)+history(i)
!saving results in 'Xforces3D.dat'
write(4,1034) (n-1)*dt,history(1),buoyancy(1),drag(1),addedmass(1),wallforce(1)
1034 format(E14.6,' ',E16.8,' ',E16.8,' ',E16.8,' ',E16.8,' ',E16.8)

!saving results in 'Yforces3D.dat'
write(5,1035) (n-1)*dt,history(2),buoyancy(2),drag(2),addedmass(2),wallforce(2)
1035 format(E14.6,' ',E16.8,' ',E16.8,' ',E16.8,' ',E16.8,' ',E16.8)

!saving results in 'Zforces3D.dat'
write(10,1030) (n-1)*dt,history(3),buoyancy(3),drag(3),addedmass(3),wallforce(3)
1030 format(E14.6,' ',E16.8,' ',E16.8,' ',E16.8,' ',E16.8,' ',E16.8)

return
close(1)
close(2)
close(4)
close(5)
close(8)
close(9)
close(10)
end subroutine save_results

!-----
! name : linear_system_solver
! purpose : solve the linear system as follow form Mh=f where h is called
! the actualized f value. here h is noted as a f actualized.
! note : LU descomposition using Doolittle method
!-----
subroutine LS_solver(M,f,ntot)
!use numerical
!use physical
implicit none
integer ntot !ntot is the total nodes number nd in main program

```

```

!local variables
integer :: i,j,k
real(kind=8):: sum1,sum2
real(kind=8),dimension(ntot,ntot):: M,Ld,Ud
real(kind=8), dimension(ntot):: f,hprim

!Ld and Ud are lower and upper arrays respectively
!arrays initialization, it is very important
do i=1,ntot
  do j=1,ntot
    Ld(i,j)=0.0d0
    Ud(i,j)=0.0d0
  end do
end do

do i=1,ntot
  hprim(i)=0.0d0
end do
!print*, Ld(1,1)

!perform LU factorization
do i=1,ntot
do j=1,ntot
  Ld(i,i)= 1.0d0
  Ud(1,j)= M(1,j)
end do
end do

do i=2,ntot
  Ld(i,1)=M(i,1)/M(1,1)
end do
do i=2,ntot
  do j=i,ntot
    sum1=0.0d0
    do k=1,i-1
      sum1=sum1+Ud(k,j)*Ld(i,k)
    end do
    Ud(i,j)=M(i,j)-sum1
  end do
  do j=i+1,ntot
    sum2=0.0d0
    do k=1,i-1
      sum2=sum2+Ld(j,k)*Ud(k,i)
    end do
    Ld(j,i)=(M(j,i)-sum2)/Ud(i,i)
  end do
end do
end do

!compute hprim
!Mh=f, but M=LU, then LUh=f hence Lh'=f next Uh=h'and h is the solution vector

!compute h' doing forward substitution as,
hprim(1)=f(1)/Ld(1,1)
do i=2,ntot
  hprim(i)=f(i)
  do j=1,i-1
    hprim(i)= hprim(i)-Ld(i,j)*hprim(j)
  end do
  hprim(i)=hprim(i)/Ld(i,i)
end do
!debug
!print*, 'hprim=',hprim

```

```

!compute h new for backward substitution, ie. compute new f
f(ntot)=hprim(ntot)/Ud(ntot,ntot)
do i=ntot-1,1,-1
  f(i)=hprim(i)
  do j=i+1,ntot
    f(i)= f(i)-Ud(i,j)*f(j)
  end do
  f(i)=f(i)/Ud(i,i)
end do

return
end subroutine LS_solver

```

```

!-----
! name      :  update
! purpose   :  under-relax and update (n-1) time step values f0
! note      :  source S. Cancelos "walling.f90"
!-----
subroutine update(ntot,f,f0,rf)
!
! -- array/data declarations
!
implicit none
integer j,ntot
double precision :: f(ntot),f0(ntot),rf

do j=1,ntot

  ! if(abs(f(j)).le.1.0d-14) f(j)=0.0
  f(j)=f0(j)*(1.-rf)+f(j)*rf
!   f(j)=f0(j)

enddo

return
end subroutine update

```

```

!-----
! name      :  resid
! purpose   :  calculate the L2-norm between two vectors
! note      :
!-----
subroutine resid(ntot,a,b,sum)
!
! -- array/data declarations
implicit none
integer :: j,ntot
real(kind=8) :: a(ntot),b(ntot)
real(kind=8) :: sum

sum=0.0d0
do j=1,ntot
  sum=abs(a(j)-b(j))+sum
enddo
sum=sum/dble(ntot)

return
end subroutine resid

```

```

!!!!!!!!!!!!!!!!!!!!!!!!!!!!!!!!!!!!!!!!!!!!!!!!!!!!!!!!!!!!!!!!!!!!!!!!!!!!!!!!!!!!!!!!!!!!!!!!!!!!!!!!!!!!!!!!!!!!!!!!

```